Molecular Pathogenesis of Fibulin-4 Associated Aortic Aneurysms

Natasja Ramnath

Molecular Pathogenesis of Fibulin-4 Associated Aortic Aneurysms

Moleculaire pathogenese van Fibuline-4 geassocieerde aorta aneurysmata

Proefschrift

ter verkrijging van de graad van doctor aan de
Erasmus Universiteit Rotterdam
op gezag van de
rector magnificus

Prof.dr. H.A.P. Pols

en volgens besluit van het College voor Promoties.

De openbare verdediging zal plaatsvinden op
woensdag 5 februari 2014 om 15.30 uur
door

Natasja Wanita Monisha Ramnath
geboren te Den Haag

ERASMUS UNIVERSITEIT ROTTERDAM

PROMOTIECOMMISSIE

Promotoren:
Prof.dr. R. Kanaar
Prof.dr. H.J.M. Verhagen

Overige leden:
Prof.dr. D.J.G.M. Duncker
Prof.dr. J.W. Roos-Hesselink
Prof.dr. J. de Backer

Copromotor:
Dr. J. Essers

Vasudhaiva Kutumbakam
The whole world is one family

Voor mijn familie

TABLE OF CONTENTS

Chapter 1

Introduction

INTRODUCTION

Aortic aneurysms

Aortic disease represents one of the major causes of morbidity and mortality in the industrialized society. Approximately 2% of all deaths are caused by aortic aneurysm and dissections [1]. Aneurysms are defined as a local widening of the artery with more than 50 percent of the normal diameter [2]. An aneurysm can result in a fatal aortic rupture or in an aortic dissection, which is a tear in the wall of the artery that causes blood to flow between the layers of the wall and forces the layers apart [3]. Dissections involving the ascending aorta, Stanford type A dissections, have a mortality rate of 1-2% per hour and should be immediately treated surgically [4], while dissections occurring in the descending aorta are usually treated medically and have an in-hospital mortality of about 10% [5]. However, an acute aortic dissection may also result in a rupture and with thoracic aortic rupture mortality is very high, approximately 94 to 100%. Both diseases have principles and techniques of surgical treatment in common. Surgery of aneurysms of the ascending aorta and arch, the descending aorta, and the thoracoabdominal aorta has been associated with a reduced operative mortality of respectively 2.9%, 3.0% and 11.9% between 1995 and 2004 [6]. However, the diagnosis of aneurysms and dissections is at the moment limited to computed tomography and echocardiography, usually in late and severe stages of the diseases. The main mechanisms by which these diseases occur are largely unknown. It is thought that aneurysm formation is the result of changes in the extracellular matrix (ECM) of the aortic wall and signaling pathways of the vasculature [3]. However, more insight into the molecular mechanisms leading to aneurysm formation is required in order to identify predisposing factors and new detection protocols for earlier detection of aortic aneurysms.

Thoracic Aortic Aneurysms (TAA) & Abdominal Aortic Aneurysms (AAA)

According to their location aneurysms can be categorized in two main groups: aneurysms of the thoracic aorta and aneurysms of the abdominal aorta. While the incidence of TAAs is approximately 10 per 100 000 persons per year and is higher in elderly males [3, 7], AAAs are much more common. Ultrasound screening studies have shown that 4 to 8 percent of older men have an occult AAA [8, 9], and that AAAs are 4 to 5 times more common in men than women [8, 10]. Interestingly, recent clinical studies also report a high frequency of TAA in patients with AAA [11, 12], while the pathophysiology underlying TAA and AAA differs to a large extent. The pathophysiology of the aorta above and below the diaphragm has demonstrated differences in embryologic origin, structure and mechanical properties of the aortic wall, atherosclerotic susceptibility, proteolytic profiles like matrix metalloproteinase (MMP) activity, immune mediators and cell signaling pathways that have implications in the development of an aortic aneurysm, such as the transforming growth factor (TGF)-β signal transduction pathway (Figure 1) [13]. Whereas the thoracic aorta originates from the neural crest, the abdominal aorta is derived from the mesoderm. In terms of aortic wall structure, the outer part of the medial layer of the thoracic aorta contains vasa vasorum (vessels which nourish the outer part of the media in large and medium-sized vessels), the medial layer has numerous lamellar units, which grows by synthesizing additional lamellar units, and has a greater elastin and collagen content compared to the abdominal aorta. In the abdominal aorta vasa vasorum are absent, the abdominal aorta contains fewer lamellar units, which grows by increasing lamellar unit thickness, and it contains lower elastin and collagen content. As such the distensibility and elasticity is greater in the thoracic aorta. Furthermore, the abdominal aorta is the site of most severe atherosclerosis formation and has slightly different MMP/ tissue inhibitor of metalloproteinases (TIMP) ratios compared to
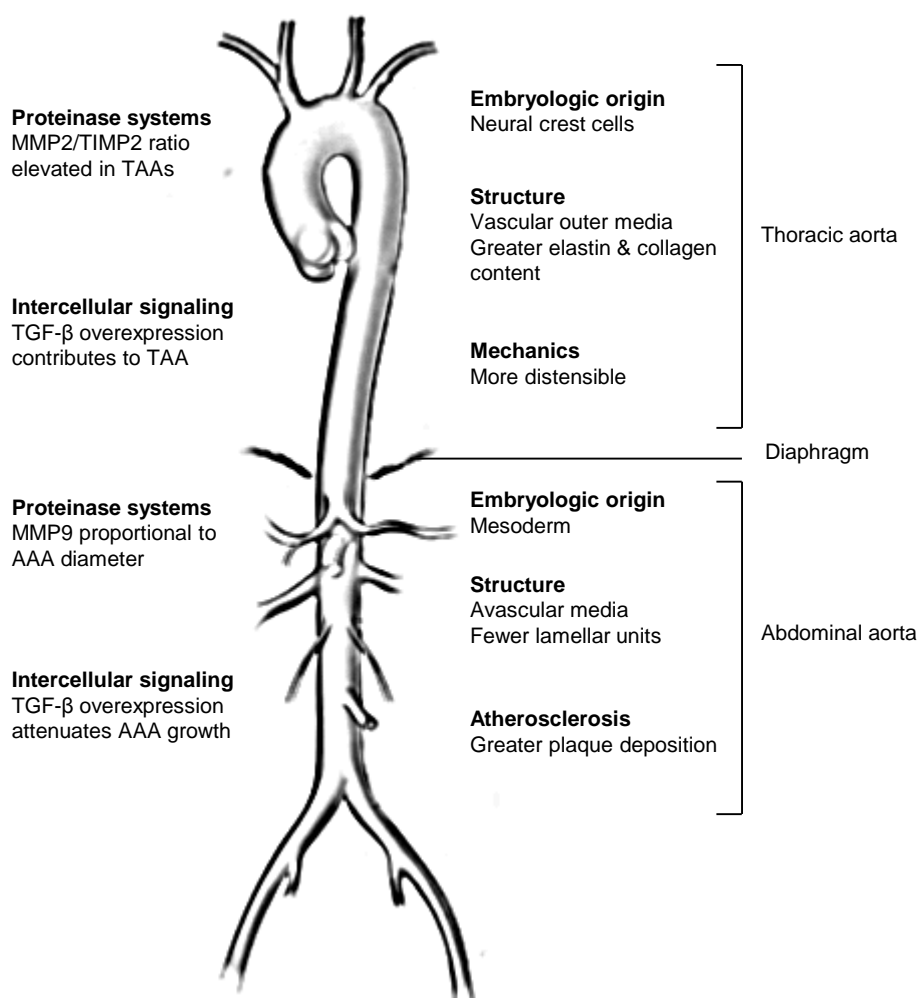
Figure 1: Differences in pathophysiology of the thoracic and abdominal aorta. Schematic overview of the aorta showing differences between the thoracic and abdominal aorta in embryologic origin, structure, mechanics, proteinase systems, molecular signaling and atherosclerosis. Image partially retrieved from http://my.clevelandclinic.org/heart/heart-blood-vessels/aorta.aspx and from Ruddy et al [11].

the thoracic aorta. In the thoracic aorta increased TGF-β signaling contributes to aneurysm disease, while overexpression of TGF-β has been reported to attenuate the proteolytic state in the abdominal aorta [13].

Pathogenesis and heritability of TAAs

Aneurysms of the thoracic aorta, in particular the aortic ascendens, are characterized by degeneration of the medial layer of the aortic wall, also called cystic medial degeneration, which is histologically characterized by smooth muscle cell (SMC) dropout and elastic fiber degeneration. While aneurysms are mostly associated with atherosclerosis, ascending

1

aortic aneurysms can occur due to a genetic mutation inherited in an autosomal dominant pattern. Generally, patients with TAA can be categorized in 3 groups: I) inherited TAA syndromes such as Marfan Syndrome (MFS), Ehlers Danlos Syndrome (EDS) and Loeys-Dietz Syndrome (LDS), II) familial non-syndromic TAA disease, which is usually associated with cardiovascular features such as bicuspid aortic valve, patent ductus arteriosus and cerebrovascular disease, with an occurrence at variable ages (20% of TAA cases) [14], and III) sporadic TAA cases with no family history of TAA, detected at older age and representing 80% of the patients with a TAA [15, 16]. Mutations in several genes related to the ECM, the TGF-β signal transduction pathway and SMCs are usually involved (Table 1), but do not always specifically associate with one of these groups. Other diseases that are associated with TAA include inflammatory disorders/vasculitis (eg, giant cell arteritis, mycotic aneurysm, Takayasu's aortitis) and bicuspid aortic valve disease.

Mutations in genes involved in the ECM leading to TAA involve Fibrillin-1, procollagen type III (COL3A1), Elastin (ELN) and Fibulin-4 (FBLN4). Mutations in Fibrillin-1 (Fbn1) lead to MFS, which is one of the most common hereditable connective tissue disorders in young patients. Currently a large number of mutations have been identified, which affect the skeletal, ocular, pulmonary and cardiovascular system, including severe ascending aortic dilation [17-21]. The EDS vascular type (EDS type IV) is caused by mutations in the COL3A1 gene, which encodes for procollagen type III. Patients with a mutation in this gene develop thoracic aortic and aortic arch dissection and rupture due to affected synthesis, secretion and structure of procollagen type III [22]. Dissections also occur in vertebral arteries and in carotids in extra- and intra-cranial segments. In addition, the skin is thin and translucent with highly visible subcutaneous vessels as compared to other EDS types. Furthermore, spontaneous rupture of organs, including pneumothorax are reported [23]. ELN mutations in patients lead to Cutis laxa, a connective tissue disorder characterized by loose, pendulous, redundant and inelastic skin, and is associated with lung emphysema and thoracic aortic root dilation [24-26]. Additionally, homozygous or compound heterozygous Fibulin-4 mutations in patients results in Cutis laxa, ascending aortic aneurysms and pulmonary diseases. On further examination some of these patients also presented with abdominal tortuosity and dilation. These patients usually present within a severe stage of the disease during the first months or years of their life [27-33].

Deficiencies in TGF-β pathway related proteins leading to TAA involve TGF-β receptor type (TβR) I, TβRII, (mothers against decapentaplegic) Smad3 and TGF-β2. TβRI and TβRII mutations are related to the LDS, which is clinically characterized by hypertelorism, cleft palate, aortic aneurysms and arterial tortuosity, also of medium sized arteries, including cerebral arteries, splanchnic arteries and renal arteries. It is generally characterized by a more severe progression of cardiovascular disease compared to MFS, as dissections have been observed at smaller aortic root diameters [34]. It has been estimated that mutations in the TβRII gene are responsible for about 5 percent of familial cases [35]. Furthermore, heterozygous loss-of-function mutations in Smad3, which is an intracellular TGF-β signaling regulator involved in transcriptional activation and repression, have been identified in families with familial forms of TAA together with some skeletal features and the occurrence of early arthritis. This syndrome is referred to as aneurysm-osteoarthritis syndrome (AOS). Similarly to LDS, a more aggressive progression of the disease than (observed in MFS) occurs for the cardiovascular manifestations of AOS, with already mildly increased ascending aortic diameters resulting in aortic dissections, and involvement of the entire arterial tree [36-39]. Recently, mutations in the gene encoding for TGF-β2, the ligand of the TGF-β receptor complex that has a higher binding affinity for TβRIII, has been observed to cause ascending aortic aneurysms in association with cerebrovascular

disease and systemic features of MFS or LDS [40, 41].

Furthermore, mutations in actin and myosin, which are the two main contractile proteins within SMCs have been reported in families with ascending aortic aneurysms [42]. Mutations in myosin heavy chain 11 (MYH11) cause familial TAA in association with patent ductus arteriosus (PDA) [43-45]. Mutations in smooth muscle α-actin (ACTA2) cause familial TAA in association with vascular and extravascular features, including PDA, bicuspid aortic valve, coronary artery disease, stroke, Moyamoya disease and gastrointestinal and urogenital tract complications [42, 45, 46]. TAA patients with a myosin light chain kinase (MYLK) mutation, which is important in the control of SMC contractile function, causes acute ascending aortic dissection with small or no aortic enlargement before dissection, and involve the gastrointestinal tract. It accounts for approximately 2.6% of all familial TAA cases [47]. Recently, a gain-of-function mutation in an additional gene involved in the contractility of SMCs, protein kinase, cGMP-dependent, type I (PRKG1), has been identified in patients with familial TAA or acute thoracic aortic dissections (Stanford type A, B and unspecified) [48]. Thoracic aortic aneurysms and dissections occur at relative young ages in these patients. Moreover, many individuals with this mutation present with hypertension and additional vascular disease of the descending and abdominal aorta, and other arteries.

Table 1 - TAA associated genes related to the ECM, the TGF-β pathway and SMCs.

Location	Genes	Disease	Reference
Extracellular matrix	Fibrillin-1	Marfan syndrome	[17-21]
	COL3A1	Ehlers-Danlos syndrome type IV	[22]
	ELN	Cutis laxa	[24-26]
	Fibulin-4	Cutis laxa	[27-33]
TGF-β pathway	TβRI	Loeys-Dietz syndrome	[34]
	TβRII	Loeys-Dietz syndrome	[34, 35]
	Smad3	Aneurysm-Osteoarthritis syndrome	[36-39]
	TGF-β2	TAA, cerebrovascular disease	[40, 41]
Smooth muscle cells	MYH11	Familial TAA, PDA	[42-45]
	ACTA2	Familial TAA, PDA, BAV	[42, 45, 46]
	MYLK	Familial TAA, gastrointestinal disease	[47]
	PRKG1	Familial TAA	[48]

TAA, thoracic aortic aneurysm; PDA, patent ductus arteriosus; BAV, bicuspid aortic valve

Pathogenesis of AAAs

Aneurysms of the abdominal aorta are thought to be caused by a multifactorial process, including genetic, environmental, hemodynamic and immunologic factors [49]. Although no dominant gene defects have been identified like in TAAs, genetic make-up seems to influence AAA formation. The risk of developing the disease is increased by a family history of abdominal aneurysm. In a previous surgery practice, three-fourths of operated

1

aneurysms were familial [50]. Several genetic polymorphisms found by genome-wide association studies are known or suspected to increase the risk for AAA including genes controlling angiotensin converting enzyme, Angiotensin II type 1 (AT1) receptor, methylene tetrahydrofolate reductase, and matrix metalloproteinase-9 (MMP9). In addition, a possible locus on chromosome 19q13 was identified in a genome scan of 36 families with AAA [51]. Other chromosomes linked to AAA include the long arm of chromosome 16, and chromosomes 4q32-34, 11q24, and 9p21 [52, 53]. Furthermore, atherosclerosis and inflammatory infiltrates have been implicated to contribute to ECM degradation in the abdominal aortic wall, which allows aneurysm development. MMPs, produced by smooth muscle and inflammatory cells, like MMP2 and MMP9, and other proteinases, like plasminogen activators, serine elastases and cathepsins, may participate in this process [13, 49].

Association with Atherosclerosis
Important risk factors for both thoracic and abdominal aortic aneurysms formation are age, male gender, smoking, a family history of aortic aneurysms, the presence of other large aneurysms and atherosclerosis. These risk factors for patients with aneurysms and those with atherosclerotic disease overlap to a large extent [54, 55]. While atherosclerosis is infrequently associated with ascending aortic aneurysms, the vast majority of descending thoracic aneurysms are associated with atherosclerosis [49]. In addition, atherosclerotic changes frequently coexist with AAA [9]. However, it is still unknown whether atherosclerosis actually leads to the generation of aortic aneurysm [56]. Contemporary research suggests that atherosclerosis is not causal and that a multifactorial, systemic process, such as a defect in vascular structural proteins, might be responsible, with atherosclerosis occurring secondarily [57]. However, the molecular mechanisms underlying aneurysm formation and the relation between atherosclerosis and aortic dilation are largely unknown.

Aortic aneurysms & lung diseases
Furthermore, an aortic aneurysm, both thoracic and abdominal, are one of the cardiovascular diseases observed in patients with chronic obstructive pulmonary disease (COPD) [58, 59]. COPD is one of the leading causes of morbidity and mortality worldwide [60], and is characterized by chronic airflow obstruction due to airway inflammation and alveolar destruction resulting in lung emphysema. In addition, COPD is associated with multiple manifestations beyond the pulmonary system, including cardiovascular diseases [61-64]. These manifestations complicate the health status and the management of COPD patients.
The nature of the relationship between aortic aneurysms and COPD is currently unknown. Patients with COPD and those with aortic aneurysms have overlapping risk factors, including age, hypertension, and tobacco smoking [56, 65]. The resemblance in risk profiles between these conditions, most notably smoking, or a systemic inflammatory response may account for the relation between AA and COPD [66]. Moreover, in patients with Fibulin-4 mutations lung abnormalities and aortic aneurysms co-occur and coincide with upregulation of TGF-β signaling [30]. The involvement of TGF-β in lung emphysema is additionally seen in MFS and Smad3 knockout mice, which develop progressive airspace enlargement [67, 68].
The lung is an elastic organ involved in the exchange of gas between the pulmonary vasculature and the external air. The lung parenchyma is composed of several differentiated cell types forming conducting airways and alveolar regions. The airways consist of the trachea, which bifurcate into two main extrapulmonary bronchi entering the lungs and becoming intrapulmonary bronchi and bronchioles. The alveolar regions of the

1

lung consist of alveolar ducts, alveolar sacs and alveoli. The interstitium of the alveolar walls is composed of contractile interstitial and collagen synthesizing fibroblasts, SMCs and pericytes [69]. Elastin is also an important component of the alveolar interstitium and is localized in a ring around each alveolus. Elastic fibers contribute to the maintenance of the structure and function of the mature lung, and destruction or loss of elastin is involved in the pathogenesis of emphysema, which is characterized by destruction of alveolar walls and abnormal alveolar airspace enlargement [69, 70]. Impaired alveolarization can be caused by the lack of elastin, which is produced by alveolar myofibroblasts during alveologenesis, possibly having an instructive role for septation, distal airway branching and structuring of the lung [68, 70]. Furthermore, excessive or impaired TGF-β signaling may also contribute to defective alveolarization.

The aortic wall and extracellular matrix composition

The normal aortic wall is composed of three main layers: the tunica intima, the tunica media and the tunica adventitia (Figure 2). These layers are composed of different cell-types: endothelial cells and the lamina elastic interna in the tunica intima, lamellar units formed by vascular SMCs embedded in parallel concentric layers of elastic fibers, collagen and proteoglycan in the medial layer, and fibroblasts, nerve fibers and vasa vasorum in the tunica adventitia [71]. The ECM is a complex and heterogeneous structural entity, which specifically supports and connects tissues, but also transmits specific environmental signals to cells influencing their development, proliferation, migration, polarization and metabolic functions. Additionally, it regulates the bioavailability of growth factors and cellular signaling
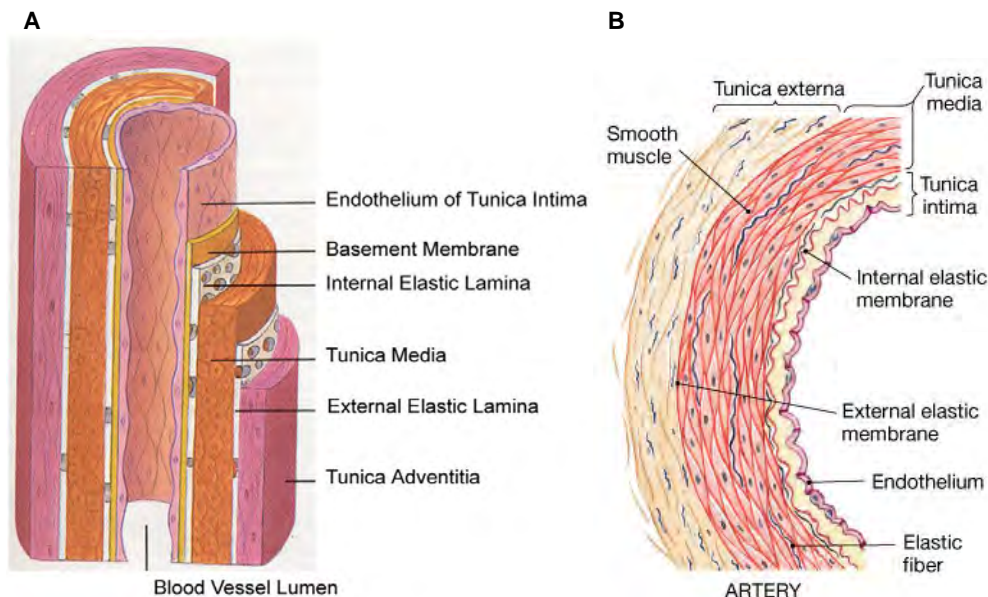

Figure 2: Schematic overview of the aortic wall layers. (A) 3D view of the aortic wall with the indicated main layers: tunica intima, tunica media and tunica adventitia. Image adapted from http://bme.ccny.cuny.edu/faculty/jtarbell/SMC%20images.htm. (B) Cross-section of the aortic wall displaying the three layers and their main components. Image adapted from Martini FH [136].

1

Figure 3: Modular structure of the fibulins. Alternative splice variants for Fibulin-1, designated A-D are displayed.

[72-76]. The ECM is constructed from glycosaminoglycan polysaccharide chains, usually in the form of proteoglycans, and of fibrous proteins such as collagen and elastin. The fibrous proteins are embedded in a gel-like substance, which is highly hydrated and formed by the proteoglycan molecules. The specific components of the ECM are produced locally by cells in the matrix and provide tissue specific properties. In the aorta the specific components of the ECM are produced by endothelial cells, SMCs and fibroblasts.

Elastic fibers in the ECM of the medial and outer layer of the aortic wall are important components for elasticity [77, 78]. Together with collagen fibers, another component of the ECM, they provide the main mechanical properties of the vascular wall, with a small contribution from the contractile function of the SMCs in the medial layer [79]. Elastic fibers are mainly composed of an insoluble elastin core and a surrounding Fibrillin-rich microfibrillar network. The elastin core is mainly composed of tropoelastin, which is highly cross-linked by lysyl oxidase (Lox) ensuring the protein's stability and insolubility [80, 81]. Microfibrils, mainly composed of the large glycoprotein fibrillin, provide structural integrity and are important for the sequestering and bioavailability of growth factors such as TGF-β
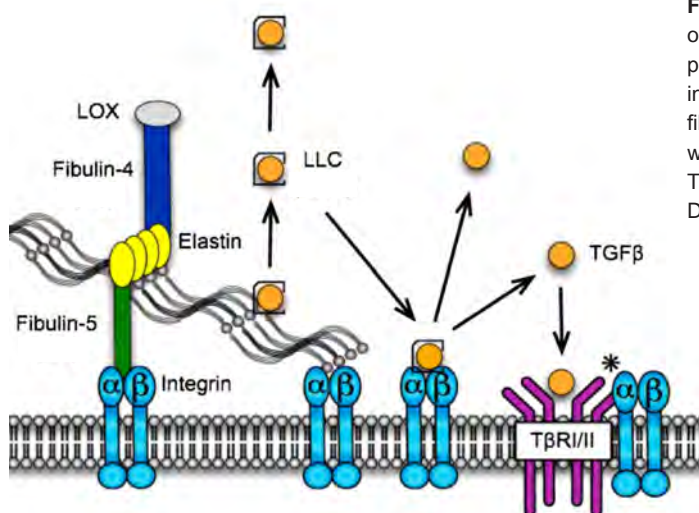
Figure 4: Schematic representation of the relation between ECM proteins and TGF-β. Fibulin-4 is involved in crosslinking of elastic fibers through recruitment of Lox, which is involved in activation of the TGF-β ligand. Image adapted from Doyle JJ et al [91].

and bone morphogenetic protein (BMP) [75, 76].

An important group of proteins that are associated with elastic fibers are fibulins, a 7-member protein family (Figure 3) [82-84]. Fibulins all share a series of calcium-binding epidermal growth factor (cbEGF) modules and a C-terminal fibulin specific domain. The 7 fibulins are prominently expressed in blood vessels by different cell types. A part of the fibulins are thought to function as intermolecular bridges that stabilize and organize extracellular elastic fibers and basement membranes [85]. Fibulin-4 and -5 are the only fibulins so far detected to be involved in elastogenesis [86-89]. They contribute to cross-linking of secreted tropoelastin aggregates and facilitate the primary deposition of larger tropoelastin aggregates onto microfibrils. Mutations in the genes encoding the different fibulins are associated with different diseases, but only mutations in the Fibulin-4 gene are associated with aortic aneurysms [78, 82, 85, 90, 91]. Fibulin-4 is mainly located in the medial layers of large veins and arteries and is found in some small capillaries [78]. The Fibulin-4 gene is a 6.37 kb gene, located on chromosome 11q13 and consists of 11 exons. The Fibulin-4 protein consists of 443 amino-acids and can bind to the first hybrid domain of Fibrillin-1 [92]. In addition, Fibulin-4 is involved in crosslinking of elastic fibers through recruitment of Lox (Figure 4), which can directly inactivate the TGF-β1 ligand through its amine oxidase activity [93-95].

The TGF-β signaling pathway
A crucial role for the TGF-β pathway has become evident in the pathogenesis of aortic aneurysms. The TGF-β cytokines belong to the TGF-β superfamily, which consists of approximately 30 members, including the BMPs and activins. These individual family members have crucial roles in multiple developmental processes and in the maintenance of tissue homeostasis in adults. Three known highly homologous isoforms of TGF-β exist: TGF-β1, -2 and -3. TGF-β is synthesized as precursor pre-pro-TGF-β, which is cleaved due to convertase into the C-terminal mature TGF-β peptide and the N-terminal precursor remnant, referred to as latency associated protein (LAP) [96, 97]. All mature TGF-β isoforms are bound to the LAP, which is called the small latent complex (SLC) and via the latent TGF-β binding protein (LTBP), forming the large latent complex (LLC), secreted and
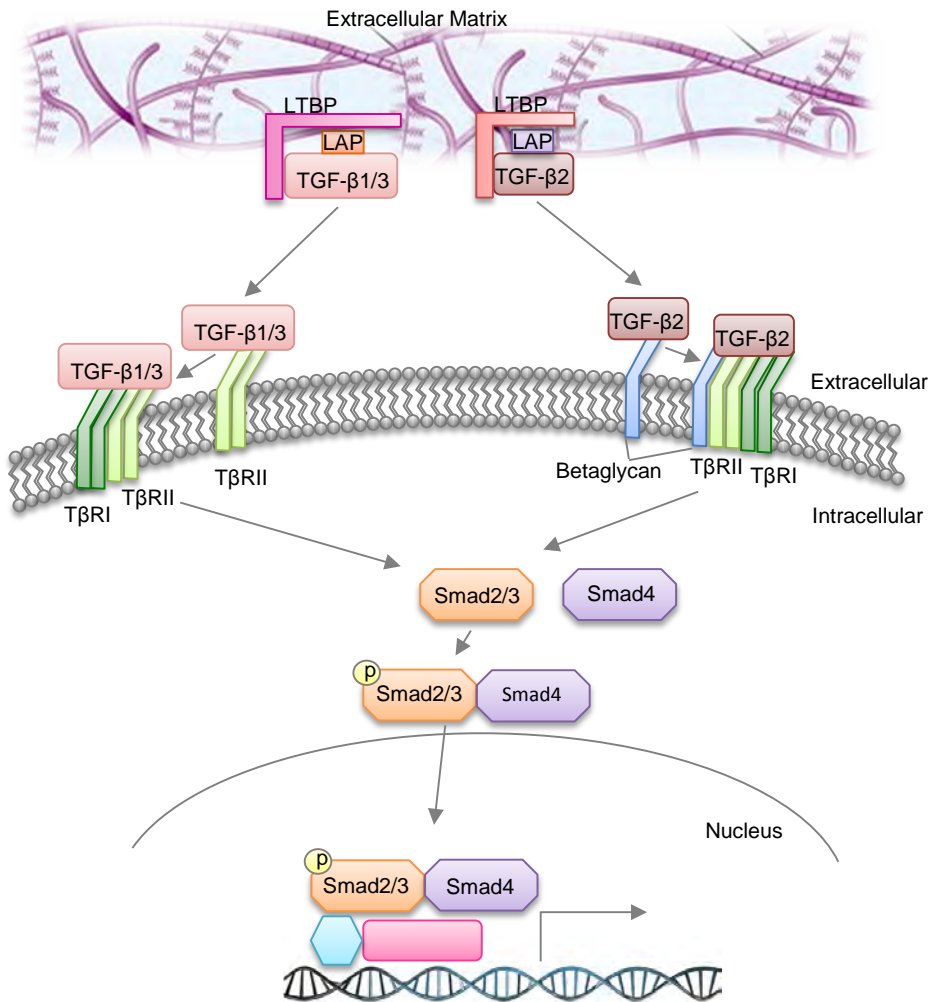
1

Figure 5: Schematic representation of TGF-β ligand specific receptor binding and canonical TGF-β signaling. TGF-β1 and -3 have a high affinity for binding to TβRII which afterwards recruits TβRI, while TGF-β2 binds with a higher affinity to betaglycan (type III TGF-β receptor) and recruits the TβRII/TβRI receptor complex. Both lead to phosphorylation and activation of TβRI and subsequent phosphorylation of Smad2/3. Smad2/3 binds to Smad4, translocates to the nucleus and initiates transcription of genes in association with coactivators and corepressors.

bound to the extracellular matrix via the N-terminal domain of LTBP, supported by covalent transglutaminase-induced crosslinks. The LLC is linked to elastic microfibrils through binding of the C-terminal region of LTBP1 to the N-terminal region of Fibrillin-1, one of the major components of microfibrils and belonging to the same gene family as LTBPs [68]. In this way Fibrillin-1 is involved in sequestering of the LLC. This complex is stored in the ECM in order to control the level of TGF-β activity and to facilitate spatiotemporal control of the response to TGF-β by concentrating the cytokine in a certain location [98]. The LLC can be released from the ECM and microfibrils by proteolytic enzymes, such as elastase and bone morphogenetic protein (BMP)-1-like metalloproteinase. Cleavage of the SLC can be achieved by proteases such as MMPs. Finally, the mature TGF-β is liberated from LAP by

1

different proteases, such as plasmin and MMPs, by Thrombospondin-1, by integrins or by reactive oxygen species (ROS), which varies according to cell type and context [99-103]. In this way the regulation of the bioavailability of TGF-β occurs at multiple levels, including the control and localization of convertases, secretion, sequestration to the ECM, and the activation process.

Upon activation, TGF-β1 and -3 have a high affinity for binding to the TβRII, which recruits, transphosphorylates and activates the TβRI, also called activin receptor like kinase (ALK)-5 (Figure 5). On the other hand, TGF-β2 has a high affinity for binding to the TGF-β receptor III betaglycan and subsequently interacts with the heterotetrameric TβRI-TβRII signaling complex (2 TβRI and 2 TβRII proteins) [104]. Activated TβRI subsequently phosphorylates downstream Smad proteins (i.e. Smad2 or -3), which form complexes with Smad4. These complexes translocate to the nucleus, and in association with co-activators and corepressors lead to transcription of target genes, including plasminogen activator inhibitor (PAI)-I, MMPs, extracellular matrix proteins and TGF-β itself, providing a positive feedback loop [105]. Dysregulation of the TGF-β- pathway due to mutations in various TGF-β related genes is associated with a variety of diseases. Interestingly, enhanced TGF-β signaling, which is additionally associated with loss of function TGF-β and TGF-β receptor mutations, have been observed in aneurysm formation, and complicates the understanding of the role for TGF-β in aneurysm development [106].

Genetic mouse models for thoracic & abdominal aortic aneurysms

Various genetically and chemically induced mouse models have been generated to mimic human thoracic and abdominal aortic aneurysms and to study their molecular pathogenesis and phenotypic features (Table 2). In contrast to patients, mouse models have a highly homogenous background, which provides the possibility to investigate the pathogenesis and outcome of specific gene associated diseases. They provide the opportunity to perform analyses ranging from pathology to molecular biology, and permit the investigation and development of tools for disease-monitoring and effective therapeutic approaches.

Different mouse models for Marfan syndrome have been generated by defined mutations in the extracellular matrix glycoprotein Fibrillin-1, which is involved in sequestering of the LLC through LTBP binding [68]. These different mouse models differ in the severity of the disease. While homozygous $Fbn1^{mg\Delta}$, $Fbn1^{C1039G}$, $Fbn1^{mgN}$ and $Fbn1^{GT-8}$ mice all die at an early postnatal age due to cardiovascular events, homozygous $Fbn1^{mgR}$ mice, with reduced expression of normal Fbn1, have a milder form of the disease and die at approximately 4 months due to aortic dissection or pulmonary insufficiency [107-111]. Heterozygosity resulting in mild aortic and lung abnormalities are only reported in viable $Fbn1^{GT-8}$ and $Fbn1^{C1039G}$ mice. Interestingly, $Fbn1^{H1\Delta}$ mice with a deletion of the LTBP binding site do not develop features of Marfan syndrome [110], suggesting that not only reduced TGF-β sequestration is responsible for increased TGF-β signaling in Fbn1 deficient mice. An additional hypothesis currently proposed is that a defective ECM is detected through integrins by mesenchymal cells (either fibroblasts or SMCs), which subsequently respond in order to repair the ECM by producing active TGF-β and required activators of latent TGF-β [112]. The increased TGF-β signaling in Marfan syndrome is associated with elevated circulating TGF-β1 levels, which is decreased after administration of losartan, an angiotensin II type 1 receptor blocker (ARB), which prevents aortic aneurysm formation [113-117]. This suggests that TGF-β1 could be a prognostic biomarker in Marfan syndrome. Additionally, Marfan mice have developmental impairment of distal alveolar septation, evident from the postnatal period and associated with an upregulated TGF-β signaling. In aged Fibrillin-1 deficient mice (6 months) destructive changes, peribronchiolar inflammation and higher

expression of MMPs are present, recapitulating the human emphysema disease [68].

The co-occurrence of lung emphysema and vascular abnormalities in association with deregulated TGF-β signaling has also been observed in mice with a deficiency in Fibulin-5, an important fibulin protein family member involved in elastic fiber organization [88]. Fibulin-5 is a molecule that bridges elastic fibers and cells through interaction with both elastin and integrins and promotes the higher order organization of thick elastic fibers or elastic lamellae. These mice develop Cutis laxa and tortuous arteries, including the aorta, but no aneurysms have been observed. Thin, fragmented and irregular elastic fibers were found in aortic sections of these mice [88].

Additionally, germline and conditional knockout mouse models have been generated for TβRI and TβRII to determine their effects on aortic aneurysm formation. Germline TβRI and TβRII knock-out mice develop defects in vascular development of the yolk sac and placenta and die during embryonic development [118, 119]. Conditional tissue specific knockout mice have been created targeting endothelial cells, vascular smooth muscle cells and neural crest cells. These mice develop specific craniofacial and cardiovascular abnormalities including aneurysm of the ductus arteriosus, persistent truncus arteriosus and an interrupted aortic arch, suggestive of LDS, and die between mid-gestation and the immediate postnatal period [120-123]. However, these mouse models do not recapitulate all symptoms of the human LDS syndrome.

In contrast to the observed phenotype of the patients, mice deficient for TGF-β2 display multiple developmental defects including cardiovascular, pulmonary, skeletal, ocular, inner ear and urogenital manifestations, and die in the perinatal period [124, 125]. In addition, Smad3 deficient mice had not been described with cardiovascular defects, but instead displayed metatastic colorectal cancer, impaired immunity, chronic infection, accelerated wound healing and progressive airspace enlargement [67, 126-129]. However, very recently progressive cardiovascular defects including aortic root and ascending aortic dilation were reported in a proportion of Smad3 deficient mice, which overcame infection. The development of the aortic disease was associated with enhanced inflammation and increased secretion of granulocyte-macrophage colony-stimulating factor (GM-CSF) from CD4^{+} T cells, while increased TGF-β signaling was detected in a later stage of the disease [130].

Furthermore, mouse models with mutations in genes involved in the contractile function of SMC have been generated to determine their effects on aortic disease. Although aortic aneurysms have not been observed in MYH11 null and Acta2 null mice, MYH11 deficiency results in delayed closure of the ductus arteriosus and Acta2 knockout mice develop abnormal vascular contractility, tone and blood flow [131, 132]. Selective ablation of integrin-linked kinase (ILK), which is located at focal adhesions and links the ECM to the actin cytoskeleton via integrins, in conditional mutant mice results in TAA and PDA in embryos. These embryos are able to complete embryonic development, but die in the perinatal period [133].

Genetically induced mouse models for AAA, hyperlipidemic apolipoprotein E (ApoE) and low density lipoprotein receptor (LDLR) knockout mice, were initially generated for atherosclerosis research, but seemed to develop abdominal aortic dilation after prolonged high fat diet feeding. In addition, compound deficient hyperlipidemic mice develop AAAs: male mice on a high fat diet deficient for ApoE and endothelial nitric oxide synthase, an enzyme involved in regulating vascular tone, and mice with a compound deficiency for LDLR and specific smooth muscle cell depleted low density lipoprotein receptor-related protein (LRP), a multifunctional protein that binds biologically diverse ligands [134].

Some genetically induced mouse models develop both thoracic and abdominal

aortic aneurysms, for instance mice with deficiencies in components of the MMP system, including MMP3 and TIMP1. Furthermore, the Blotchy mouse has a mutation on the X chromosome leading to abnormal intestinal copper absorption, which is a required co-factor for Lox, and has a tendency to develop AAA [134]. They additionally develop generalized problems such as aneurysms in other parts of the vasculature and emphysema. However, Lysyl oxidase-null mice develop predominantly TAA and ruptures spontaneously, rather than developing aneurysms of the abdominal aorta [135].

Chemically induced mouse models for thoracic & abdominal aortic aneurysms
In addition, chemically induced mouse models have been generated to study the pathogenesis of thoracic and abdominal aortic aneurysms and dissections. In this way, Lox could be inhibited by administration of β-aminopropionitrile monofumarate (BAPN), which induced cystic medial degeneration, and consequently in combination with induced hypertension, thoracic and abdominal aortic aneurysms [136, 137]. These models affecting Lox activity have been used for aneurysm studies, but these aortic aneurysms and dissections are only observed by chance.

Other chemically induced mouse models that have been used widely to study the pathogenesis of aortic aneurysm are obtained by chronic subcutaneous induction of angiotensin II, which is the main effector peptide of the renin-angiotensin system (RAS). The RAS is important for the regulation of blood pressure, electrolyte balance and body fluid homeostasis and is known to be involved in aneurysm formation. Chronic subcutaneous angiotensin II induction results in aortic aneurysm formation in ApoE or LDLR knockout mice [138-140]. In ApoE$^{-/-}$ mice infused with Angiotensin II, abdominal and ascending aortic aneurysms were observed. In 20% of the LDL receptor mice receiving Angiotensin II, large aneurysms of the abdominal aorta were found. Furthermore, Angiotensin II infusions in ApoE$^{-/-}$ mice led to an increased severity of aortic atherosclerotic lesions composed of lipid-laden macrophages and lymphocytes, while in Angiotensin II infused LDLR$^{-/-}$ mice the content of cholesterol (esterified and unesterified) in lesions of the arch, thoracic, and abdominal aorta was significantly increased. Additionally, Angiotensin II infusions in a mouse model of vascular Ehlers-Danlos syndrome, heterozygous type III collagen Col3a1$^{+/-}$ mice which have no spontaneous early vascular phenotype, led to a higher mortality rate due to thoracic aortic ruptures and dissections [141].

Furthermore, as both increased elastase activity and calcification leads to fragmentation of elastic tissue, their role in aneurysm formation were determined using elastase and calcium chloride exposure. Adventitial intraluminal elastase exposure, resulting in extensive destruction of the elastic lamellae and inflammatory infiltrates in the adventitial region, and calcium chloride exposure, resulting in structural disruption of the medial layer and inflammatory response, both generated abdominal aortic aneurysms in mice [134]. In addition, recent evidence suggests that the mineralocorticoid receptor plays an important role in cardiovascular diseases. Indeed, activation of the mineralocorticoid receptor by deoxycorticosterone acetate (DOCA) and salt, or aldosterone and salt, induced age-related abdominal and thoracic aortic aneurysm formation and rupture, with elastin degradation, inflammatory cell infiltration, SMC degeneration and apoptosis, and oxidative stress in C57BL/6 mice. DOCA or aldosterone in combination with salt induced aortic aneurysms could be significantly attenuated with mineralcorticoid receptor antagonists, but not with the angiotensin-converting enzyme inhibitor, enalapril, or with losartan [142].

Moreover, an increased ascending aortic lumen diameter has been observed after transverse aortic constriction (TAC) in mice, which is a common experimental method used to induce pressure overload cardiac hypertrophy and heart failure [143]. These mice

1

Fibulin-4^{+/+}   Fibulin-4^{+/R}   Fibulin-4^{R/R}

Fibulin-4^{+/+}   Fibulin-4^{+/R}   Fibulin-4^{R/R}
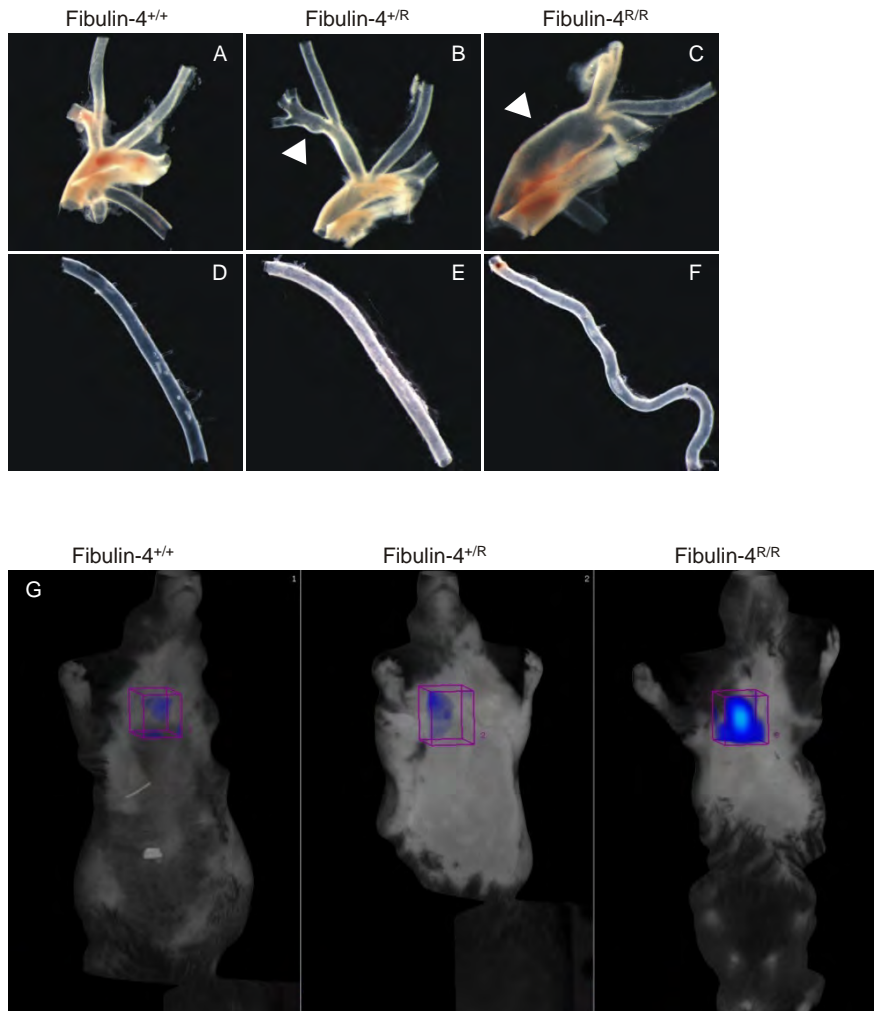
Figure 6: Aortic pathology in Fibulin-4 deficient mice. (A-F) Newborn Fibulin-4$^{+/R}$ mice showed abnormal ballooning of the innominate artery, indicative for aneurysm (indicated with arrow in B) and a less translucent aorta compared to Fibulin-4$^{+/+}$ mice (indicated in D and E). Homozygous newborn Fibulin-4$^{R/R}$ mice showed dramatic dilation of the ascending aorta (indicated with arrow in C). All Fibulin-4$^{R/R}$ mice analyzed had a tortuous aorta. (G) In vivo 3D registration of MMP activity with protease sensing optical probes showed a gradual increased activity in Fibulin-4$^{+/R}$ and Fibulin-4$^{R/R}$ mice. Images A-F adapted from Hanada et al [81]. Image G adapted from Kaijzel et al [135].

develop increased ascending aortic diameter and aortic wall thickening, with increased aortic expression of TGF-β1 and TGF-β2. The vascular remodeling associated with TAC was significantly reduced after inhibition of the AT_1 receptor using losartan. Losartan treatment also reduced TGF-β2 expression, while it did not completely reduce the increased TGF-β1 expression, adventitial Smad2 signaling, and collagen accumulation.

Fibulin-4 mouse model
In this thesis we focused on the Fibulin-4 based aneurysm mouse model. This mouse model was generated by a gradual reduction of the expression of the extracellular matrix protein Fibulin-4. Fibulin-4 knockout mice with complete disruption of the Fibulin-4 gene are not viable and die just before birth due to arterial hemorrhage and aneurysm rupture [79, 86]. The replacement of a TKneo targeting construct in a downstream gene of Fibulin-4, Mus81, resulted in a viable Fibulin-4 mouse model with reduced expression of Fibulin-4, resulting from transcriptional interference. Compared to wild type mice, heterozygous Fibulin-4[+/R] (R= Reduced) and homozygous Fibulin-4[R/R] mice contain respectively 2- and 4- fold less Fibulin-4 mRNA expression in the aorta, heart and lung. The reduced Fibulin-4 expression correlates with the severity of the cardiovascular disease seen in these mouse models. This was associated with a gradual increase in pSmad2 phosphorylation and nuclear translocation, and an enhanced production of connective tissue growth factor and collagen fibers, indicating increased TGF-β signaling [85]. Additionally, smooth muscle cell-specific Fibulin-4 knockdown mice (Fibulin-4[SMKO]) develop aneurysms in the ascending thoracic aorta with a differentiation defect of SMCs and increased phosphorylated extracellular signal-regulated kinase (ERK)1/2 signaling, suggesting an important role for Fibulin-4 in the intrinsic properties of SMCs [144].

Similar to homozygous or compound heterozygous Fibulin-4 deficient patients, Fibulin-4[R/R] mice present with thoracic ascending aortic aneurysm, tortuosity and aortic wall degeneration (Figure 6C and F) [85]. These mice therefore provide a good model to study the molecular pathogenesis leading to early aortic aneurysm formation. Interestingly, already heterozygous Fibulin-4[+/R] mice develop a milder form of the aortic disease (Figure 6B and E). Although they do not develop aortic aneurysms spontaneously, they present with less translucent aortas compared to wild type mice, and aortic wall degeneration, including elastic fiber fragmentation and significantly more local regions of disorganized extracellular matrix and collagen fibers. Gene expression profiling of the aortas of Fibulin-4 knockdown mice pointed to dysregulated TGF-β signaling and indicated that MMP9, a pro-gelatinase which degrades extracellular matrix proteins, such as collagen and elastin, might be upregulated in the aortas of these mice [85]. Fibulin-4[+/R] and Fibulin-4[R/R] mice indeed showed gradually increased MMP activity compared to wild type littermates (Figure 6G) [85, 145]. The Fibulin-4 heterozygous mice might therefore be a good model for an intermediate phenotype of connective tissue disease. In combination with additional risk factors and environmental triggers, such as atherosclerosis and infections, this mouse model might develop cardiovascular and connective tissue disorders representative for late-onset diseases, and might therefore indicate that a haploinsuffciency for Fibulin-4 leads to a pathogenic outcome. Additionally, Fibulin-4 deficient mice might be relevant models to determine early detection methods for early as well as late onset aortic diseases, by providing insight into phenotypic alterations as well as molecular mechanisms associated with aneurysm formation.

Table 2 - Genetically and chemically induced mouse models for thoracic and abdominal aortic disease.

1

Mode of induction	Mouse model	Aortic disease	Reference
Genetic	Fibrillin-1	Marfan syndrome, TAA, lung emphysema	(68, 113-117)
	Fibulin-4	TAA, dissection, rupture, tortuous and stiffened aorta, cardiac abnormalities, aortic valve stenosis	(85, 86, 145)
	Fibulin-5	Cutis laxa, tortuous arteries, lung emphysema	(88)
	TβRI, TβRII	Suggestive of LDS, postnatal mortality	(118-123)
	TGF-β2	Multiple developmental defects, perinatal mortality	(124, 125)
	Smad3	TAA in a specific proportion	(130)
	MYH11	Delayed closure of ductus arteriosus	(131)
	Acta2	Abnormal vascular contractility, tone and blood flow	(132)
	ILK	Embryonic TAA and PDA, perinatal mortality	(134)
	ApoE	Abdominal aortic dilation after prolonged HFD	(135)
	LDLR	Abdominal aortic dilation after prolonged HFD	(135)
	ApoE/eNOS	AAA	(135)
	LDLR/SMC-specific LRP	AAA	(135)
	MMP3	TAA and AAA	(135)
	TIMP1	TAA and AAA	(135)
	Blotchy mouse	AAA, generalized aneurysms and lung emphysema	(135)
	Lox	TAA and rupture	(136)
Chemical	BAPN	TAA and AAA after induced hypertension	(137, 138)
	Angiotensin II/ ApoE	TAA and AAA	(139-141)
	Angiotensin II/ LDLR	AAA in 20% of mice	(139-141)
	Angiotensin II/ COL3A1	Thoracic aortic ruptures and dissections	(142)
	Elastase	AAA	(135)
	Calcium chloride	AAA	(135)
	DOCA with salt or aldosterone with salt	Age-related TAA and AAA and rupture	(143)
	TAC	Thoracic aortic dilation and wall thickening	(144)

TAA, thoracic aortic aneurysm; LDS, Loeys-Dietz syndrome; ILK, Integrin-linked kinase; PDA, patent ductus arteriosus; HFD, high fat diet; AAA, abdominal aortic aneurysm; LRP, Low density lipoprotein receptor related protein; Lox, lysyl oxidase; BAPN, β-aminopropionitrile monofumarate ; DOCA, deoxycorticosterone acetate; TAC, transverse aortic constriction

SCOPE OF THE THESIS

The aorta is the largest artery of the body, which is important for the transportation of oxygenated blood from the heart to all organs. The elastic properties of the aorta provide the possibility to withstand the high pressure generated by the heart, which is important to pump the blood through the arteries to all parts of the body. An aneurysm of the aorta is defined as a local widening, usually due to degeneration of the arterial wall, which forms a life-threatening risk for aortic dissection or rupture. As the progression of aortic aneurysms is usually asymptomatic, they are mostly detected in a very late and severe stage of the disease. More insight into the pathogenesis of aortic aneurysm formation is required to determine the possibilities for earlier detection, follow-up and treatment of patients predisposed to aortic aneurysms. In general, two types of aortic aneurysm patients can be identified: patients displaying a genetic heritable form of the disease, which usually present with cardiovascular abnormalities at younger age, and those with a still unidentified cause, usually presenting at older age. In this thesis I aimed to determine early detection methods for aortic aneurysms, by determining phenotypic alterations as well as molecular and genetic analyses, based on a combination of clinical data and a Fibulin-4 deficient mouse model. Fibulin-4 is an extracellular matrix protein important for the structural organization of elastic fibers in large arteries. Aortas of mice homozygous for a Fibulin-4 reduced expression allele (Fibulin-4^R) generally resemble those from patients with a genetic and severe form of TAA, while heterozygous mice are primary asymptomatic, with mild aortic wall degeneration.

In **chapter 2** of this thesis we show that protease-activatable fluorescent sensors are promising new tools to monitor the matrix metalloproteinase activity non-invasively in the aortic wall of Fibulin-4 deficient mice that do not yet display aortic aneurysm formation. In **chapter 3** we show that aortic aneurysms coincide with chronic obstructive pulmonary disease (COPD) in a large patient cohort, and that this association is additionally observed in extracellular matrix defective Fibulin-4 deficient mice. While homozygous Fibulin-4^R mice present with severe lung emphysema from birth on, adult heterozygous Fibulin-4^R mice develop a milder form of alveolar airspace enlargement, with an enhanced inflammatory response after an induced infection. **Chapter 4** additionally shows that heterozygosity for Fibulin-4^R can predispose for late-onset diseases in association with risk factors, as the induction of atherosclerosis in the mice results in thoracic and abdominal aortic wall dilation at adult age. This is associated with increased and altered plaque formation, leading to paralysis symptoms and a reduced survival outcome. In **chapter 5** we demonstrate that the increased TGF-β signaling observed in the smooth muscle cells (SMCs) of the aortic wall of Fibulin-4 deficient mice occurs due to increased secretion of TGF-β1 and TGF-β2 from SMCs, which is associated with increased detection of TGF-β2 in plasma of homozygous Fibulin-4^R mice. Interestingly, mutations in TGF-β2 have recently been identified to cause TAAs in humans. Finally, in **chapter 6** we describe the results of screening of the Fibulin-4 gene in patient cohorts with either syndromic, familial and/or sporadic forms of TAAs and a group of patients with AAAs.

1

REFERENCES

1. Lindsay ME, Dietz HC. Lessons on the pathogenesis of aneurysm from heritable conditions. Nature. 2011 May 19;473(7347):308-16.

2. Johnston KW, Rutherford RB, Tilson MD, Shah DM, Hollier L, Stanley JC. Suggested standards for reporting on arterial aneurysms. Subcommittee on Reporting Standards for Arterial Aneurysms, Ad Hoc Committee on Reporting Standards, Society for Vascular Surgery and North American Chapter, International Society for Cardiovascular Surgery. J Vasc Surg. 1991 Mar;13(3):452-8.

3. Olsson C, Thelin S, Stahle E, Ekbom A, Granath F. Thoracic aortic aneurysm and dissection: increasing prevalence and improved outcomes reported in a nationwide population-based study of more than 14,000 cases from 1987 to 2002. Circulation. 2006 Dec 12;114(24):2611-8.

4. Nienaber CA, Eagle KA. Aortic dissection: new frontiers in diagnosis and management: Part I: from etiology to diagnostic strategies. Circulation. 2003 Aug 5;108(5):628-35.

5. Suzuki T, Mehta RH, Ince H, Nagai R, Sakomura Y, Weber F, Sumiyoshi T, Bossone E, Trimarchi S, Cooper JV, Smith DE, Isselbacher EM, Eagle KA, Nienaber CA, International Registry of Aortic D. Clinical profiles and outcomes of acute type B aortic dissection in the current era: lessons from the International Registry of Aortic Dissection (IRAD). Circulation. 2003 Sep 9;108 Suppl 1:II312-7.

6. Achneck HE, Rizzo JA, Tranquilli M, Elefteriades JA. Safety of thoracic aortic surgery in the present era. Ann Thorac Surg. 2007 Oct;84(4):1180-5; discussion 5.

7. Ramanath VS, Oh JK, Sundt TM, 3rd, Eagle KA. Acute aortic syndromes and thoracic aortic aneurysm. Mayo Clin Proc. 2009 May;84(5):465-81.

8. Singh K, Bonaa KH, Jacobsen BK, Bjork L, Solberg S. Prevalence of and risk factors for abdominal aortic aneurysms in a population-based study : The Tromso Study. Am J Epidemiol. 2001 Aug 1;154(3):236-44.

9. Lederle FA, Johnson GR, Wilson SE, Chute EP, Hye RJ, Makaroun MS, Barone GW, Bandyk D, Moneta GL, Makhoul RG. The aneurysm detection and management study screening program: validation cohort and final results. Aneurysm Detection and Management Veterans Affairs Cooperative Study Investigators. Arch Intern Med. 2000 May 22;160(10):1425-30.

10. Lederle FA. The rise and fall of abdominal aortic aneurysm. Circulation. 2011 Sep 6;124(10):1097-9.

11. Agricola E, Slavich M, Tufaro V, Fisicaro A, Oppizzi M, Melissano G, Bertoglio L, Marone E, Civilini E, Margonato A, Chiesa R. Prevalence of thoracic ascending aortic aneurysm in adult patients with known abdominal aortic aneurysm: An echocardiographic study. Int J Cardiol. 2013 May 10.

12. Larsson E, Vishnevskaya L, Kalin B, Granath F, Swedenborg J, Hultgren R. High frequency of thoracic aneurysms in patients with abdominal aortic aneurysms. Ann Surg. 2011 Jan;253(1):180-4.

13. Ruddy JM, Jones JA, Spinale FG, Ikonomidis JS. Regional heterogeneity within the aorta: relevance to aneurysm disease. J Thorac Cardiovasc Surg. 2008 Nov;136(5):1123-30.

14. Coady MA, Davies RR, Roberts M, Goldstein LJ, Rogalski MJ, Rizzo JA, Hammond GL, Kopf GS, Elefteriades JA. Familial patterns of thoracic aortic aneurysms. Arch Surg. 1999 Apr;134(4):361-7.

15. Booher AM, Eagle KA. Diagnosis and management issues in thoracic aortic aneurysm. Am Heart J. 2011 Jul;162(1):38-46 e1.

16. Albornoz G, Coady MA, Roberts M, Davies RR, Tranquilli M, Rizzo JA, Elefteriades JA. Familial thoracic aortic aneurysms and dissections--incidence, modes of inheritance, and phenotypic patterns. Ann Thorac Surg. 2006 Oct;82(4):1400-5.

17. Dietz HC, Cutting GR, Pyeritz RE, Maslen CL, Sakai LY, Corson GM, Puffenberger EG, Hamosh A, Nanthakumar EJ, Curristin SM, et al. Marfan syndrome caused by a recurrent de novo missense mutation in the fibrillin gene. Nature. 1991 Jul 25;352(6333):337-9.

18. Turner CL, Emery H, Collins AL, Howarth RJ, Yearwood CM, Cross E, Duncan PJ, Bunyan DJ, Harvey JF, Foulds NC. Detection of 53 FBN1 mutations (41 novel and 12 recurrent) and genotype-phenotype correlations in 113 unrelated probands referred with Marfan syndrome, or a related fibrillinopathy. Am J Med Genet A. 2009 Feb;149A(2):161-70.

19. Li D, Yu J, Gu F, Pang X, Ma X, Li R, Liu N, Ma X. The roles of two novel FBN1 gene mutations in the genotype-phenotype correlations of Marfan syndrome and ectopia lentis

patients with marfanoid habitus. Genet Test. 2008 Jun;12(2):325-30.

20. Rommel K, Karck M, Haverich A, von Kodolitsch Y, Rybczynski M, Muller G, Singh KK, Schmidtke J, Arslan-Kirchner M. Identification of 29 novel and nine recurrent fibrillin-1 (FBN1) mutations and genotype-phenotype correlations in 76 patients with Marfan syndrome. Hum Mutat. 2005 Dec;26(6):529-39.

21. Robinson PN, Booms P, Katzke S, Ladewig M, Neumann L, Palz M, Pregla R, Tiecke F, Rosenberg T. Mutations of FBN1 and genotype-phenotype correlations in Marfan syndrome and related fibrillinopathies. Hum Mutat. 2002 Sep;20(3):153-61.

22. Germain DP. Ehlers-Danlos syndrome type IV. Orphanet J Rare Dis. 2007;2:32.

23. De Paepe A, Malfait F. The Ehlers-Danlos syndrome, a disorder with many faces. Clin Genet. 2012 Jul;82(1):1-11.

24. Zhang MC, He L, Giro M, Yong SL, Tiller GE, Davidson JM. Cutis laxa arising from frameshift mutations in exon 30 of the elastin gene (ELN). J Biol Chem. 1999 Jan 8;274(2):981-6.

25. Callewaert B, Renard M, Hucthagowder V, Albrecht B, Hausser I, Blair E, Dias C, Albino A, Wachi H, Sato F, Mecham RP, Loeys B, Coucke PJ, De Paepe A, Urban Z. New insights into the pathogenesis of autosomal-dominant cutis laxa with report of five ELN mutations. Hum Mutat. 2011 Apr;32(4):445-55.

26. Szabo Z, Crepeau MW, Mitchell AL, Stephan MJ, Puntel RA, Yin Loke K, Kirk RC, Urban Z. Aortic aneurysmal disease and cutis laxa caused by defects in the elastin gene. J Med Genet. 2006 Mar;43(3):255-8.

27. Hoyer J, Kraus C, Hammersen G, Geppert JP, Rauch A. Lethal cutis laxa with contractural arachnodactyly, overgrowth and soft tissue bleeding due to a novel homozygous fibulin-4 gene mutation. Clin Genet. 2009 Sep;76(3):276-81.

28. Hucthagowder V, Sausgruber N, Kim KH, Angle B, Marmorstein LY, Urban Z. Fibulin-4: a novel gene for an autosomal recessive cutis laxa syndrome. Am J Hum Genet. 2006 Jun;78(6):1075-80.

29. Dasouki M, Markova D, Garola R, Sasaki T, Charbonneau NL, Sakai LY, Chu ML. Compound heterozygous mutations in fibulin-4 causing neonatal lethal pulmonary artery occlusion, aortic aneurysm, arachnodactyly, and mild cutis laxa. Am J Med Genet A. 2007 Nov 15;143A(22):2635-41.

30. Renard M, Holm T, Veith R, Callewaert BL, Ades LC, Baspinar O, Pickart A, Dasouki M, Hoyer J, Rauch A, Trapane P, Earing MG, Coucke PJ, Sakai LY, Dietz HC, De Paepe AM, Loeys BL. Altered TGFbeta signaling and cardiovascular manifestations in patients with autosomal recessive cutis laxa type I caused by fibulin-4 deficiency. Eur J Hum Genet. 2010 Aug;18(8):895-901.

31. Erickson LK, Opitz JM, Zhou H. Lethal osteogenesis imperfecta-like condition with cutis laxa and arterial tortuosity in MZ twins due to a homozygous fibulin-4 mutation. Pediatr Dev Pathol. 2012 Mar-Apr;15(2):137-41.

32. Sawyer SL, Dicke F, Kirton A, Rajapkse T, Rebeyka IM, McInnes B, Parboosingh JS, Bernier FP. Longer term survival of a child with autosomal recessive cutis laxa due to a mutation in FBLN4. Am J Med Genet A. 2013 May;161A(5):1148-53.

33. Kappanayil M, Nampoothiri S, Kannan R, Renard M, Coucke P, Malfait F, Menon S, Ravindran HK, Kurup R, Faiyaz-Ul-Haque M, Kumar K, De Paepe A. Characterization of a distinct lethal arteriopathy syndrome in twenty-two infants associated with an identical, novel mutation in FBLN4 gene, confirms fibulin-4 as a critical determinant of human vascular elastogenesis. Orphanet J Rare Dis. 2012;7:61.

34. Loeys BL, Chen J, Neptune ER, Judge DP, Podowski M, Holm T, Meyers J, Leitch CC, Katsanis N, Sharifi N, Xu FL, Myers LA, Spevak PJ, Cameron DE, De Backer J, Hellemans J, Chen Y, Davis EC, Webb CL, Kress W, Coucke P, Rifkin DB, De Paepe AM, Dietz HC. A syndrome of altered cardiovascular, craniofacial, neurocognitive and skeletal development caused by mutations in TGFBR1 or TGFBR2. Nat Genet. 2005 Mar;37(3):275-81.

35. Pannu H, Fadulu VT, Chang J, Lafont A, Hasham SN, Sparks E, Giampietro PF, Zaleski C, Estrera AL, Safi HJ, Shete S, Willing MC, Raman CS, Milewicz DM. Mutations in transforming growth factor-beta receptor type II cause familial thoracic aortic aneurysms and dissections. Circulation. 2005 Jul 26;112(4):513-20.

36. van de Laar IM, Oldenburg RA, Pals G, Roos-Hesselink JW, de Graaf BM, Verhagen JM, Hoedemaekers YM, Willemsen R, Severijnen LA, Venselaar H, Vriend G, Pattynama PM, Collee M, Majoor-Krakauer D, Poldermans D, Frohn-Mulder IM, Micha D, Timmermans J, Hilhorst-Hofstee Y, Bierma-Zeinstra SM, Willems PJ, Kros JM, Oei EH, Oostra BA, Wessels

1

MW, Bertoli-Avella AM. Mutations in SMAD3 cause a syndromic form of aortic aneurysms and dissections with early-onset osteoarthritis. Nat Genet. 2011 Feb;43(2):121-6.

37. van der Linde D, van de Laar IM, Bertoli-Avella AM, Oldenburg RA, Bekkers JA, Mattace-Raso FU, van den Meiracker AH, Moelker A, van Kooten F, Frohn-Mulder IM, Timmermans J, Moltzer E, Cobben JM, van Laer L, Loeys B, De Backer J, Coucke PJ, De Paepe A, Hilhorst-Hofstee Y, Wessels MW, Roos-Hesselink JW. Aggressive cardiovascular phenotype of aneurysms-osteoarthritis syndrome caused by pathogenic SMAD3 variants. J Am Coll Cardiol. 2012 Jul 31;60(5):397-403.

38. van de Laar IM, van der Linde D, Oei EH, Bos PK, Bessems JH, Bierma-Zeinstra SM, van Meer BL, Pals G, Oldenburg RA, Bekkers JA, Moelker A, de Graaf BM, Matyas G, Frohn-Mulder IM, Timmermans J, Hilhorst-Hofstee Y, Cobben JM, Bruggenwirth HT, van Laer L, Loeys B, De Backer J, Coucke PJ, Dietz HC, Willems PJ, Oostra BA, De Paepe A, Roos-Hesselink JW, Bertoli-Avella AM, Wessels MW. Phenotypic spectrum of the SMAD3-related aneurysms-osteoarthritis syndrome. J Med Genet. 2012 Jan;49(1):47-57.

39. Regalado ES, Guo DC, Villamizar C, Avidan N, Gilchrist D, McGillivray B, Clarke L, Bernier F, Santos-Cortez RL, Leal SM, Bertoli-Avella AM, Shendure J, Rieder MJ, Nickerson DA, Project NGES, Milewicz DM. Exome sequencing identifies SMAD3 mutations as a cause of familial thoracic aortic aneurysm and dissection with intracranial and other arterial aneurysms. Circ Res. 2011 Sep 2;109(6):680-6.

40. Boileau C, Guo DC, Hanna N, Regalado ES, Detaint D, Gong L, Varret M, Prakash SK, Li AH, d'Indy H, Braverman AC, Grandchamp B, Kwartler CS, Gouya L, Santos-Cortez RL, Abifadel M, Leal SM, Muti C, Shendure J, Gross MS, Rieder MJ, Vahanian A, Nickerson DA, Michel JB, National Heart L, Blood Institute Go Exome Sequencing P, Jondeau G, Milewicz DM. TGFB2 mutations cause familial thoracic aortic aneurysms and dissections associated with mild systemic features of Marfan syndrome. Nat Genet. 2012 Aug;44(8):916-21.

41. Lindsay ME, Schepers D, Bolar NA, Doyle JJ, Gallo E, Fert-Bober J, Kempers MJ, Fishman EK, Chen Y, Myers L, Bjeda D, Oswald G, Elias AF, Levy HP, Anderlid BM, Yang MH, Bongers EM, Timmermans J, Braverman AC, Canham N, Mortier GR, Brunner HG, Byers PH, Van Eyk J, Van Laer L, Dietz HC, Loeys BL. Loss-of-function mutations in TGFB2 cause a syndromic presentation of thoracic aortic aneurysm. Nat Genet. 2012 Aug;44(8):922-7.

42. Jondeau G, Boileau C. Genetics of thoracic aortic aneurysms. Curr Atheroscler Rep. 2012 Jun;14(3):219-26.

43. Pannu H, Tran-Fadulu V, Papke CL, Scherer S, Liu Y, Presley C, Guo D, Estrera AL, Safi HJ, Brasier AR, Vick GW, Marian AJ, Raman CS, Buja LM, Milewicz DM. MYH11 mutations result in a distinct vascular pathology driven by insulin-like growth factor 1 and angiotensin II. Hum Mol Genet. 2007 Oct 15;16(20):2453-62.

44. Zhu L, Vranckx R, Khau Van Kien P, Lalande A, Boisset N, Mathieu F, Wegman M, Glancy L, Gasc JM, Brunotte F, Bruneval P, Wolf JE, Michel JB, Jeunemaitre X. Mutations in myosin heavy chain 11 cause a syndrome associating thoracic aortic aneurysm/aortic dissection and patent ductus arteriosus. Nat Genet. 2006 Mar;38(3):343-9.

45. Renard M, Callewaert B, Baetens M, Campens L, MacDermot K, Fryns JP, Bonduelle M, Dietz HC, Gaspar IM, Cavaco D, Stattin EL, Schrander-Stumpel C, Coucke P, Loeys B, De Paepe A, De Backer J. Novel MYH11 and ACTA2 mutations reveal a role for enhanced TGFbeta signaling in FTAAD. Int J Cardiol. 2013 May 10;165(2):314-21.

46. Disabella E, Grasso M, Gambarin FI, Narula N, Dore R, Favalli V, Serio A, Antoniazzi E, Mosconi M, Pasotti M, Odero A, Arbustini E. Risk of dissection in thoracic aneurysms associated with mutations of smooth muscle alpha-actin 2 (ACTA2). Heart. 2011 Feb;97(4):321-6.

47. Wang L, Guo DC, Cao J, Gong L, Kamm KE, Regalado E, Li L, Shete S, He WQ, Zhu MS, Offermanns S, Gilchrist D, Elefteriades J, Stull JT, Milewicz DM. Mutations in myosin light chain kinase cause familial aortic dissections. Am J Hum Genet. 2010 Nov 12;87(5):701-7.

48. Guo DC, Regalado E, Casteel DE, Santos-Cortez RL, Gong L, Kim JJ, Dyack S, Horne SG, Chang G, Jondeau G, Boileau C, Coselli JS, Li Z, Leal SM, Shendure J, Rieder MJ, Bamshad MJ, Nickerson DA, Gen TACRC, National Heart L, Blood Institute Grand Opportunity Exome Sequencing P, Kim C, Milewicz DM. Recurrent Gain-of-Function Mutation in PRKG1 Causes Thoracic Aortic Aneurysms and Acute Aortic Dissections. Am J Hum Genet. 2013 Aug 8;93(2):398-404.

49. Isselbacher EM. Thoracic and abdominal aortic aneurysms. Circulation. 2005 Feb 15;111(6):816-28.

1

50. Sterpetti AV, Feldhaus RJ, Schultz RD, Blair EA. Identification of abdominal aortic aneurysm patients with different clinical features and clinical outcomes. Am J Surg. 1988 Dec;156(6):466-9.

51. Shibamura H, Olson JM, van Vlijmen-Van Keulen C, Buxbaum SG, Dudek DM, Tromp G, Ogata T, Skunca M, Sakalihasan N, Pals G, Limet R, MacKean GL, Defawe O, Verloes A, Arthur C, Lossing AG, Burnett M, Sueda T, Kuivaniemi H. Genome scan for familial abdominal aortic aneurysm using sex and family history as covariates suggests genetic heterogeneity and identifies linkage to chromosome 19q13. Circulation. 2004 May 4;109(17):2103-8.

52. Thompson AR, Drenos F, Hafez H, Humphries SE. Candidate gene association studies in abdominal aortic aneurysm disease: a review and meta-analysis. Eur J Vasc Endovasc Surg. 2008 Jan;35(1):19-30.

53. Ruigrok YM, Elias R, Wijmenga C, Rinkel GJ. A comparison of genetic chromosomal loci for intracranial, thoracic aortic, and abdominal aortic aneurysms in search of common genetic risk factors. Cardiovasc Pathol. 2008 Jan-Feb;17(1):40-7.

54. Kent KC, Zwolak RM, Egorova NN, Riles TS, Manganaro A, Moskowitz AJ, Gelijns AC, Greco G. Analysis of risk factors for abdominal aortic aneurysm in a cohort of more than 3 million individuals. J Vasc Surg. 2010 Sep;52(3):539-48.

55. Lederle FA, Johnson GR, Wilson SE, Chute EP, Littooy FN, Bandyk D, Krupski WC, Barone GW, Acher CW, Ballard DJ. Prevalence and associations of abdominal aortic aneurysm detected through screening. Aneurysm Detection and Management (ADAM) Veterans Affairs Cooperative Study Group. Ann Intern Med. 1997 Mar 15;126(6):441-9.

56. Reed D, Reed C, Stemmermann G, Hayashi T. Are aortic aneurysms caused by atherosclerosis? Circulation. 1992 Jan;85(1):205-11.

57. Tilson MD. Aortic aneurysms and atherosclerosis. Circulation. 1992 Jan;85(1):378-9.

58. Meijer CA, Kokje VB, van Tongeren RB, Hamming JF, van Bockel JH, Moller GM, Lindeman JH. An Association between Chronic Obstructive Pulmonary Disease and Abdominal Aortic Aneurysm beyond Smoking: Results from a Case-control Study. Eur J Vasc Endovasc Surg. 2012 Jun 14.

59. Sakamaki F, Oya H, Nagaya N, Kyotani S, Satoh T, Nakanishi N. Higher prevalence of obstructive airway disease in patients with thoracic or abdominal aortic aneurysm. J Vasc Surg. 2002 Jul;36(1):35-40.

60. WHO. World health report: Chronic Obstructive Pulmonary Disease. 2007 [cited; Available from: www.who.int/respiratory/copd

61. Mannino DM, Thorn D, Swensen A, Holguin F. Prevalence and outcomes of diabetes, hypertension and cardiovascular disease in COPD. Eur Respir J. 2008 Oct;32(4):962-9.

62. Anthonisen NR, Connett JE, Enright PL, Manfreda J. Hospitalizations and mortality in the Lung Health Study. Am J Respir Crit Care Med. 2002 Aug 1;166(3):333-9.

63. Fabbri LM, Luppi F, Beghe B, Rabe KF. Complex chronic comorbidities of COPD. Eur Respir J. 2008 Jan;31(1):204-12.

64. Corsonello A, Antonelli Incalzi R, Pistelli R, Pedone C, Bustacchini S, Lattanzio F. Comorbidities of chronic obstructive pulmonary disease. Curr Opin Pulm Med. 2011 Dec;17 Suppl 1:S21-8.

65. Johnsen SH, Forsdahl SH, Singh K, Jacobsen BK. Atherosclerosis in abdominal aortic aneurysms: a causal event or a process running in parallel? The Tromso study. Arterioscler Thromb Vasc Biol. 2010 Jun;30(6):1263-8.

66. Fowkes FG, Anandan CL, Lee AJ, Smith FB, Tzoulaki I, Rumley A, Powell JT, Lowe GD. Reduced lung function in patients with abdominal aortic aneurysm is associated with activation of inflammation and hemostasis, not smoking or cardiovascular disease. J Vasc Surg. 2006 Mar;43(3):474-80.

67. Bonniaud P, Kolb M, Galt T, Robertson J, Robbins C, Stampfli M, Lavery C, Margetts PJ, Roberts AB, Gauldie J. Smad3 null mice develop airspace enlargement and are resistant to TGF-beta-mediated pulmonary fibrosis. J Immunol. 2004 Aug 1;173(3):2099-108.

68. Neptune ER, Frischmeyer PA, Arking DE, Myers L, Bunton TE, Gayraud B, Ramirez F, Sakai LY, Dietz HC. Dysregulation of TGF-beta activation contributes to pathogenesis in Marfan syndrome. Nat Genet. 2003 Mar;33(3):407-11.

69. Maronpot R.R. BGA, Gaul B.W. Pathology of the mouse. In: R.R. M, ed. 1 ed. Saint Louis: Cache River Press 1999.

70. Wendel DP, Taylor DG, Albertine KH, Keating MT, Li DY. Impaired distal airway development in mice lacking elastin. American journal of respiratory cell and molecular biology. 2000

1

Sep;23(3):320-6.

71. V. Kumar RC SR. Robbins Basic Pathology. ed. : Philadelphia: Saunders, an imprint of Elsevier Science 2003.

72. Jarvelainen H, Sainio A, Koulu M, Wight TN, Penttinen R. Extracellular matrix molecules: potential targets in pharmacotherapy. Pharmacol Rev. 2009 Jun;61(2):198-223.

73. Alberts B. JA, Lewis J., Raff M., Roberts K., Walter P. Molecular Biology of the Cell. Fifth ed: Garland Publishing New York 2008.

74. E. H. Cell Biology of Extracellular Matrix: Plenum Press, New York 1991.

75. Charbonneau NL, Ono RN, Corson GM, Keene DR, Sakai LY. Fine tuning of growth factor signals depends on fibrillin microfibril networks. Birth Defects Res C Embryo Today. 2004 Mar;72(1):37-50.

76. Rifkin DB. Latent transforming growth factor-beta (TGF-beta) binding proteins: orchestrators of TGF-beta availability. J Biol Chem. 2005 Mar 4;280(9):7409-12.

77. Kielty CM, Sherratt MJ, Shuttleworth CA. Elastic fibres. Journal of cell science. 2002 Jul 15;115(Pt 14):2817-28.

78. Argraves WS, Greene LM, Cooley MA, Gallagher WM. Fibulins: physiological and disease perspectives. EMBO Rep. 2003 Dec;4(12):1127-31.

79. Cudilo E, Al Naemi H, Marmorstein L, Baldwin AL. Knockout mice: is it just genetics? Effect of enriched housing on fibulin-4(+/-) mice. PLoS ONE. 2007;2(2):e229.

80. Gray WR, Sandberg LB, Foster JA. Molecular model for elastin structure and function. Nature. 1973 Dec 21-28;246(5434):461-6.

81. Bellingham CM, Woodhouse KA, Robson P, Rothstein SJ, Keeley FW. Self-aggregation characteristics of recombinantly expressed human elastin polypeptides. Biochim Biophys Acta. 2001 Nov 26;1550(1):6-19.

82. Kobayashi N, Kostka G, Garbe JH, Keene DR, Bachinger HP, Hanisch FG, Markova D, Tsuda T, Timpl R, Chu ML, Sasaki T. A comparative analysis of the fibulin protein family. Biochemical characterization, binding interactions, and tissue localization. The Journal of biological chemistry. 2007 Apr 20;282(16):11805-16.

83. Yanagisawa H, Schluterman MK, Brekken RA. Fibulin-5, an integrin-binding matricellular protein: its function in development and disease. J Cell Commun Signal. 2009 Dec;3(3-4):337-47.

84. de Vega S, Iwamoto T, Nakamura T, Hozumi K, McKnight DA, Fisher LW, Fukumoto S, Yamada Y. TM14 is a new member of the fibulin family (fibulin-7) that interacts with extracellular matrix molecules and is active for cell binding. J Biol Chem. 2007 Oct 19;282(42):30878-88.

85. Hanada K, Vermeij M, Garinis GA, de Waard MC, Kunen MG, Myers L, Maas A, Duncker DJ, Meijers C, Dietz HC, Kanaar R, Essers J. Perturbations of vascular homeostasis and aortic valve abnormalities in fibulin-4 deficient mice. Circ Res. 2007 Mar 16;100(5):738-46.

86. McLaughlin PJ, Chen Q, Horiguchi M, Starcher BC, Stanton JB, Broekelmann TJ, Marmorstein AD, McKay B, Mecham R, Nakamura T, Marmorstein LY. Targeted disruption of fibulin-4 abolishes elastogenesis and causes perinatal lethality in mice. Mol Cell Biol. 2006 Mar;26(5):1700-9.

87. Chen Q, Zhang T, Roshetsky JF, Ouyang Z, Essers J, Fan C, Wang Q, Hinek A, Plow EF, Dicorleto PE. Fibulin-4 regulates the expression of the tropoelastin gene and consequent elastic fiber formation by human fibroblasts. The Biochemical journal. 2009 Jul 23.

88. Nakamura T, Lozano PR, Ikeda Y, Iwanaga Y, Hinek A, Minamisawa S, Cheng CF, Kobuke K, Dalton N, Takada Y, Tashiro K, Ross Jr J, Honjo T, Chien KR. Fibulin-5/DANCE is essential for elastogenesis in vivo. Nature. 2002 Jan 10;415(6868):171-5.

89. Yanagisawa H, Davis EC, Starcher BC, Ouchi T, Yanagisawa M, Richardson JA, Olson EN. Fibulin-5 is an elastin-binding protein essential for elastic fibre development in vivo. Nature. 2002 Jan 10;415(6868):168-71.

90. Timpl R, Sasaki T, Kostka G, Chu ML. Fibulins: a versatile family of extracellular matrix proteins. Nature reviews. 2003 Jun;4(6):479-89.

91. Chu ML, Tsuda T. Fibulins in development and heritable disease. Birth Defects Res C Embryo Today. 2004 Mar;72(1):25-36.

92. El-Hallous E, Sasaki T, Hubmacher D, Getie M, Tiedemann K, Brinckmann J, Batge B, Davis EC, Reinhardt DP. Fibrillin-1 interactions with fibulins depend on the first hybrid domain and provide an adaptor function to tropoelastin. The Journal of biological chemistry. 2007 Mar 23;282(12):8935-46.

93. Horiguchi M, Inoue T, Ohbayashi T, Hirai M, Noda K, Marmorstein LY, Yabe D, Takagi K,

Akama TO, Kita T, Kimura T, Nakamura T. Fibulin-4 conducts proper elastogenesis via interaction with cross-linking enzyme lysyl oxidase. Proc Natl Acad Sci U S A. 2009 Nov 10;106(45):19029-34.

94. Atsawasuwan P, Mochida Y, Katafuchi M, Kaku M, Fong KS, Csiszar K, Yamauchi M. Lysyl oxidase binds transforming growth factor-beta and regulates its signaling via amine oxidase activity. J Biol Chem. 2008 Dec 5;283(49):34229-40.

95. Doyle JJ, Gerber EE, Dietz HC. Matrix-dependent perturbation of TGFbeta signaling and disease. FEBS Lett. 2012 Jul 4;586(14):2003-15.

96. Dubois CM, Laprise MH, Blanchette F, Gentry LE, Leduc R. Processing of transforming growth factor beta 1 precursor by human furin convertase. J Biol Chem. 1995 May 5;270(18):10618-24.

97. Saharinen J, Taipale J, Keski-Oja J. Association of the small latent transforming growth factor-beta with an eight cysteine repeat of its binding protein LTBP-1. EMBO J. 1996 Jan 15;15(2):245-53.

98. Kaartinen V, Warburton D. Fibrillin controls TGF-beta activation. Nat Genet. 2003 Mar;33(3):331-2.

99. Sato Y, Rifkin DB. Inhibition of endothelial cell movement by pericytes and smooth muscle cells: activation of a latent transforming growth factor-beta 1-like molecule by plasmin during co-culture. J Cell Biol. 1989 Jul;109(1):309-15.

100. Yu Q, Stamenkovic I. Cell surface-localized matrix metalloproteinase-9 proteolytically activates TGF-beta and promotes tumor invasion and angiogenesis. Genes Dev. 2000 Jan 15;14(2):163-76.

101. Annes JP, Munger JS, Rifkin DB. Making sense of latent TGFbeta activation. J Cell Sci. 2003 Jan 15;116(Pt 2):217-24.

102. Sheppard D. Integrin-mediated activation of latent transforming growth factor beta. Cancer Metastasis Rev. 2005 Sep;24(3):395-402.

103. Barcellos CK, Schetinger MR, Battastini AM, Silva LB, Dias RD, Sarkis JJ. Inhibitory effect of cadmium acetate on synaptosomal ATP diphosphohydrolase (EC 3.6.1.5; apyrase) from adult rat cerebral cortex. Braz J Med Biol Res. 1994 May;27(5):1111-5.

104. Lopez-Casillas F, Wrana JL, Massague J. Betaglycan presents ligand to the TGF beta signaling receptor. Cell. 1993 Jul 2;73(7):1435-44.

105. ten Dijke P, Arthur HM. Extracellular control of TGFbeta signalling in vascular development and disease. Nat Rev Mol Cell Biol. 2007 Nov;8(11):857-69.

106. Jones JA, Spinale FG, Ikonomidis JS. Transforming growth factor-beta signaling in thoracic aortic aneurysm development: a paradox in pathogenesis. J Vasc Res. 2009;46(2):119-37.

107. Pereira L, Lee SY, Gayraud B, Andrikopoulos K, Shapiro SD, Bunton T, Biery NJ, Dietz HC, Sakai LY, Ramirez F. Pathogenetic sequence for aneurysm revealed in mice underexpressing fibrillin-1. Proc Natl Acad Sci U S A. 1999 Mar 30;96(7):3819-23.

108. Judge DP, Biery NJ, Keene DR, Geubtner J, Myers L, Huso DL, Sakai LY, Dietz HC. Evidence for a critical contribution of haploinsufficiency in the complex pathogenesis of Marfan syndrome. J Clin Invest. 2004 Jul;114(2):172-81.

109. Carta L, Pereira L, Arteaga-Solis E, Lee-Arteaga SY, Lenart B, Starcher B, Merkel CA, Sukoyan M, Kerkis A, Hazeki N, Keene DR, Sakai LY, Ramirez F. Fibrillins 1 and 2 perform partially overlapping functions during aortic development. J Biol Chem. 2006 Mar 24;281(12):8016-23.

110. Charbonneau NL, Carlson EJ, Tufa S, Sengle G, Manalo EC, Carlberg VM, Ramirez F, Keene DR, Sakai LY. In vivo studies of mutant fibrillin-1 microfibrils. J Biol Chem. 2010 Aug 6;285(32):24943-55.

111. Pereira L, Andrikopoulos K, Tian J, Lee SY, Keene DR, Ono R, Reinhardt DP, Sakai LY, Biery NJ, Bunton T, Dietz HC, Ramirez F. Targetting of the gene encoding fibrillin-1 recapitulates the vascular aspect of Marfan syndrome. Nat Genet. 1997 Oct;17(2):218-22.

112. Horiguchi M, Ota M, Rifkin DB. Matrix control of transforming growth factor-beta function. J Biochem. 2012 Oct;152(4):321-9.

113. Lavoie P, Robitaille G, Agharazii M, Ledbetter S, Lebel M, Lariviere R. Neutralization of transforming growth factor-beta attenuates hypertension and prevents renal injury in uremic rats. J Hypertens. 2005 Oct;23(10):1895-903.

114. Franken R, den Hartog AW, de Waard V, Engele L, Radonic T, Lutter R, Timmermans J, Scholte AJ, van den Berg MP, Zwinderman AH, Groenink M, Mulder BJ. Circulating transforming growth factor-beta as a prognostic biomarker in Marfan syndrome. Int J Cardiol.

1

1

2013 Apr 10.

115. Matt P, Schoenhoff F, Habashi J, Holm T, Van Erp C, Loch D, Carlson OD, Griswold BF, Fu Q, De Backer J, Loeys B, Huso DL, McDonnell NB, Van Eyk JE, Dietz HC, Gen TACC. Circulating transforming growth factor-beta in Marfan syndrome. Circulation. 2009 Aug 11;120(6):526-32.

116. Habashi JP, Judge DP, Holm TM, Cohn RD, Loeys BL, Cooper TK, Myers L, Klein EC, Liu G, Calvi C, Podowski M, Neptune ER, Halushka MK, Bedja D, Gabrielson K, Rifkin DB, Carta L, Ramirez F, Huso DL, Dietz HC. Losartan, an AT1 antagonist, prevents aortic aneurysm in a mouse model of Marfan syndrome. Science. 2006 Apr 7;312(5770):117-21.

117. Brooke BS, Habashi JP, Judge DP, Patel N, Loeys B, Dietz HC, 3rd. Angiotensin II blockade and aortic-root dilation in Marfan's syndrome. N Engl J Med. 2008 Jun 26;358(26):2787-95.

118. Larsson J, Goumans MJ, Sjostrand LJ, van Rooijen MA, Ward D, Leveen P, Xu X, ten Dijke P, Mummery CL, Karlsson S. Abnormal angiogenesis but intact hematopoietic potential in TGF-beta type I receptor-deficient mice. EMBO J. 2001 Apr 2;20(7):1663-73.

119. Oshima M, Oshima H, Taketo MM. TGF-beta receptor type II deficiency results in defects of yolk sac hematopoiesis and vasculogenesis. Dev Biol. 1996 Oct 10;179(1):297-302.

120. Carvalho RL, Itoh F, Goumans MJ, Lebrin F, Kato M, Takahashi S, Ema M, Itoh S, van Rooijen M, Bertolino P, Ten Dijke P, Mummery CL. Compensatory signalling induced in the yolk sac vasculature by deletion of TGFbeta receptors in mice. J Cell Sci. 2007 Dec 15;120(Pt 24):4269-77.

121. Choudhary B, Zhou J, Li P, Thomas S, Kaartinen V, Sucov HM. Absence of TGFbeta signaling in embryonic vascular smooth muscle leads to reduced lysyl oxidase expression, impaired elastogenesis, and aneurysm. Genesis. 2009 Feb;47(2):115-21.

122. Choudhary B, Ito Y, Makita T, Sasaki T, Chai Y, Sucov HM. Cardiovascular malformations with normal smooth muscle differentiation in neural crest-specific type II TGFbeta receptor (Tgfbr2) mutant mice. Dev Biol. 2006 Jan 15;289(2):420-9.

123. Wang J, Nagy A, Larsson J, Dudas M, Sucov HM, Kaartinen V. Defective ALK5 signaling in the neural crest leads to increased postmigratory neural crest cell apoptosis and severe outflow tract defects. BMC Dev Biol. 2006;6:51.

124. Sanford LP, Ormsby I, Gittenberger-de Groot AC, Sariola H, Friedman R, Boivin GP, Cardell EL, Doetschman T. TGFbeta2 knockout mice have multiple developmental defects that are non-overlapping with other TGFbeta knockout phenotypes. Development. 1997 Jul;124(13):2659-70.

125. Bartram U, Molin DG, Wisse LJ, Mohamad A, Sanford LP, Doetschman T, Speer CP, Poelmann RE, Gittenberger-de Groot AC. Double-outlet right ventricle and overriding tricuspid valve reflect disturbances of looping, myocardialization, endocardial cushion differentiation, and apoptosis in TGF-beta(2)-knockout mice. Circulation. 2001 Jun 5;103(22):2745-52.

126. Ashcroft GS, Yang X, Glick AB, Weinstein M, Letterio JL, Mizel DE, Anzano M, Greenwell-Wild T, Wahl SM, Deng C, Roberts AB. Mice lacking Smad3 show accelerated wound healing and an impaired local inflammatory response. Nat Cell Biol. 1999 Sep;1(5):260-6.

127. Datto MB, Frederick JP, Pan L, Borton AJ, Zhuang Y, Wang XF. Targeted disruption of Smad3 reveals an essential role in transforming growth factor beta-mediated signal transduction. Mol Cell Biol. 1999 Apr;19(4):2495-504.

128. Zhu Y, Richardson JA, Parada LF, Graff JM. Smad3 mutant mice develop metastatic colorectal cancer. Cell. 1998 Sep 18;94(6):703-14.

129. Yang X, Letterio JJ, Lechleider RJ, Chen L, Hayman R, Gu H, Roberts AB, Deng C. Targeted disruption of SMAD3 results in impaired mucosal immunity and diminished T cell responsiveness to TGF-beta. EMBO J. 1999 Mar 1;18(5):1280-91.

130. Ye P, Chen W, Wu J, Huang X, Li J, Wang S, Liu Z, Wang G, Yang X, Zhang P, Lv Q, Xia J. GM-CSF contributes to aortic aneurysms resulting from SMAD3 deficiency. J Clin Invest. 2013 May 1;123(5):2317-31.

131. Morano I, Chai GX, Baltas LG, Lamounier-Zepter V, Lutsch G, Kott M, Haase H, Bader M. Smooth-muscle contraction without smooth-muscle myosin. Nat Cell Biol. 2000 Jun;2(6):371-5.

132. Schildmeyer LA, Braun R, Taffet G, Debiasi M, Burns AE, Bradley A, Schwartz RJ. Impaired vascular contractility and blood pressure homeostasis in the smooth muscle alpha-actin null mouse. FASEB J. 2000 Nov;14(14):2213-20.

133. Bee KJ, Wilkes DC, Devereux RB, Basson CT, Hatcher CJ. TGFbetaRIIb mutations trigger aortic aneurysm pathogenesis by altering transforming growth factor beta2 signal

transduction. Circ Cardiovasc Genet. 2012 Dec;5(6):621-9.

134. Shen D, Li J, Lepore JJ, Anderson TJ, Sinha S, Lin AY, Cheng L, Cohen ED, Roberts JD, Jr., Dedhar S, Parmacek MS, Gerszten RE. Aortic aneurysm generation in mice with targeted deletion of integrin-linked kinase in vascular smooth muscle cells. Circ Res. 2011 Sep 2;109(6):616-28.

135. Daugherty A, Cassis LA. Mouse models of abdominal aortic aneurysms. Arterioscler Thromb Vasc Biol. 2004 Mar;24(3):429-34.

136. Maki JM, Rasanen J, Tikkanen H, Sormunen R, Makikallio K, Kivirikko KI, Soininen R. Inactivation of the lysyl oxidase gene Lox leads to aortic aneurysms, cardiovascular dysfunction, and perinatal death in mice. Circulation. 2002 Nov 5;106(19):2503-9.

137. Kurihara T, Shimizu-Hirota R, Shimoda M, Adachi T, Shimizu H, Weiss SJ, Itoh H, Hori S, Aikawa N, Okada Y. Neutrophil-derived matrix metalloproteinase 9 triggers acute aortic dissection. Circulation. 2012 Dec 18;126(25):3070-80.

138. Kanematsu Y, Kanematsu M, Kurihara C, Tsou TL, Nuki Y, Liang EI, Makino H, Hashimoto T. Pharmacologically induced thoracic and abdominal aortic aneurysms in mice. Hypertension. 2010 May;55(5):1267-74.

139. Daugherty A, Manning MW, Cassis LA. Angiotensin II promotes atherosclerotic lesions and aneurysms in apolipoprotein E-deficient mice. J Clin Invest. 2000 Jun;105(11):1605-12.

140. Daugherty A, Cassis L. Chronic angiotensin II infusion promotes atherogenesis in low density lipoprotein receptor -/- mice. Ann N Y Acad Sci. 1999 Nov 18;892:108-18.

141. Daugherty A, Rateri DL, Charo IF, Owens AP, Howatt DA, Cassis LA. Angiotensin II infusion promotes ascending aortic aneurysms: attenuation by CCR2 deficiency in apoE-/- mice. Clin Sci (Lond). 2010 Jun;118(11):681-9.

142. Faugeroux J, Nematalla H, Li W, Clement M, Robidel E, Frank M, Curis E, Ait-Oufella H, Caligiuri G, Nicoletti A, Hagege A, Messas E, Bruneval P, Jeunemaitre X, Bergaya S. Angiotensin II promotes thoracic aortic dissections and ruptures in Col3a1 haploinsufficient mice. Hypertension. 2013 Jul;62(1):203-8.

143. Liu S, Xie Z, Daugherty A, Cassis LA, Pearson KJ, Gong MC, Guo Z. Mineralocorticoid receptor agonists induce mouse aortic aneurysm formation and rupture in the presence of high salt. Arterioscler Thromb Vasc Biol. 2013 Jul;33(7):1568-79.

144. Kuang SQ, Geng L, Prakash SK, Cao JM, Guo S, Villamizar C, Kwartler CS, Peters AM, Brasier AR, Milewicz DM. Aortic Remodeling After Transverse Aortic Constriction in Mice Is Attenuated With AT1 Receptor Blockade. Arterioscler Thromb Vasc Biol. 2013 Sep;33(9):2172-9.

145. Huang J, Davis EC, Chapman SL, Budatha M, Marmorstein LY, Word RA, Yanagisawa H. Fibulin-4 deficiency results in ascending aortic aneurysms: a potential link between abnormal smooth muscle cell phenotype and aneurysm progression. Circ Res. 2010 Feb 19;106(3):583-92.

146. Kaijzel EL, van Heijningen PM, Wielopolski PA, Vermeij M, Koning GA, van Cappellen WA, Que I, Chan A, Dijkstra J, Ramnath NW, Hawinkels LJ, Bernsen MR, Lowik CW, Essers J. Multimodality imaging reveals a gradual increase in matrix metalloproteinase activity at aneurysmal lesions in live fibulin-4 mice. Circ Cardiovasc Imaging. 2010 Sep;3(5):567-77.

147. FH M. Fundamentals of Anatomy and Physiology. Pearson Education 2006.

1

Chapter 2

Multimodality Imaging reveals a gradual increase in Matrix Metalloproteinase Activity at Aneurysmal Lesions in Live Fibulin-4 Mice

**E.L Kaijzel[1] PhD, P.M. van Heijningen[2] MSc,
P.A. Wielopolski[3] PhD, M. Vermeij[4] MSc, G.A. Koning[5] PhD,
W.A. van Cappellen[6] PhD, I. Que[1] MSc, A. Chan[7] PhD,
J. Dijkstra[8] PhD, N.W.M. Ramnath[2,9] MSc, L.J.A.C Hawinkels[10]
PhD, M.R. Bernsen[3] PhD, C.W.G.M. Löwik[1] PhD, and J. Essers[2,9, 11] PhD,**

[1]Department of Endocrinology and Metabolic Diseases, [8]Department of Radiology, Division of Image Processing, [10]Department of Molecular Cell Biology and Centre for Biomedical Genetics, Leiden University Medical Center, Leiden.

[2]Department of Cell Biology and Genetics, [3]Department of Radiology, [4]Department of Pathology, [5]Department of Surgical Oncology [9]Department of Vascular Surgery,[11]Department of Radiation Oncology, [6]Department of Reproduction and Development, Erasmus MC, PO Box 2040, 3000CA Rotterdam, The Netherlands.

[7]Percuros B.V., Enschede, The Netherlands

ABSTRACT

Background: We imaged the protease activity of matrix metalloproteinases (MMPs) upregulated during aneurysm formation, using protease-activatable near-infrared fluorescence (NIRF) probes. We tested whether these protease-activatable sensors can directly report the *in vivo* activity of the key biomarkers in aneurysm using our genetically modified Fibulin-4 mouse models for aneurysm formation. Mice homozygous for the Fibulin-4 reduced expression allele (Fibulin-4$^{R/R}$) show dilatation of the ascending aorta and a tortuous, stiffened aorta resulting from disorganized elastic fiber networks. Strikingly, even a moderate reduction in expression of Fibulin-4 in the heterozygous Fibulin-4$^{+/R}$ mice occasionally results in modest aneurysm formation.

Methods and Results: Aorta transcriptome and protein expression analysis of Fibulin-4$^{+/R}$ and Fibulin-4$^{R/R}$ animals identified excessive TGFβ signaling as the critical event in the pathogenesis of aneurysm formation. To determine whether perturbed elastin lamellar structure arose from induction of TGFβ regulated MMPs, we performed gelatin-zymography and used a protease-activatable NIRF probe to monitor and quantify MMP upregulation in animals using various *in vivo* optical imaging modules and co-registration of the fluorescence signal with CT images of the same animals. Gelatin-zymography demonstrated a significant increase in the presence of the active form of MMP-9 in the aortic arch of Fibulin-4$^{R/R}$ mice. *In vivo* analysis of MMP upregulation using the NIRF probe and subsequent isosurface concentration mapping from reconstructed tomographic images from Fibulin-4$^{+/R}$ and Fibulin-4$^{R/R}$ mice revealed a graded increase in activation of MMPs within the aneurysmal lesions.

Conclusions: We aimed to develop molecular imaging procedures for faster, earlier and easier recognition of aortic aneurysms. Here we show that *in vivo* co-registration of MMP activity by non-invasive tomographic imaging methods allows the detection of increased MMP activity, even before the aneurysm has actually formed.

INTRODUCTION

A thoracic aortic aneurysm (TAA) is a bulge in the aorta which can cause the aorta's diameter to expand to several times its normal size. Such an aneurysm may rupture, leading to extensive internal bleeding that is frequently fatal. Aortic aneurysms can be identified with ultrasound imaging and can be treated by open or endovascular surgery once they have formed. However, the loss of vessel wall integrity that precedes aortic dilatation can neither be detected nor treated. An essential protein for maintaining arterial integrity is the extracellular matrix protein Fibulin-4 (FBLN4). FBLN4 is an elastic fiber-associated glycoprotein involved in stabilizing the organization of extracellular matrix structures such as elastic fibers and basement membranes. Complete elimination of FBLN4 in mice resulted in embryonic death due to arterial hemorrhage [1]. In a Fibulin-4 knockdown mouse-model we have identified a dose-dependent requirement for FBLN4 for proper elastic fiber composition [2]. Homozygous Fibulin-4$^{R/R}$ (Fibulin-4$^{R/R}$) mice with a systemic 4-fold reduced Fibulin-4 expression level, show severe dilatation of the ascending aorta as well as a tortuous and stiffened aorta, resulting from disorganized elastic fiber networks. Interestingly, already a modest 2-fold reduction in expression of FBLN4 in the heterozygous Fibulin-4$^{+/R}$ mice resulted in clear aberrations in elastin formation with occasionally small aneurysm formation. This milder phenotype of heterozygous Fibulin-4$^{+/R}$ mice provides an informative aneurysm model system to delineate the early events in the pathogenetic sequence that culminate in aneurysm. The subtle manifestations of aberrant elastin formation in the Fibulin-4$^{+/R}$ mice might resemble those patients suffering from "sporadic" and barely detectable forms of aneurysms. Therefore these Fibulin-4$^{+/R}$ mice provide the opportunity to unravel the biological processes within early onset of aortic degeneration. This dose-dependent requirement for FBLN4 in the development of the elastic fibers in arteries has recently been confirmed using either heterozygous Fibulin-4$^{+/-}$ mice [3] and using a mouse model with a smooth muscle specific Cre-mediated Fibulin-4 deletion [4], both causing a gradual disorganization of elastic laminae in the medial layer in the aortic wall.

Transcriptome and protein expression analysis implicated perturbation of TGFβ signaling in the pathogenesis of aneurysm in Fibulin-4 deficient mice. Analysis of aortic tissue from Fibulin-4$^{+/R}$ and Fibulin-4$^{R/R}$ mice revealed a graded increase in TGFβ signaling in comparison to wild type animals. Increased TGFβ signaling has previously been documented in the context of other well-established aortic aneurysm syndromes, including Marfan Syndrome (MFS), Loeys-Dietz Syndrome (LDS) and Arterial Tortuosity Syndrome (ATS) [5, 6]. The prominent perturbation of normal elastin lamellar structure may arise from induction of TGFβ regulated matrix metalloproteinases (MMPs), a family of zinc-dependent endopeptidases that are responsible for the degradation of the extracellular matrix (ECM) in aortic aneurysms [7, 8]. Studies of aneurysm tissues from patients with MFS suggest that upregulation of MMP-2 and MMP-9 may also play a primary role in MFS [9]. Based on these data we used our Fibulin-4 knockdown mouse models to explore molecular imaging methods for the *in vivo* registration of MMP upregulation during aneurysm formation.

Optical imaging is an important new technology in translational medicine and three-dimensional (3D) quantitative techniques like Fluorescence Molecular Tomography (FMT) emerged as powerful quantitative modalities for non-invasive whole mouse imaging [10, 11]. Rapidly developing molecular sensing strategies permit visualization of key biological processes in aneurysm formation. In this study, we aimed at molecular imaging of upregulated MMP activity during aneurysm formation, using protease-activatable near-infrared fluorescence (NIRF) probes. These long circulating protease-sensing optical probes that can be used to detect and quantitate protease activity are autoquench

2

fluorescent probes that convert from a nonfluorescent state to a fluorescent state by proteolytic activation. This proteolytic activity comes from MMPs that can cleave an MMP specific recognition sequence between the carrier and the fluorochromes of these probes [12, 13]. In this way, these protease-activatable sensors can directly report the *in vivo* activity of a key biomarker in aneurysm such as MMP-9.

To be able to accurately localize the fluorescent signal obtained from a living mouse reference imaging to visualize anatomy is required. To achieve this, reference imaging with microCT on the same animals was performed immediately after FMT. With this hybrid approach of FMT-CT imaging, localization of MMP activity can be visualized in the different stages of aneurysm development and correlated with anatomical structures. These hybrid technologies, where multiple modalities for both anatomical as well as functional imaging are combined become increasingly available and transform the imaging of vascular disease from a method of diagnosing to a tool for the non-invasive detection of early sub clinical abnormalities [14].

At first, in order to carefully analyze and compare the overall vasculature between wildtype and Fibulin-4 mice we used contrast-enhanced magnetic resonance angiography (MRA) [15]. Clinically, 3D MRA is the imaging modality of choice for stable aortic disease. The increase in vascular signal that gadolinium (Gd) based contrast agents provide when compared with unenhanced MRA allows for faster imaging with improved spatial resolution using 3D techniques, flow independent signal enhancement and reduced magnetic susceptibility artifacts. Advantages of magnetic resonance imaging (MRI) for vascular diagnosis include safety, non-invasive nature (except for giving intravenous contrast agents), a wide field-of-view and imaging depth unimpaired by acoustic shadowing or beam-hardening artifact, and isotropic data collection making it possible to show complicated 3D relationships using multi-planar reformats and 3D rendering [16]. The non-invasive and multi-contrast capabilities of MRI were used to understand the pathology of the Fibulin-4 mice.

In this study, we investigated methods identifying early aneurysm onset (using Fibulin-4$^{+/R}$) and advanced aneurysms (Fibulin-4$^{R/R}$) in mature animals using NIR protease-activatable probes in combination with optical quantitative *in vivo* detection methods and multimodality co-registration. Our studies indicate that this protease activatable probe can be used to image MMP activity during both the onset and maturation of aneurysm formation. This approach supersedes existing methods analyzing MMP levels and activity, such as zymography, immunohistochemistry, Western blotting, and scintigraphy [17] since it enables reliable quantitative *in vivo* registration allowing longitudinal analysis during treatment.

METHODS

Mouse model

While complete Fibulin-4 knockout mice have recently been generated and showed embryonic lethality [1], we previously generated a Fibulin-4 allele with reduced expression by transcriptional interference through placement of a TKneo targeting construct in the downstream Mus81 gene [2]. Heterozygous Fibulin-4$^{+/R}$ mice in a mixed C57Bl/6J;129Sv background were mated to generate Fibulin-4$^{+/+}$, Fibulin-4$^{+/R}$, and Fibulin-4$^{R/R}$ littermates analyzed in this study. Mice were kept in individually ventilated cages to keep animals consistently micro-flora and disease free. To avoid stress-related vascular injury mice were earmarked and genotyped 4 weeks after birth.

Histological analysis

Mice (120 days old) were sacrificed by an overdose of anaesthesia or CO_2, fixed by perfusion fixation with 4% formaldehyde and autopsied according to standard protocols (e.g. Eumorphia protocol). Organ weights were determined and macroscopic abnormalities noted. Organs and tissues were fixed in formalin. Hearts and aortas of Fibulin-4^{+/+}, Fibulin-4[+/R] and Fibulin-4[R/R] mice were isolated and after removing fibrous connective tissue, macroscopical images were taken using a stereoscope. Then aortas were paraffin embedded and 4 μm sections were haematoxylin and eosin stained, stained for cartilage (alcian blue) and elastin (Verhoeff-van Giesson). Immunohistochemistry for phosphorylated smad-2 was performed as described before [18, 19] using rabbit anti-phospho-smad-2 antibodies (Cell Signaling Technology, Danvers, MA, USA). Immunohistochemistry for MMP-9 (Santa Cruz) was performed on 6μm aortic cryosections of Fibulin-4^{+/+}, Fibulin-4[+/R] and Fibulin-4[R/R] mouse aortas counterstained with haematoxylin.

Zymography

Protein was extracted from the mouse aortic arch. The samples were homogenized at 4°C in 350 μl lysisbuffer (50 mM Tris-HCl Ph 8.8, 100 mM NaCl, 1% SDS, 1/25 protease inhibitor mix (Roche) using a rotor homogenizer (Ika Works Inc., Wilmington, NC, USA). After, lysis samples were spun down (10 min, 4000 rpm) and heated for 3 min. at 55°C to denature the gelatinases. Samples were further homogenized by shearing through a 25G needle. The protein content of the aortic samples was determined according to the method of Lowry et al [20] and samples were equalized for protein content. Gelatin-zymography was conducted using sodium dodecyl sulfate (SDS)-polyacrylamide gels containing 1.0% gelatin. After electrophoresis, the gels were washed 2 times in a Triton X-100 solution (2.5%) to remove the SDS and renature the gelatinases. Gels were then developed in development buffer (5mM $CaCl_2$, 50 mM Tris.HCl, pH8.8, 0.02% NaN_3) overnight at 37°C. Enzymatic activities were visualized as negative stainings with 0.1% Coomassie Brilliant. The molecular sizes of gelatinolytic activity were determined by comparison with native molecular weight markers (Invitrogen, Carlsbad, CA, USA) and quantified using ImageJ software. *In situ* zymography on 6μm aortic cryosections of Fibulin-4^{+/+}, Fibulin-4[+/R] and Fibulin-4[R/R] mouse aortas was performed using quenched fluorogenic DQ gelatin (Invitrogen) as described by the manufacturer.

Magnetic resonance imaging and angiography

In order to fully understand the complex nature of aortic vascular pathology in Fibulin-4[R/R] mice we used homemade Gd-liposomes (as previously described [21]) as an intravascular contrast agent to acquire high-resolution whole-body MRA on a 3.0T clinical MRI scanner (General Electric Healthcare, Milwaukee, USA; software release 12X) with a 4-channel phased array receiver interface providing an effective 7 cm field-of-view (FOV) cranial-caudal. A 3D fat-supressed T1-weighted scan (TR/TE = 41.7/2.8 ms, flip angle = 40°, FOV = 60 mm, acquisition time = 35 minutes) was performed after the injection of the Gd-liposomes through the tail vein with an effective voxel resolution of 117 x 187 x 100 μm^3. Subsequently, MRAs were processed using surface rendering 3D on the MRI scanner console to visualize the entire aorta from the aortic root until the branching of the iliac arteries.

In vivo lifetime fluorescence imaging

We used MMPSense 680 (VisEN Medical, Bedford, MA, USA), which according to supplier's information can be activated *in vitro* in the presence of MMP-13, MMP-12, MMP-

2

2

9, MMP-7, MMP-2, and MMP-1, to monitor the upregulation of MMPs *in vivo*. Four nmol MMPSense 680 was injected into the tail vein of 120 days old Fibulin-4$^{+/+}$, Fibulin-4$^{+/R}$ and Fibulin-4$^{R/R}$ male littermates. Twenty hours later, the anaesthetized mice were scanned using the Optix MX2 optical imaging system (ART, Montreal, QC, Canada). Excitation was performed with a 670 nm pulsing laser and emission was detected with a 693 nm long pass filter. Time-of-flight distribution enabled fluorescence lifetime to be determined. The scanning was performed over a Cartesian grid in prioritized raster fashion. The fluorescent intensity of the tissues was quantified using the Optiview software (version 2.2) provided as part of the Optix MX2 imaging package. Lifetime analysis was used to confirm the specificity of MMP-activated MMPSense 680. Fluorescence intensities and fluorescence lifetime were expressed in pseudo colors and projected on the bright field grayscale image of the mouse. Data analysis was performed using the Optiview 2.2 software to allow for background subtraction and then lifetime analysis of MMPSense was performed. The temporal dispersion of fluorescent photons is measured by time-correlated single photon counting after excitation of the fluorophore by laser pulse. Analysis of this temporal dispersion curve, the fluorescent temporal point spread function, was used to verify the intensity of MMPSense 680 in the tissue. The fluorescent intensity value was gated (synchronized) at the fluorescent lifetime range as determined for MMPSense 680.

Macroscopic *ex vivo* fluorescence reflectance imaging
Complete hearts with aortas attached were harvested after *in vivo* fluorescence imaging and analyzed using the FMT2500 (VisEN Medical, Bedford, MA, USA) or the Odyssey Imaging system (LI-COR Biosciences, Lincoln, NE, USA). Near-infrared images were obtained in the 680 and 700 nm channels, respectively.

FMT-CT imaging
We employed vascular FMT-CT imaging as previously described [22]. In short, mice were shaved and depilated to remove all hair that otherwise absorb light and interfere with optical imaging. Prior to FMT scanning, mice received 5 ml per kg of body weight eXIA™ 160 contrast agent (Binitio Biomedical Inc, Ottawa, ON, Canada) via tail vein injection for subsequent CT-analysis. FMT imaging of Fibulin-4 mice was then performed using an FMT 2500 system (VisEN Medical, Bedford, MA, USA) at 680/700 nm excitation/emission wavelengths at 20 hrs after tail-vein injection of 5 nmol of MMPSense 680. Mice were anaesthetized (Isoflurane 1.5%, O$_2$ 2L/min) and fixed into the portable animal imaging cassette that lightly compressed the anesthetized mouse between optically translucent windows thereby preventing motion during FMT and CT imaging. This multi-modal animal holder facilitates coregistration of FMT to CT data through fiducial landmarks on its frame. The FMT 2500 Quantitative Tomography software was then used to calculate three-dimensional fluorochrome concentration distribution of MMPSense 680. Immediately after FMT imaging, the animal holder with the anaesthetized mouse was transferred to the microCT (Skyscan 1076, Kontich, Belgium) to identify the heart and aortic root region of the animal. The CT X-ray source operated at 70 KV and 142 µA with an exposure time of 110 ms to acquire 1500 projections (rotation steps of 0,7 degrees). The effective 3D resolution was 35 µm isotropic. We then imported data into 'CVP' (Cyttron Visualization Platform), an in-house developed image registration and visualization program to coregister FMT and CT images. Fiducial markers on the imaging cartridge were visualized and tagged in FMT and CT images with point markers to define their XYZ coordinates. Using these coordinates, data were resampled, rotated, and translated to match the image matrices and finally displayed in one hybrid image.

RESULTS

Fibulin-4 mice as model system for the detection of aneurysm specific biomarkers
In order to fully understand the complex nature of aortic vascular pathology in Fibulin-4$^{R/R}$ mice, we performed MRI and MRA using Gadolineum (Gd)-liposomes as an intravascular contrast agent to acquire high-resolution whole-body angiograms. To be able to perform these experiments on a clinical MRI scanner, we developed a specialized receiver interface using 4 loop coils for signal reception [23]. MR angiograms were subsequently processed using a 3D reconstruction platform to visualize the entire aorta from the aortic root until the branching of the iliac arteries. We compared the aortic arch and the descending aorta of wild type, Fibulin-4$^{+/R}$ and Fibulin-4$^{R/R}$ mice (Figure 1A). 3D MRA reconstructions allowed accurate analysis of the thoraceous aortic aneurysma in Fibulin-4$^{R/R}$ mice. We observed variations in size and location of TAA in the ascending aorta of Fibulin-4$^{R/R}$ mice. Tortuosity is clearly visible in the descending aorta and is limited to the thoraceous part of the aorta. Surface rendering of a high resolution MR angiograms acquired in living Fibulin-4$^{R/R}$ mice not only showed aortic dilatation and a tortuous descending aorta, but also allowed detailed examination of the surrounding aorta, collateral vessels and heart abnormalities (Figure 1B and online supplemental Figure 1 for 3D animation). Since careful examination of the collateral vessels revealed no other aberrations, we concluded that the vascular pathology we observe is highly specific for the thoraceous aorta. These Fibulin-4$^{R/R}$ mice can therefore be used as an attractive model for the *in vivo* detection of aneurysm specific biomarkers.

We then compared the *ex vivo* morphology of the adult aorta of wild type, Fibulin-4$^{+/R}$ and Fibulin-4$^{R/R}$ mice. All homozygous Fibulin-4$^{R/R}$ mice showed a dramatic dilatation of the ascending aorta and a tortuous and stiffened aorta (Figure 2A). In comparison to wild type mice the aortas of Fibulin$^{+/R}$ mice were less translucent, possibly also due to increased deposition of amorphous extracellular matrix material and reactive cartilage proteoglycans as identified by Alcian blue staining (Figure 2B, 2C). Thus, already a moderate 2-fold decrease in Fibulin-4 expression results in aberrations of the aortic wall. Analysis of the elastic fiber network of the aorta of the Fibulin-4 mice, pointed to significant changes in the architecture of the elastic laminae, consisting of a granular appearance of elastin in the outer layers of the aorta in adult Fibulin-4$^{R/R}$ mice. In addition, the inner layers showed fragmentation and disarray of elastic fibers and increased thickness of the aortic wall (Figure 2D). Interestingly, fragmentation of elastic fibers, but not the granular appearance, was also observed in adult heterozygous Fibulin-4$^{+/R}$ mice, indicative for a gene dosage effect of Fibulin-4.

Disturbed TGFβ signaling and MMP upregulation in Fibulin-4 mice
Aorta transcriptome analysis of Fibulin-4$^{+/R}$ and Fibulin-4$^{R/R}$ animals identified excessive TGFβ signaling as the critical event in the pathogenesis of aneurysm formation [2]. We performed protein expression analysis by immunolabeling of aortic tissue slices from the different mice. These stainings revealed an increase in TGFβ signaling in comparison to wild type animals, as evidenced by increased phosphorylation and nuclear localization of Smad2 in Fibulin-4$^{+/R}$ mice (Figure 3A). In addition, Fibulin-4$^{R/R}$ mice also showed an increase in pSmad2. There were large areas that showed loss of vascular smooth muscle cells and severe thickening (data not shown). From the elastin and immunostainings we realized that this perturbed elastin lamellar structures in the Fibulin-4 mice might have been caused by the induction of TGFβ regulated MMPs, also because previously we found MMPs upregulated in both Fibulin-4$^{+/R}$ mice and Fibulin$^{R/R}$ mice in our microarray expression analysis [2].

2

A

Fibulin-4⁺/⁺ Fibulin-4⁺/R Fibulin-4R/R

B

Fibulin-4⁺/⁺ Fibulin-4⁺/R Fibulin-4R/R
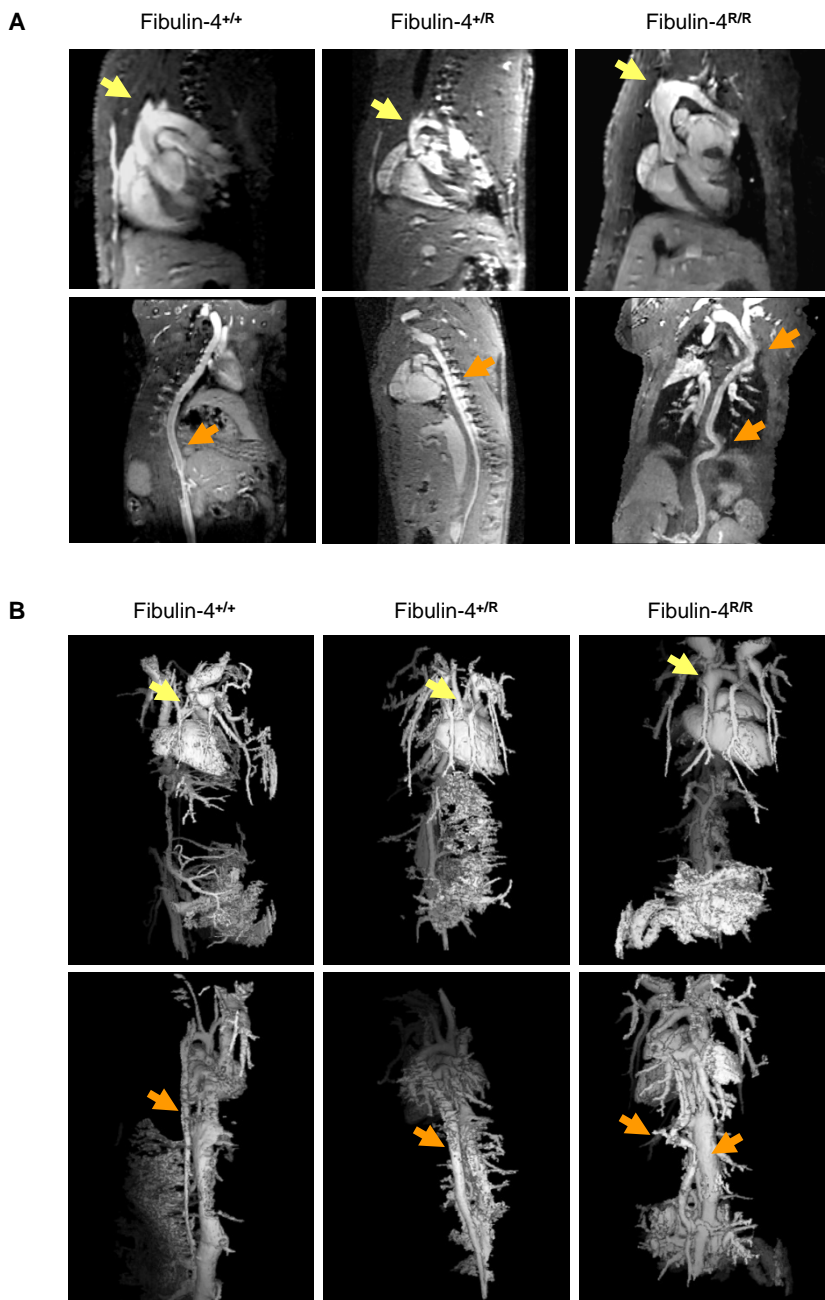

Figure 1: (A) Using Gd-liposomes as an intravascular contrast agent high-resolution whole-body MRAs on a 3.0T MR imaging scanner were acquired. Homozygous knockdown mice (Fibulin-4$^{R/R}$) underexpressing Fibulin-4 show an aortic dilatation and a tortuous descending aorta. (B) Surface rendering of a high resolution MRA acquired in a live mouse using intravascular Gd-liposomes.

To determine whether and which MMPs are increased in aortas of Fibulin-4 mice we performed gelatin-zymography. Homogenates of the aortic arches of Fibulin-4 mice were generated and separated by SDS-PAGE, after which the gelatinolytic activity was determined. Based on molecular weights we conclude that the gelatinolytic activities were consistent with the presence of MMP-2 and MMP-9. Where both protein extracts of Fibulin-4$^{+/R}$ and Fibulin-4$^{R/R}$ aortic arches showed an increase in MMP-2, densitometric analyses of the active form of MMP-9 also demonstrated a clear increase in the presence of the active form of MMP-9 in the aortic arch of Fibulin-4$^{R/R}$ mice (Figure 3B and C). Moreover, a decrease in pro-MMP-9 coincides with an increase of active MMP-9 in the Fibulin-4$^{+/R}$ and Fibulin$^{R/R}$ genotypes.

To provide histological support for the increase in MMP-9 activity detected in the Fibulin-4$^{+/R}$ and Fibulin$^{R/R}$ genotypes, we performed *in situ* MMP-9 enzyme localization and MMP enzyme activity-localization experiments. Firstly, we performed MMP-9 peroxidase immunohistochemistry on cryosections of aortic slices of the different genotypes which showed a gradual increase in MMP-9 levels in the medial layers of Fibulin-4$^{+/R}$ and Fibulin-4$^{R/R}$ mouse aortas (figure 4A, left panel). Secondly, to accurately localize the increase of MMP activity, we performed *in situ* zymography on cryosections which showed a gradual increase in DQ-gelatin derived fluorescence throughout the aortic wall (see figure 4A, right panel DQ-gelatin, DAPI and merged image). Thirdly, we compared cryosections of aortas of MMPSense 680, an MMP specific activatable NIRF probe developed for *in vivo* imaging, injected mice with non-injected control aortas by confocal microscopy which showed that both the elastin layers as well as the amorphous material between the layers showed increased near-infrared fluorescence after MMPsense 680 injections. From these experiments we conclude that while there is a Fibulin-4 dose dependent increase in the MMP-9 protein levels in the medial layers of Fibulin-4$^{+/R}$ and Fibulin-4$^{R/R}$ aortas, this results in an overall increase of fluorescence in the overall structure of the vessel, including the elastin layers, probably due to a local redistribution of the cleaved fluorescent MMPSense probe throughout the aortic wall.

In vivo imaging of MMP activity in aneurysmal Fibulin-4 mice

MMP activity was monitored *in vivo* using MMPsense 680, after injection of this protease sensor into live mice. After excitation, fluorescent molecules can be characterized by their specific decay time from an excited to a ground state, known as their lifetime fluorescence. The measurement of this parameter was used to verify the signal intensity against background in the determination of MMP activity in the heart and aortic arch region during aneurysm formation. A weighted histogram showed that the lifetime of MMPSense 680 was centered around a maximum peak of 1.85ns with a distribution curve of between 1.79 ns and 2.02 ns as shown on the histogram (Figure 5A). Figure 5B shows the localization and distribution of the 1.79 ns and 2.02 ns lifetime signal range for the Fibulin-4$^{+/R}$ and Fibulin-4$^{R/R}$ genotypes. The specificity of the MMPSense 680 is indicated as intensity for Fibulin-4$^{+/R}$ (Figure 5C left) and Fibulin-4$^{R/R}$ (Figure 5C right) genotypes, gated at a lifetime of between 1.79 ns and 2.02 ns. The total gated intensity (in normalized counts) showed an increase of MMP Sense 680 activity in the Fibulin-4$^{R/R}$ genotype. Non-injected control mice had a lifetime of less than 1 ns in the aortic arch area, which underscores the specificity of the fluorescent MMPsense signal (data not shown).

After the *in vivo* imaging the mice were euthanized, the hearts with the aortas attached excised, and *ex vivo* fluorescence in the aortic arch and aorta of the Fibulin-4 mice compared using the Odyssey imaging system (Li-COR Biosciences, Lincoln, NE, USA). We measured a graded increase of MMPSense 680 activation in the Fibulin-4$^{+/R}$ and
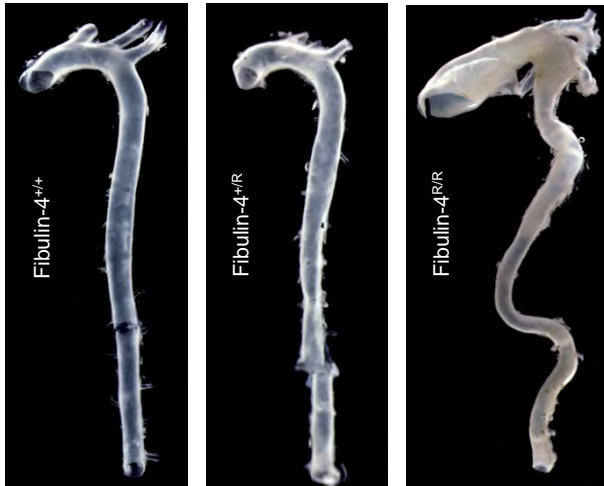
2

A

B   Fibulin-4+/+   Fibulin-4+/R   Fibulin-4R/R

C

D

Figure 2: (A) Gross aortic abnormalities of Fibulin-4+/R and Fibulin-4R/R mice. Representative aortas (from aortic root until the branching of the iliac arteries) of 120 days old Fibulin-4+/+, Fibulin-4+/R and Fibulin-4R/R mice. Note the severe aneurysm in the Fibulin-4R/R mice. The ascending aorta of Fibulin-4R/R mice is elongated and severely dilated. Aortas of Fibulin-4+/R mice are less translucent compared to the littermate control and aortas of Fibulin-4R/R mice are elongated and tortuous. (B and C) Comparison of the architecture of the aortic wall in Fibulin-4+/+, Fibulin-4+/R, and Fibulin-4R/R mice. (B) Haematoxylin and eosin staining of cross-sections from 120-days old mice. (C) Alcian blue (cartilage bone) stained section. (D) Verhoeff-Van Gieson (elastin) staining of cross sections. Elastic laminae changes consisted of a granular appearance of elastin in the outer layers of the aorta. In heterozygous Fibulin-4+/R mice, areas in the aortic wall with a granular appearance of elastic laminae are present indicating a gene dosage effect. Note the irregularity of the elastic laminae in Fibulin-4+/R and in Fibulin-4R/R mice, particularly.
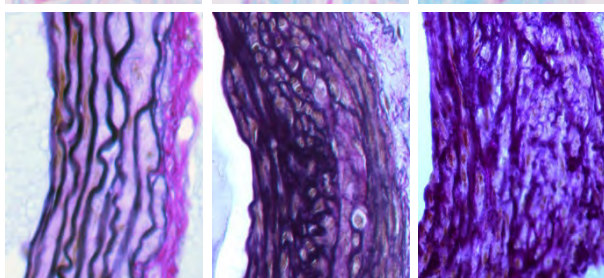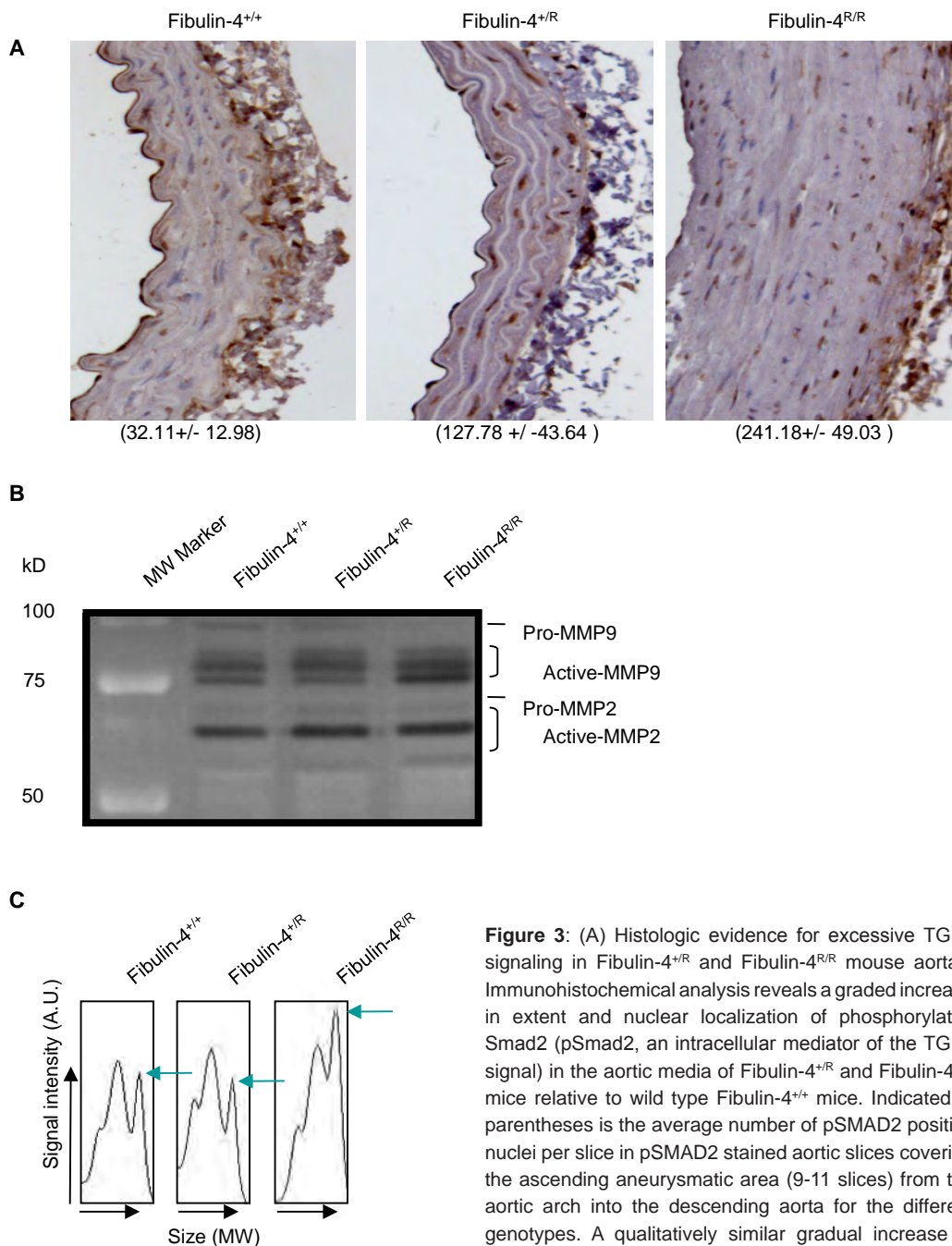
A

Fibulin-4$^{+/+}$ Fibulin-4$^{+/R}$ Fibulin-4$^{R/R}$

(32.11+/- 12.98)   (127.78 +/ -43.64)   (241.18+/- 49.03)

2

B

C
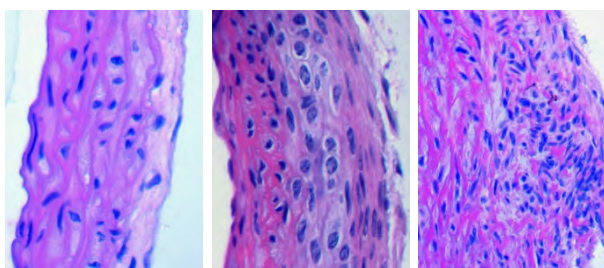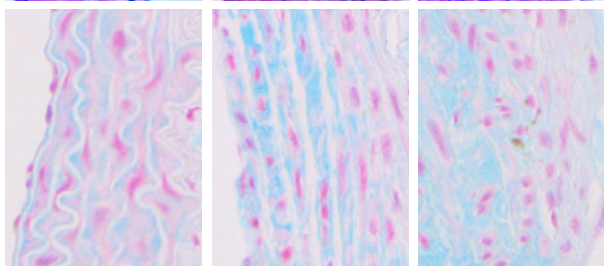
Figure 3: (A) Histologic evidence for excessive TGFβ signaling in Fibulin-4$^{+/R}$ and Fibulin-4$^{R/R}$ mouse aortas. Immunohistochemical analysis reveals a graded increase in extent and nuclear localization of phosphorylated Smad2 (pSmad2, an intracellular mediator of the TGFβ signal) in the aortic media of Fibulin-4$^{+/R}$ and Fibulin-4$^{R/R}$ mice relative to wild type Fibulin-4$^{+/+}$ mice. Indicated in parentheses is the average number of pSMAD2 positive nuclei per slice in pSMAD2 stained aortic slices covering the ascending aneurysmatic area (9-11 slices) from the aortic arch into the descending aorta for the different genotypes. A qualitatively similar gradual increase in pSMAD2 was observed in an additional set of Fibulin-4 mice of the indicated genotypes. (B) Gelatin-zymography of aortic arch homogenates of Fibulin-4 mice. The molecular weights of the gelatinolytic activities were consistent with the presence of MMP-2 and MMP-9. (C) Densitometric analyses of active MMP-9 demonstrated a strong increase in the presence of active MMP-9 in the aortic arch of Fibulin-4$^{R/R}$ mice.

Fibulin-4$^{R/R}$ mice compared to wildtype Fibulin-4$^{+/+}$ mice (Figure 5D). In the wildtype Fibulin-4$^{+/+}$ mouse, basic activity of the MMPSense 680 was primarily detected in the aortic arch region and reached a level of 19,75 relative fluorescence units. In the Fibulin-4$^{+/R}$ and Fibulin-4$^{R/R}$ mice, an increasing amount of MMP-9 activity induced fluorescence was detected in the dilated aortic arch and further down the extended descending aorta. Relative fluorescence units were increased to 26.53 and 105.77 for the Fibulin-4$^{+/R}$ and Fibulin-4$^{R/R}$, respectively. The fluorescent intensity of the aortas was quantified using the Odyssey software package. In conclusion, *in vivo* life-time imaging of aneurysmal Fibulin-4 mice and *ex vivo* analyses of the aortas of these animals demonstrated specific near infrared fluorescent signals for MMP activity in Fibulin-4 mice in the region of the aortic arch.

3D FMT-CT co-registration locates MMP activation in the aortic arch

To accurately localize a fluorescent signal retrieved from a living mouse and identify the organ from which the fluorescence is emitted reference imaging is needed to visualize anatomical detail. After we found that MRA revealed no other abnormalities in the vascular system then the aortic aneurysm we switched to a less technical demanding imaging modality to acquire reference anatomy pictures. Using a microCT scanner dedicated for small animal imaging in combination with the vascular contrast agent EXia160, we generated 3D datasets for the different Fibulin-4 mice. CT angiography allowed to identify and demonstrate an increased heart size and the aortic aneurysm in the ascending aorta in the homozygous Fibulin-4$^{R/R}$ knockdown animals compared to the Fibulin-4$^{+/R}$ mice (Figure 6A). Using the MMPSense 680 we monitored MMP activity in live animals using a fluorescence molecular tomographic (FMT) imaging system, and coregistered the fluorescence signal with CT images of the same animals. To coregister FMT and CT data sets, mice were placed in a multimodal imaging cartridge containing fiducial markers detectable by both imaging modalities. Figure 6B represents a two-dimensional (2D) data set of fluorescence derived from the MMPSense 680 in Fibulin-4$^{+/R}$ and Fibulin-4$^{R/R}$ animals coregistered with CT. Clear fluorescent signals could be detected in the homozygous Fibulin-4$^{R/R}$ knockdown animal at the position of the aortic arch. Interestingly, already in the modestly affected heterozygote Fibulin-4$^{+/R}$ mice FMT allows the detection of specific fluorescence as a result of MMP activity even before the onset of aneurysm formation. Metabolization of the fluorescent probe in the liver also leads to release of the fluorescence and is similar in Fibulin-4$^{+/R}$ and Fibulin-4$^{R/R}$ mice. Accurate coregistered 3D FMT-CT images as illustrated in Figure 6C are useful for quantitative analysis of fluorescence levels detected in the animals and thus for quantitative analysis of MMP activity (See supplemental Figure S2 for animation of 3D FMT-CT coregistration). Taken together, with this hybrid approach of FMT-CT imaging, localization of MMP activity can be visualized in the different stages of aneurysm development and correlated with anatomical structures.

Quantitative FMT analysis detects MMP activation before the onset of aneurysm formation

Ex vivo analysis confirmed the *in vivo* observed graded increase in MMPs within the aortic arches in Fibulin-4$^{+/R}$ and Fibulin-4$^{R/R}$ mice compared to Fibulin-4$^{+/+}$ wildtype animals (Figure 7A). Using the FMT imaging modality, a direct comparison of isolated heart and aorta of the different genotypes showed that the graded increase in fluorescence can evidently be detected. Ultimately, we wanted to rigorously address whether we can detect upregulation of protease activity already in Fibulin-4$^{+/R}$ mice. For that reason we directly compared the MMP upregulation in Fibulin-4$^{+/+}$ and Fibulin-4$^{+/R}$ (Figure 7B, 7C and Table I). Finally we
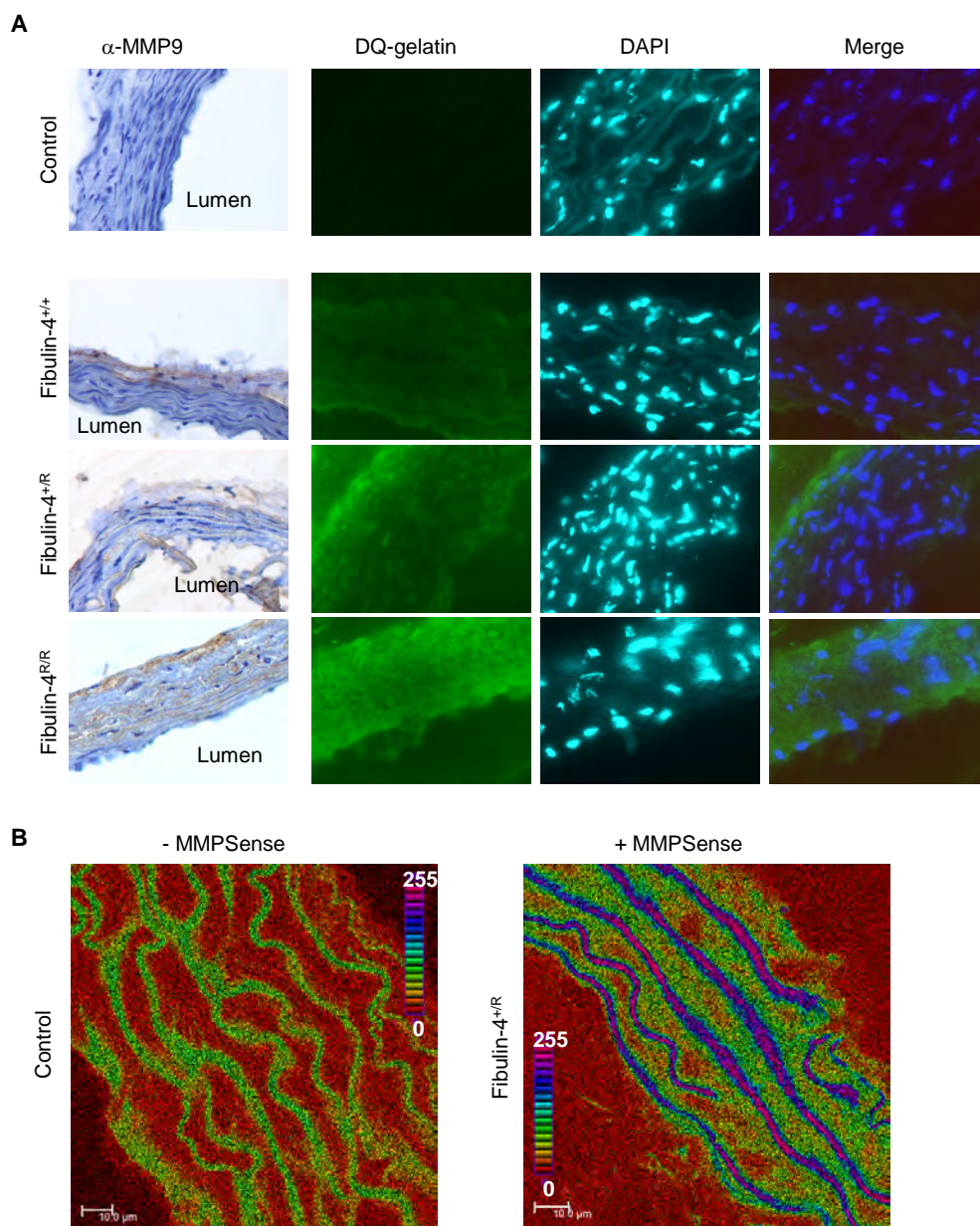
Figure 4: (A) MMP-9 peroxidase immunohistochemistry on cryosections of aortic slices of the indicated genotypes and control tissue staining in which the primary MMP-9 antibody was excluded (left panel). To accurately localize the increase of MMP activity, *in situ* zymography was performed on aortic cryosections using DQ-gelatin after which the sections were counterstained with DAPI (right panel DQ-gelatin, DAPI and merged image). (B) Confocal images of aortic cryosections of MMPSense 680 injected mice (24 hrs prior preparation of the slices) and non-injected control sections. Both images are displayed on the same relative fluorescence intensity scale (0-255) in a stepwise rainbow color scale. Note that both the elastin layers as well as the amorphous material between the layers showed increased near-infrared fluorescence.

2

Fluorescence Lifetime

Fluorescence Intensity

Fibulin-4$^{+/R}$ Fibulin-4$^{R/R}$

Fibulin-4$^{+/R}$ Fibulin-4$^{R/R}$

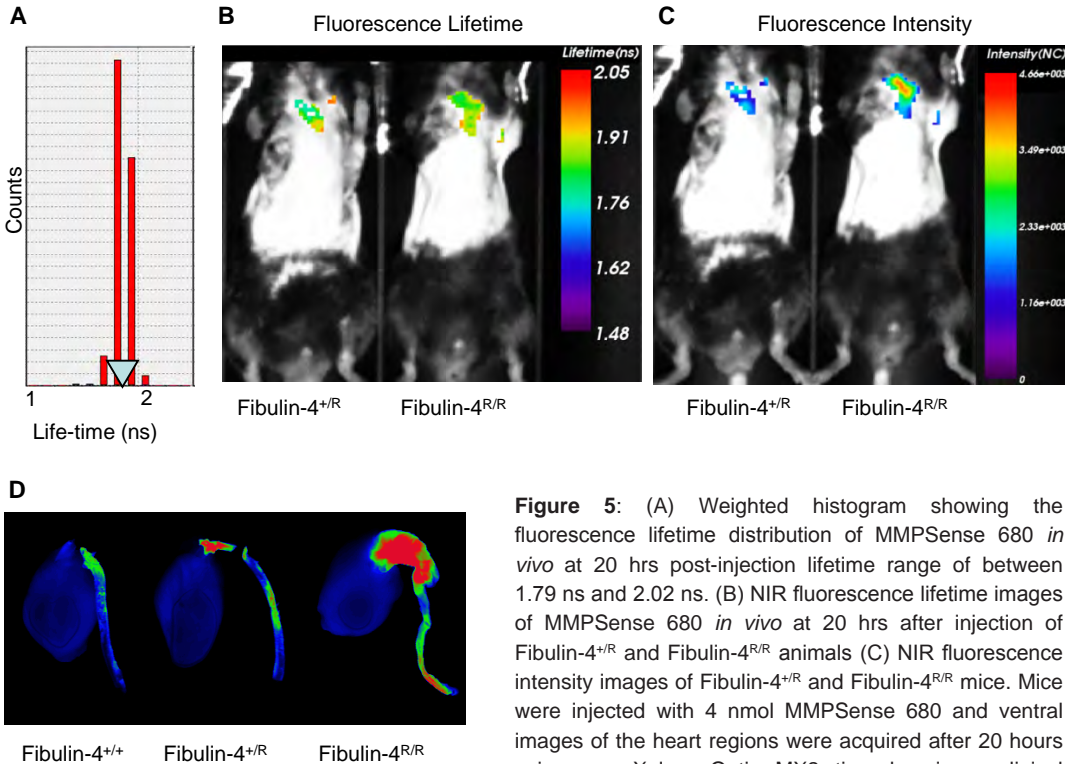Fibulin-4$^{+/+}$ Fibulin-4$^{+/R}$ Fibulin-4$^{R/R}$

Figure 5: (A) Weighted histogram showing the fluorescence lifetime distribution of MMPSense 680 *in vivo* at 20 hrs post-injection lifetime range of between 1.79 ns and 2.02 ns. (B) NIR fluorescence lifetime images of MMPSense 680 *in vivo* at 20 hrs after injection of Fibulin-4$^{+/R}$ and Fibulin-4$^{R/R}$ animals (C) NIR fluorescence intensity images of Fibulin-4$^{+/R}$ and Fibulin-4$^{R/R}$ mice. Mice were injected with 4 nmol MMPSense 680 and ventral images of the heart regions were acquired after 20 hours using an eXplore Optix MX2 time-domain preclinical imager. (D) *Ex vivo* analysis confirmed the *in vivo* observed graded increase in MMP activity within the aneurysmal lesions in Fibulin-4$^{+/R}$ and Fibulin-4$^{R/R}$ mice.

performed a comparative analysis of 5 mice in total, two wild type Fibulin-4$^{+/+}$ mice and three heterozygous Fibulin-4$^{+/R}$ mice. Quantitative analysis confirmed the upregulation of MMP activity in all heterozygous Fibulin-4$^{+/R}$ mice compared to wild type Fibulin-4$^{+/+}$ animals analyzed by both FMT *in vivo* (Figure 7C, 7D and Table I) and 2D fluorescence imaging of the hearts and aortas *ex vivo* (Figure 7C). Whereas the absolute amount of the fluorescent signal of activated MMPsense 680 was 3-4 pmol, the fluorescence level of MMPSense 680 varied from 7-11 pmol per animal in the heterozygous animals. Importantly, these Fibulin-4$^{+/R}$ mice did not display any detectable signs of aneurysm formation. The fluorescence level determined for MMPSense 680 in non-injected control mice imaged under the same FMT imaging settings was 0 pmol (data not shown). Figure 7D shows the qualitative analysis of MMP activity in the different mouse models after reconstruction of the tomographic images. Twenty hours after intravenous injection of the MMPSense 680 probe we observed a graded increase in MMP activity in heterozygous Fibulin-4$^{+/R}$ animals and homozygous Fibulin-4$^{R/R}$ animal compared to normal wildtype mice. A 3D FMT-CT reconstruction of the fluorescence and the CT signal of the same Fibulin-4$^{+/R}$ mouse is depicted in Figure 7E and shows that, while the diameter of the ascending aorta is unaffected, there is clear fluorescence detectable pointing to MMP activity at this position (see also supplemental Figure S3 for animation of 3D FMT-CT coregistration).
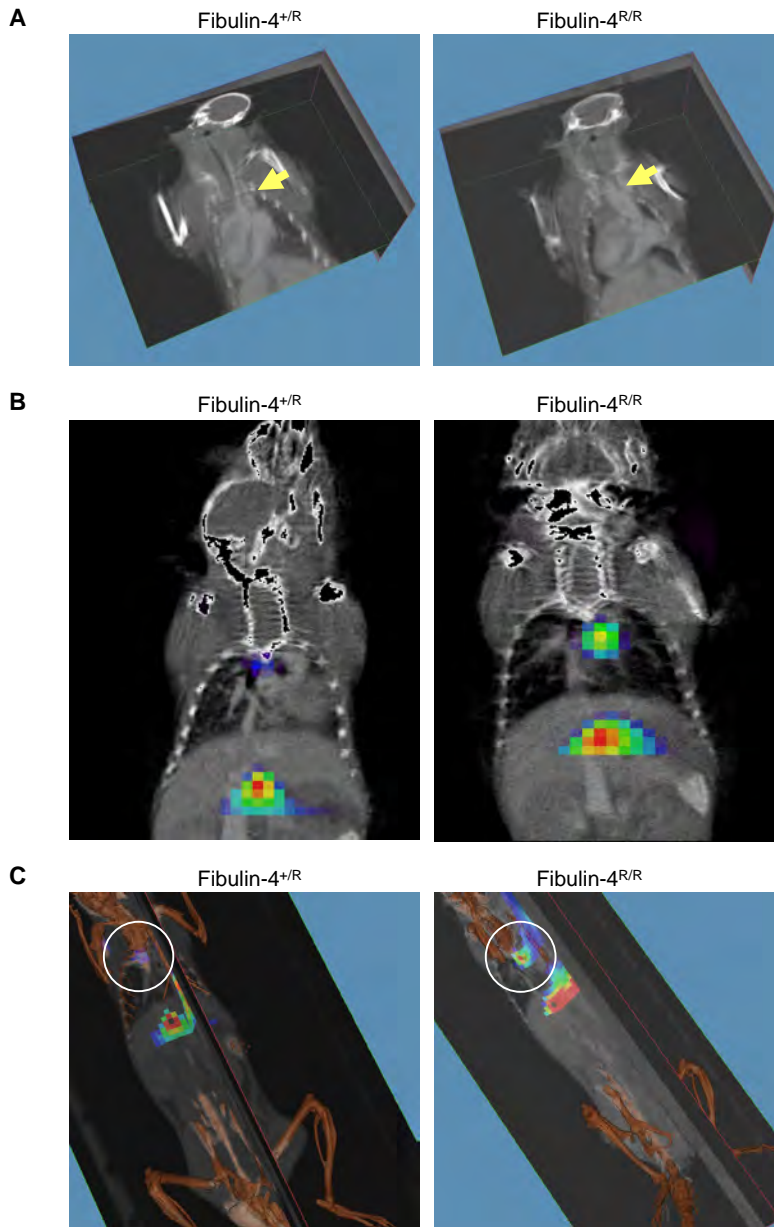
A Fibulin-4$^{+/R}$ Fibulin-4$^{R/R}$

B Fibulin-4$^{+/R}$ Fibulin-4$^{R/R}$

C Fibulin-4$^{+/R}$ Fibulin-4$^{R/R}$

Figure 6: (A) CT images of Fibulin-4$^{+/R}$ and Fibulin-4$^{R/R}$ mice. (B) 2D FMT-CT co-registration of Fibulin-4$^{+/R}$ and Fibulin-4$^{R/R}$ mice. Using MMPSense 680 we monitored and quantified MMP upregulation in live animals with FMT and coregistered the fluorescence signal with CT images of the same animals. (C) 3D FMT-CT co-registration. To reliably identify the region of interest within the heart, FMT-imaging was hybridized with CT-imaging for anatomic reference. After completion of FMT, the animal fixed in the multimodal animal holder with fiducial markers was analyzed with CT. Within both data sets, fiducial points were tagged to define their X-Y-Z-coordinates. Using these coordinates, FMT data were then resampled, rotated and translated to match the CT image matrix, and finally fused. After identification of the aneurysm on CT, regions of interest were defined in both FMT channels.
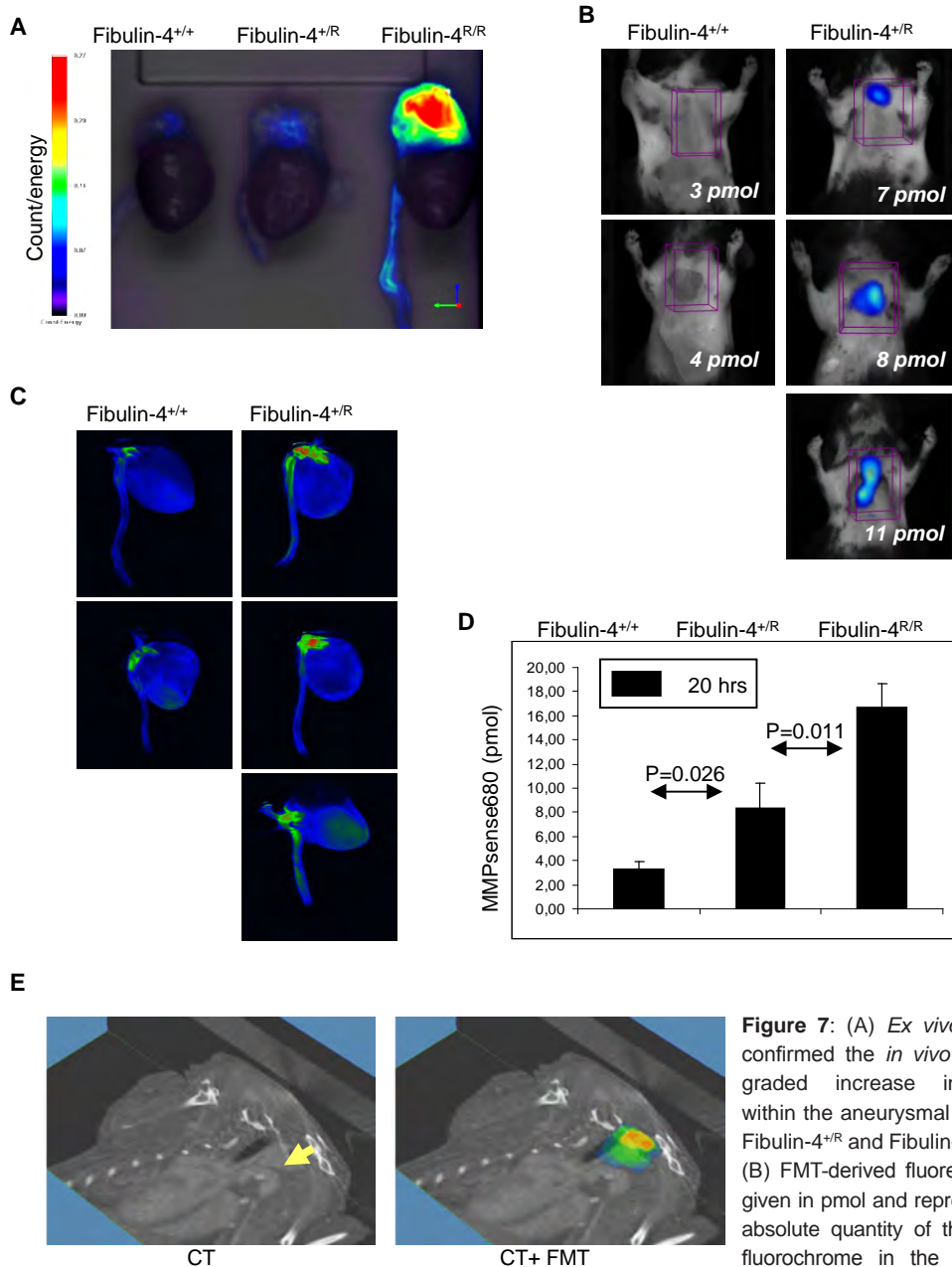
2

A Fibulin-4+/+ Fibulin-4+/R Fibulin-4R/R

Count/energy

B Fibulin-4+/+ Fibulin-4+/R

3 pmol *7 pmol*

4 pmol *8 pmol*

11 pmol

C Fibulin-4+/+ Fibulin-4+/R

D Fibulin-4+/+ Fibulin-4+/R Fibulin-4R/R

20 hrs

P=0.011

P=0.026

MMPsense680 (pmol)

E

CT CT+ FMT

Figure 7: (A) *Ex vivo* analysis confirmed the *in vivo* observed graded increase in MMPs within the aneurysmal lesions in Fibulin-4+/R and Fibulin-4R/R mice. (B) FMT-derived fluorescence is given in pmol and represents the absolute quantity of the excited fluorochrome in the aorta (C) *Ex vivo* analysis of the MMP increase within the aortic arch area in Fibulin-4+/+ and Fibulin-4+/R mice. (D) Isosurface concentration mapping from reconstructed tomographic images revealed a graded increase in activation of intravenously injected MMPSense 680 within the aortic arch area of Fibulin-4+/R and Fibulin-4R/R mice compared to wildtype Fibulin-4+/+ animals. Data are given as the mean MMPSense 680 quantity (pmol) with *bars* indicating S.D. (n=5). Statistical differences were determined using Student's *t* test and indicated are the p-values between the different groups. (E) 3D FMT-CT co-registration of the heart and aorta of a heterozygous Fibulin-4+/R mouse.

Table I - Isosurface concentration mapping from reconstructed tomographic images after in vivo imaging of MMPSense 680 (see also figure 6C). FMT-derived fluorescence is measured in mean concentration (nM) and the absolute quantity of the excited fluorochrome is given in pmol in the indicated volume.

Mouse	Genotype	Size (mm^3)	Concentration (nM)			Stdev	Total (pmol)
			min	max	mean		
08-26501-03F	Fibulin-4$^{+/R}$	853.10	0.01	47.55	12.48	10.07	10.65
08-24732-06M	Fibulin-4$^{+/R}$	2376.42	0.00	26.34	2.74	3.67	6.52
08-26501-00F	Fibulin-4$^{+/R}$	927.92	0.06	41.37	8.44	7.52	7.83
08-25959-01F	Fibulin-4$^{+/+}$	1931.69	0.00	11.63	1.96	1.95	3.78
08-24941-04M	Fibulin-4$^{+/+}$	1293.68	0.00	11.44	2.22	2.75	2.87

2

DISCUSSION

The size and growth rate of an aortic aneurysm likely predicts the onset of risk for aortic dissection or rupture [24, 25]. In addition to conventional imaging modalities (e.g. ultrasound imaging or CT) new diagnostic tools that interrogate the aneurysmatic lesion could potentially serve to test pathophysiological hypotheses to identify the risk while the disease remains undetected and to evaluate novel therapeutic strategies. Accumulating evidence, mainly from *in vitro* studies, implicates the increase in MMP activity, most notably MMP-9, in the disease state [26]. While no conventional structural imaging technique can measure the protease level at the site of the aortic aneurysm, we tested whether NIRF protease-activatable probes to detect MMP action *in vivo* followed by quantitative assessment of the actual level of protease activity, renders non-invasive macroscopic observation of aortic aneurysm staging in living mice feasible.

Our focus was to investigate early detection methods of aortic aneurysms using genetically modified mouse models for thoracic aortic aneurysms. The aortic arch is distinct from the other parts of the arterial tree especially due to the presence of a large amount of elastic fibers. A critical component for the elasticity is the FBLN4 protein. Based on the knockdown of the Fibulin-4 gene, we have recently developed mouse models displaying both mild and severe forms of aneurysm due to reduced amounts of FBLN4 protein. By a combination of pathological analyses and *in vivo* experiments we demonstrated a reproducible aortic dilatation of the ascending aorta in the homozygous Fibulin-4$^{R/R}$ mice. Strikingly, already a modest 2-fold reduction in expression of FBLN4 in the heterozygous Fibulin-4$^{+/R}$ mice occasionally resulted in aneurysm formation [2]. Here we show, with a variety of molecular imaging methods, using protease-activatable NIRF probes, that the protease activity of MMPs becomes gradually upregulated during aneurysm formation. Using the MMPSense 680 probe we monitored MMP activity in living animals using a fluorescence molecular tomographic imaging system, and coregistered the fluorescence signal with CT images of the same animals. We detected bright fluorescence in the homozygous (Fibulin-4$^{R/R}$) knockdown animals at the position of the dilated aortic arch. However, already in the modestly affected heterozygous Fibulin-4$^{+/R}$ animals, an increased activity of MMPs at the position of the non-dilated aortic arch could be detected. Accurate 3D images are the key to quantitative analysis of fluorescence levels detected in the animals and thus the quantitative analysis of MMP activity. Previously, MMP activatable probes have been used *in vivo* to detect MMP-2/MMP-9 action non-invasively in macrophage-rich atherosclerotic aortas in hypercholesterolemic mice [27]. However, our genetically engineered Fibulin-4

mouse models do not require induction of the aneurysm using either high-fat diet, causing atherosclerosis or angiotensin-II infusion protocols [28], but spontaneously and highly reproducibly develop aortic aneurysm due to cystic medial degeneration. Thus, the MMP activation we detect is not atherosclerosis induced. Immunohistochemical analysis of aortic tissue from Fibulin-4[+/R] and Fibulin-4[R/R] mice revealed a graded increase in TGFβ signaling in comparison to wild type animals, as evidenced by increased phosphorylation and nuclear localization of Smad2, indicative for increased TGFβ signaling. The mechanism by which Fibulin-4 deficiency initiates excessive TGFβ signaling could reflect disruption of other elastic fiber components known to regulate TGFβ such as Fibrillin-1 or Emilin [29, 30]. TGF-β is synthesized as a latent complex consisting of the active TGF-β dimer, the latency associated protein and the latent TGFβ binding protein (LTBP). This LTBP is bound to fibrillin-1 in the extracellular matrix [31]. LTBP mediated incorporation into the ECM is necessary for subsequent effective activation of TGFβ. There are several mechanisms for activation including proteolysis of the ECM proteins such as fibrillin or LTBPs [32]. MMP-2 has been shown to be involved in activation of TGFβ within the arterial wall [33]. In addition cell surface localized MMP-9 is capable of activating latent TGFβ [34]. Since we show increased active MMP-2 and MMP-9 levels in the arterial walls of fibulin-4 deficient mice, these proteases could be involved in increased TGFβ activation. In contrast or in addition TGFβ has been shown to upregulate both MMP-2 and MMP-9 expression *in vitro* [35, 36]. Moreover TGFβ levels have been shown to correlate to MMP-2 and MMP-9 expression in colorectal cancer [18]. So increased TGFβ activity could also be causally involved in increased MMP expression, and in turn mediate increased TGFβ activation creating a positive feedback loop.

Using MRA, we find combined manifestations of general aortic vascular pathology, including TAA, and a tortuous descending aorta. We observed variations in size and location of TAA in ascending aorta of Fibulin-4[R/R] mice. Strikingly, we also noticed incidental cases of aortic coarctation (data not shown), a type of aortic pathology that in humans is also associated with aneurysm formation [37]. While the unsurpassed resolution of Gd liposome enhanced MRI was extremely useful to analyze the location of the aneurysm and the presence of additional abnormalities in the collateral vessels in mice, CT imaging was the modality of choice to routinely determine aortic root diameter and to perform multimodality imaging.

Following FMT by microCT imaging, the upregulation of this MMP biomarker was compared with the actual increase in aneurysmal size and a consistent upregulation of MMP activity in all Fibulin-4[+/R] animals was detected. Fusing the 3D optical images with CT images from the same animal allowed us to obtain structural anatomic information enhancing spatial resolution. This multimodal approach of molecular sensing by FMT and anatomic CT imaging including fiducial markers in the field of view is a promising and useful quantitative imaging modality that has recently been applied to detect protease activity in atherosclerotic lesions of apoE^{-/-} mice [22] and amyloid-β plaques in a mouse model of Alzheimer's disease [38]. In this study, we show that this hybrid method based on FMT fluorescence measurements combined with CT anatomical information is an important tool for *in vivo* imaging of aneurysmal disease progression within a single mouse. Information from studies like these could provide real time evaluation of the efficacy therapeutic treatments such as AngiotensinII AT1 receptor blockage treatments by Losartan [39]. By utilizing the same method at several spectral windows, with corresponding fluorochromes or expressed fluorescent proteins emitting at different spectral bands, different aneurysmal disease biomarkers such as cathepsins or changes in renin-angiotensin levels could be visualized simultaneously.

Our aim was to develop molecular imaging procedures for faster, earlier and easier recognition of aneurysms. What we show here is that *in vivo* co-registration of MMP activity and vascular pathology, using quantitative FMT imaging and contrast enhanced CT imaging allows the detection of increased MMP activity, already before the aneurysm has actually formed. This study reveals that TGFβ induced MMP activity is a leading indicator for (non-atherosclerotic) aneurysm formation and that this key biomarker for aortic aneurysm can be monitored *in vivo*.

2

ACKNOWLEDGEMENTS

REFERENCES

1. McLaughlin PJ, Chen Q, Horiguchi M, Starcher BC, Stanton JB, Broekelmann TJ, Marmorstein AD, McKay B, Mecham R, Nakamura T, Marmorstein LY. Targeted disruption of fibulin-4 abolishes elastogenesis and causes perinatal lethality in mice. *Mol Cell Biol.* 2006;26:1700-1709.
2. Hanada K, Vermeij M, Garinis GA, de Waard MC, Kunen MG, Myers L, Maas A, Duncker DJ, Meijers C, Dietz HC, Kanaar R, Essers J. Perturbations of vascular homeostasis and aortic valve abnormalities in fibulin-4 deficient mice. *Circ Res.* 2007;100:738-746.
3. Cudilo E, Al Naemi H, Marmorstein L, Baldwin AL. Knockout mice: is it just genetics? Effect of enriched housing on fibulin-4(+/-) mice. *PLoS One.* 2007;2:e229.
4. Horiguchi M, Inoue T, Ohbayashi T, Hirai M, Noda K, Marmorstein LY, Yabe D, Takagi K, Akama TO, Kita T, Kimura T, Nakamura T. Fibulin-4 conducts proper elastogenesis via interaction with cross-linking enzyme lysyl oxidase. *Proc Natl Acad Sci U S A.* 2009.
5. Coucke PJ, Willaert A, Wessels MW, Callewaert B, Zoppi N, De Backer J, Fox JE, Mancini GM, Kambouris M, Gardella R, Facchetti F, Willems PJ, Forsyth R, Dietz HC, Barlati S, Colombi M, Loeys B, De Paepe A. Mutations in the facilitative glucose transporter GLUT10 alter angiogenesis and cause arterial tortuosity syndrome. *Nat Genet.* 2006;38:452-457.
6. Judge DP, Dietz HC. Marfan's syndrome. *Lancet.* 2005;366:1965-1976.
7. Lemaitre V, Soloway PD, D'Armiento J. Increased medial degradation with pseudo-aneurysm formation in apolipoprotein E-knockout mice deficient in tissue inhibitor of metalloproteinases-1. *Circulation.* 2003;107:333-338.
8. Longo GM, Xiong W, Greiner TC, Zhao Y, Fiotti N, Baxter BT. Matrix metalloproteinases 2 and 9 work in concert to produce aortic aneurysms. *J Clin Invest.* 2002;110:625-632.
9. Segura AM, Luna RE, Horiba K, Stetler-Stevenson WG, McAllister HA, Jr., Willerson JT, Ferrans VJ. Immunohistochemistry of matrix metalloproteinases and their inhibitors in thoracic aortic aneurysms and aortic valves of patients with Marfan's syndrome. *Circulation.* 1998;98:II331-337; discussion II337-338.
10. Ntziachristos V, Tung CH, Bremer C, Weissleder R. Fluorescence molecular tomography resolves protease activity in vivo. *Nat Med.* 2002;8:757-760.
11. Weissleder R, Ntziachristos V. Shedding light onto live molecular targets. *Nat Med.* 2003;9:123-128.
12. Bremer C, Tung CH, Weissleder R. In vivo molecular target assessment of matrix metalloproteinase inhibition. *Nat Med.* 2001;7:743-748.
13. Bremer C, Tung CH, Weissleder R. Molecular imaging of MMP expression and therapeutic MMP inhibition. *Acad Radiol.* 2002;9 Suppl 2:S314-315.
14. Sanz J, Fayad ZA. Imaging of atherosclerotic cardiovascular disease. *Nature.* 2008;451:953-957.
15. Koning GA, Krijger GC. Targeted multifunctional lipid-based nanocarriers for image-guided drug delivery. *Anticancer Agents Med Chem.* 2007;7:425-440.
16. Hartnell GG. Imaging of aortic aneurysms and dissection: CT and MRI. *J Thorac Imaging.* 2001;16:35-46.
17. Schafers M, Riemann B, Kopka K, Breyholz HJ, Wagner S, Schafers KP, Law MP, Schober O, Levkau B. Scintigraphic imaging of matrix metalloproteinase activity in the arterial wall in vivo. *Circulation.* 2004;109:2554-2559.
18. Hawinkels LJ, Verspaget HW, van der Reijden JJ, van der Zon JM, Verheijen JH, Hommes DW, Lamers CB, Sier CF. Active TGF-beta1 correlates with myofibroblasts and malignancy in the colorectal adenoma-carcinoma sequence. *Cancer Sci.* 2009;100:663-670.
19. Hawinkels LJ, Zuidwijk K, Verspaget HW, de Jonge-Muller ES, van Duijn W, Ferreira V, Fontijn RD, David G, Hommes DW, Lamers CB, Sier CF. VEGF release by MMP-9 mediated heparan sulphate cleavage induces colorectal cancer angiogenesis. *Eur J Cancer.* 2008;44:1904-1913.
20. Lowry OH, Rosebrough NJ, Farr AL, Randall RJ. Protein measurement with the Folin phenol reagent. *J Biol Chem.* 1951;193:265-275.
21. Mulder WJ, Douma K, Koning GA, van Zandvoort MA, Lutgens E, Daemen MJ, Nicolay K, Strijkers GJ. Liposome-enhanced MRI of neointimal lesions in the ApoE-KO mouse. *Magn Reson Med.* 2006;55:1170-1174.
22. Nahrendorf M, Waterman P, Thurber G, Groves K, Rajopadhye M, Panizzi P, Marinelli B, Aikawa E, Pittet MJ, Swirski FK, Weissleder R. Hybrid in vivo FMT-CT imaging of protease

activity in atherosclerosis with customized nanosensors. *Arterioscler Thromb Vasc Biol.* 2009;29:1444-1451.

23. Zhang Z, van den Bos EJ, Wielopolski PA, de Jong-Popijus M, Bernsen MR, Duncker DJ, Krestin GP. In vitro imaging of single living human umbilical vein endothelial cells with a clinical 3.0-T MRI scanner. *Magma.* 2005;18:175-185.

24. Hellenthal FA, Buurman WA, Wodzig WK, Schurink GW. Biomarkers of abdominal aortic aneurysm progression. Part 2: inflammation. *Nat Rev Cardiol.* 2009;6:543-552.

25. Hellenthal FA, Buurman WA, Wodzig WK, Schurink GW. Biomarkers of AAA progression. Part 1: extracellular matrix degeneration. *Nat Rev Cardiol.* 2009;6:464-474.

26. Zhang X, Shen YH, LeMaire SA. Thoracic aortic dissection: are matrix metalloproteinases involved? *Vascular.* 2009;17:147-157.

27. Deguchi JO, Aikawa M, Tung CH, Aikawa E, Kim DE, Ntziachristos V, Weissleder R, Libby P. Inflammation in atherosclerosis: visualizing matrix metalloproteinase action in macrophages in vivo. *Circulation.* 2006;114:55-62.

28. Daugherty A, Cassis LA. Mouse models of abdominal aortic aneurysms. *Arterioscler Thromb Vasc Biol.* 2004;24:429-434.

29. Neptune ER, Frischmeyer PA, Arking DE, Myers L, Bunton TE, Gayraud B, Ramirez F, Sakai LY, Dietz HC. Dysregulation of TGF-beta activation contributes to pathogenesis in Marfan syndrome. *Nat Genet.* 2003;33:407-411.

30. Zacchigna L, Vecchione C, Notte A, Cordenonsi M, Dupont S, Maretto S, Cifelli G, Ferrari A, Maffei A, Fabbro C, Braghetta P, Marino G, Selvetella G, Aretini A, Colonnese C, Bettarini U, Russo G, Soligo S, Adorno M, Bonaldo P, Volpin D, Piccolo S, Lembo G, Bressan GM. Emilin1 links TGF-beta maturation to blood pressure homeostasis. *Cell.* 2006;124:929-942.

31. ten Dijke P, Arthur HM. Extracellular control of TGFbeta signalling in vascular development and disease. *Nat Rev Mol Cell Biol.* 2007;8:857-869.

32. Hynes RO. The extracellular matrix: not just pretty fibrils. *Science.* 2009;326:1216-1219.

33. Wang M, Zhao D, Spinetti G, Zhang J, Jiang LQ, Pintus G, Monticone R, Lakatta EG. Matrix metalloproteinase 2 activation of transforming growth factor-beta1 (TGF-beta1) and TGF-beta1-type II receptor signaling within the aged arterial wall. *Arterioscler Thromb Vasc Biol.* 2006;26:1503-1509.

34. Yu Q, Stamenkovic I. Cell surface-localized matrix metalloproteinase-9 proteolytically activates TGF-beta and promotes tumor invasion and angiogenesis. *Genes Dev.* 2000;14:163-176.

35. Kim ES, Kim MS, Moon A. TGF-beta-induced upregulation of MMP-2 and MMP-9 depends on p38 MAPK, but not ERK signaling in MCF10A human breast epithelial cells. *Int J Oncol.* 2004;25:1375-1382.

36. Seomun Y, Kim J, Lee EH, Joo CK. Overexpression of matrix metalloproteinase-2 mediates phenotypic transformation of lens epithelial cells. *Biochem J.* 2001;358:41-48.

37. Pemberton J, Sahn DJ. Imaging of the aorta. *Int J Cardiol.* 2004;97 Suppl 1:53-60.

38. Hyde D, de Kleine R, MacLaurin SA, Miller E, Brooks DH, Krucker T, Ntziachristos V. Hybrid FMT-CT imaging of amyloid-beta plaques in a murine Alzheimer's disease model. *Neuroimage.* 2009;44:1304-1311.

39. Habashi JP, Judge DP, Holm TM, Cohn RD, Loeys BL, Cooper TK, Myers L, Klein EC, Liu G, Calvi C, Podowski M, Neptune ER, Halushka MK, Bedja D, Gabrielson K, Rifkin DB, Carta L, Ramirez F, Huso DL, Dietz HC. Losartan, an AT1 antagonist, prevents aortic aneurysm in a mouse model of Marfan syndrome. *Science.* 2006;312:117-121.

2

SUPPLEMENTARY

<div align="center">Fibulin-4^{+/+}   Fibulin-4^{+/R}   Fibulin-4^{R/R}</div>
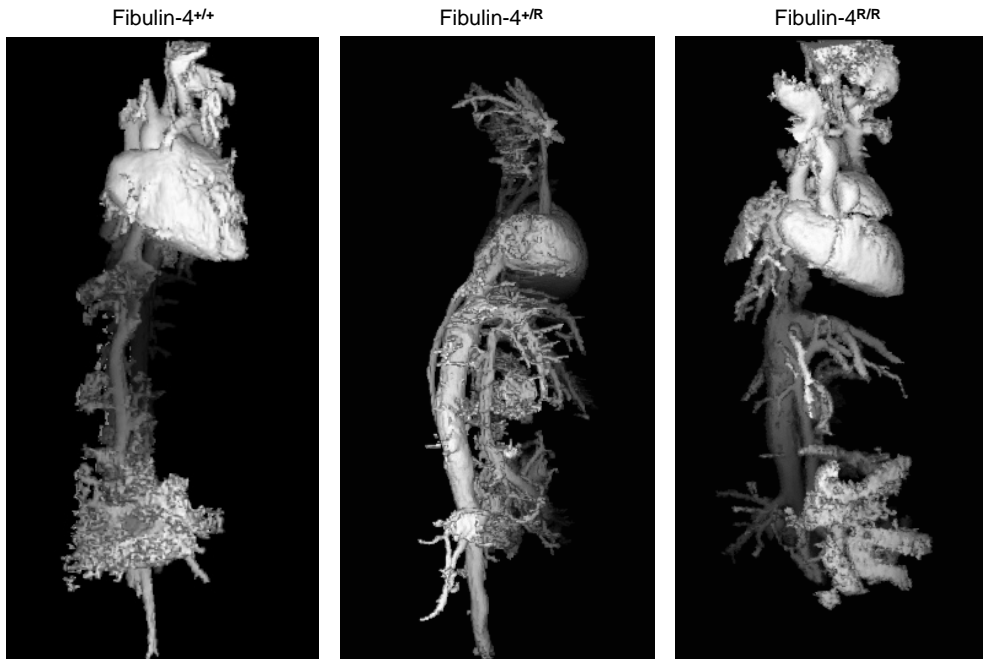
Supplemental figure 1: 3D presentation after whole body MRA. Surface rendering of a high resolution MRA acquired in living Fibulin-4$^{+/+}$, Fibulin-4$^{+/R}$ and Fibulin-4$^{R/R}$ mice using intravascular Gd-liposomes on a 3.0T clinical MRI scanner. Homozygous Fibulin-4 knockdown animals (Fibulin-4$^{R/R}$) show a severe aneurysm at the position of the aortic arch and a tortuous descending aorta.

Supplemental figures 2 and 3 are available online
http://circimaging.ahajournals.org/content/3/5/567.long

Supplemental figure 2: FMT-CT co-registration 20 hrs after injection of MMPSense 680 in a Fibulin-4$^{R/R}$ mouse. FMT-CT datasets were processed as described in material and methods section. The resulting 3D animation shows a severe aneurysm in the ascending aorta and aortic arch. The superimposed 3D fluorescence colocalizes with the aneurysmatic lesion.

Supplemental figure 3: FMT-CT co-registration 20 hrs after injection of MMPSense 680 in a Fibulin-4$^{+/R}$ mouse. FMT-CT datasets were processed as described in material and methods section. The resulting 3D animation shows that, while the diameter of the ascending aorta is unaffected, there is clear fluorescence detectable at this position.

Multimodality Imaging reveals a gradual increase in Matrix Metalloproteinase Activity at Aneurysmal Lesions in Live Fibulin-4 Mice

2

Chapter 3
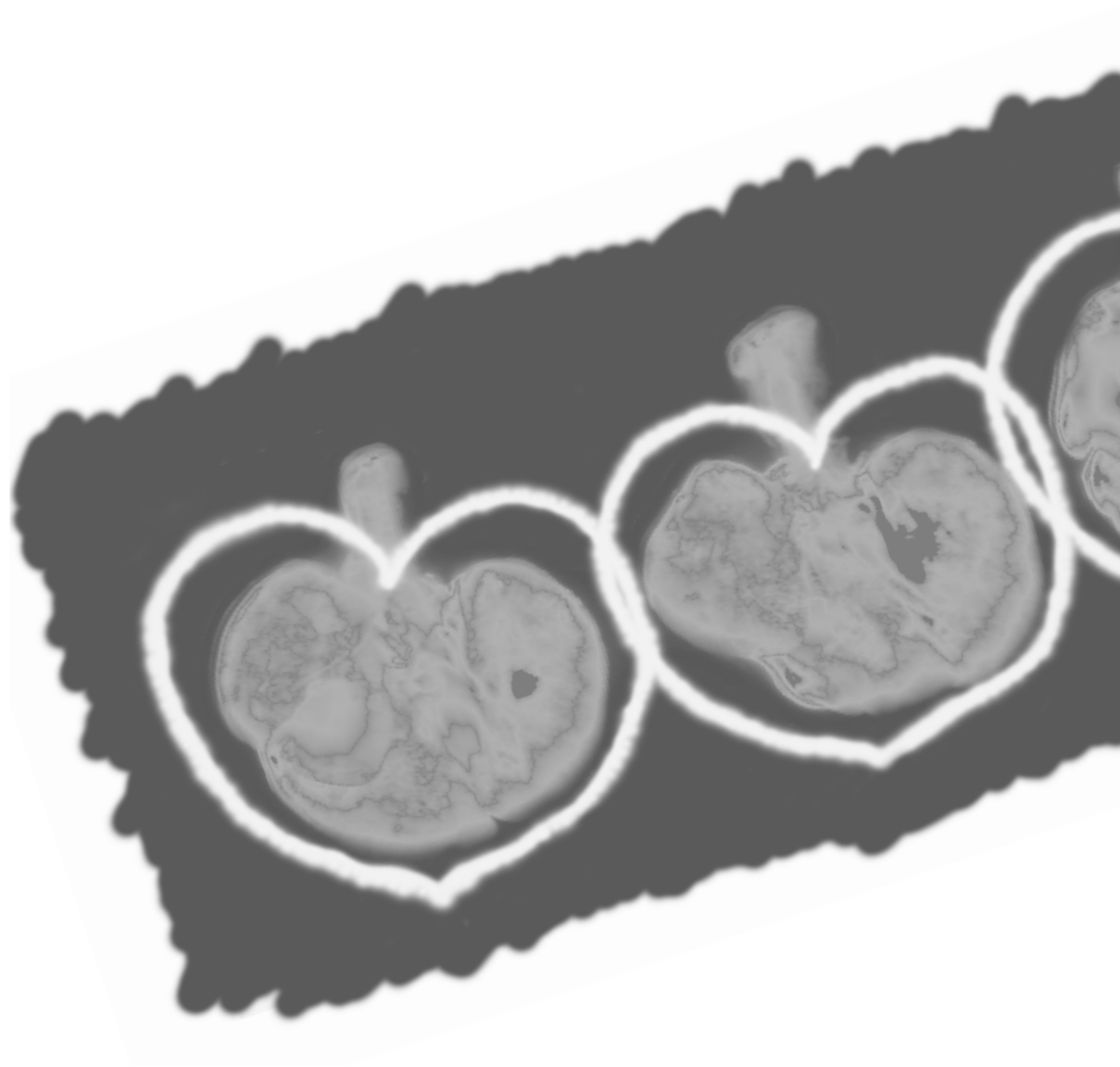
Extracellular matrix defects in aneurysmal Fibulin-4 mice predispose to lung emphysema

Natasja W.M. Ramnath[1,7],
Koen M. van de Luijtgaarden[7],
Ingrid van der Pluijm[1,7],
Menno van Nimwegen[2],
Paula M. van Heijningen[1],
Sigrid M.A. Swagemakers[1,3],
Bibi S. van Thiel[1,7,8],
Ruziedi Y. Ridwan[1,7,8],
Nicole van Vliet[1],
Marcel Vermeij[4], Luuk J.A.C. Hawinkels[9],
Anne de Munck[10], Oleh Dzyubachyk[5,11], Erik Meijering[5],
Peter van der Spek[3], Robbert Rottier[10], H. Yanagisawa[12],
Rudi W. Hendriks[2], Roland Kanaar[1,6], Ellen V. Rouwet[7],
Alex KleinJan[2], Jeroen Essers[1,6,7]

[1]Department of Cell Biology & Genetics, Cancer Genomics Centre, [2]Department of Pulmonary Diseases, [3]Department of Bioinformatics, [4]Department of Pathology, [5]Department of Medical Informatics and Department of Radiology, [6]Department of Radiation Oncology, [7]Department of Vascular Surgery, [8]Department of Pharmacology, [10]Department of Paediatric Surgery, Erasmus MC, Rotterdam, The Netherlands

[9]Department of Molecular Cell Biology and Centre for Biomedical Genetics, [11]Department of Radiology, Leiden University Medical Centre, Leiden, The Netherlands

[12]Department of Molecular Biology, University of Texas Southwestern Medical Center, Dallas, Texas, U.S.A.

ABSTRACT

***Background*:** In this study we set out to investigate the clinically observed relationship between chronic obstructive pulmonary disease (COPD) and aortic aneurysms. We tested the hypothesis that an inherited deficiency of connective tissue might play a role in the combined development of pulmonary emphysema and vascular disease.

***Methods*:** We first determined the prevalence of chronic obstructive pulmonary disease in a clinical cohort of aortic aneurysms patients and arterial occlusive disease patients. Subsequently, we used a combined approach comprising pathological, functional, molecular imaging, immunological and gene expression analysis to reveal the sequence of events that culminates in pulmonary emphysema in aneurysmal Fibulin-4 deficient (Fibulin-4^R) mice.

***Results*:** Here we show that COPD is significantly more prevalent in aneurysm patients compared to arterial occlusive disease patients, independent of smoking, other clinical risk factors and inflammation. In addition, we demonstrate that aneurysmal Fibulin-4$^{R/R}$ mice display severe developmental lung emphysema, whereas Fibulin-4$^{+/R}$ mice acquire alveolar breakdown with age and upon infectious stress. This vicious circle is further exacerbated by the diminished antiprotease capacity of the lungs and ultimately results in the development of pulmonary emphysema.

***Conclusions*:** Our experimental data identify genetic susceptibility to extracellular matrix degradation and secondary inflammation as the common mechanisms in both COPD and aneurysm formation.

3

INTRODUCTION

Chronic obstructive pulmonary disease (COPD) is worldwide one of the major causes of morbidity and mortality[1]. In addition to chronic airflow obstruction due to airway inflammation and alveolar destruction, COPD is associated with extrapulmonary manifestations, including cardiovascular diseases[2-5]. These comorbid conditions contribute to the overall disability of patients and complicate the management of COPD.

Aortic aneurysm (AA) is one of the cardiovascular diseases related to COPD[6, 7]. The nature of this relationship is currently unknown. Patients with COPD, AA, and/or atherosclerosis share a number of risk factors, including age, hypertension, and tobacco smoking[8, 9]. Resemblances in risk profiles between these conditions, most notably smoking, may account for the relation between AA and COPD. Furthermore, a systemic inflammatory response has been suggested as a common denominator[10].

The association between COPD and AA prompted us to investigate the prevalence of COPD in a large cohort of patients with aneurysmal or arterial occlusive disease (AOD) in relation to their clinical risk profiles. Here, we found that COPD is much more prevalent in patients with AA compared to those with AOD, irrespective of common clinical risk factors. Since AA[11, 12] and COPD[13] are associated with destruction of the extracellular matrix (ECM), we hypothesized that a primary ECM defect may provide a common ground for the combined development of COPD and aneurysm formation. We previously demonstrated that mice with reduced expression of the ECM glycoprotein Fibulin-4 exhibit ECM degradation in the aortic wall and AA formation[14, 15]. We here investigated the role of Fibulin-4 deficiency in the development of lung emphysema.

RESULTS

Clinical study

Patient characteristics
We included 1393 patients; 614 patients (44%) were diagnosed with AA and 779 patients (56%) with AOD. Clinical characteristics of both groups are presented in Table 1. Patients with AA were on average older and more frequently of male gender. Patients with AOD had higher rates of diabetes, hypercholesterolemia, and cerebrovascular disease. In addition, there were differences in medication use between the two groups: statins and antiplatelet drugs were more commonly used by patients with AOD, whereas beta-blockers were more often used by patients with AA. Importantly, smoking rates were similar in the two patient groups.

Association between COPD and AA
COPD was more common in AA patients as compared to AOD patients (42% vs. 26%, p<0.001, Figure 1A). Univariate logistic regression analysis showed a significant association between COPD and AA (odds ratio 2.08, 95%CI: 1.66-2.61, p<0.001; Supplemental Table 1). Since patients with COPD, AA, and AOD shared a number of cardiovascular risk factors, we subsequently performed a multivariable regression analysis. Even after adjustment for potentially confounding factors the association between COPD and AA remained significant (odds ratio 1.56, 95%CI: 1.16-2.10, p=0.003; Supplemental Table 1).

As inflammation is involved in aneurysm development, atherosclerosis, and COPD, we measured serum levels of the systemic inflammatory biomarker high-sensitivity

3

Table 1 - Clinical characteristics of patients with aortic aneurysm (AA) or arterial occlusive disease (AOD)

	AA	AOD	P-value
	n=614	n=779	
Baseline characteristics			
Male gender (%)	525 (85.5)	521 (66.9)	<0.001
Age (years ± SD)	71.4 ± 7.8	65.6 ± 11.0	<0.001
Body mass index (kg/m2, mean ± SD)	26.1 ± 3.9	26.2 ± 4.3	0.540
Cardiovascular comorbidities (%)			
Congestive heart failure	66 (10.7)	89 (11.4)	0.692
Ischemic heart disease	272 (44.3)	306 (39.3)	0.059
Cerebrovascular disease	89 (14.5)	366 (47.0)	<0.001
Cardiovascular risk factors (%)			
Kidney disease	94 (15.3)	106 (13.6)	0.368
Diabetes mellitus	103 (16.8)	225 (28.9)	<0.001
Hypertension	408 (66.4)	524 (67.2)	0.761
Hypercholesterolemia	534 (87.0)	706 (90.6)	0.030
Smoking – current	236 (38.4)	338 (43.3)	0.068
Smoking – ever	473 (77.0)	613 (78.7)	0.459
Medication (%)			
Statins	446 (72.6)	633 (81.2)	<0.001
Renin-angiotensin system inhibitors	271 (44.1)	369 (47.3)	0.247
Diuretics	138 (22.4)	211 (27.0)	0.052
Antiplatelets	353 (57.4)	581 (74.5)	<0.001

C-reactive protein (hs-CRP). The median serum hs-CRP concentration was higher in patients with AA compared to AOD (5.9 [IQR 2.9-12.5] vs 4.8 mg/L [IQR 2.1-11.1], p=0.02). However, there were no differences in hs-CRP levels between arterial disease patients with COPD and those without COPD (median 5.4 vs 5.2 mg/L, p=0.776; Figure 1B). These data strongly support the association between AA and COPD in patients independently of smoking and other cardiovascular risk factors.

Experimental study

Alveolar airspace enlargement in Fibulin-4 deficient mice
We next investigated whether ECM abnormalities may provide a common ground for COPD and aneurysm formation using Fibulin-4 deficient mice. While complete Fibulin-4 knockout mice have been described[16] and showed embryonic lethality (E12.5), we previously generated a hypomorphic Fibulin-4 allele (Fibulin4R) with reduced expression by transcriptional interference through placement of a TKneo targeting construct in a downstream gene (Mus81)[14]. Mus81 knockout mice from which the selectable marker was removed were born at expected Mendelian frequencies and were indistinguishable from wild type littermates in terms of development, growth, immune function and fertility[17].
    Fibulin-4 hypomorphic mice display a 2-fold lower expression of Fibulin-4 in
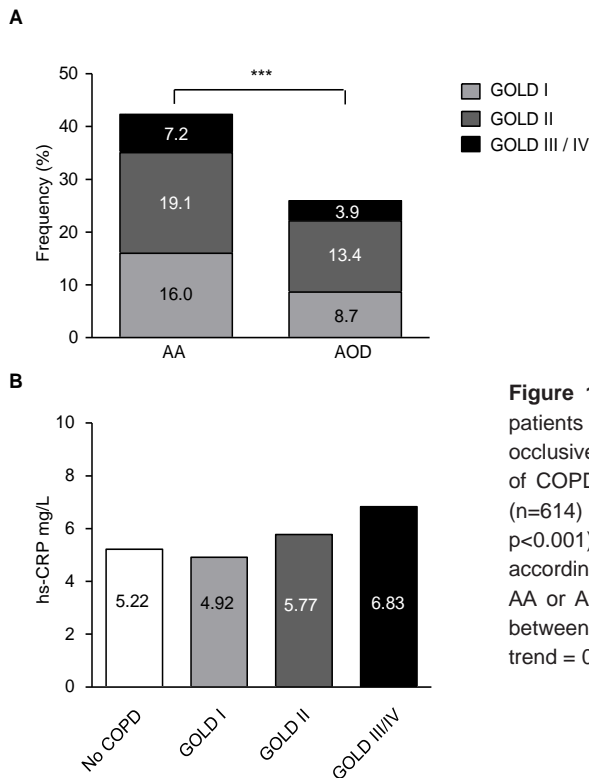
A

B

Figure 1: Prevalence and severity of COPD in patients with an aortic aneurysm (AA) or arterial occlusive disease (AOD). (A) The prevalence of COPD in all GOLD classes was higher in AA (n=614) compared to AOD patients (n=779, *** p<0.001). (B) Serum high-sensitivity CRP levels according to severity of COPD in patients with AA or AOD. There was no significant difference between patients with and without COPD (p for trend = 0.123).

Fibulin-4$^{+/R}$ aortas and a 4-fold down-regulation in Fibulin-4$^{R/R}$ aortas, resulting in ECM defects and vascular abnormalities, including AAs[14]. We now tested whether the transcriptional down-regulation of Fibulin-4 also occurs in the lungs of these mutant mice and whether Fibulin-4 animals display lung emphysema. Expression levels of Fibulin-4 mRNA in newborn and adult lungs of Fibulin-4$^{+/R}$ and Fibulin-4$^{R/R}$ mice were significantly lower compared to Fibulin-4$^{+/+}$ mice (Figure 2A).

Assessment of respiratory performance by whole-body plethysmography showed similar breathing frequencies and Peak Inspiratory Flows (PIF) after a 9-minute adaptation period in adult Fibulin-4 deficient mice and Fibulin-4$^{+/+}$ littermates, whereas the Peak Expiratory Flow (PEF) tended to decrease over time in Fibulin-4$^{R/R}$ mice (Figure 2B). Significance could not be determined since 2 out of 4 Fibulin-4$^{R/R}$ mice died during the course of the experiment.

Down-regulation of Fibulin-4 was accompanied by alveolar airspace enlargement in adult Fibulin-4$^{+/R}$ and Fibulin-4$^{R/R}$ lungs. In newborn mice, reduced pulmonary Fibulin-4 expression levels coincided with clear alveolar airspace enlargements in Fibulin-4$^{R/R}$ lungs, but not Fibulin-4$^{+/R}$ lungs (Figures 2C and 2D, Supplemental Figure 1). Immunohistochemistry on lung tissue with antibodies specific for certain lung cell markers, including thyroid transcription factor 1 (TTF-1), Clara-cell-specific protein (CC-10), and α-smooth muscle actin (α-SMA) demonstrated no differences in the presence and relative distribution of the major cell types in the lungs of Fibulin-4$^{+/R}$ and Fibulin-4$^{R/R}$ mice (Supplemental Figure 2), which may exclude altered airway-cell differentiation.
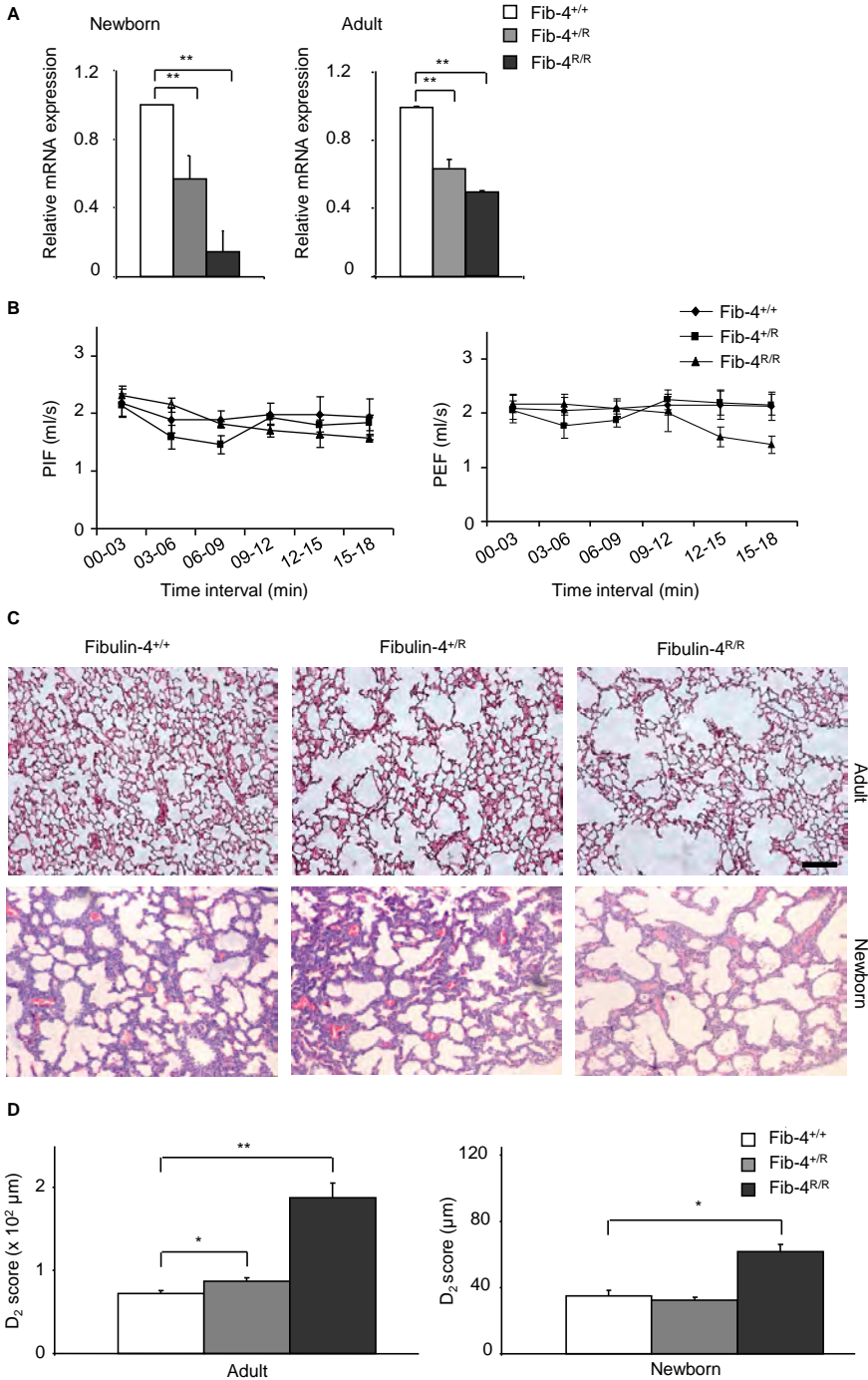
Figure 2: Enlarged alveolar airspaces in lungs of Fibulin-4 knockdown mice. (A) Expression levels of Fibulin-4 in lungs isolated from newborn (n=4, n=4, n=3) and adult (n=4, n=4, n=4) Fibulin-4+/+, Fibulin-4+/R and Fibulin-4R/R mice relative to Fibulin-4+/+ lungs (** p<0.01). (B) Mean peak inspiratory flow (PIF) and peak expiratory flow (PEF) values for Fibulin-4+/+ (n=4), Fibulin-4+/R (n=4) and Fibulin-4R/R mice (observed for n=4, but two animals died during

the procedure) at 3-minute intervals. After an adaptation period of the first three time intervals, PIF follows similar trends in Fibulin-4^{+/+}, Fibulin-4[+/R] and Fibulin-4[R/R] mice, while Fibulin-4[R/R] mice show a decrease in PEF. (C) HE stained sections of formalin fixed lungs of male mice. Enlarged alveolar airspaces are observed in Fibulin-4[+/R] (middle, n=3) and Fibulin-4[R/R] lungs (right, n=3), with the latter being more pronounced, compared to Fibulin-4^{+/+} (n=3). Enlarged alveolar airspaces are already present in Fibulin-4[R/R] newborn lungs (n=3), while lungs of Fibulin-4[+/R] littermates (n=5) show no difference compared to Fibulin-4^{+/+} lungs (n=4). Scale bar 100 μm. Magnification 10x. (D) The D_2 quantification of the alveolar airspaces revealed a significant difference between adult Fibulin-4^{+/+} and Fibulin-4[+/R] (* $p<0.05$) and between adult Fibulin-4^{+/+} and Fibulin-4[R/R] lungs (** $p<0.01$) as well as between newborn Fibulin-4^{+/+} and Fibulin-4[R/R] lungs (* $p<0.05$).

These results show that in addition to aortic abnormalities, a decrease in Fibulin-4 expression leads to gene dose-dependent alterations in the lung. While the emphysematous changes in the lungs of newborn Fibulin-4[R/R] mice suggest a developmental defect, Fibulin-4[+/R] mice acquired the COPD phenotype with age.

Transcriptome analysis of Fibulin-4[+/R] and Fibulin-4[R/R] lungs
Comparison of RNA expression between newborn Fibulin-4^{+/+}, Fibulin-4[+/R] and Fibulin-4[R/R] lungs with Significance Analysis of Microarrays (SAM) revealed a limited set of differentially regulated genes. Comparison of RNA expression between adult Fibulin-4^{+/+} and Fibulin-4[R/R] lungs using SAM (FDR 10%) revealed 374 deregulated genes, whereas no deregulated genes were found between Fibulin-4^{+/+} and Fibulin-4[+/R] lungs.

Of the 20 most significantly up-regulated genes in adult Fibulin-4[R/R] lungs, 50% were involved in inflammation processes (Table 2 and Supplemental Table 2). Network analysis with Ingenuity pathway analysis (IPA) on the 374 deregulated probes revealed many significantly deregulated pathways involved in the immune system (Supplemental

Table 2 - The most significantly up-regulated genes in adult Fibulin-4R/R lungs. Genes are indicated with their ratios compared to Fibulin-4+/+ lungs and the process involved.

Top up-regulated genes		
Genes	Ratio	Function
Arg1	3.68	Urea cycle
Slpi	3.37	Inhibitor serine proteases
Ms4a4b	2.38	T-cell regulation
Wisp2	2.26	Inhibits proliferation of vascular smooth muscle cells
Prkcb	2.03	B-cell activation, apoptosis
Emr4	1.98	Mediate between myeloid- and B-cells
Cd300a	1.92	Leukocyte cell surface proteins
Gzma	1.93	Cytotoxic T-cell and natural killer cell specific serine proteases
Klra4	1.91	Natural killer cell receptor
Nkg7	1.90	Natural killer cell granule protein
Ctsw	1.84	Regulation of T-cell cytolytic activity
Wisp1	1.83	Matrix remodelling
Lrat	1.64	Retinoid cycle
Plac8	1.81	Defence response to bacterium
Ccl5	1.78	Chemotactic cytokine and plays active role in recruiting leukocytes
Tspan32	1.73	Tumour suppressing fragment
Cyp51a1	1.70	Production of sterols
Rbm3	1.68	Temperature induced
Bcl2	1.66	Apoptosis regulator
Mef2c	1.65	Transcription factor important for vascular development

Table 3). This suggests that the severe airspace enlargement in adult Fibulin-4$^{R/R}$ lungs coincides with overexpression of genes involved in inflammatory processes.

Spontaneous inflammation in adult Fibulin-4$^{R/R}$ lungs

Flow cytometric analysis of broncho-alveolar lavage (BAL) samples showed more inflammatory cells, in particular granulocytes (Gr-1+) and B-cells (CD19+), in adult Fibulin-4$^{R/R}$ compared to Fibulin-4$^{+/+}$ and Fibulin-4$^{+/R}$ mice (Figure 3A). Cell suspensions of Fibulin-4$^{R/R}$ lungs contained significantly more macrophages (F4/80+) compared to Fibulin-4$^{+/+}$ and Fibulin-4$^{+/R}$ lungs (Figure 3B), and tended to contain more T-cells (CD3+) and dendritic cells (CD11c+). Immunohistochemical analysis showed focal infiltrations of inflammatory cells around veins and bronchi in adult Fibulin-4$^{R/R}$ lungs (Figure 3C), mainly consisting of T-cells and dendritic cells. Cytokine analysis of BAL samples showed significantly higher levels of interleukin (IL)-1β, a pro-inflammatory cytokine which is mainly produced by activated macrophages and which is increased in patients with COPD [18, 19], in Fibulin-4$^{R/R}$ but not in Fibulin-4$^{+/R}$ as compared to Fibulin-4$^{+/+}$ mice (Figure 3D). These data indicate that the severe airspace enlargement was accompanied by up-regulation of inflammatory pathways in lungs of adult Fibulin-4$^{R/R}$ mice, whereas the milder lung abnormalities in Fibulin-4$^{+/R}$ animals were not associated with an explicit inflammation process.
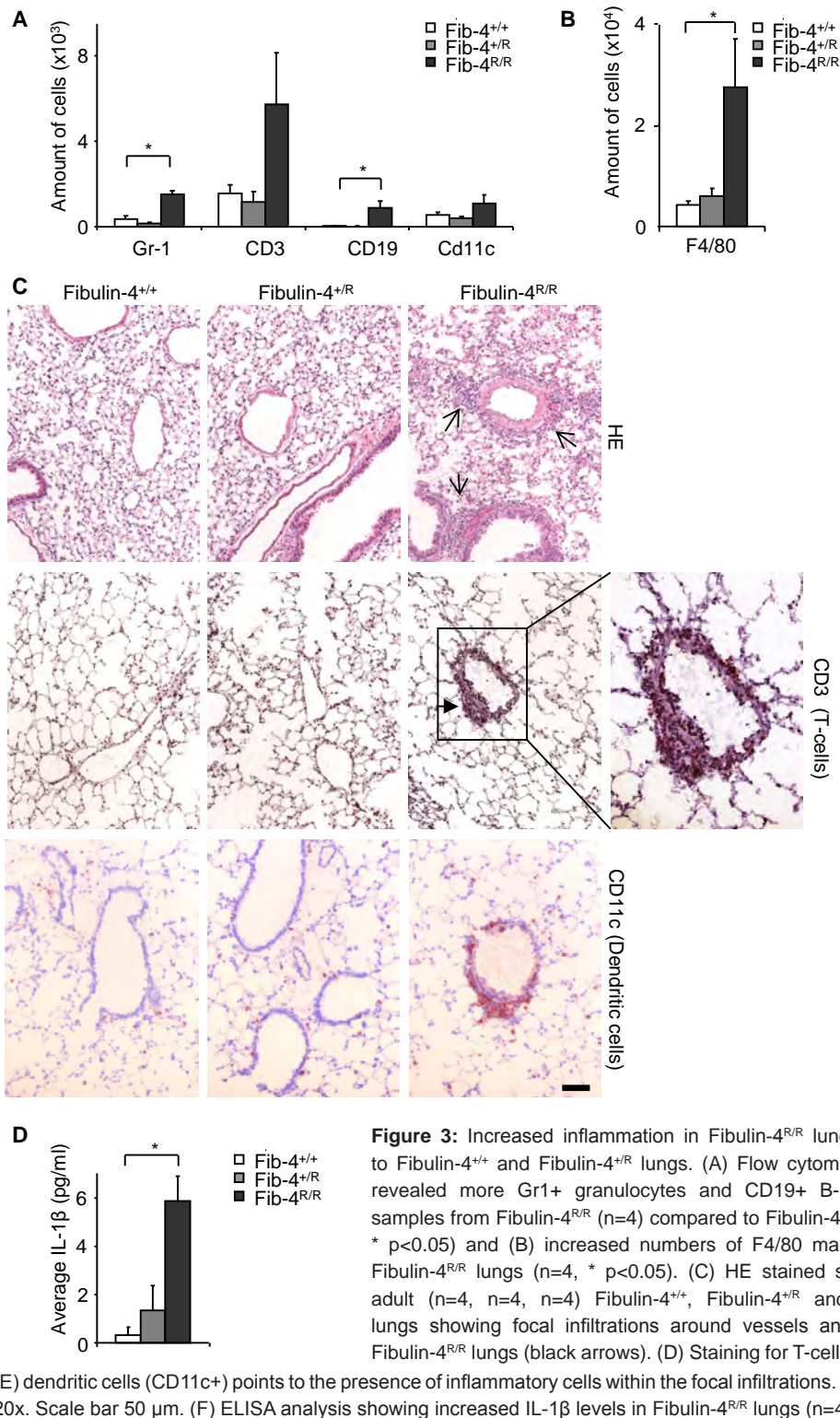
Disturbed TGF-β signalling in Fibulin-4 deficient lungs

Since degradation of the vascular wall in aortic aneurysms is related to disturbances in the TGF-β signalling pathway[14, 20], we next investigated the role of TGF- signalling in alveolar wall degradation in Fibulin-4 deficient mice. Expression analysis revealed down-regulation of the Pias4 gene in newborn Fibulin-4$^{R/R}$ compared to Fibulin-4$^{+/+}$ lungs (1.2-fold, p<0.05, Supplemental Table 4). In adults Fibulin-4$^{R/R}$ lungs we identified up-regulation of TGF-β2 and down-regulation of type 2b activin A receptor. In adult Fibulin-4$^{+/R}$ lungs the 'SMAD specific E3 ubiquitin protein ligase 1' (Smurf1) gene was significantly down-regulated compared to Fibulin-4$^{+/+}$ lungs.

Immunoblot analysis for phosphorylation of Smad2 (pSmad2), an intracellular mediator of the TGF-β pathway, showed a gradual increase in pSmad2 in adult Fibulin-4 deficient lungs, indicating increased TGF-β activity. In Fibulin-4$^{+/R}$ lungs we observed a 1.32-fold change for pSmad2 relative to total Smad and a 1.23-fold change relative to actin when compared to Fibulin-4$^{+/+}$ lungs. In Fibulin-4$^{R/R}$ lungs we observed a 1.67-fold and 1.5-fold change, respectively (Figure 4A and data not shown). Immunohistochemistry confirmed increased pSmad2 expression in Clara cells lining the bronchioles of the lungs as well as in inflammatory cell infiltrates (Figure 4B). Together these data show that TGF-β activity is mildly increased in adult Fibulin-4$^{+/R}$ and Fibulin-4$^{R/R}$ lungs, which may contribute to the breakdown of alveolar walls in adult Fibulin-4 deficient mice.

Overlapping down-regulation of SERPINA1 in lungs of Fibulin-4 deficient mice and COPD patients

To investigate a potential common underlying mechanism of the observed lung emphysema phenotype in our Fibulin-4 animals and COPD patients, we compared our mouse dataset to gene lists related to COPD and gene expression datasets from lung emphysema patients. A search in IPA with the search term 'chronic obstructive pulmonary disease' gave 248 records. Gene expression data from the comparison between Fibulin-4$^{+/+}$ and Fibulin-4$^{R/R}$ lungs (374 genes) were compared to this list of COPD-related genes in IPA, where we found an overlap of 6 genes: PDE3B (1.28 ↑), HCK (1.55 ↑), PRF1 (1.47 ↑), SERPINA1 (1.38 ↓),

Figure 3: Increased inflammation in Fibulin-4[R/R] lungs compared to Fibulin-4^{+/+} and Fibulin-4[+/R] lungs. (A) Flow cytometric analysis revealed more Gr1+ granulocytes and CD19+ B-cells in BAL samples from Fibulin-4[R/R] (n=4) compared to Fibulin-4^{+/+} mice (n=4, * p<0.05) and (B) increased numbers of F4/80 macrophages in Fibulin-4[R/R] lungs (n=4, * p<0.05). (C) HE stained sections from adult (n=4, n=4, n=4) Fibulin-4^{+/+}, Fibulin-4[+/R] and Fibulin-4[R/R] lungs showing focal infiltrations around vessels and airways in Fibulin-4[R/R] lungs (black arrows). (D) Staining for T-cells (CD3+) and (E) dendritic cells (CD11c+) points to the presence of inflammatory cells within the focal infiltrations. Magnification 20x. Scale bar 50 μm. (F) ELISA analysis showing increased IL-1β levels in Fibulin-4[R/R] lungs (n=4, * p<0.05).
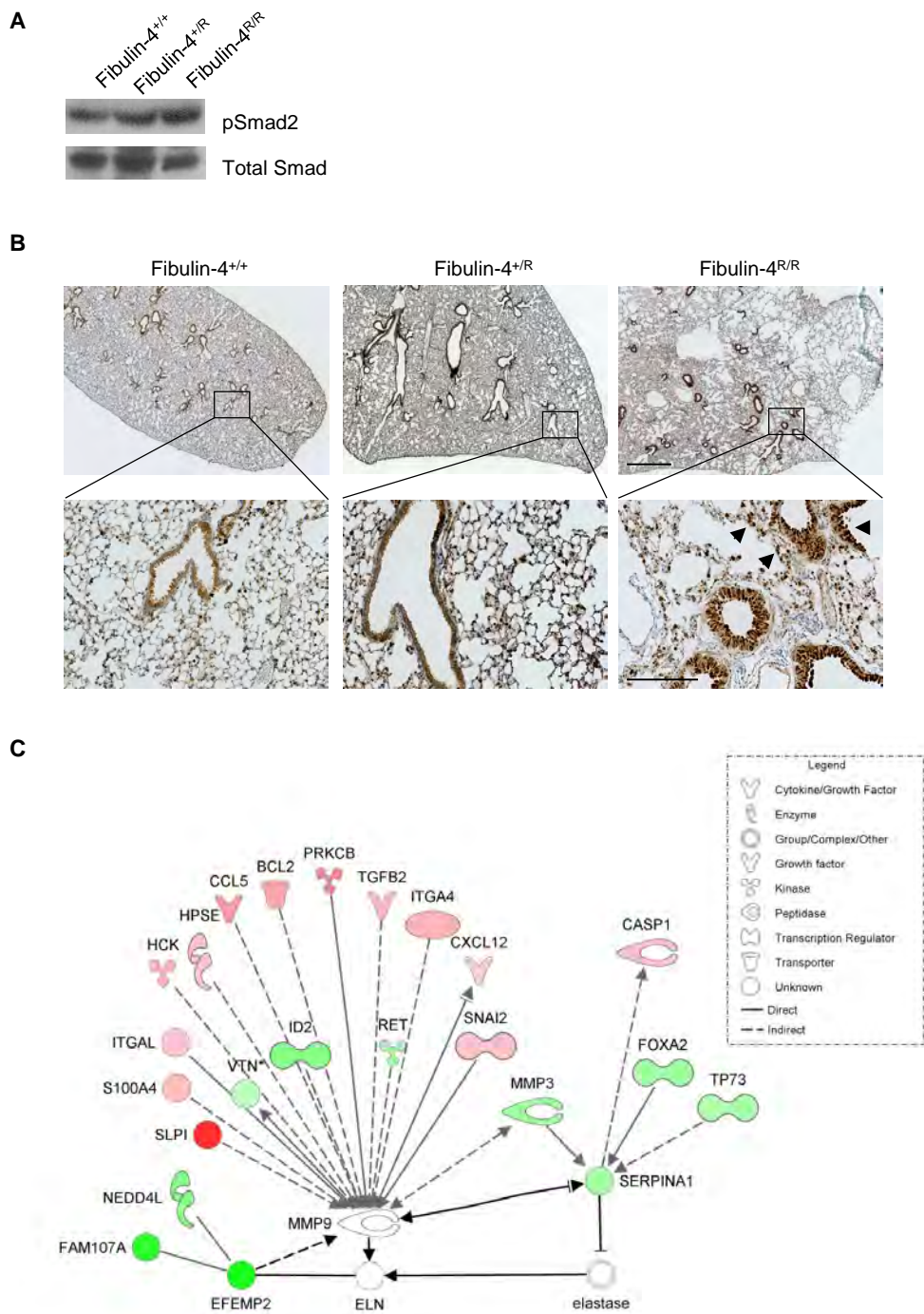
A

B

C

Figure 4: Increased TGF-β signalling in Fibulin-4[+/R] and Fibulin-4[R/R] lungs. (A) Immuno blot analysis of pSmad2 in lung homogenates shows an increase in the amount of pSmad2 in Fibulin-4[+/R] (n=3) and Fibulin-4[R/R] (n=3) lungs, compared to the total amount of Smad, and to their Fibulin-4^{+/+} control (n=3). (B) Increased pSmad2 staining of

inflammatory and endogenous cells on Fibulin-4$^{+/R}$ (n=3) and Fibulin-4$^{R/R}$ (n=3) lung sections. Magnification 2.5x (scale bar 1 mm) upper panel and 20x (scale bar 200 µm) lower panel. (C) Ingenuity pathway explorer showed MMP9 as the shortest connection between Fibulin-4 and SERPINA1. SERPINA1 inhibits neutrophil elastase, which affects elastin. MMP9 itself was not deregulated in Fibulin-4$^{R/R}$ lungs (n=4), but could be connected to 16 deregulated genes in Fibulin-4$^{R/R}$ compared to Fibulin-4$^{+/+}$ lungs (n=4, red, up-regulated; green, down-regulated). Black arrows indicate the connection between Fibulin-4 (EFEMP2), MMP9, SERPINA1, elastase and ELN. Grey arrows indicate the connection of these genes with deregulated genes between Fibulin-4$^{+/+}$ and Fibulin-4$^{R/R}$ lungs.

FGFR3 (1.28 ↓), and EFEMP2 (i.e. Fibulin-4, 3.57 ↓). Comparison of our mouse lung gene expression data to GEO dataset GSE8581 of lung emphysema patients showed an overlap of ITPKC (1.28 ↓), KIAA1377 (1.45 ↓), and SERPINA1 (1.38 ↓). Interestingly, these two independent methods both identified SERPINA1 as an overlapping down-regulated gene. SERPINA1 encodes for the serine protease inhibitor α-1 antitrypsin, whose targets include elastase. Local expression by airway epithelial cells has been detected in gene expression studies. The gene portal bioGPS identified expression of α-1 antitrypsin in the lung in the human Geneatlas U133A and mouse GeneAtlas MOE430 datasets. In addition, deficiency in α-1 antitrypsin in patients is associated with lung emphysema[21, 22].

SERPINA1 was 1.38-fold down-regulated in Fibulin-4$^{R/R}$ lungs and 1.59-fold down-regulated in Fibulin-4$^{+/R}$ lungs compared to Fibulin-4$^{+/+}$ lungs (p<0.01). We used Path explorer in IPA that identifies pathways between differentially expressed genes, in order to determine the relation between Fibulin-4 and SERPINA1. By calculating the shortest path between Fibulin-4 (EFEMP2) and SERPINA1, an indirect connection of Fibulin-4 to MMP9 and a direct connection of MMP9 to SERPINA1 was revealed, as indicated by the black arrows in Figure 4C[14, 23, 24]. Surprisingly, by connecting Fibulin-4, MMP9 and SERPINA1 both direct and indirect to deregulated genes from the SAM comparison between Fibulin-4$^{+/+}$ and Fibulin-4$^{R/R}$ lungs (grey arrows), we found an interaction of 16 significantly deregulated genes from our dataset with MMP9 (Figure 4C). Since our gene expression analysis did not show a deregulation of MMP9 at the mRNA level, we next investigated MMP9 protein activity in Fibulin-4$^{R/R}$ and Fibulin-4$^{+/R}$ lungs.

Increased MMP and neutrophil elastase activity in Fibulin-4 deficient lungs
Fluorescent imaging using protease activatable probes showed increased pulmonary MMP activity in adult Fibulin-4 deficient mice (Figure 5A). The observed decrease in the elastase inhibitor SERPINA1 and the increased MMP activity, which is associated with cleavage of α-1 antitrypsin[23], might lead to increased activity of neutrophil elastase (NE). Indeed, we observed a graded increase in NE activity in adult Fibulin-4$^{+/R}$ and Fibulin-4$^{R/R}$ lungs compared to Fibulin-4$^{+/+}$ lungs (Figures 5B and C). In line with this, pulmonary elastin staining demonstrated interruptions in the elastin layers in Fibulin-4$^{+/R}$ lungs and even more in Fibulin-4$^{R/R}$ lungs compared to those of Fibulin-4$^{+/+}$ animals (Figure 5D), as previously found in the aortas of these mice[14]. Newborn Fibulin-4$^{R/R}$ lungs also displayed elastin abnormalities, while newborn Fibulin-4$^{+/R}$ lungs were comparable to those of Fibulin-4$^{+/+}$ mice (data not shown).

Increased and prolonged inflammatory response in LPS exposed Fibulin-4$^{+/R}$ mice
Fibulin-4$^{+/R}$ mice developed alveolar airspace enlargement with age together with increased MMP9 and NE activity in the absence of inflammation. However, when adult Fibulin-4$^{+/R}$ lungs were triggered by LPS, flow cytometric analyses of BAL samples and pulmonary cell suspensions showed an increased and prolonged inflammatory response as compared to Fibulin-4$^{+/+}$ mice. There was a significantly greater influx of macrophages (F4/80+) in the lungs 18 hours after LPS exposure and significantly higher numbers of dendritic
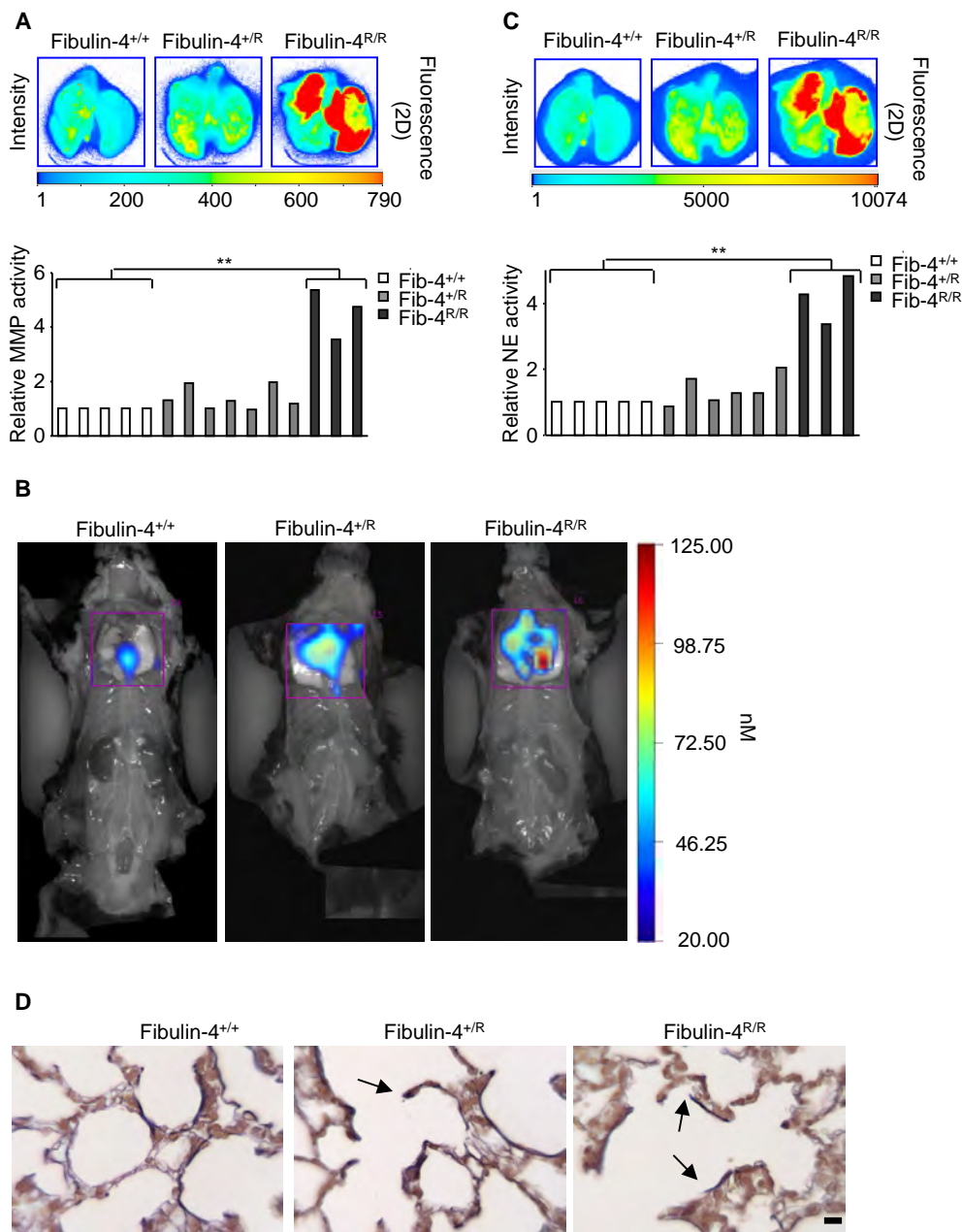
Figure 5: Higher MMP and NE activity in Fibulin-4$^{+/R}$ and Fibulin-4$^{R/R}$ lungs. (A) and (C) Ex-vivo imaging of excised lungs using Odyssey shows increased activity of MMP and NE respectively in Fibulin-4$^{+/R}$ (n=7) and Fibulin-4$^{R/R}$ lungs (observed for n=5, but two animals died during the procedure) as compared to Fibulin-4$^{+/+}$ lungs (n=5), with a significant upregulation for Fibulin-4$^{R/R}$ lungs (** p<0.01). (B) Open-chest registration of NE activity with Neutrophil Elastase FAST 680 probes shows increased activity in Fibulin-4$^{+/R}$ and Fibulin-4$^{R/R}$ lungs as compared to Fibulin-4$^{+/+}$ lungs. (D) Elastin staining of Fibulin-4$^{+/+}$, Fibulin-4$^{+/R}$ and Fibulin-4$^{R/R}$ lungs (n=3, n=3, n=3) shows fragmented elastin layers in Fibulin-4$^{+/R}$ and Fibulin-4$^{R/R}$ lungs, indicated by arrows. Magnification 40x. Scale bar 10 μm.

cells (CD11c+), T-cells (CD3+), and granulocytes (GR1+) 72 hours after LPS exposure (Figure 6 and Supplemental Figure 3). Moreover, opposite dynamics were observed; in the Fibulin-4+/+ lungs the amount of GR-1+ cells decreased after 18 hours, while an increase was observed in Fibulin-4+/R lungs 72 hours after LPS exposure. The increase of inflammatory cells after LPS exposure was significantly higher when compared to PBS. The levels of pro-inflammatory cytokines released upon LPS exposure, including IL-1β, TNF-α, and keratinocyte-derived chemokine, were not different between groups (data not shown). These data indicate that Fibulin-4+/R mice exhibit an intensified inflammatory response in the lungs.

DISCUSSION

In this study we show that COPD is more common in patients with AA than in patients with atherosclerotic arterial disease. This relationship was independent of cigarette smoking and other known risk factors. Furthermore, there was no difference in serum hs-CRP levels between patients with and without COPD, indicating that inflammation per se is unlikely to account for the observed relation between COPD and AA. The findings in this large patient cohort are in line with previous observations of reduced respiratory function in smaller series of AAA patients[6, 7, 10]. However, our findings suggest that factors other than cardiovascular risk profiles or systemic inflammation contribute to the association between COPD and AA.
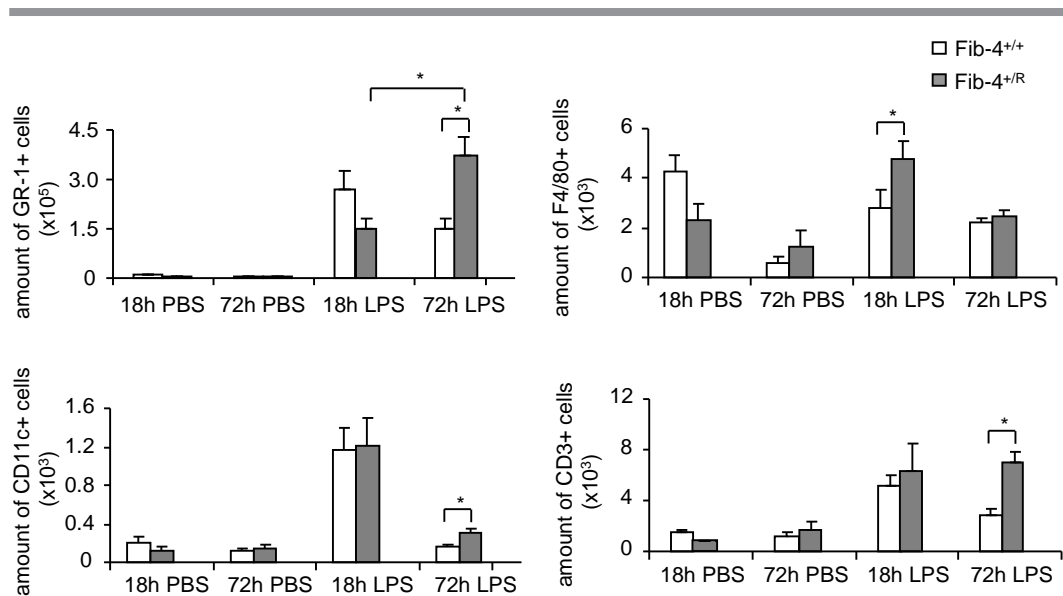

Figure 6: Increased and prolonged inflammatory response in LPS exposed Fibulin-4+/R mice. Quantification of immune cells shows significantly increased F4/80+ cells after 18 hours of LPS exposure in Fibulin-4+/R lungs (n=4) and a significantly higher number of Gr1+, CD11c+, and CD3+ cells after 72 hours of LPS exposure as compared to Fibulin-4+/+ lungs (n=4, * p<0.05).

Since both diseases, COPD and AA, are characterized by breakdown of the ECM in the airways and –spaces and in the aortic wall, we investigated whether a primary ECM defect provides the pathogenic link between these two diseases. Analogous to the previously observed degradation of the aortic wall and formation of AAs in mice deficient in the ECM component Fibulin-4, we found that gradual down-regulation of Fibulin-4 in the lungs correlated with destruction of alveolar walls and airspace enlargement that is characteristic for lung emphysema. Similar to embryonically lethal, complete Fibulin-4 knockout mice[16], in Fibulin-4$^{R/R}$ mice alveolar breakdown was already present in newborn lungs, and became progressive with age. In contrast, Fibulin-4$^{+/R}$ mice, which have only a 2-fold reduction in the amount of Fibulin-4, had normal elastin structures and alveolar airspaces at birth, but acquired alveolar breakdown with ageing.

Analogous to the activation of the TGF-β pathway in the aortas of the Fibulin-4 deficient mice[14], we here demonstrate enhanced activation of the TGF-β pathway in the lungs of Fibulin-4$^{+/R}$ and Fibulin-4$^{R/R}$ mice. The co-occurrence of lung emphysema and vascular abnormalities in association with deregulated TGF-β signalling has also been shown in another mouse model with a deficiency in an ECM protein, for example mice with mutations in the ECM protein Fibrillin-1 which are a model for Marfan syndrome[25]. Moreover, the co-occurrence of lung abnormalities and aortic aneurysms coinciding with upregulation of TGF-β signalling has also been shown in patients with Fibulin-4 mutations[26]. The role for TGF-β in this process is further supported by the development of progressive airspace enlargement in Smad3 knockout mice, which are deficient for an intracellular regulator of the TGF-β pathway[27]. Overall, these data point to deregulated TGF- signalling and ECM defects as common underlying factors for aortic and pulmonary abnormalities.

Expression analysis further revealed down-regulation of the SERPINA1 gene, encoding for the serine protease inhibitor α-1 antitrypsin whose targets include elastase. Interestingly, overlapping gene expression profiles of our Fibulin-4 deficient mice with those of COPD patients revealed down-regulation of SERPINA1 as a common denominator. As it is known that patients with α-1 antitrypsin deficiency develop COPD[21, 28] we explored the link between SERPINA1 and Fibulin-4. Pathway exploration in IPA revealed a direct link to MMP9, TGF-β deregulation and 15 other deregulated genes from our dataset. Although MMP9 itself was not overexpressed, molecular imaging showed that the MMP activity was gradually higher in Fibulin-4$^{+/R}$ and Fibulin-4$^{R/R}$ lungs. In line with the observed downregulation of SERPINA1, fluorescent imaging showed a gradual upregulation of elastase in Fibulin-4$^{+/R}$ and Fibulin-4$^{R/R}$ lungs, which correlated with elastin fragmentation. The decreased expression of SERPINA1 may either be a direct effect of Fibulin-4 deficiency, or indirectly through its cleavage by MMP9[23]. This combination of increased protease activity and decreased antiprotease activity may account for the breakdown of alveolar walls, resulting in emphysema.

Another hallmark of adult Fibulin-4 mice was the inflammatory response in the lungs. Lungs of adult Fibulin-4$^{R/R}$ mice already displayed pulmonary inflammation in a specific pathogen free environment, including influx of a wide range of inflammatory cells with elevated levels of the pro-inflammatory cytokine IL-1β, which coincided with the overexpression of genes involved in inflammatory pathways. In contrast, adult Fibulin-4$^{+/R}$ animals did not exhibit pulmonary inflammation under baseline conditions, but displayed an enhanced respiratory inflammatory response upon LPS inhalation. These findings indicate that although inflammation may contribute to the progressive breakdown of alveolar walls in adult Fibulin-4$^{R/R}$ mice, it is unlikely to be the primary causative factor in Fibulin-4$^{+/R}$ mice. Conversely, ECM degradation by proteases is known to induce the

3

release of bioactive fragments that may act as chemo-attractants for leukocytes and modulate the activity of resident immune cells[29]. Our data suggest that a mild Fibulin-4 deficiency induces disruption of the ECM, which subsequently predisposes to an enhanced inflammatory response with further breakdown of alveolar walls. This vicious circle is further exacerbated by the diminished antiprotease capacity of the lungs and ultimately results in the development of pulmonary emphysema. The Fibulin-4$^{R/R}$ mouse can therefore provide as a model for adverse lung development, while the heterozygous Fibulin-4$^{+/R}$ mouse may serve as a postnatal challenge model.

The traditional inflammatory model of COPD proposes that in susceptible patients cigarette smoking leads to inflammation, which subsequently induces loss of ECM and alveoli, resulting in airspace enlargement. We propose that genetic ECM defects are one of the initiating events contributing to this susceptibility, which are associated with a heightened inflammatory response to environmental triggers, such as microorganisms and smoking. Such a generalized genetic susceptibility to ECM degradation and secondary inflammation in combination with increased protease activity and decreased anti-protease activity might be the common pathophysiologic mechanism underlying the tissue destruction in both COPD and aneurysm formation. Genetic screening for mutations related to ECM defects may be a new strategy to identify people at risk for developing both aneurysms and COPD with age.

3

ACKNOWLEDGEMENTS

REFERENCES

[1]   WHO. World health report: Chronic Obstructive Pulmonary Disease. 2007 [cited; Available from: www.who.int/respiratory/copd

[2]   Mannino DM, Thorn D, Swensen A, Holguin F. Prevalence and outcomes of diabetes, hypertension and cardiovascular disease in COPD. Eur Respir J. 2008 Oct;32(4):962-9.

[3]   Anthonisen NR, Connett JE, Enright PL, Manfreda J. Hospitalizations and mortality in the Lung Health Study. Am J Respir Crit Care Med. 2002 Aug 1;166(3):333-9.

[4]   Fabbri LM, Luppi F, Beghe B, Rabe KF. Complex chronic comorbidities of COPD. Eur Respir J. 2008 Jan;31(1):204-12.

[5]   Corsonello A, Antonelli Incalzi R, Pistelli R, Pedone C, Bustacchini S, Lattanzio F. Comorbidities of chronic obstructive pulmonary disease. Curr Opin Pulm Med. 2011 Dec;17 Suppl 1:S21-8.

[6]   Meijer CA, Kokje VB, van Tongeren RB, Hamming JF, van Bockel JH, Moller GM, Lindeman JH. An Association between Chronic Obstructive Pulmonary Disease and Abdominal Aortic Aneurysm beyond Smoking: Results from a Case-control Study. Eur J Vasc Endovasc Surg. 2012 Jun 14.

[7]   Sakamaki F, Oya H, Nagaya N, Kyotani S, Satoh T, Nakanishi N. Higher prevalence of obstructive airway disease in patients with thoracic or abdominal aortic aneurysm. J Vasc Surg. 2002 Jul;36(1):35-40.

[8]   Reed D, Reed C, Stemmermann G, Hayashi T. Are aortic aneurysms caused by atherosclerosis? Circulation. 1992 Jan;85(1):205-11.

[9]   Johnsen SH, Forsdahl SH, Singh K, Jacobsen BK. Atherosclerosis in abdominal aortic aneurysms: a causal event or a process running in parallel? The Tromso study. Arterioscler Thromb Vasc Biol. 2010 Jun;30(6):1263-8.

[10]   Fowkes FG, Anandan CL, Lee AJ, Smith FB, Tzoulaki I, Rumley A, Powell JT, Lowe GD. Reduced lung function in patients with abdominal aortic aneurysm is associated with activation of inflammation and hemostasis, not smoking or cardiovascular disease. J Vasc Surg. 2006 Mar;43(3):474-80.

[11]   Lindsay ME, Dietz HC. Lessons on the pathogenesis of aneurysm from heritable conditions. Nature. 2011 May 19;473(7347):308-16.

[12]   Antoniou GA, Georgiadis GS, Antoniou SA, Granderath FA, Giannoukas AD, Lazarides MK. Abdominal aortic aneurysm and abdominal wall hernia as manifestations of a connective tissue disorder. J Vasc Surg. 2011 Oct;54(4):1175-81.

[13]   Wendel DP, Taylor DG, Albertine KH, Keating MT, Li DY. Impaired distal airway development in mice lacking elastin. Am J Respir Cell Mol Biol. 2000 Sep;23(3):320-6.

[14]   Hanada K, Vermeij M, Garinis GA, de Waard MC, Kunen MG, Myers L, Maas A, Duncker DJ, Meijers C, Dietz HC, Kanaar R, Essers J. Perturbations of vascular homeostasis and aortic valve abnormalities in fibulin-4 deficient mice. Circ Res. 2007 Mar 16;100(5):738-46.

[15]   Kaijzel EL, van Heijningen PM, Wielopolski PA, Vermeij M, Koning GA, van Cappellen WA, Que I, Chan A, Dijkstra J, Ramnath NW, Hawinkels LJ, Bernsen MR, Lowik CW, Essers J. Multimodality imaging reveals a gradual increase in matrix metalloproteinase activity at aneurysmal lesions in live fibulin-4 mice. Circ Cardiovasc Imaging. 2010 Sep;3(5):567-77.

[16]   McLaughlin PJ, Chen Q, Horiguchi M, Starcher BC, Stanton JB, Broekelmann TJ, Marmorstein AD, McKay B, Mecham R, Nakamura T, Marmorstein LY. Targeted disruption of fibulin-4 abolishes elastogenesis and causes perinatal lethality in mice. Mol Cell Biol. 2006 Mar;26(5):1700-9.

[17]   Dendouga N, Gao H, Moechars D, Janicot M, Vialard J, McGowan CH. Disruption of murine Mus81 increases genomic instability and DNA damage sensitivity but does not promote tumorigenesis. Mol Cell Biol. 2005 Sep;25(17):7569-79.

[18]   Lappalainen U, Whitsett JA, Wert SE, Tichelaar JW, Bry K. Interleukin-1beta causes pulmonary inflammation, emphysema, and airway remodeling in the adult murine lung. Am J Respir Cell Mol Biol. 2005 Apr;32(4):311-8.

[19]   Pauwels NS, Bracke KR, Dupont LL, Van Pottelberge GR, Provoost S, Vanden Berghe T, Vandenabeele P, Lambrecht BN, Joos GF, Brusselle GG. Role of IL-1alpha and the Nlrp3/caspase-1/IL-1beta axis in cigarette smoke-induced pulmonary inflammation and COPD. Eur Respir J. 2011 Nov;38(5):1019-28.

[20]   Lindsay ME, Schepers D, Bolar NA, Doyle JJ, Gallo E, Fert-Bober J, Kempers MJ, Fishman

EK, Chen Y, Myers L, Bjeda D, Oswald G, Elias AF, Levy HP, Anderlid BM, Yang MH, Bongers EM, Timmermans J, Braverman AC, Canham N, Mortier GR, Brunner HG, Byers PH, Van Eyk J, Van Laer L, Dietz HC, Loeys BL. Loss-of-function mutations in TGFB2 cause a syndromic presentation of thoracic aortic aneurysm. Nat Genet. 2012;44(8):922-7.

[21]   Greene CM, Hassan T, Molloy K, McElvaney NG. The role of proteases, endoplasmic reticulum stress and SERPINA1 heterozygosity in lung disease and alpha-1 anti-trypsin deficiency. Expert Rev Respir Med. 2011 Jun;5(3):395-411.

[22]   Wu C, Orozco C, Boyer J, Leglise M, Goodale J, Batalov S, Hodge CL, Haase J, Janes J, Huss JW, 3rd, Su AI. BioGPS: an extensible and customizable portal for querying and organizing gene annotation resources. Genome Biol. 2009;10(11):R130.

[23]   Liu Z, Zhou X, Shapiro SD, Shipley JM, Twining SS, Diaz LA, Senior RM, Werb Z. The serpin alpha1-proteinase inhibitor is a critical substrate for gelatinase B/MMP-9 in vivo. Cell. 2000 Sep 1;102(5):647-55.

[24]   Lapierre M, Siegfried G, Scamuffa N, Bontemps Y, Calvo F, Seidah NG, Khatib AM. Opposing function of the proprotein convertases furin and PACE4 on breast cancer cells' malignant phenotypes: role of tissue inhibitors of metalloproteinase-1. Cancer Res. 2007 Oct 1;67(19):9030-4.

[25]   Neptune ER, Frischmeyer PA, Arking DE, Myers L, Bunton TE, Gayraud B, Ramirez F, Sakai LY, Dietz HC. Dysregulation of TGF-beta activation contributes to pathogenesis in Marfan syndrome. Nat Genet. 2003 Mar;33(3):407-11.

[26]   Renard M, Holm T, Veith R, Callewaert BL, Ades LC, Baspinar O, Pickart A, Dasouki M, Hoyer J, Rauch A, Trapane P, Earing MG, Coucke PJ, Sakai LY, Dietz HC, De Paepe AM, Loeys BL. Altered TGFbeta signaling and cardiovascular manifestations in patients with autosomal recessive cutis laxa type I caused by fibulin-4 deficiency. Eur J Hum Genet. 2010 Aug;18(8):895-901.

[27]   Bonniaud P, Kolb M, Galt T, Robertson J, Robbins C, Stampfli M, Lavery C, Margetts PJ, Roberts AB, Gauldie J. Smad3 null mice develop airspace enlargement and are resistant to TGF-beta-mediated pulmonary fibrosis. J Immunol. 2004 Aug 1;173(3):2099-108.

[28]   Stoller JK, Aboussouan LS. A review of alpha1-antitrypsin deficiency. Am J Respir Crit Care Med. 2012 Feb 1;185(3):246-59.

[29]   Taraseviciene-Stewart L, Voelkel NF. Molecular pathogenesis of emphysema. J Clin Invest. 2008 Feb;118(2):394-402.

3

SUPPLEMENTARY

MATERIAL AND METHODS

Clinical study

Patients
Consecutive patients undergoing elective open or endovascular surgery for aortic aneurysm, peripheral arterial disease, or carotid artery disease between 2002 and 2011 in the Erasmus MC, Rotterdam were included. Patients with an aortic aneurysm (AA) were classified as aneurysmal disease. Patients with atherosclerotic peripheral arterial or carotid artery disease were classified as arterial occlusive disease (AOD). Patients treated with combined AA and symptomatic AOD and patients with a genetic aneurysm syndrome like Marfan, Loeys-Dietz or vascular Ehlers-Danlos syndrome were excluded. The study complies with the declaration of Helsinki and was approved by the Institutional Review Board.

Clinical characteristics
Medical history was obtained from every patient, including the cardiovascular risk factors age, gender, body mass index (BMI), smoking status, hypertension (blood pressure ≥140/90 mmHg in non-diabetics, ≥130/80 mmHg in diabetics, or use of antihypertensive medication), hypercholesterolemia (low-density lipoprotein [LDL] cholesterol ≥3.5 mmol/L or use of lipid lowering medication), diabetes mellitus (fasting plasma glucose ≥7.0 mmol/L, non-fasting glucose ≥11.1 mmol/L, or use of anti-diabetic medication), and kidney disease (serum creatinine ≥2.0 mg/dl). Cardiovascular comorbidities were recorded, including congestive heart failure (defined as history of congestive heart failure), ischemic heart disease (defined as a history of angina pectoris, myocardial infarction, coronary revascularisation, or presence of pathologic Q-waves on the electrocardiogram), cerebrovascular disease (defined as a history of ischemic/haemorrhagic stroke or transient ischemic attack). Prescription medications were recorded and included the use of statins, beta-blockers, renin-angiotensin system inhibitors, diuretics, and antiplatelet drugs. Serum concentrations of the inflammatory biomarker high-sensitivity C-reactive protein (hs-CRP) were measured prior to surgery using immunochemistry (Beckman Coulter, Woerden, the Netherlands).

Chronic obstructive pulmonary disease
The diagnosis and classification of COPD was made using spirometry, which was part of the routine preoperative workup and was obtained in 92% of COPD patients. COPD was defined as the presence of a forced expiratory volume in one second (FEV1) to forced vital capacity (FVC) ratio (FEV1/FVC) <0.70. In the presence of a FEV1/FVC ratio of <0.70, mild COPD was defined as a FEV1 >80% of the predicted FEV1 (GOLDI), moderate COPD was defined as a FEV1 of 50-80% of the predicted FEV1 (GOLDII), and severe COPD was defined as a FEV1 <50% of the predicted FEV1[1]. Patients without spirometry were classified based on the presence of pulmonary symptoms (i.e. cough, dyspnea, sputum) and the use of pulmonary medication.

Statistical analysis
Dichotomous data are presented as numbers and percentages. Continuous variables are presented as mean ± standard deviation or median and IQR when not normally distributed. Categorical data were analysed with chi-square tests and continuous variables with

ANOVA or Kruskal-Wallis tests. Multivariable binary logistic regression analysis was used to calculate odds for having COPD between AA and AOD. Adjustments were made for age, gender, BMI, congestive heart failure, ischemic heart disease, cerebrovascular disease, kidney disease, diabetes mellitus, hypertension, hypercholesterolemia, smoking, statins, beta-blockers, renin-angiotensin system inhibitors, diuretics, antiplatelets, and hs-CRP. Furthermore, we performed a propensity score to adjust for the possibility of receiving a pulmonary function test prior to surgery. Covariates were chosen on the bases of biological plausibility. For all tests, a p-value <0.05 (two-sided) was considered significant. All analyses were performed using IBM SPSS Statistics version 20.0 (SPSS Inc., Chicago, IL, USA).

Experimental study

Animals

Fibulin-4 animals were generated as previously described[2]. All mice used were bred in a C57Bl/6J background and were kept in individually ventilated cages to keep animals consistently micro-flora and disease free. To avoid stress-related vascular injury, mice were earmarked and genotyped 4 weeks after birth. Mice used were either newborn or adult (110 ± 10 days). Adult mice were challenged by a single intratracheal injection with either 80 µl ultra-pure, sterile Lipopolysaccharide (LPS) 1 mg/ml from *E. coli* Serotype R515 (Alexis Corporation Switzerland) or 80 µl PBS (Lonza). Animals were housed at the Animal Resource Centre (Erasmus University Medical Centre), which operates in compliance with the "Animal Welfare Act" of the Dutch government, using the "Guide for the Care and Use of Laboratory Animals" as its standard. As required by Dutch law, formal permission to generate and use genetically modified animals was obtained from the responsible local and national authorities. All animal studies were approved by an independent Animal Ethical Committee (Dutch equivalent of the IACUC).

Quantitative real time PCR

RNA was isolated using the RNeasy minikit from Qiagen according to the provided protocol and synthesized to cDNA with the RevertAid H Minus First Strand cDNA Synthesis Kit according to the provided instructions. Quantitative Real-Time PCR was performed using Maxima SYBR Green qPCR Master Mix 2x (Fermentas) also according to the provided protocol. Reactions were performed in triplicates per gene for each sample. The primers used for Fibulin-4, Gadph and Hprt (Invitrogen) are indicated in supplemental table 5. Product specificity was determined by melting curve analysis and gel electrophoresis. The average Ct values of the triple reactions were calculated for each gene according to cell type. The relative gene expression level was calculated by the following formula for each gene:

Relative gene expression level = $2^{\text{(Ct control – Ct sample) gene}} / 2^{\text{(Ct control – Ct sample) housekeeping gene}}$

The levels of fold-change for each gene were calculated by dividing the relative gene expression levels in Fibulin-4$^{+/R}$ or $^{R/R}$ lungs to the relative gene expression levels in wild type lungs.

Whole body plethysmography

Conscious mice were placed in a single-chamber whole body plethysmograph (Emka Technologies, Paris, France) as described previously[3]. In 6 time blocks of 3 minutes, the Peak Inspiration Flow (PIF) and Peak Expiration Flow (PEF) were measured. Differences in PIF and PEF indicate differences in inspiration and expiration strength. During the first blocks of 3 minutes we observed enhanced Peak Inspiration flow (PIF) and Peak Expiration

3

Flow (PEF) due to the stress by placing the animals in the chamber, which subsided after acclimatization.

Lung morphometry

Mice were euthanized with a lethal dose of pentobarbital (60 mg/ml, 0.1-1.5 ml per mouse according to weight). Lung lobes were excised and the left lobe was pressure fixed through the bronchi at a pressure of 25 cm H_2O with 4% paraformaldehyde (PFA), and fixed overnight at 4°C before paraffin embedding. Lungs from newborn mice were immersion fixed. The 5-µm sections were prepared from the paraffin embedded lungs and put on Superfrost Ultra plus slides (Menzel-Glaser). For histological analysis paraffin sections of the lungs were stained with Haematoxylin-Eosin (HE) and Resorcine-Fuchsine (Elastin von Gieson). A random selection of images of HE stained alveoli were obtained with the Leica DFC280DFC480 (Aristoplan) with a magnification of 10x. Large airways and vessels were generally avoided. Next, alveolar airspace size quantification was performed according to the fully automated D_2 method as described in Jacob RE et. al, where it was compared to the semi-automated mean linear intercept measurements, and turned out to be more sensitive and specific for subtle airspace enlargement expected to be found in mild or early stage emphysema[4]. All images were converted to grayscale before performing the analysis. Fuzzy-c-means clustering with simultaneous correction of potential luminance inhomogeneity was applied to each image for pre-segmenting it into two classes: the foreground and the background. The final segmentation was obtained by the graph-cut method with the energies given by the class membership functions calculated on the previous step. The resulting foreground was split into separate compartments corresponding to the connected components belonging to this class. Vector of the compartment sizes obtained in such a way was converted from pixels to micrometres. For each of the vectors we calculated the D_2 measure, an index based on the equivalent diameters of airspaces and by incorporating higher moment factors from the airspace diameter distributions, where enlarged airspaces are weighed more heavily. This measure is useful to detect early or mild emphysema. The compartments whose sizes were less than 138 µm were disregarded according to the threshold previously described[4].

Immunohistochemistry

For histological analysis 100-day-old female mice were dissected. Mice were euthanized by CO_2-inhalation. After opening thorax and abdomen, mice were fixed by perfusion fixation through the left ventricle, with PBS and 4% paraformaldehyde (PFA). Lungs were dehydrated through the histokinette processor (Microm), and paraffin embedded, after which 5-µm sections were prepared. Sections were emerged in 3% H_2O_2 in PBS to inhibit endogenous peroxidase. Antigen retrieval was performed by boiling slides in 10 mM citrate buffer, pH 6.0, at 600 W for 15 minutes in a microwave for TTF-1 and CC10 staining, 100 mM Tris 10 mM EDTA buffer, pH 9.0, at 300 W for 20 minutes for pSmad-2 staining, or with pronase treatment for α-SMA. Slides were first blocked in 5% Bovine Serum Albumin (BSA) in PBS and 0.5% Tween (and 5% Protifar in PBS and 0.025% Triton X-100 for pSmad-2), and incubated with the primary antibodies overnight at 4 °C; TTF-1 (1:250 mouse monoclonal Ab-1 Clone 8G7G3/1 Thermo Fisher Scientific), CC10 (1:100 goat Ab (T-18): sc-9772 Santa Cruz Biotechnology), Anti-Human Smooth Muscle Actin (1:250 mouse, clone 1A4 Biogenex Laboratories Inc.), and pSmad-2 (1:100 monoclonal Rabbit anti-pSmad2 (S465|467 (138D4) Cell Signaling). The next day slides were incubated with Horse Radish Peroxidase (HRP) labelled secondary antibodies (1:100 DAKO) and avidin-biotinylated secondary antibodies (Vectastain Universal Elite ABC kit Vector Laboratories)

for pSmad-2. DAB chromogen (DAKO Liquid Dab substrate-chromogen system) was used as substrate and slides were counterstained with haematoxylin.

Immunohistochemical stainings for inflammatory cells were performed in a half-automatic stainer (Sequenza, Amsterdam, the Netherlands). Acetone-fixed slides were blocked in diluted normal goat serum (CLB, Amsterdam, the Netherlands) and stained against mouse CD3 (1:10 rat monoclonal antibodies KT3 AbD Serotec) and against mouse CD11c (1:20 hamster antibodies N418 Ebioscience). Primary antibodies were revealed by incubation with diluted appropriate secondary antibodies coupled to alkaline phosphatase for 30 min. Slides were subsequently incubated with New Fuchsin substrate for alkaline phosphatase conjugates. Finally, the sections were counterstained with Gills triple-strength haematoxylin and mounted in VectaMount (Brunschwig, Amsterdam).

Micro-array hybridizations

RNA was isolated using the RNeasy minikit from Qiagen with the provided protocol and delivered to the department of Biomics, Erasmus MC. Synthesis of double stranded cDNA and biotin labelled cRNA was performed according to the instructions of the manufacturer (Affymetrix). Fragmented cRNA was hybridized to Mouse Genome 430 V2.0 arrays, using a hybridization Oven 640 (Affymetrix), washed and subsequently scanned on a GeneChip Scanner 3000 (Affymetrix). To examine the quality of the various arrays, several R packages (including affyQCreport and affyPLM) were run starting from the CEL files. All created plots including RNA degradation, RLE and NUSE plots indicated a high quality of all samples and an overall comparability, except for one sample (Fibulin-4$^{R/R}$ newborn lung), which was excluded from further analysis. Raw intensities values of all samples were normalized by robust multichip analysis normalization (background correction and quantile normalization) using Partek version 6.4 (Partek Inc., St. Louis, MO). The normalized data file was transposed and imported into OmniViz version 6.0.1 (Biowisdom, Ltd., Cambridge, UK) for further analysis. For each probe set, the geometric mean of the hybridization intensities of all samples was calculated. The level of expression of each probe set was determined relative to this geometric mean and ^{2}log transformed. The geometric mean of the hybridization signal of all samples was used to ascribe equal weight to gene expression levels with similar relative distances to the geometric mean. Differentially expressed genes were identified using ANOVA (Partek), SAM (Omniviz). The cut-off value for significantly expressed genes was FDR 10% for adult Fibulin-4$^{R/R}$ lungs compared to Fibulin-4$^{+/+}$ lungs. Functional and network analysis was done using Ingenuity Pathway Analysis (IPA; Ingenuity® Systems, www.ingenuity.com, Mountain View, CA). Ingenuity pathway analysis is a web-based software application that enables to analyse and integrate data derived from gene expression microarrays into biological networks and pathways. All Ingenuity products leverage the Ingenuity Knowledge Base, which houses biological and chemical relationships extracted from the scientific literature.

Significantly expressed genes from the adult Fibulin-4$^{R/R}$ to Fibulin-4$^{+/+}$ lungs comparison were compared to COPD-associated genes in Ingenuity and a list of literature based genes associated with COPD. CEL files from GEO dataset GSE8581 were obtained and were analysed following the above described procedures. Cut-off values for significantly expressed genes were FDR 30% and 1.5-fold. Comparison to significantly expressed genes from the adult Fibulin-4$^{R/R}$ to Fibulin-4$^{+/+}$ lungs comparison was done using IPA.

Preparation of cell suspensions, flow cytometry and ELISA

Broncho Alveolar Lavage (BAL) was performed with 3 times 1 ml of Ca^{2+}- and Mg^{2+}-free PBS, containing 10 mM EDTA. Furthermore, lungs were enzymatically digested using

collagenase type III (Worthington) for 1 hour at 37° C, followed by washing and filtering. Cell suspensions were stained with antibodies specific for F4/80-Fitc, MHC class II-PE, CD11c-PeTexasRed, CD3-PECy5, CD19-APCCy7, CD25-APC and GR-1-PECy7 (Becton Dickinson or eBiosciences). Nonspecific binding to Fc-receptors was blocked by incubation with 2.4G2 antibodies and DAPI (Invitrogen) was used as life/dead marker. Acquisitions were performed on an LSRII flow cytometer (Becton Dickinson) and data were analysed by FlowJo (Treestar, Costa Mesa, CA) software. Supernatants of BAL fluid were stored for ELISA. BAL fluid cytokines were measured by commercially available specific ELISA systems for IL-6, KC, MCP-1, TARC, IL-10, IL-12, IL-1β, TNF-α, IFN-gamma and IL-17 according to the manufacturers' instructions. In a separate set of experiments, flow cytometric analyses of BAL samples and pulmonary cell suspensions were performed 18 or 72 hours after a single intratracheal injection with either sterile lipopolysaccharide (LPS) 1 mg/ml in PBS or PBS alone in adult (100-days-old) Fibulin-4$^{+/R}$ and Fibulin-4$^{+/+}$ mice.

Western blot analysis

Western blot analysis was performed as described before[5]. In short, equal amounts of lung tissue homogenates (40 ug) were separated under reducing conditions on 10% SDS-PAGE. Proteins were transferred to nitrocellulose membranes (Whatman, Germany) and blocked with 5% milk. After washing, membranes were incubated with rabbit anti-phosphorylated Smad2 (Cell Signaling Technologies, USA) followed by HRP labelled secondary antibodies (GE Healthcare) and detection with a chemoluminiscent substrate (Pierce). Afterwards membranes were stripped and reprobed with anti Smad2/3 antibodies (BD biosciences) and β-actin (Sigma) as a loading control.

Fluorescence imaging

We used vascular fluorescent mediated tomography (FMT) imaging with near-infrared fluorescent protease activatable probes as previously described[6, 7]. Open chest FMT imaging of fibulin-4 mice was performed using an FMT 2500 system (Perkin Elmer Inc.) at 680- and 750-nm excitation and emission wavelengths, respectively, at five hours after tail vein injection of 4 nmol of Neutrophil Elastase 680 FAST and 2 nmol of MMPSense 750 FAST (Perkin Elmer Inc.). Mice with open chests were fixed into the portable animal imaging cassette that lightly compressed the mouse between optically translucent windows. The FMT 2500 quantitative tomography software was then used to calculate 3D fluorochrome concentration distribution of Neutrophil Elastase 680 FAST and MMPSense 750 FAST.

After open chest fluorescence imaging, complete lungs were harvested and fluorescence was quantified using the FMT 2500 or Odyssey imaging systems (LI-COR Inc.). Near-infrared images were obtained in the 680- and 700 nm channels, respectively.

Statistical analysis

Data are presented as mean ± SEM. Statistical analysis for lung morphometry was performed using the Kolmogorov-Smirnov test. The Kruskal-Wallis one-way ANOVA was used to determine any significant differences between groups. The nonparametric Mann-Whitney U-test was performed to analyse the specific sample pairs for significant differences. A p-value of <0.05 was considered to indicate a significant difference between groups. All analyses were performed using IBM SPSS Statistics version 20.0 (SPSS Inc., Chicago, IL, USA).

SUPPLEMENTAL TABLES & FIGURES

Supplemental Table 1 – Association between COPD and aneurysmal disease.

	Univariable			Multivariable[*]		
	odds ratio	95%CI	P-value	odds ratio	95%CI	P-value
No COPD	1.00			1.0		
COPD	2.08	[1.66 – 2.61]	<0.001	1.56	[1.16– 2.10]	0.003
Mild COPD	2.34	[1.67 – 3.28]	<0.001	1.66	[1.08 – 2.57]	0.022
Moderate COPD	1.83	[1.36 – 2.46]	<0.001	1.40	[0.97 – 2.04]	0.075
Severe COPD	2.38	[1.47 – 3.86]	<0.001	1.63	[0.85 – 3.15]	0.142

[*] Adjusted for: age, gender, BMI, congestive heart failure, ischemic heart disease, cerebrovascular disease, kidney disease, diabetes mellitus, hypertension, hypercholesterolemia, smoking, statins, beta-blockers, renin-angiotensin system inhibitors, diuretics, antiplatelets and hs-CRP.

3

Supplemental Table 2 - The most significantly down-regulated genes in lungs of adult Fibulin-4$^{R/R}$ mice. The genes are indicated with their ratios compared to Fibulin-4$^{+/+}$ and the process involved.

Top down-regulated genes		
Genes	Ratio	Function
Efemp2	3.56	Extracellular matrix protein
Myrip	2.25	Melanosome transport
Krtap17-1	2.20	Interfilamentous matrix proteins
Fam107a	2.10	Tumor development
Gdpd2	1.87	Hydrolyzes glycerophosphoinositol
Dcdc2	1.82	Microtubule polymerization
Mus81	1.82	Endonuclease
Acot1	1.78	Catalyze the hydrolysis of acyl-CoAs
Apob	1.76	LDL apolipoprotein
Slc15a2	1.74	Proton-coupled peptide transporter in small intestine
Hspa4l	1.70	Chaperone activity
Galntl2	1.69	Oligosaccharide biosynthesis
Hist2h3c	1.67	Nucleosome structure
Hmgcs2	1.67	Mitochondrial enzyme involved in ketogenesis
Slc6a2	1.65	Neurotransmitter transporter
Lonrf3	1.65	Protein-protein and protein-DNA interactions
Ccl20	1.65	Chemotactic factor that attracts lymphocytes and slightly neutrophils
Msc	1.63	Downstream target of B-cell receptor signal transduction pathway
Fmo3	1.58	Oxidative metabolism

Supplemental Table 3 - Over-expressed canonical pathways, based on IPA, in lungs of adult Fibulin-$4^{R/R}$ mice ($p<0.05$). Genes associated with these pathways are shown with their log ratio changes compared to Fibulin-$4^{+/+}$ lungs.

Canonical pathways	P-value	Involved genes (log ratio)
Cholesterol Biosynthesis	$6.27\ 10^{-5}$	HSD17B7, MSMO1, SC5DL, CYP51A1
Zymosterol Biosynthesis	$1.09\ 10^{-4}$	HSD17B7, MSMO1, CYP51A1
Tumoricidal Function of Hepatic Natural Killer Cells	$8.66\ 10^{-3}$	ENDOG, PRF1, ITGAL
Aldosterone Signalling in Epithelial Cells	$1.03\ 10^{-2}$	HSPA12B, HSPB2, HSP90AA1, PLCL2, DNAJB2, HSPA2, HSPA4L, PRKCB
Sonic Hedgehog Signalling	$1.08\ 10^{-2}$	STK36, PTCH1, HHIP
Granzyme A Signalling	$2.18\ 10^{-2}$	GZMA, PRF1
Acyl-CoA Hydrolysis	$2.18\ 10^{-2}$	ACOT2, ACOT1
Cytotoxic T Lymphocyte-mediated Apoptosis of Target Cells	$3.01\ 10^{-2}$	PRF1, TRA, BCL2
Glucocorticoid Receptor Signalling	$3.15\ 10^{-2}$	FKBP4, SLPI, TGFB2, HSP90AA1, CCL5, CD163, HSPA2, TRA, BCL2
Granzyme B Signalling	$3.24\ 10^{-2}$	ENDOG, PRF1
Hepatic Fibrosis / Hepatic Stellate Cell Activation	$3.32\ 10^{-2}$	MYH10, MYH14, IL10RA, TGFB2, CCL5, BCL2
Atherosclerosis Signalling	$4.19\ 10^{-2}$	APOB, MMP3, SERPINA1, APOC2, ITGA4
p38 MAPK Signalling	$4.29\ 10^{-2}$	HSPB2, MAPT, HIST2H3C, TGFB2, MEF2C
Reelin Signalling in Neurons	$4.17\ 10^{-2}$	MAPT, HCK, ITGAL, ITGA4
LXR/RXR Activation	$4.89\ 10^{-2}$	APOB, VTN, SERPINA1, APOC2, CYP51A1

Supplemental Table 4 - Deregulated TGF-β pathway genes in adult and newborn Fibulin-4 deficient lungs compared to Fibulin-$4^{+/+}$ lungs ($p<0.05$).

Comparison	Deregulated TGF-β pathway genes	Gene symbol	Fold change
Adult Fibulin-$4^{R/R}$ vs Fibulin-$4^{+/+}$	Transforming growth factor β2	Tgfb2	↑ 1.46
	Activin A receptor type 2b	Acvr2b	↓ 1.24
Adult Fibulin-$4^{+/R}$ vs Fibulin-$4^{+/+}$	SMAD specific E3 ubiquitin protein ligase 1	Smurf1	↓ 1.23
Newborn Fibulin-$4^{R/R}$ vs Fibulin-$4^{+/+}$	Protein inhibitor of activated STAT 4	Pias4	↓ 1.25
Newborn Fibulin-$4^{+/R}$ vs Fibulin-$4^{+/+}$	None	-	-

Supplemental Table 5 - Primers used for quantitative real time PCR. Forward and reverse primers are displayed for each gene from 5' to 3'.

Genes	Forward primers	Reverse primers
Fibulin-4	5'-GGGTTATTTGTGTCTGCCTCG-3'	5'-TGGTAGGAGCCAGGAAGGTT-3'
Gadph	5'-ACCACAGTCCATGCCATCAC-3'	5'-TCCACCACCCTGTTGCTGTA-3'
Hprt	5'-CGAAGTGTTGGATACAGGCC-3'	5'-GGCAACATCAACAGGACTCC-3'

Fibulin-4$^{+/+}$ Fibulin-4$^{+/R}$ Fibulin-4$^{R/R}$
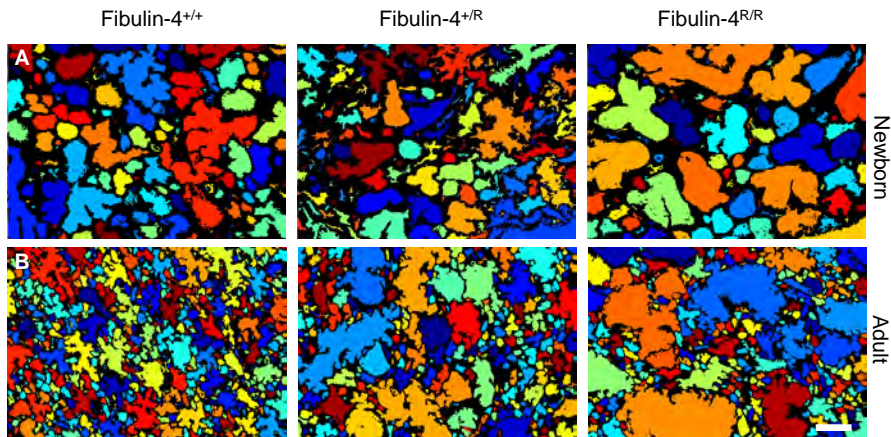
Supplemental Figure 1: Larger alveolar airspaces in newborn Fibulin-4$^{R/R}$ lungs (A) and adult Fibulin-4$^{+/R}$ and Fibulin-4$^{R/R}$ lungs (B). The compartments from the different alveolar airspaces were segmented on the HE images. Each segmented compartment was given a different colour and quantified. Magnification 10x. Scale bar 100 µm.

3

Fibulin-4$^{+/+}$ Fibulin-4$^{+/R}$ Fibulin-4$^{R/R}$
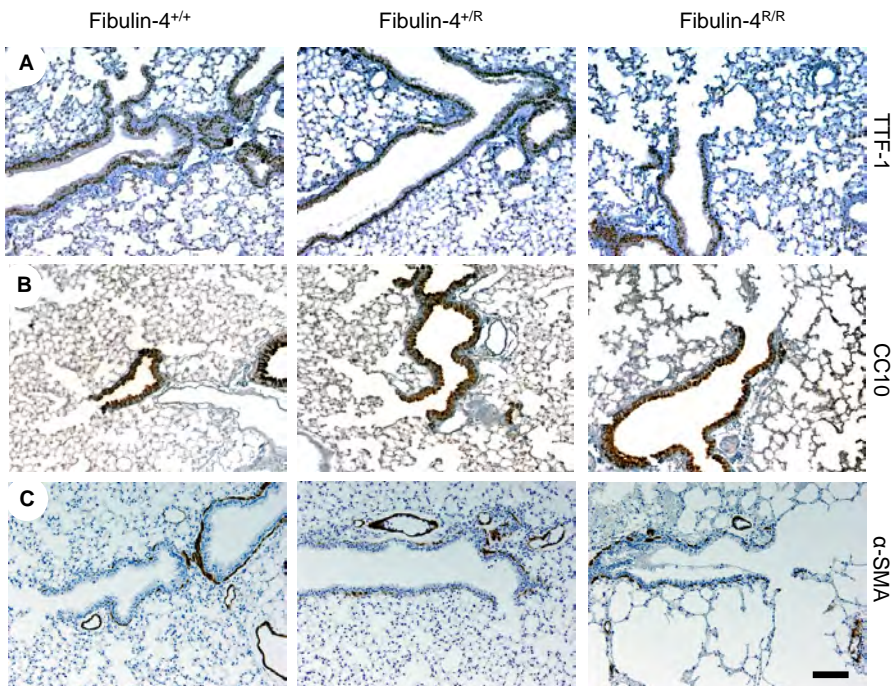
Supplemental Figure 2: Similar cell structures in wild type and Fibulin-4 knockdown lungs. Stainings for (A) respiratory epithelial cells with TTF-1, (B) Clara cells with CC10 and (C) smooth muscle cells with α-SMA show similar cell structures in Fibulin-4$^{+/+}$ (n=3), Fibulin-4$^{+/R}$ (n=3) and Fibulin-4$^{R/R}$ (n=2) lungs. Magnification 10x. Scale bar 100 µm.
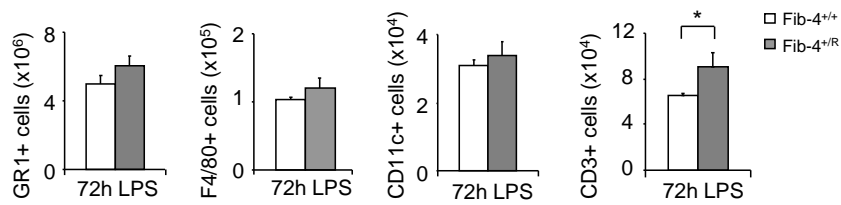
Supplemental Figure 3: LPS infection induces infiltration of inflammatory cells in the alveolar compartments. Quantification of immune cells in alveolar compartments shows increased CD3+ cells after 72 hours of LPS exposure in Fibulin-4$^{+/R}$ (n=4) as compared to Fibulin-4$^{+/+}$ lungs (n=4, * p<0.05).

3

REFERENCES

[1]   Rabe KF, Hurd S, Anzueto A, Barnes PJ, Buist SA, Calverley P, Fukuchi Y, Jenkins C, Rodriguez-Roisin R, van Weel C, Zielinski J. Global strategy for the diagnosis, management, and prevention of chronic obstructive pulmonary disease: GOLD executive summary. Am J Respir Crit Care Med. 2007 Sep 15;176(6):532-55.

[2]   Hanada K, Vermeij M, Garinis GA, de Waard MC, Kunen MG, Myers L, Maas A, Duncker DJ, Meijers C, Dietz HC, Kanaar R, Essers J. Perturbations of vascular homeostasis and aortic valve abnormalities in fibulin-4 deficient mice. Circ Res. 2007 Mar 16;100(5):738-46.

[3]   Hamelmann E, Schwarze J, Takeda K, Oshiba A, Larsen GL, Irvin CG, Gelfand EW. Noninvasive measurement of airway responsiveness in allergic mice using barometric plethysmography. Am J Respir Crit Care Med. 1997 Sep;156(3 Pt 1):766-75.

[4]   Jacob RE, Carson JP, Gideon KM, Amidan BG, Smith CL, Lee KM. Comparison of two quantitative methods of discerning airspace enlargement in smoke-exposed mice. PLoS One. 2009;4(8):e6670.

[5]   Hawinkels LJ, Kuiper P, Wiercinska E, Verspaget HW, Liu Z, Pardali E, Sier CF, ten Dijke P. Matrix metalloproteinase-14 (MT1-MMP)-mediated endoglin shedding inhibits tumor angiogenesis. Cancer Res. 2010 May 15;70(10):4141-50.

[6]   Kaijzel EL, van Heijningen PM, Wielopolski PA, Vermeij M, Koning GA, van Cappellen WA, Que I, Chan A, Dijkstra J, Ramnath NW, Hawinkels LJ, Bernsen MR, Lowik CW, Essers J. Multimodality imaging reveals a gradual increase in matrix metalloproteinase activity at aneurysmal lesions in live fibulin-4 mice. Circ Cardiovasc Imaging. 2010 Sep;3(5):567-77.

[7]   Nahrendorf M, Waterman P, Thurber G, Groves K, Rajopadhye M, Panizzi P, Marinelli B, Aikawa E, Pittet MJ, Swirski FK, Weissleder R. Hybrid in vivo FMT-CT imaging of protease activity in atherosclerosis with customized nanosensors. Arterioscler Thromb Vasc Biol. 2009 Oct;29(10):1444-51.

3

Chapter 4

Fibulin-4 deficiency induces thoracic and abdominal aortic wall dilation and altered plaque morphology in apolipoprotein E-deficient mice

N.W.M. Ramnath[1,2]*, B.S. van Thiel[1,2,4]*, K. Van der Heiden[3]*, L. Speelman[3], R.Y. Ridwan[1,2,4], P.M. van Heijningen[1], M. Vermeij[5], E.V. Rouwet[2], R. Kanaar[1,6], I. van der Pluijm[1,2], J. Essers[1,2,6]

[1]Department of Genetics, [2]Department of Vascular Surgery, [3]Department of Biomedical Engineering, [4]Department of Pharmacology, [5]Department of Pathology, [6]Department of Radiation Oncology, Erasmus Medical Center, Rotterdam, The Netherlands

* Equal contributors

ABSTRACT

Objective: Extracellular matrix degradation plays an important role in aortic aneurysm formation. In Fibulin-4$^{R/R}$ mice, deficiency of the extracellular matrix protein Fibulin-4 induces upregulation of matrix metalloproteinases (MMP) and elastin irregularities, resulting in early thoracic aortic aneurysms. In humans, aneurysms usually develop in the abdominal aorta with increasing age and are often associated with atherosclerosis. To investigate the molecular mechanisms of the interaction between aneurysm formation and atherosclerotic disease we crossbred Fibulin-4$^{+/R}$ mice, with minor extracellular matrix (ECM) abnormalities such as increased ECM deposition and slight MMP activation in the thoracic aorta, but without aortic dilation yet, onto an atherosclerotic Apolipoprotein E knockout (ApoE$^{-/-}$) background.

Approach: Double ApoE$^{-/-}$Fibulin-4$^{+/R}$ mutant mice were fed a high fat diet (HFD) for 10, 20 or 30 weeks and compared to ApoE$^{-/-}$Fibulin-4$^{+/+}$ control mice. MMP activity in the aorta was determined using protease-activatable near-infrared fluorescent probes. Thoracic and abdominal aortic diameters were assessed using high-frequency ultrasound. After sacrifice, atherosclerotic burden in the aorta was evaluated.

Results: Interestingly, after 10 weeks of HFD, ApoE$^{-/-}$Fibulin-4$^{+/R}$ mice displayed increased MMP activity in the abdominal aorta and after 20 weeks of diet thoracic and abdominal aortic dilations were observed as compared to ApoE$^{-/-}$Fibulin-4$^{+/+}$ mice. In addition, ApoE$^{-/-}$Fibulin-4$^{+/R}$ mice showed increased plaque formation after 10 weeks of HFD and histological plaque analysis showed a distinct plaque architecture. Moreover, part of the ApoE$^{-/-}$Fibulin-4$^{+/R}$ mice developed symptoms of paralysis between 20 and 30 weeks of HFD and 30% did not survive beyond 30 weeks.

Conclusions: These results indicate that a subtle defect in the extracellular matrix of the aortic wall predisposes to the development of thoracic and abdominal aortic dilation upon atherosclerosis, and induces altered plaque morphology.

INTRODUCTION

Aortic aneurysm and dissections account for 1-2% of all deaths in the developed countries [1]. According to their location, aneurysms can be categorized in two main groups: thoracic aortic aneurysms (TAA) and abdominal aortic aneurysms (AAA). Aneurysms of the thoracic aorta, in particular the aortic arch, are characterized by necrosis of the medial layer of the aortic wall, also called cystic medial necrosis. TAAs usually occur due to a genetic mutation, for example aneurysms in Marfan's disease. Aneurysms of the distal aorta, in particular AAAs, are much more common and are thought to be caused by a multifactorial process [2]. Interestingly, recent clinical studies report a high frequency of TAAs in patients with aneurysms of the abdominal aorta [3, 4]. Important risk factors for aortic aneurysm formation are age and atherosclerosis, and these risk factors are similar for patients with aneurysms and those with arterial occlusive disease, which is characterized by narrowing of the arteries due to atherosclerosis [5]. However, the molecular mechanisms underlying aneurysm formation and the relation with atherosclerosis are largely unknown.

It is known that extracellular matrix degeneration plays an important role in TAA formation. Elastin is a crucial component of the extracellular matrix that is responsible for maintaining vessel wall elasticity [6]. Fibulin-4 is an extracellular matrix protein, which plays an important role in elastic fiber assembly and function and is a regulatory factor in elastogenesis [7, 8]. Indeed, Fibulin-4 deficient patients described so far present with TAAs, due to homozygous or compound heterozygous mutations, which usually develop to a severe stage of the disease within the first months or years of their life [9-15]. A proportion of these patients also presented with abdominal tortuosity and/or dilation on further examination [12, 15].

Similar to Fibulin-4 deficient patients, previously developed mutant mice with a systemic 4-fold (Fibulin-4$^{R/R}$) reduced expression of Fibulin-4 present with aortic wall degeneration and thoracic aortic aneurysm [16-18]. Additionally, they develop impaired vascular contractility and increased arterial stiffness. Interestingly, a 2-fold reduced expression of Fibulin-4, in Fibulin-4$^{+/R}$ mice, also induces aortic disease but in a milder form. Although they do not develop aortic aneurysms spontaneously at adult age, they present with aortic wall degeneration, including elastic fiber fragmentation and slightly increased TGF-β signaling [17, 19]. Additionally, destruction of the extracellular matrix in the aortic wall of these Fibulin-4 mice is associated with increased expression and activation of matrix metalloprotease (MMPs), which are involved in degradation of the extracellular matrix [17, 19]. Molecular imaging using a near-infrared in vivo imaging probe for MMP activity (MMPsense 680) shows a graded increase in MMP activity in aneurysmal lesions of the aortic arch of Fibulin-4$^{+/R}$ and Fibulin-4$^{R/R}$ mice, showing that MMP activity is a leading indicator in these hypomorfic Fibulin-4 mice for aneurysm formation [19].

To study whether and how a primary extracellular matrix defect can be involved in aortic dilation and atherosclerosis, we developed a mouse model in which we combined the subtle defect in the extracellular matrix of the Fibulin-4$^{+/R}$ mouse with the most commonly used model for atherosclerosis, the apolipoprotein E knockout (ApoE$^{−/−}$) mouse. At the age of 9 weeks, the double mutant mice were fed a high fat diet (HFD) to induce atherosclerotic plaque formation. Since MMP-induced elastin and collagen degradation are known to affect atherosclerotic plaque morphology [20, 21], we additionally analyzed whether plaque morphology in ApoE$^{-/-}$ mice is affected by Fibulin-4 deficiency. This model mimics the human situation as it combines the clinically observed association between (thoracic and abdominal) aortic dilation and atherosclerosis by combining an atherosclerosis mouse model (ApoE) and a subtle inherited defect present in the aortic wall (Fibulin-4$^{+/R}$) that

4

might predispose these animals for the development of atherosclerosis associated aortic disease.

MATERIAL AND METHODS

Mouse model
Mice containing the Fibulin-4^R allele were generated as previously described (2). All mice used were bred in a C57Bl/6J background and were kept in individually ventilated cages to keep them consistently micro-flora and disease free. Fibulin-4^R mice were crossbred with ApoE$^{-/-}$ mice (C57Bl/6J background) to obtain ApoE$^{-/-}$Fibulin-4$^{+/+}$ and ApoE$^{-/-}$Fibulin-4$^{+/R}$ mice. Female and male ApoE$^{-/-}$Fibulin-4$^{+/+}$ and ApoE$^{-/-}$Fibulin-4$^{+/R}$ mice were fed either a normal chow diet (Standard CRM (P), Special Diets Services, UK), a HFD containing 16% fat (Purified diet W 4021.06, AB diets Animal Nutrition, Woerden, the Netherlands) or a control fat diet (CFD) containing 5% fat (Purified diet W control 4021.69, AB diets Animal Nutrition, Woerden, the Netherlands) starting at the age of 9 weeks. Hind limb paralyses was observed by dragging of the limbs, and facial paralyses by loss of eye blink reflects, a bulging eye and abnormal vibrissae orientation with fibers flattened posterior against the head. Animals were housed at the Animal Resource Center (Erasmus University Medical Center), which operates in compliance with the "Animal Welfare Act" of the Dutch government, using the "Guide for the Care and Use of Laboratory Animals" as its standard. As required by Dutch law, formal permission to generate and use genetically modified animals was obtained from the responsible local and national authorities. All animal studied were approved by an independent Animal Ethical Committee (Dutch equivalent of the IACUC).

MMP imaging
Per 25 grams of body weight 2 nmol specific MMP activatable NIRF probes, MMPSense 680 (PerkinElmer), was injected into the tail vein of anesthetized mice after 10 and 20 weeks of HFD or normal chow diet. Intact aortas were harvested 24 hours after injection for *ex vivo* fluorescence imaging, and analyzed using the Odyssey Imaging system (LI-COR Biosciences, Lincoln, NE, USA). Near-infrared images were obtained in the 700 nm channel.

Ultrasound imaging
Animals were sedated with 4% isoflurane and maintained on 1-3% isoflurane for anaesthesia, adjusted to the vital parameters of the mouse (heart rate > 400 bpm, breath rate 30 strokes/min). Mice were placed on a heating pad to maintain body temperature at 37°C. *In vivo* ultrasound imaging of the aortic arch, abdominal aorta and left ventricle (LV) was performed with a Vevo2100 (Visualsonics Inc., Toronto, Canada) using a 40-MHz linear interfaced array transducer (MS550S). B-mode and M-mode images of the aorta were captured. Diameters of the aortic arch were measured from the parasternal window at the level of the ascending aorta. Distensibility of the aortic arch was measured as the systolic to diastolic aortic diameter ratio in M-mode image data (calculated as systolic diameter minus diastolic diameter, divided by the diastolic diameter).

Analysis of plaque area and composition
To quantify the surface area affected by atherosclerosis, aortas were stained with Oil-red-O after 10 and 20 weeks of HFD and macro photographs of *en face* preparations were

made (n=minimal 5 mice in each group). The Oil-red-O stained surface areas in the aortic arch, descending and abdominal aorta were quantified using ImageJ (Fiji). Additionally, plaque size and morphology were histologically analyzed after 10 and 20 weeks of HFD (n=minimal 5 mice in each group). The aortas with the branching brachiocephalic artery, left carotid artery and left subclavian artery of mice on 10 weeks of HFD were perfusion fixed with 1% paraformaldehyde after PBS flush, dehydrated and embedded in paraffin. Serial longitudinal sections of the aortic arch and cross sections of the abdominal aorta (5 µm) were prepared for histological analysis. Total plaque size in the inner curvature of the aortic arch and in the brachiocephalic artery was measured on haematoxylin-eosin stained slides using BioPix iQ 2.0 imaging software (BioPix, Göteborg, Sweden). Aortic wall structure and plaque morphology were additionally analyzed by histochemical staining with Resorcin-Fuchsin (elastin). Elastin content was analyzed on elastin stained slides with ImageJ (Fiji).

To further determine differences in plaque phenotype, including lipid content, cryosections were made of mice on 20 weeks HFD. After PBS flush aortic arches were embedded in Tissue-Tek (O.C.T. compound) and serial longitudinal cryosections were made (5 µm). Plaque size in the aortic arch and brachiocephalic artery was quantified on haematoxylin-eosin stained slides using Biopix. Oil-red-O staining was used to determine lipid content of the plaques.

Statistical analysis

All results are expressed as mean ± SEM (continuous results) or median (lower to upper limit) (aortic arch diameters). The unpaired 2-tailed Student t-test was performed to analyze the specific sample groups for significant differences. A p-value <0.05 was considered to indicate a significant difference between groups. All analyses were performed using IBM SPSS Statistics version 20.0 (SPSS Inc., Chicago, IL, USA).

4

RESULTS

Abdominal aorta of ApoE$^{-/-}$Fibulin-4$^{+/R}$ mice shows increased MMP activity

We have previously shown that extracellular matrix degeneration in Fibulin-4$^{+/R}$ and Fibulin-4$^{R/R}$ mice is associated with increased MMP activity in the thoracic aorta [19]. In this study, we tested whether extracellular matrix degeneration in the aortic wall of Fibulin-4 deficient mice could contribute to abdominal aortic lesions. Measurements of MMP activity in the abdominal aorta using the MMPSense 680 probes indeed revealed a mild increased activity of 1.2 fold in Fibulin-4$^{+/R}$ abdominal aortas as compared to Fibulin-4$^{+/+}$ mice (Figure 1A). However, these Fibulin-4$^{+/R}$ mice do not yet develop abdominal aortic dilations.

As atherosclerosis can be associated with aortic aneurysms, we next tested whether the induction of atherosclerosis in Fibulin-4^R heterozygous mice, which have minor extracellular matrix defects in the aortic wall, could lead not only to thoracic, but also abdominal aortic dilation. To induce atherosclerosis, Fibulin-4$^{+/R}$ mice were crossbred with ApoE$^{-/-}$ mice, which develop atherosclerosis spontaneously after 12 weeks [22-24]. Starting from the age of 9 weeks the double mutant ApoE$^{-/-}$Fibulin-4$^{+/R}$ and ApoE$^{-/-}$Fibulin-4$^{+/+}$ littermate controls were fed a HFD for 10 or 20 weeks to accelerate atherosclerotic plaque formation. ApoE$^{+/+}$Fibulin-4$^{+/+}$ and ApoE$^{+/+}$Fibulin-4$^{+/R}$ mice on a HFD for 10 or 20 weeks did not develop atherosclerosis and did not show additional vascular abnormalities as compared to Fibulin-4$^{+/+}$ and Fibulin-4$^{+/R}$ mice.

Interestingly, after 10 weeks of HFD, MMP activity measurement on whole aortas revealed a strongly increased MMP activity in the abdominal aortas of ApoE$^{-/-}$Fibulin-4$^{+/R}$
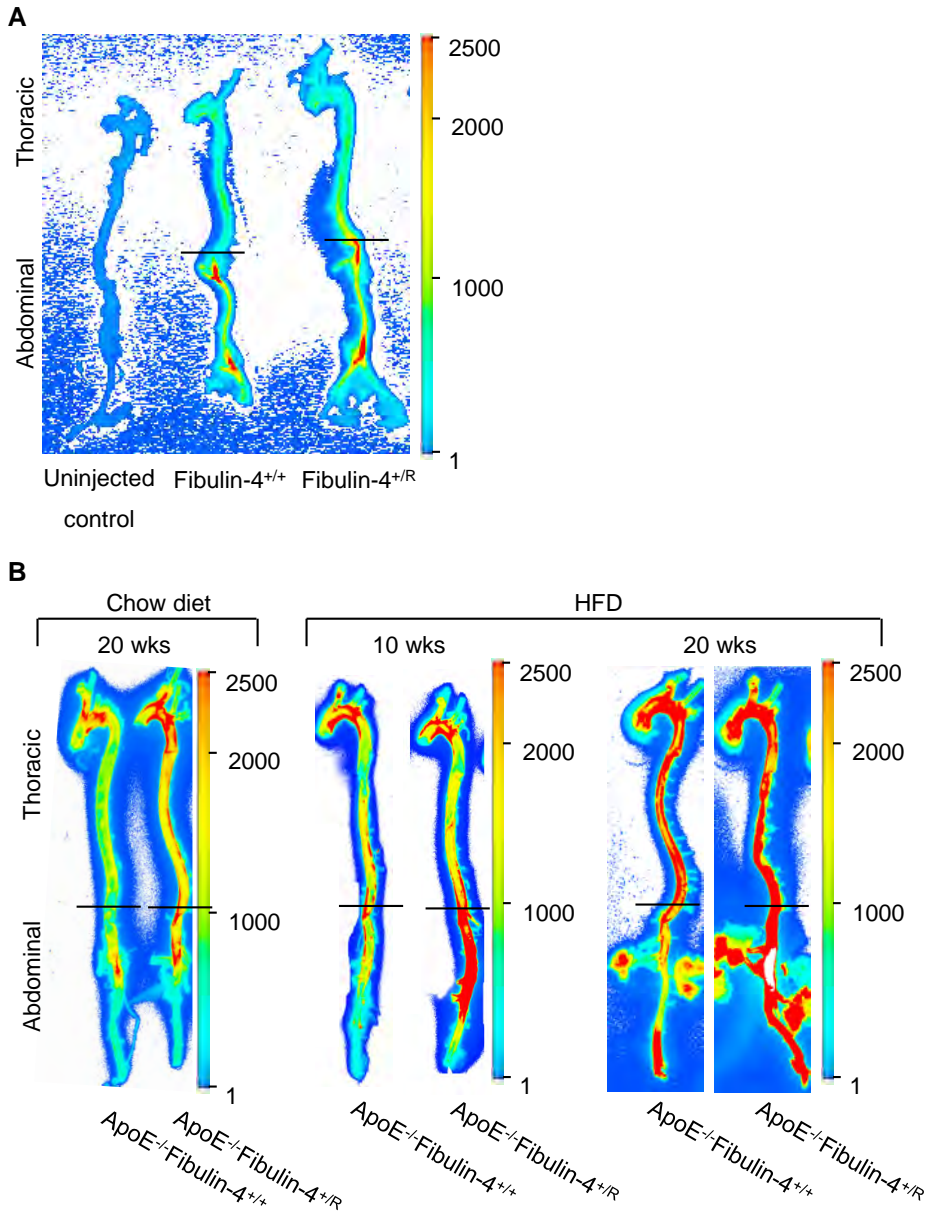
Figure 1: Increased MMP activity in ApoE$^{-/-}$Fibulin-4$^{+/R}$ abdominal aortas after 10 and 20 weeks of HFD. (A) E*x vivo* imaging of isolated aortas shows 1.2 fold higher MMP activity in the abdominal aortas of Fibulin-4$^{+/R}$ mice (n=6) as compared to Fibulin-4$^{+/+}$ abdominal aortas (n=4). (B) *Ex vivo* imaging of aortas after 10 and 20 weeks of HFD and chow diet shows a further increase in MMP activity in the abdominal aorta of ApoE$^{-/-}$Fibulin-4$^{+/R}$ mice (n=3) with a 2.7 fold increase after 10 weeks of HFD as compared to ApoE$^{-/-}$Fibulin-4$^{+/+}$ aortas (n=3), and a 13 fold increase after 20 weeks of HFD in the abdominal aortas of ApoE$^{-/-}$Fibulin-4$^{+/R}$ mice (n=5) as compared to ApoE$^{-/-}$Fibulin-4$^{+/+}$ aortas (n=5) as well as compared to ApoE$^{-/-}$Fibulin-4$^{+/R}$ mice after 20 weeks of chow diet (n=5), which had a 1.6 fold increase compared to ApoE$^{-/-}$Fibulin-4$^{+/+}$ aortas (n=3). Horizontal lines depict the level of the diaphragm, indicating the transition of the thoracic into the abdominal part of the aorta.

mice of 2.7 fold as compared to ApoE$^{-/-}$Fibulin-4$^{+/+}$ mice, and also compared to ApoE$^{-/-}$Fibulin-4$^{+/R}$ mice on a chow diet, which had a 1.6 fold increase compared to ApoE$^{-/-}$Fibulin-4$^{+/+}$ mice on chow diet (Figure 1B). This highly increased MMP activity in the abdominal aortas of ApoE$^{-/-}$Fibulin-4$^{+/R}$ mice was further increased after 20 weeks of HFD. ApoE$^{-/-}$Fibulin-4$^{+/R}$ mice on 20 weeks of HFD had a 13 fold increase as compared to ApoE$^{-/-}$Fibulin-4$^{+/+}$ mice. This indicates that induction of atherosclerosis in ApoE$^{-/-}$Fibulin-4$^{+/R}$ mice enhanced the already slightly increased MMP activity observed in the abdominal aorta of Fibulin-4$^{+/R}$ mice, which suggests that abdominal aortic wall lesions worsened progressively in ApoE$^{-/-}$Fibulin-4$^{+/R}$ mice on a HFD.

ApoE$^{-/-}$Fibulin-4$^{+/R}$ aortas display increased thoracic and abdominal aortic diameters
To subsequently determine whether the combination of atherosclerosis and an extracellular matrix defect can result in aortic dilation in ApoE$^{-/-}$Fibulin-4$^{+/R}$ mice, we measured thoracic and abdominal aortic diameters using *in vivo* ultrasound imaging of ApoE$^{-/-}$Fibulin-4$^{+/+}$ and ApoE$^{-/-}$Fibulin-4$^{+/R}$ mice after 10 and 20 weeks of HFD and after 10 or 20 weeks of CFD, which has a similar nutrient composition as HFD, but a lower fat percentage. We also included mice after 20 weeks of chow diet and mice of 9 weeks old (without starting a diet: 0 weeks HFD/CFD) as controls. Interestingly, significantly increased thoracic aortic diameters were observed in ApoE$^{-/-}$Fibulin-4$^{+/R}$ mice after 20 weeks of CFD compared to ApoE$^{-/-}$Fibulin-4$^{+/+}$ mice, but no difference was observed between the two genotypes on HFD or chow diet (Figure 2A and Supplemental Figure 1A). The thoracic aortic diameters of the ApoE$^{-/-}$Fibulin-4$^{+/R}$ mice on 20 weeks CFD were also significantly larger compared to ApoE$^{-/-}$Fibulin-4$^{+/R}$ mice on 10 weeks CFD and ApoE$^{-/-}$Fibulin-4$^{+/R}$ mice on 20 weeks chow diet. ApoE$^{-/-}$Fibulin-4$^{+/+}$ and ApoE$^{-/-}$Fibulin-4$^{+/R}$ mice on 10 and 20 weeks of HFD displayed similar distributions with large variations in aortic arch diameters, which seemed to show some dilation in both ApoE$^{-/-}$Fibulin-4$^{+/+}$ and ApoE$^{-/-}$Fibulin-4$^{+/R}$ mice. Since increased aortic arch diameters were also observed in ApoE$^{-/-}$Fibulin-4$^{+/+}$ mice on HFD, this probably indicates that HFD induces aortic arch dilations in both ApoE$^{-/-}$Fibulin-4$^{+/+}$ and ApoE$^{-/-}$Fibulin-4$^{+/R}$ mice. Aortic arch diameter measurements at 0 weeks of diet or after 20 weeks of chow diet, showed no difference between ApoE$^{-/-}$Fibulin-4$^{+/+}$ and ApoE$^{-/-}$Fibulin-4$^{+/R}$ mice. In short, after a subtle increase in fat diet (CFD) ApoE$^{-/-}$Fibulin-4$^{+/R}$ mice developed thoracic aortic dilations compared to ApoE$^{-/-}$Fibulin-4$^{+/+}$ mice, while a diet with even more fat (HFD) results in a large variation in thoracic aortic diameters between animals in both the ApoE$^{-/-}$Fibulin-4$^{+/+}$ and ApoE$^{-/-}$Fibulin-4$^{+/R}$ group.

Additionally, to determine the effect of atherosclerosis on the stiffness of the aortic wall, we performed calculations on the distensibility of the aortic arch, which is an elasticity index of the aorta and inversely correlates with aortic wall stiffness. A slight reduction was already observed in adult Fibulin-4$^{+/R}$ aortas compared to Fibulin-4$^{+/+}$ aortas (Supplemental Figure 2A). A similar slight reduction was observed in ApoE$^{-/-}$Fibulin-4$^{+/R}$ mice after 10 and 20 weeks of CFD as compared to ApoE$^{-/-}$Fibulin-4$^{+/+}$ mice (data not shown). The same measurements in ApoE$^{-/-}$Fibulin-4$^{+/R}$ mice after 10 and 20 weeks of HFD revealed a further decreased distensibility as compared to ApoE$^{-/-}$Fibulin-4$^{+/+}$ mice (Supplemental Figure 2B). This decrease was significant after 10 weeks of HFD, whereas after 20 weeks of HFD ApoE$^{-/-}$Fibulin-4$^{+/+}$ aortas also showed a slight decrease in aortic arch distensibility. In conclusion, these results indicate that CFD, probably inducing modest atherosclerosis formation, results in aortic arch dilation in extracellular matrix defective ApoE$^{-/-}$Fibulin-4$^{+/R}$ mice, while a HFD leads to an equal distribution of aortic arch diameters in both ApoE$^{-/-}$Fibulin-4$^{+/R}$ and ApoE$^{-/-}$Fibulin-4$^{+/+}$ mice, (including aortic arch dilations in some of both). This could point to the fact that under the same conditions Fibulin-4$^{+/R}$ animals are more susceptible than Fibulin-4$^{+/+}$ animals to atherosclerosis induction, which is therefore already
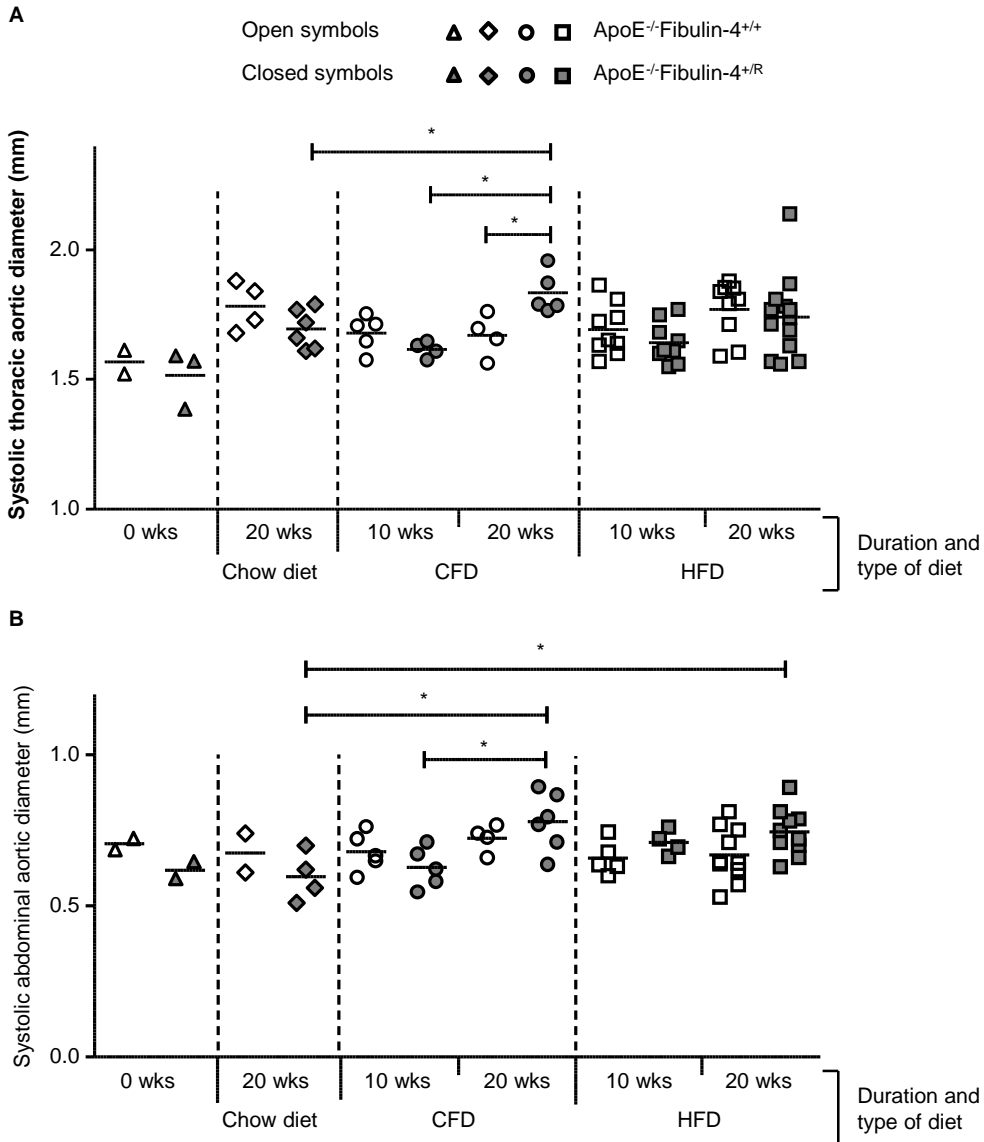
4

Figure 2: Increased thoracic and abdominal aortic diameters in ApoE^{-/-}Fibulin-4[+/R] mice. (A) Aortic arch diameter measurements by ultrasound imaging in M-mode show significant increased systolic aortic arch diameters in ApoE^{-/-}Fibulin-4[+/R] mice after 20 weeks of CFD (n=5) compared to ApoE^{-/-}Fibulin-4^{+/+} mice after 20 weeks of CFD (n=5), ApoE^{-/-}Fibulin-4[+/R] mice after 10 weeks of CFD (n=5), and compared to ApoE^{-/-}Fibulin-4[+/R] mice after 20 weeks of chow diet (n=6). Aortic arch diameters after 10 and 20 weeks HFD appear to be equally distributed in ApoE^{-/-}Fibulin-4^{+/+} and ApoE^{-/-}Fibulin-4[+/R] mice, with an increased variation in diameters. No differences are observed in mice fed a chow diet for 0 or 20 weeks. (B) Abdominal aortic measurements at the level of the iliac artery bifurcation also show significantly increased aortic diameters in ApoE^{-/-}Fibulin-4[+/R] mice after 20 weeks of CFD compared to ApoE^{-/-}Fibulin-4[+/R] mice after 10 weeks of CFD and 20 weeks of chow diet. Furthermore, increased abdominal aortic diameters are observed in ApoE^{-/-}Fibulin-4[+/R] mice after 20 weeks of HFD compared to ApoE^{-/-}Fibulin-4[+/R] mice after 20 weeks of chow diet (*p<0.05). Open symbols indicate aortic diameters of ApoE^{-/-}Fibulin-4^{+/+} mice, closed symbols indicate aortic diameters of ApoE^{-/-}Fibulin-4[+/R] mice.

apparent on a low fat diet. In addition, HFD leads to increased aortic wall stiffness in ApoE$^{-/-}$Fibulin-4$^{+/R}$ mice.

Interestingly, assessment of abdominal aortic diameters at the level of the iliac artery bifurcation showed significantly increased diameters in ApoE$^{-/-}$Fibulin-4$^{+/R}$ mice after 20 weeks on CFD as compared to 10 weeks on CFD, and also compared to ApoE$^{-/-}$ Fibulin-4$^{+/R}$ mice after 20 weeks chow diet (Figure 2B and Supplemental Figure 1B). Moreover, significantly increased abdominal diameters were observed in ApoE$^{-/-}$Fibulin-4$^{+/R}$ mice on 20 weeks of HFD compared to ApoE$^{-/-}$Fibulin-4$^{+/R}$ mice on 20 weeks of chow diet. Abdominal aortic diameters in ApoE$^{-/-}$Fibulin-4$^{+/+}$ mice were not increased when compared among different diets and diet durations. Altogether, these data suggest that Fibulin-4 deficient ApoE$^{-/-}$ mice already develop thoracic and abdominal aortic dilation on a low fat diet, while in addition HFD induces abdominal aortic dilation in ApoE$^{-/-}$Fibulin-4$^{+/R}$ mice and increases aortic arch stiffness.

ApoE$^{-/-}$Fibulin-4$^{+/R}$ aortas present increased plaque area in the thoracic and abdominal aorta

Next, we investigated the effect of a primary extracellular matrix defect on atherosclerotic plaque formation after 10 or 20 weeks of HFD feeding. Plaque area was quantified on *en face* preparations of Oil-red-O stained aortas. The descending and abdominal aorta of ApoE$^{-/-}$Fibulin-4$^{+/R}$ mice after 10 weeks of HFD showed significantly increased plaque area as compared to ApoE$^{-/-}$Fibulin-4$^{+/+}$ mice (Figure 3A and C). However, the plaque area in the aortic arch was similar between ApoE$^{-/-}$Fibulin-4$^{+/R}$ and ApoE$^{-/-}$Fibulin-4$^{+/+}$ mice at this age. After 20 weeks of HFD increased plaque area was detected in the aortic arch and abdominal aorta of ApoE$^{-/-}$Fibulin-4$^{+/R}$ mice compared to ApoE$^{-/-}$Fibulin-4$^{+/+}$ mice, but this was not significant due to large variability in plaque area between ApoE$^{-/-}$Fibulin-4$^{+/+}$ mice (Figure 3B and D). This suggests that Fibulin-4 deficiency accelerates plaque formation such that these are present after 10 weeks of HFD, while plaque occurrence after 20 weeks of HFD also increases in ApoE$^{-/-}$Fibulin-4$^{+/+}$ mice. Interestingly, increased plaque area in individual ApoE$^{-/-}$Fibulin-4$^{+/+}$ mice significantly correlated with increased aortic arch diameter (Figure 4), while plaque area in ApoE$^{-/-}$Fibulin-4$^{+/R}$ mice did not correlate with aortic arch diameter. These data indicate that the observed dilation in ApoE$^{-/-}$Fibulin-4$^{+/+}$ aortas is due to progression of atherosclerosis. However, in ApoE$^{-/-}$Fibulin-4$^{+/R}$ mice this correlation is absent, which is probably due to the fact that aortic dilation is already present at an earlier stage or with mild atherosclerosis, which means that in these mice the extracellular matrix defect is the underlying cause of the aortic dilation. At the same time, these results together indicate that the extracellular matrix defect in ApoE$^{-/-}$Fibulin-4$^{+/R}$ mice contributes to the increase in plaque area observed in thoracic and abdominal aortas.

ApoE$^{-/-}$Fibulin-4$^{+/R}$ aortas show altered plaque morphology

Results of the *en face* Oil-red-O staining of the aortic arches were confirmed by quantification of plaque size on haematoxylin-eosin stained sections of the aortic arch, showing no significantly increased plaque size in ApoE$^{-/-}$Fibulin-4$^{+/R}$ animals after 10 and 20 weeks of HFD as compared to ApoE$^{-/-}$Fibulin-4$^{+/+}$ mice. Although a small increase in plaque size and lipid content was observed after 20 weeks of HFD in histological sections of aortic arches of ApoE$^{-/-}$Fibulin-4$^{+/R}$ mice, this increase was not significant due to the low amount of samples (Supplemental Figure 3). Interestingly, a different plaque morphology was observed in aortic arches of ApoE$^{-/-}$Fibulin-4$^{+/R}$ mice after just 10 weeks of HFD; ApoE$^{-/-}$Fibulin-4$^{+/R}$ aortas showed either 1) partially loose plaques (which will be referred to as disconnected plaques) or 2) plaques grown over existing plaques (which will be referred to as overlying plaques) or
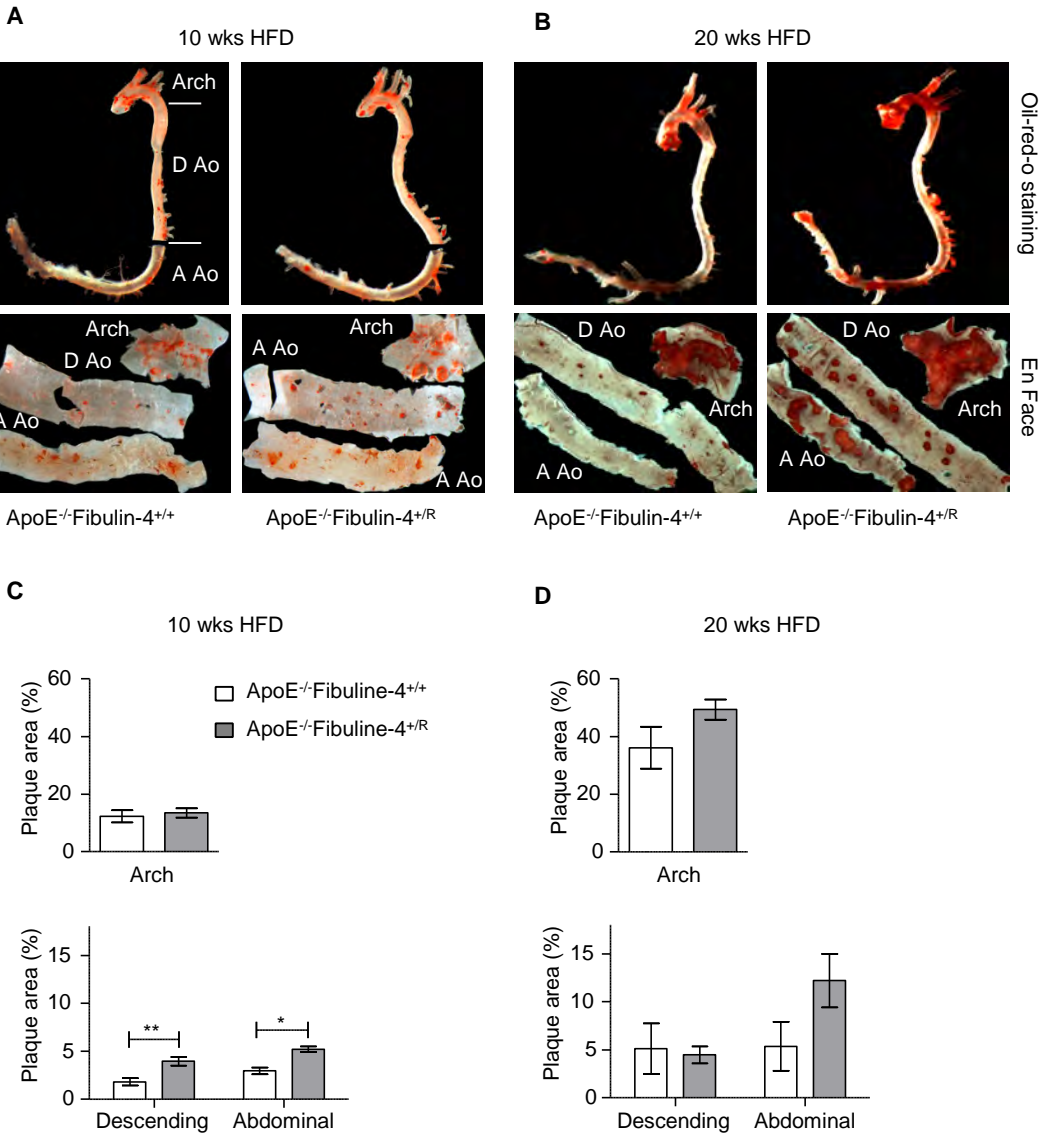
4

Figure 3: Increased plaque deposition in thoracic and abdominal aortas of ApoE$^{-/-}$Fibulin-4$^{+/R}$ mice. Oil-red-O staining and *en face* preparations of ApoE$^{-/-}$Fibulin-4$^{+/+}$ and ApoE$^{-/-}$Fibulin-4$^{+/R}$ aortas after (A) 10 and (B) 20 weeks of HFD show increased plaque areas in the thoracic and abdominal aortas of ApoE$^{-/-}$Fibulin-4$^{+/R}$ mice. Images in B represent aortas from ApoE$^{-/-}$Fibulin-4$^{+/R}$ mice, which show increased plaque areas as compared to their littermate ApoE$^{-/-}$Fibulin-4$^{+/+}$. Arch= aortic arch, D Ao= descending aorta, A Ao= abdominal aorta. (C) Quantification of the Oil-red-O stained *en face* preparations of ApoE$^{-/-}$Fibulin-4$^{+/R}$ aortas after 10 weeks of HFD (n=5) shows significantly increased plaque areas in the descending and abdominal aortas as compared to ApoE$^{-/-}$Fibulin-4$^{+/+}$ aortas (n=5). (D) After 20 weeks of HFD no significant differences could be observed between ApoE$^{-/-}$Fibulin-4$^{+/R}$ mice (n=10) and ApoE$^{-/-}$Fibulin-4$^{+/+}$ mice (n=5), as some ApoE$^{-/-}$Fibulin-4$^{+/+}$ aortas also displayed an increase in plaque areas (* $p<0.05$, ** $p<0.01$).

20 wks HFD

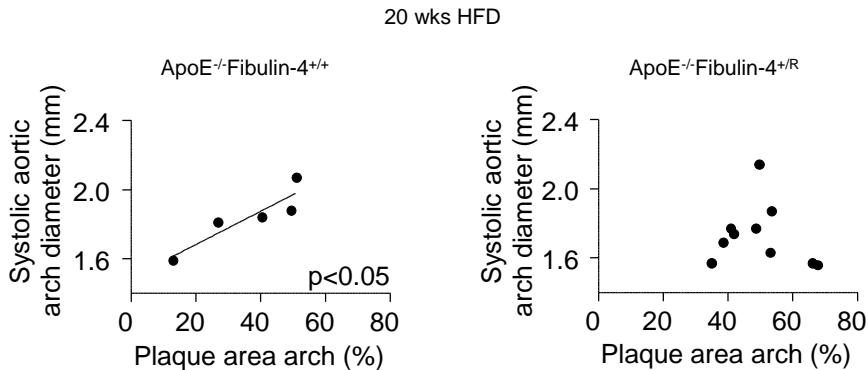ApoE$^{-/-}$Fibulin-4$^{+/+}$ ApoE$^{-/-}$Fibulin-4$^{+/R}$

Figure 4: Increased plaque formation correlates with aortic arch dilation in ApoE$^{-/-}$Fibulin-4$^{+/+}$ mice. After 20 weeks of HFD, ApoE$^{-/-}$Fibulin-4$^{+/+}$ mice significantly develop increased aortic arch diameters with increased plaque formation, whereas no such correlation is present in ApoE$^{-/-}$Fibulin-4$^{+/R}$ mice (*p<0.05).

3) a combination of both, in the brachiocephalic artery and in the inner curvature of the aortic arch (Figure 5A and C). Out of the eight ApoE$^{-/-}$Fibulin-4$^{+/R}$ animals examined, all displayed either disconnected plaques or overlying plaques, or both, in the brachiocephalic artery, whereas one out of eight ApoE$^{-/-}$Fibulin-4$^{+/+}$ mice displayed a disconnected plaque and one an overlying plaque (Table 1). To determine whether this altered plaque morphology is associated with elastin abnormalities due to Fibulin-4 deficiency, we performed histological elastin analysis. This revealed a significantly decreased elastin content in plaques of the brachiocephalic artery of ApoE$^{-/-}$Fibulin-4$^{+/R}$ animals (Figure 5B). In the inner curvature of the aortic arch, three out of seven ApoE$^{-/-}$Fibulin-4$^{+/R}$ animals had either a disconnected or an overlying plaque, or both, as compared to one out of eight ApoE$^{-/-}$Fibulin-4$^{+/+}$ mice with a disconnected plaque, which is the same animal that showed the disconnected plaque in the brachiocephalic artery (Table 1). Plaques of the inner curvature of the aortic arch of ApoE$^{-/-}$Fibulin-4$^{+/R}$ animals additionally contained a decrease in elastin content (Figure 5D). Histological analysis on cross-sections of abdominal aortas showed thickening of the abdominal aortic wall with increased spaces between the elastic laminae in ApoE$^{-/-}$Fibulin-4$^{+/R}$ animals after both 10 and 20 weeks of HFD, which is also observed at sites of plaque formation in the abdominal aorta as compared to ApoE$^{-/-}$Fibulin-4$^{+/+}$ animals

Table 1 – Amount of disconnected and overlying plaques found in the inner curvature of the aortic arch and in the brachiocephalic artery of ApoE$^{-/-}$Fibulin-4$^{+/R}$ mice as compared to ApoE$^{-/-}$Fibulin-4$^{+/+}$ mice.

Genotype	Inner Curvature			Brachiocephalic artery		
	Disconnected plaque	Overlying plaque	Total	Disconnected plaque	Overlying plaque	Total
ApoE$^{-/-}$Fibulin-4$^{+/+}$	1/8	-/8	1/8	1/8	1/8	2/8
ApoE$^{-/-}$Fibulin-4$^{+/R}$	2/7	3/7	3/7	5/8	6/8	8/8

*One arch could not be analyzed
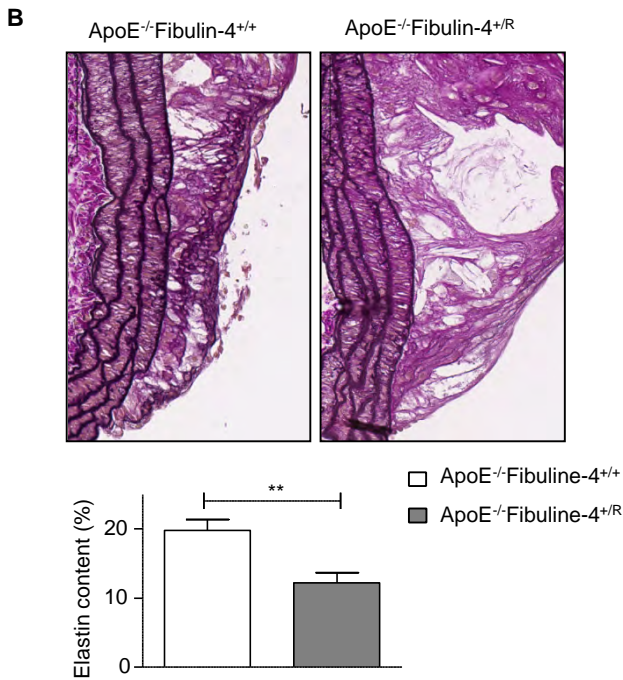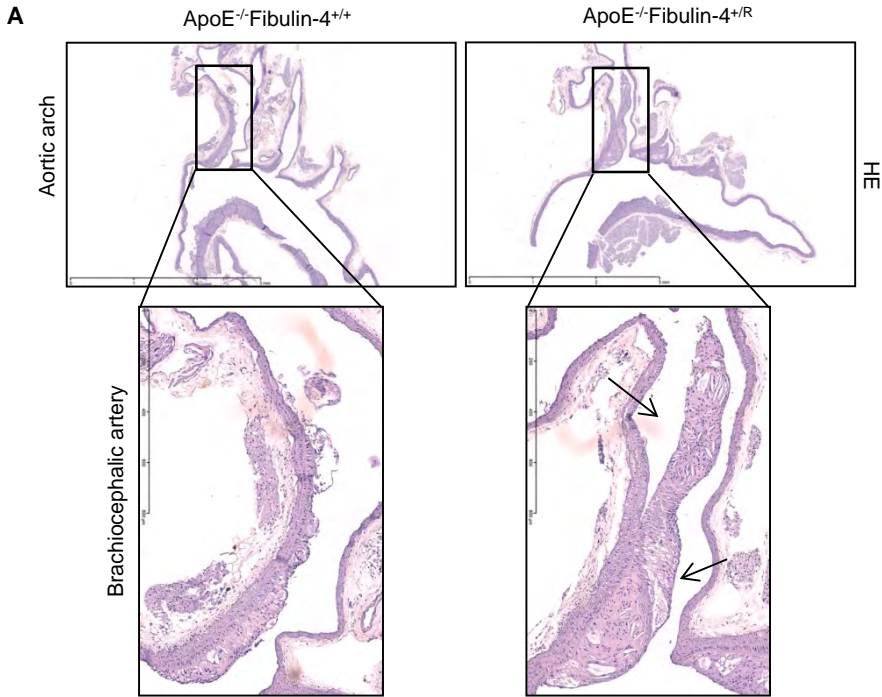
A

B

Figure 5: Plaque morphological changes in ApoE$^{-/-}$Fibulin-4$^{+/R}$ aortic arches after 10 weeks of HFD. HE analysis points to more disconnected and overlying plaques in (A) the brachiocephalic artery and (C) inner curvature of the arch of ApoE$^{-/-}$Fibulin-4$^{+/R}$ aortas after 10 weeks of HFD compared to ApoE$^{-/-}$Fibulin-4$^{+/+}$ aortas. (B and D) Elastin staining and quantification of the elastin content in plaques revealed significantly less elastin in plaques in (B) the brachiocephalic artery of ApoE$^{-/-}$Fibulin-4$^{+/R}$ mice. (D) Plaques of the inner curvature of the aortic arch of ApoE$^{-/-}$Fibulin-4$^{+/R}$ mice also show a tendency towards less elastin (*p<0.05).
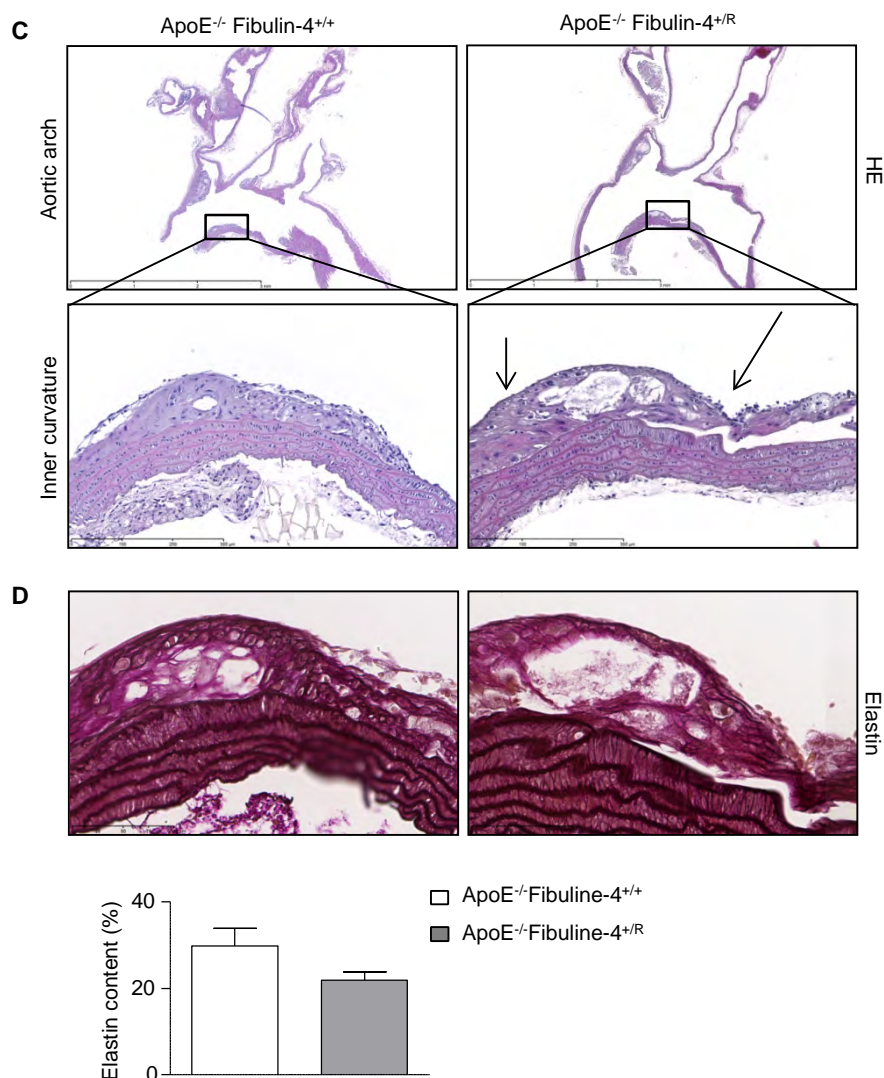
(Supplemental Figure 4 and 5). This was also previously observed in the thoracic aortas of homozygous Fibulin-4[R/R] mice and is associated with degeneration of the aortic wall [17]. No differences in plaque morphology could be observed in the abdominal aorta. Altogether, these results suggest that a deficiency in the extracellular matrix protein Fibulin-4 leads to the formation of morphologically different atherosclerotic plaques in the thoracic aorta.

Decreased survival of atherosclerotic ApoE^{-/-}Fibulin-4[+/R] mice between 20 and 30 weeks of HFD

Interestingly, approximately 30% of ApoE^{-/-}Fibulin-4[+/R] animals that were fed a HFD with the aim to be analyzed at 30 weeks, died suddenly between 20 and 30 weeks on the diet as compared to a 100% survival of ApoE^{-/-}Fibulin-4^{+/+} control animals (Figure 6). Moreover, symptoms of paralysis were observed after handling of 4 out of 16 ApoE^{-/-}Fibulin-4[+/R]

animals that survived between 20 and 30 weeks of CFD or HFD, while none of these symptoms were observed in ApoE$^{-/-}$Fibulin-4$^{+/+}$ mice (n=9) (Table 2). These results indicate that atherosclerotic Fibulin-4 deficient ApoE$^{-/-}$Fibulin-4$^{+/R}$ animals display a worsened survival outcome, possibly due to atherosclerosis-induced events, which may cause the paralysis symptoms.
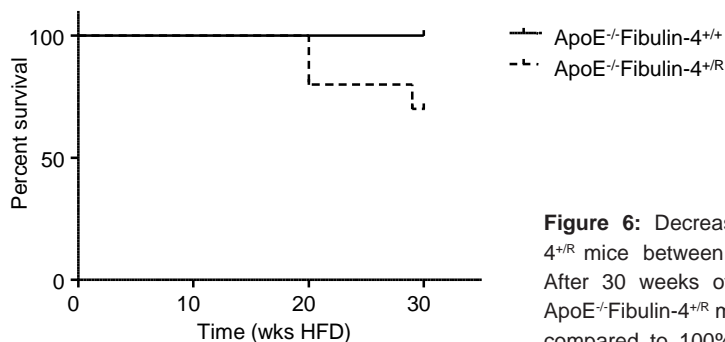

Figure 6: Decreased survival of ApoE$^{-/-}$Fibulin-4$^{+/R}$ mice between 20 and 30 weeks of HFD. After 30 weeks of HFD approximately 30% of ApoE$^{-/-}$Fibulin-4$^{+/R}$ mice (n=10) did not survive as compared to 100% survival of ApoE$^{-/-}$Fibulin-4$^{+/+}$ mice (n=3).

Table 2 – Observed paralysis symptoms after handling in ApoE$^{-/-}$Fibulin-4$^{+/R}$ mice on indicated durations of diet. wks= weeks

Mouse	Diet	Diet duration	Handling	Symptoms
1	CFD	20 wks	Anesthesia; echocardiography	Both hind limbs paralyzed
2	HFD	25 wks	Anesthesia; echocardiography	Left hind limb paralyzed; convulsions
3	HFD	30 wks	Anesthesia; injection MMPSense	Facial paralysis
4	HFD	30 wks	Anesthesia; echocardiography	Both hind limbs paralyzed

DISCUSSION

In this study we demonstrate that a genetic defect leading to subtle changes in the extracellular matrix structure of the aortic wall, in combination with atherosclerosis, may predispose for thoracic and abdominal aortic disease, including morphologically altered atherosclerotic plaques, and a worsened survival outcome. Atherosclerosis induction in the double mutant ApoE$^{-/}$Fibulin-4$^{+/R}$ mice results in increased abdominal MMP activity, thoracic and abdominal aortic dilation and increased thoracic and abdominal plaque formation. Furthermore, ApoE$^{-/}$Fibulin-4$^{+/R}$ mice display altered plaque morphology and have a reduced survival rate after 20 weeks of HFD. These results indicate that an underlying extracellular matrix defect promotes a bidirectional relation between atherosclerotic disease and aortic wall dilation.

On one side, atherosclerosis induction in Fibulin-4 deficient mice leads to enhanced aortic wall degeneration in Fibulin-4 deficient mice. ApoE$^{-/}$Fibulin-4$^{+/R}$ mice already develop both thoracic and abdominal aortic wall dilations after 20 weeks on CFD. Most probably 20 weeks of CFD induces mild atherosclerosis since ApoE$^{-/}$ mice spontaneously develop atherosclerosis after 12 weeks on normal chow diet, which has a lower fat percentage and a different nutrient composition compared to CFD [22-24]. Abdominal aortic dilations also occur after 20 weeks of HFD compared to chow diet, indicating that induction of both mild and high atherosclerosis results in increased abdominal aortic dilation in ApoE$^{-/}$Fibulin-4$^{+/R}$ mice. However, after 20 weeks of HFD both ApoE$^{-/}$Fibulin-4$^{+/+}$ and ApoE$^{-/}$Fibulin-4$^{+/R}$ mice have a wide but equal distribution in thoracic aortic arch diameters. This might be explained by highly increased atherosclerotic plaque formation induced by the HFD, which probably overrules the effects of the extracellular matrix degeneration on the aortic wall.

On the other side the aortic wall degeneration in ApoE$^{-/}$Fibulin-4$^{+/R}$ mice on HFD leads to increased plaque formation and altered plaque morphology. Ten weeks of HFD induces significantly more atherosclerotic plaques in the thoracic and abdominal aorta of ApoE$^{-/}$Fibulin-4$^{+/R}$ mice, whereas 20 weeks of HFD induces increased plaque formation in both ApoE$^{-/}$Fibulin-4$^{+/+}$ and ApoE$^{-/}$Fibulin-4$^{+/R}$ mice. However, a slight increase in plaque formation in the aortic arch and abdominal aorta of ApoE$^{-/}$Fibulin-4$^{+/R}$ mice after 20 weeks of HFD can be observed. This suggests that Fibulin-4 deficiency leads to enhanced atherosclerosis progression. In ApoE$^{-/}$Fibulin-4$^{+/+}$ mice the increased plaque formation is associated with the observed increased diameters, which is in concordance with previous reports [25]. However, ApoE$^{-/}$Fibulin-4$^{+/R}$ mice show increased plaque formation independent of changes in aortic diameters, probably because this dilation already occurs in an earlier stage at a lower percentage of fat. Histological analyses of aortic plaques of ApoE$^{-/}$Fibulin-4$^{+/R}$ mice after 10 weeks of HFD show more disconnected plaques, more overlying plaques and less elastin content in plaques compared to ApoE$^{-/}$Fibulin-4$^{+/+}$ aortic plaques. The reduced elastin content in atherosclerotic plaques of ApoE$^{-/}$Fibulin-4$^{+/R}$ mice is likely to be a consequence of impaired elastogenesis since Fibulin-4 influences crosslinking of elastic fiber by affecting the recruitment of LOX [5, 7, 26, 27]. A reduction in elastin content can make these plaques less stable. Additionally, ApoE$^{-/}$Fibulin-4$^{+/R}$ mice show symptoms of paralysis and a reduced survival between 20 and 30 weeks of HFD. The histological observed alterations in plaque morphology together with the observed worsened survival outcome might indicate that Fibulin-4 deficiency increases atherosclerosis-induced events. Whether these events are caused by plaque rupture is unclear. Our data show overlying plaques, disconnected plaques, and plaques with reduced elastin content and high MMP activity in the double mutant ApoE$^{-/}$Fibulin-4$^{+/R}$ mice. These features coincide with the occurrence of paralysis and reduced survival outcome.

4

In this respect, it would be interesting to make whole body angiographies of these animals just before they succumb. However, this is complicated due to their unpredictable and sudden death. Strikingly, plaque rupture was observed in another atherosclerotic mouse model with a more severe ECM defect; the ApoE$^{-/-}$Fibrillin-1$^{+/-}$ mouse [28]. Fibrillin-1 is the major structural component of microfibrils, which provide the scaffold for the deposition and crosslinking of elastin. The C1039G mutated Fibrillin-1 mice used in these studies however are different from the Fibulin-4^R mice used here, as the Fibrillin-1 mice spontaneously develop thoracic aneurysms thereby also affecting the hemodynamic parameters. Fragmentation of elastic fibers in these double knockout mice leads to increased vascular stiffness and promoted features of multifocal plaque instability. These mouse models with a structural defect in elastic fibers associated proteins provide insight into the role of extracellular matrix degeneration in the susceptibility for altered plaque morphology and its consequences.

The bidirectional interaction between aortic wall degeneration and atherosclerosis formation in our ApoE$^{-/-}$Fibulin-4$^{+/R}$ mice may lead to a vicious circle, in which the observed increased MMP activity could play a prominent role. The MMPSense 680 probes are activated by MMP2, -3, -9 and -13, of which MMP2 and MMP9 are known to play an important role in extracellular matrix degeneration and in aortic aneurysm formation. Increased MMP activity has indeed been observed in Fibulin-4 deficient mice with these probes [17, 19]. Furthermore, MMPs, mainly MMP3, -9, -12 and -13, were shown to be involved in different stages of plaque formation [20]. Therefore, the highly increased MMP activity observed in ApoE$^{-/-}$Fibulin-4$^{+/R}$ mice might be due to aortic wall degeneration as well as increased atherosclerotic plaques, and might contribute to the altered plaque morphology in these mice.

This ApoE$^{-/-}$Fibulin-4$^{+/R}$ mouse model with diet-induced atherosclerosis shows that subtle manifestations of aberrant elastin formation in heterozygous Fibulin-4$^{+/R}$ mice might predispose to thoracic and abdominal aortic disease as well as enhanced atherosclerotic disease. This combined mouse model provides the opportunity to unravel the biological processes underlying aortic wall degeneration and to identify markers that elucidate key events in the early stages of the pathogenic sequence that might culminate in an aneurysm. In fact, the ApoE$^{-/-}$Fibulin-4 mouse model therefore indicates that a haploinsufficiency for Fibulin-4 leads to a pathogenic outcome in combination with fat diets, and therefore might resemble patients that experience late-onset 'sporadic' and barely detectable forms of aneurysms. Additionally, this model provides insight in the effect of mild extracellular matrix defects, as observed during aging, on the progression of atherosclerosis.

ACKNOWLEDGMENTS

SUPPLEMENTARY

A

Open symbols △ ◇ ○ □ ApoE$^{-/-}$Fibulin-4$^{+/+}$
Closed symbols ▲ ◆ ● ■ ApoE$^{-/-}$Fibulin-4$^{+/R}$


B
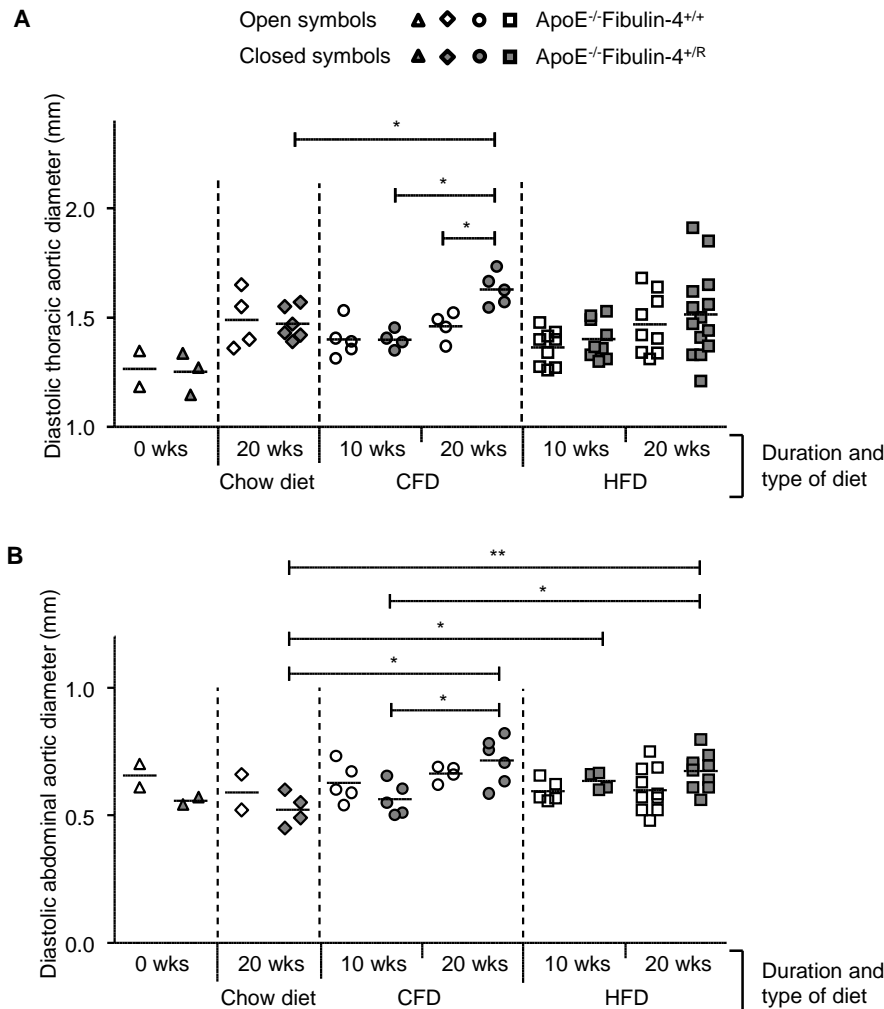
Supplemental Figure 1: Increased diastolic thoracic and abdominal aortic diameters in ApoE$^{-/-}$Fibulin-4$^{+/R}$ mice. (A) M-mode aortic diameter measurements in diastole by ultrasound imaging show significant dilation of the aortic arches of ApoE$^{-/-}$Fibulin-4$^{+/R}$ mice after 20 weeks of CFD (n=5) compared to ApoE$^{-/-}$Fibulin-4$^{+/+}$ mice after 20 weeks of CFD (n=5), ApoE$^{-/-}$Fibulin-4$^{+/R}$ mice after 10 weeks of CFD (n=5) and ApoE$^{-/-}$Fibulin-4$^{+/R}$ mice after 20 weeks of chow diet (n=6). Aortic arch diameters after 10 or 20 weeks of HFD seem to be evenly distributed in ApoE$^{-/-}$Fibulin-4$^{+/+}$ and ApoE$^{-/-}$Fibulin-4$^{+/R}$ mice, with an increased diameter variation. No differences are observed in mice fed a chow diet for 0 or 20 weeks. (B) Abdominal aortic measurements in diastole show significantly increased diameters in ApoE$^{-/-}$Fibulin-4$^{+/R}$ mice after 20 weeks of CFD compared to ApoE$^{-/-}$Fibulin-4$^{+/R}$ mice after 10 weeks of CFD and 20 weeks of chow diet. Furthermore, increased abdominal aortic diameters are observed in ApoE$^{-/-}$Fibulin-4$^{+/R}$ mice after 10 and 20 weeks of HFD compared to ApoE$^{-/-}$Fibulin-4$^{+/R}$ mice after 20 weeks of chow diet, and ApoE$^{-/-}$Fibulin-4$^{+/R}$ mice after 20 weeks of HFD compared to ApoE$^{-/-}$Fibulin-4$^{+/R}$ mice after 10 weeks of CFD (*p<0.05, **p<0.01). Open symbols indicate aortic diameters of ApoE$^{-/-}$Fibulin-4$^{+/+}$ mice, closed symbols indicate aortic diameters of ApoE$^{-/-}$Fibulin-4$^{+/R}$ mice.

4
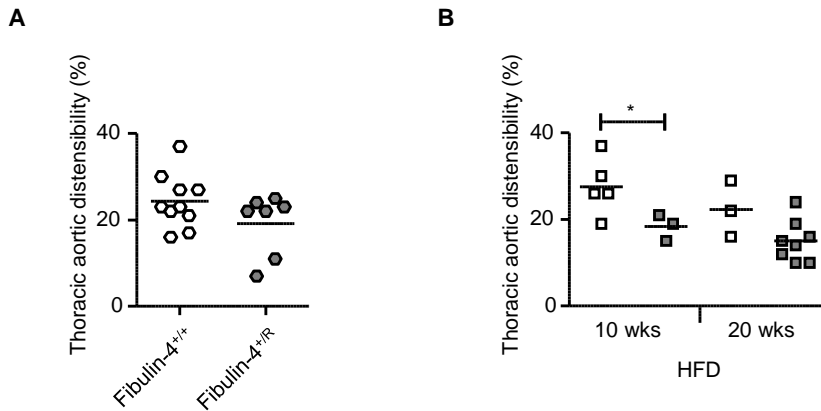
Supplemental Figure 2: Decreased distensibility of aortic arches from ApoE$^{-/-}$Fibulin-4$^{+/R}$ mice. (A) Calculations of aortic wall displacements in M-mode during systole and diastole indicate a slight non-significant reduced distensibility of 15 weeks old Fibulin-4$^{+/R}$ aortas on a chow diet compared to Fibulin-4$^{+/+}$ aortas. (B) A significantly reduced distensibility is observed in calculations of aortic wall displacements in B-mode of ApoE$^{-/-}$Fibulin-4$^{+/R}$ (n=5) aortas after 10 weeks of HFD, which further decreases after 20 weeks (n=10) of HFD compared to ApoE$^{-/-}$Fibulin-4$^{+/+}$ aortas (n=5) (*p<0.05).

4

A

B
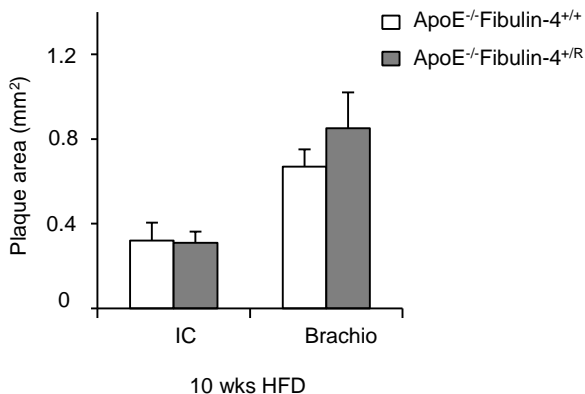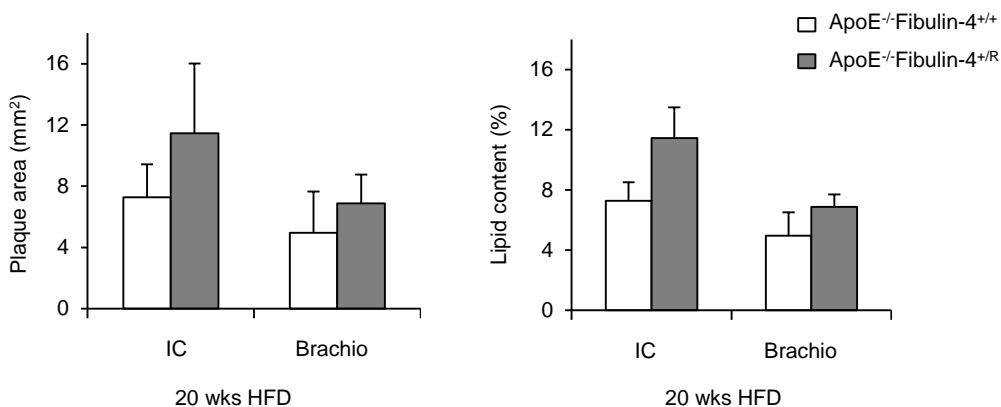
Supplemental Figure 3: Quantification of plaque area on histological sections of ApoE$^{-/-}$Fibulin-4 aortas after 10 and 20 weeks of HFD. (A) Plaque area quantified in the inner curvature of the aortic arch shows no difference between ApoE$^{-/-}$Fibulin-4$^{+/R}$ mice (n=8) and ApoE$^{-/-}$Fibulin-4$^{+/+}$ mice after 10 weeks of HFD (n=8), while a slight increase is observed in the brachiocephalic artery. (B) Quantified plaque area and percentage lipid content in plaques show a slight increase in ApoE$^{-/-}$Fibulin-4$^{+/R}$ mice after 20 weeks of HFD (n=5) compared to ApoE$^{-/-}$Fibulin-4$^{+/R}$ mice (n=3). IC= inner curvature, Brachio= brachiocephalic artery.

A

B
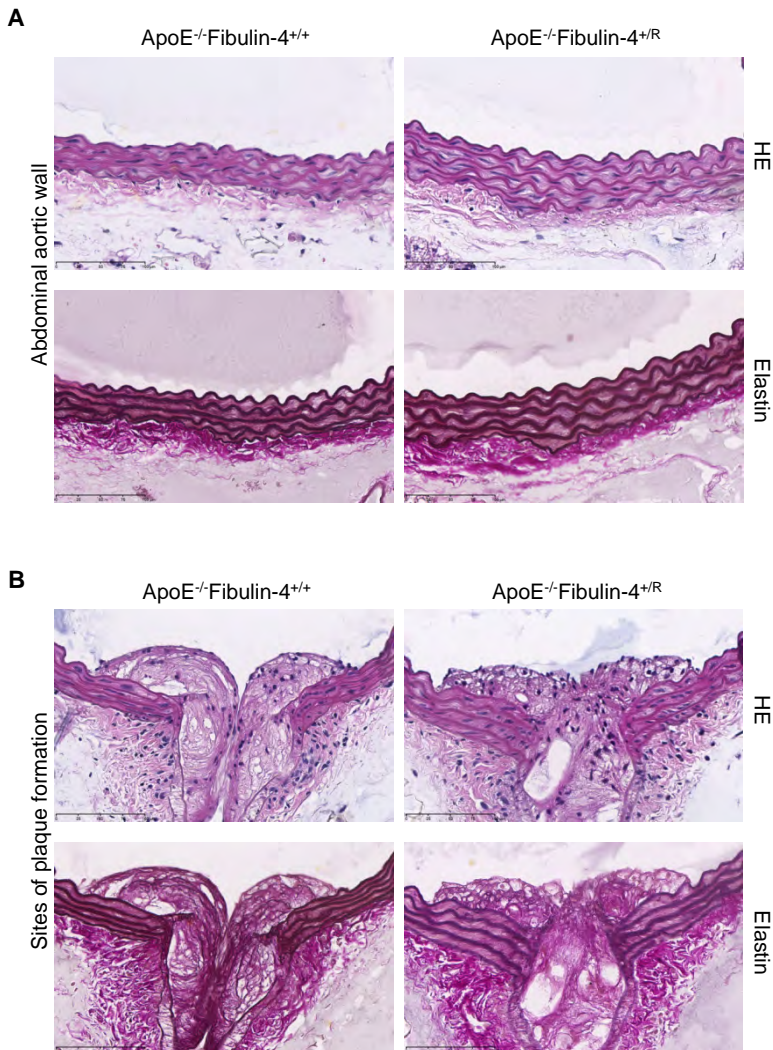
Supplemental Figure 4: Histological analysis of abdominal aortas after 10 weeks of HFD. HE and elastin analysis of the abdominal aorta revealed (A) thickened abdominal aortic wall with increased spaces between the elastic laminae in ApoE$^{-/-}$Fibulin-4$^{+/R}$ mice after 10 weeks of HFD as compared to ApoE$^{-/-}$Fibulin-4$^{+/+}$ mice, (B) which is also observed at sites of plaque formation.
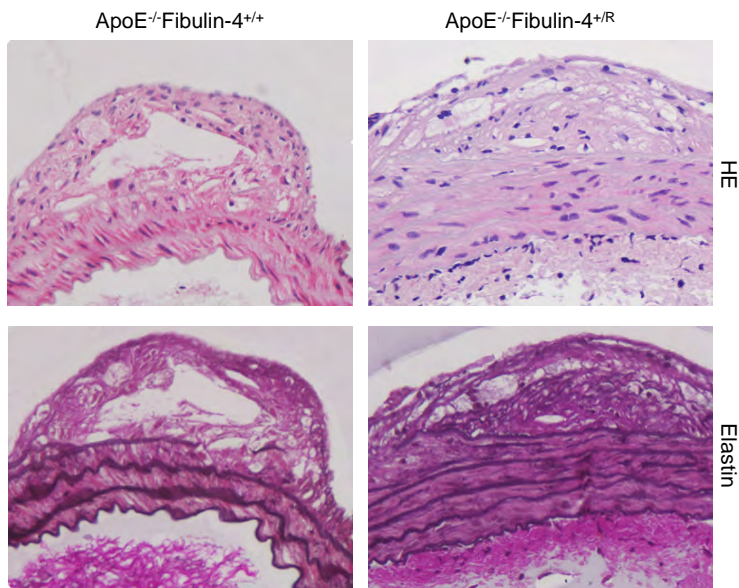
Supplemental Figure 5: Histological analysis of abdominal aortas after 20 weeks of HFD. HE and elastin analysis of the abdominal aorta after 20 weeks of HFD points to a thickened abdominal aortic wall with increased spaces between the elastic laminae in ApoE$^{-/-}$Fibulin-4$^{+/R}$ mice as compared to ApoE$^{-/-}$Fibulin-4$^{+/+}$ mice.

4

REFERENCES

1.   Lindsay ME, Dietz HC. Lessons on the pathogenesis of aneurysm from heritable conditions. Nature. 2011 May 19;473(7347):308-16.
2.   Isselbacher EM. Thoracic and abdominal aortic aneurysms. Circulation. 2005 Feb 15;111(6):816-28.
3.   Agricola E, Slavich M, Tufaro V, Fisicaro A, Oppizzi M, Melissano G, Bertoglio L, Marone E, Civilini E, Margonato A, Chiesa R. Prevalence of thoracic ascending aortic aneurysm in adult patients with known abdominal aortic aneurysm: An echocardiographic study. Int J Cardiol. 2013 May 10.
4.   Larsson E, Vishnevskaya L, Kalin B, Granath F, Swedenborg J, Hultgren R. High frequency of thoracic aneurysms in patients with abdominal aortic aneurysms. Ann Surg. 2011 Jan;253(1):180-4.
5.   Lederle FA, Johnson GR, Wilson SE, Chute EP, Littooy FN, Bandyk D, Krupski WC, Barone GW, Acher CW, Ballard DJ. Prevalence and associations of abdominal aortic aneurysm detected through screening. Aneurysm Detection and Management (ADAM) Veterans Affairs Cooperative Study Group. Ann Intern Med. 1997 Mar 15;126(6):441-9.
6.   Kielty CM, Sherratt MJ, Shuttleworth CA. Elastic fibres. J Cell Sci. 2002 Jul 15;115(Pt 14):2817-28.
7.   Argraves WS, Greene LM, Cooley MA, Gallagher WM. Fibulins: physiological and disease perspectives. EMBO Rep. 2003 Dec;4(12):1127-31.
8.   Chen Q, Zhang T, Roshetsky JF, Ouyang Z, Essers J, Fan C, Wang Q, Hinek A, Plow EF, Dicorleto PE. Fibulin-4 regulates expression of the tropoelastin gene and consequent elastic-fibre formation by human fibroblasts. Biochem J. 2009 Oct 1;423(1):79-89.
9.   Hoyer J, Kraus C, Hammersen G, Geppert JP, Rauch A. Lethal cutis laxa with contractural arachnodactyly, overgrowth and soft tissue bleeding due to a novel homozygous fibulin-4 gene mutation. Clin Genet. 2009 Sep;76(3):276-81.
10.   Hucthagowder V, Sausgruber N, Kim KH, Angle B, Marmorstein LY, Urban Z. Fibulin-4: a novel gene for an autosomal recessive cutis laxa syndrome. Am J Hum Genet. 2006 Jun;78(6):1075-80.
11.   Dasouki M, Markova D, Garola R, Sasaki T, Charbonneau NL, Sakai LY, Chu ML. Compound heterozygous mutations in fibulin-4 causing neonatal lethal pulmonary artery occlusion, aortic aneurysm, arachnodactyly, and mild cutis laxa. Am J Med Genet A. 2007 Nov 15;143A(22):2635-41.
12.   Renard M, Holm T, Veith R, Callewaert BL, Ades LC, Baspinar O, Pickart A, Dasouki M, Hoyer J, Rauch A, Trapane P, Earing MG, Coucke PJ, Sakai LY, Dietz HC, De Paepe AM, Loeys BL. Altered TGFbeta signaling and cardiovascular manifestations in patients with autosomal recessive cutis laxa type I caused by fibulin-4 deficiency. Eur J Hum Genet. 2010 Aug;18(8):895-901.
13.   Erickson LK, Opitz JM, Zhou H. Lethal osteogenesis imperfecta-like condition with cutis laxa and arterial tortuosity in MZ twins due to a homozygous fibulin-4 mutation. Pediatr Dev Pathol. 2012 Mar-Apr;15(2):137-41.
14.   Sawyer SL, Dicke F, Kirton A, Rajapkse T, Rebeyka IM, McInnes B, Parboosingh JS, Bernier FP. Longer term survival of a child with autosomal recessive cutis laxa due to a mutation in FBLN4. Am J Med Genet A. 2013 May;161A(5):1148-53.
15.   Kappanayil M, Nampoothiri S, Kannan R, Renard M, Coucke P, Malfait F, Menon S, Ravindran HK, Kurup R, Faiyaz-Ul-Haque M, Kumar K, De Paepe A. Characterization of a distinct lethal arteriopathy syndrome in twenty-two infants associated with an identical, novel mutation in FBLN4 gene, confirms fibulin-4 as a critical determinant of human vascular elastogenesis. Orphanet J Rare Dis. 2012;7:61.
16.   McLaughlin PJ, Chen Q, Horiguchi M, Starcher BC, Stanton JB, Broekelmann TJ, Marmorstein AD, McKay B, Mecham R, Nakamura T, Marmorstein LY. Targeted disruption of fibulin-4 abolishes elastogenesis and causes perinatal lethality in mice. Mol Cell Biol. 2006 Mar;26(5):1700-9.
17.   Hanada K, Vermeij M, Garinis GA, de Waard MC, Kunen MG, Myers L, Maas A, Duncker DJ, Meijers C, Dietz HC, Kanaar R, Essers J. Perturbations of vascular homeostasis and aortic valve abnormalities in fibulin-4 deficient mice. Circ Res. 2007 Mar 16;100(5):738-46.
18.   Huang J, Davis EC, Chapman SL, Budatha M, Marmorstein LY, Word RA, Yanagisawa

H. Fibulin-4 deficiency results in ascending aortic aneurysms: a potential link between abnormal smooth muscle cell phenotype and aneurysm progression. Circ Res. 2010 Feb 19;106(3):583-92.

19. Kaijzel EL, van Heijningen PM, Wielopolski PA, Vermeij M, Koning GA, van Cappellen WA, Que I, Chan A, Dijkstra J, Ramnath NW, Hawinkels LJ, Bernsen MR, Lowik CW, Essers J. Multimodality imaging reveals a gradual increase in matrix metalloproteinase activity at aneurysmal lesions in live fibulin-4 mice. Circ Cardiovasc Imaging. 2010 Sep;3(5):567-77.

20. Carmeliet P, Moons L, Lijnen R, Baes M, Lemaitre V, Tipping P, Drew A, Eeckhout Y, Shapiro S, Lupu F, Collen D. Urokinase-generated plasmin activates matrix metalloproteinases during aneurysm formation. Nat Genet. 1997 Dec;17(4):439-44.

21. Luttun A, Lutgens E, Manderveld A, Maris K, Collen D, Carmeliet P, Moons L. Loss of matrix metalloproteinase-9 or matrix metalloproteinase-12 protects apolipoprotein E-deficient mice against atherosclerotic media destruction but differentially affects plaque growth. Circulation. 2004 Mar 23;109(11):1408-14.

22. Zhang SH, Reddick RL, Piedrahita JA, Maeda N. Spontaneous hypercholesterolemia and arterial lesions in mice lacking apolipoprotein E. Science. 1992 Oct 16;258(5081):468-71.

23. Breslow JL. Mouse models of atherosclerosis. Science. 1996 May 3;272(5262):685-8.

24. Plump AS, Smith JD, Hayek T, Aalto-Setala K, Walsh A, Verstuyft JG, Rubin EM, Breslow JL. Severe hypercholesterolemia and atherosclerosis in apolipoprotein E-deficient mice created by homologous recombination in ES cells. Cell. 1992 Oct 16;71(2):343-53.

25. Lutgens E, de Muinck ED, Heeneman S, Daemen MJ. Compensatory enlargement and stenosis develop in apoE(-/-) and apoE*3-Leiden transgenic mice. Arterioscler Thromb Vasc Biol. 2001 Aug;21(8):1359-65.

26. Doyle JJ, Gerber EE, Dietz HC. Matrix-dependent perturbation of TGFbeta signaling and disease. FEBS Lett. 2012 Jul 4;586(14):2003-15.

27. Choudhury R, McGovern A, Ridley C, Cain SA, Baldwin A, Wang MC, Guo C, Mironov A, Jr., Drymoussi Z, Trump D, Shuttleworth A, Baldock C, Kielty CM. Differential regulation of elastic fiber formation by fibulin-4 and -5. J Biol Chem. 2009 Sep 4;284(36):24553-67.

28. Van Herck JL, De Meyer GR, Martinet W, Van Hove CE, Foubert K, Theunis MH, Apers S, Bult H, Vrints CJ, Herman AG. Impaired fibrillin-1 function promotes features of plaque instability in apolipoprotein E-deficient mice. Circulation. 2009 Dec 15;120(24):2478-87.
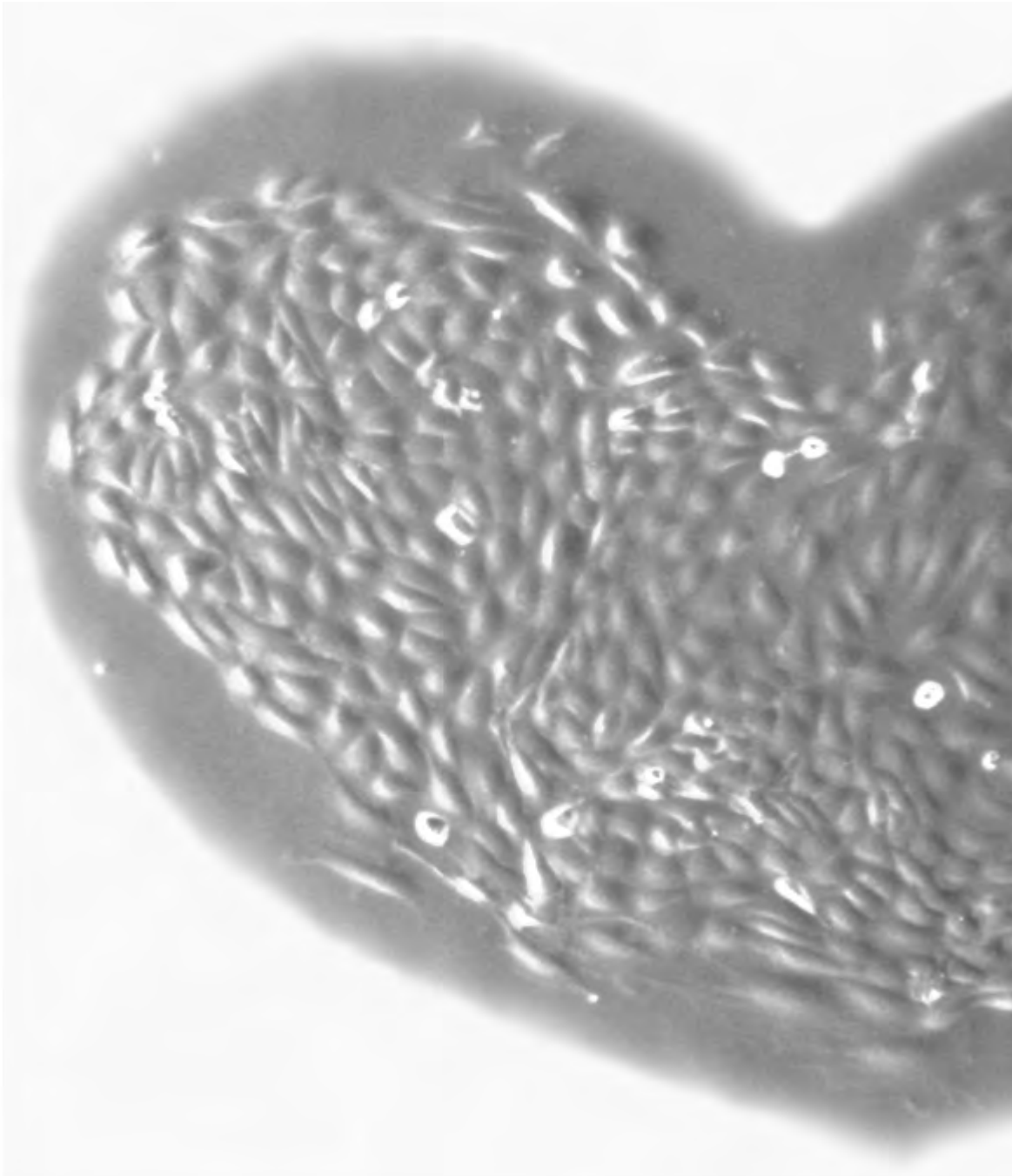
4

Chapter 5

Fibulin-4 deficiency results in enhanced TGF-β signaling in aortic smooth muscle cells and increased TGF-β2 secretion
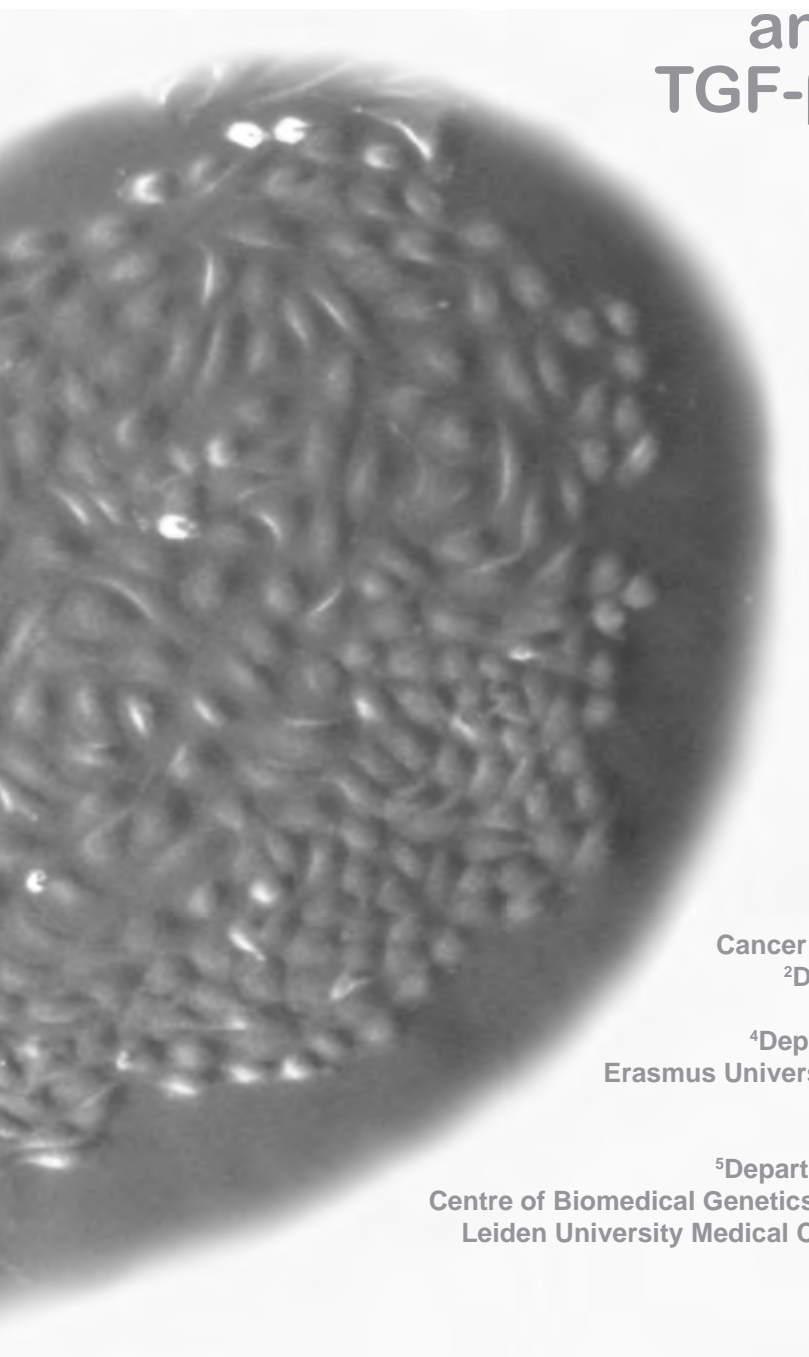
N.W.M. Ramnath[1,2] *,
L.J.A.C. Hawinkels[5] *,
P.M. van Heijningen[1],
L. te Riet[2,3], M. Paauwe[5],
R. Kanaar[1,4], P. ten Dijke[5],
J. Essers[1,2,4]

[1]Department of Genetics,
Cancer Genomics Center Netherlands,
[2]Department of Vascular Surgery,
[3]Department of Pharmacology,
[4]Department of Radiation Oncology,
Erasmus University Medical Center, Rotterdam,
The Netherlands

[5]Department of Molecular Cell Biology,
Centre of Biomedical Genetics and Cancer Genomics Centre,
Leiden University Medical Center, Leiden, The Netherlands

* Equal contributors

ABSTRACT

Fibulins are extracellular matrix proteins associated with elastic fibers, which are important for the mechanical elasticity of connective tissue such as skin, vessels and lungs. The most life threatening abnormalities caused by homozygous Fibulin-4 mutations in patients are aortic aneurysms. A previously generated mouse model with Fibulin-4 deficiency (Fibulin-4[R]) showed that Fibulin-4 expression level determines the severity of the aneurysmal disease, and was associated with upregulation of TGF-β signaling in aortic smooth muscle cells (SMCs) of Fibulin-4 deficient mice. To further determine the regulation of this pathway, we isolated aortic SMCs from Fibulin-4 deficient mice. Fibulin-4 deficient SMCs showed reduced growth, which could be reversed by treatment with TGF-β neutralizing antibodies. In Fibulin-4 deficient SMCs increased basal and ligand-induced TGF-β signaling was detected using a Smad3/Smad4-dependent transcriptional reporter assay and by increased Smad2 phosphorylation. Since the increased TGF-β/Smad signaling could be inhibited by inhibition of TGF-β type I receptor kinase activity we measured levels of all TGF-β isoforms in conditioned medium of these cells. The data revealed slightly increased TGF-β1 and, interestingly, markedly increased TGF-β2 levels. Interestingly, increased TGF-β2 bioavailability could be measured in plasma from homozygous Fibulin-4[R/R] mice, which was reduced after losartan treatment, an angiotensin II type 1 receptor blocker known to prevent aortic aneurysm formation. In conclusion, we have shown increased TGF-β signaling in isolated SMCs from Fibulin-4 deficient mouse aortas caused by increased bioavailability of TGF-β1, and especially TGF-β2. These data provide new insights in the molecular interaction between Fibulin-4 and TGF-β pathway regulation in the pathogenesis of aortic aneurysms.

5

INTRODUCTION

In developed countries 1% to 2% of all deaths are caused by aortic aneurysms and dissections [1]. In these countries the incidence of thoracic aortic aneurysm (TAA) is approximately 10 per 100,000 persons per year [2, 3]. Several genes have been identified in both syndromic and non-syndromic forms of TAA, including extracellular matrix (ECM) genes, genes encoding contractile proteins of the smooth muscle cell (SMC) and genes encoding proteins involved in the regulation of the transforming growth factor (TGF)-β pathway [4-10]. A crucial role for the TGF-β pathway in TAA became evident from both studies on mouse models and the analysis of the TGF-β pathway in patients with these disorders [6, 11-14]. TAAs are usually associated with increased TGF-β signaling, but contradictory this association has also been observed with loss of function TGF-β and TGF-β receptor mutations. Although the identification of these genes has led to new insights in the pathogenesis of aneurysm formation, the precise molecular mechanism of how deficiency in these genes results in dysregulated TGF-β signaling still remains to be elucidated.

The TGF-β superfamily consists of 30 members including the TGF-βs, the bone morphogenetic proteins and the activins. These cytokines have pleiotropic functions and are all synthesized as inactive precursors and require (proteolytic) processing before they are biologically active. Their biological functions include regulation of cell growth, differentiation and apoptosis. There are three mammalian TGF-β isoforms; TGF-β1, -β2 and -β3 are encoded by different genes, but show a high degree of amino acid sequence homology. All TGF-β isoforms are bound to the latency associated protein (LAP) and via the latent TGF-β binding protein (LTBP) bound to the extracellular matrix. Upon activation TGF-βs can bind to the type-II TGF-β receptors (TβRII), which recruit the type-I TGF-β receptor (TβRI), also called activin receptor-like kinase (ALK)-5. ALK-5 is transphosphorylated by TβRII and subsequently downstream (mothers against decapentaplegic) Smad proteins (i.e. Smad 2/3) are phosphorylated. Upon heteromeric complex formation of activated Smad2 and -3 with Smad4, the Smad complex can translocate to the nucleus and interact with target gene promoters and regulate transcription of genes encoding for plasminogen activator inhibitor (PAI)-I, matrix metalloproteinases (MMPs) and extracellular matrix proteins [15-17].

A syndromic form of TAA, Marfan syndrome, is caused by mutations in the extracellular matrix glycoprotein Fibrillin-1, which is one of the major components of microfibrils and belongs to the same gene family as LTBPs. Fibrillin-1 is involved in sequestering of the latent TGF-β complex through interaction with LTBPs and Fibrillin-1 deficiency results in a higher TGF-β bioavailability and increased TGF-β signaling in aortic and lung tissue in Marfan syndrome mice. The increased TGF-β signaling is associated with elevated circulating TGF-β1 levels, which can be decreased by administration of losartan, an angiotensin II type 1 receptor blocker (ARB) which prevents aortic aneurysm formation and lowers the expression of TGF-β ligands, receptors and activators [18-22]. This suggests TGF-β1 as a prognostic biomarker in Marfan syndrome and indicates that reduced TGF-β1 levels lead to reversal of the aortic pathology.

In addition to Marfan syndrome, upregulated TGF-β signaling has been observed in another heritable form of TAA caused by a deficiency in the extracellular matrix protein Fibulin-4 [13, 23-29]. Fibulin-4 is mainly expressed in large vessels and elastic organs (e.g. lungs, skin) and plays an important role in elastogenesis [30, 31]. In addition, Fibulin-4 is involved in crosslinking of elastic fibers through recruitment of lysyl oxidase (LOX), which can directly inactivate the TGF-β ligands [32-34]. In Fibulin-4 deficient patients and mice

5

elevated TGF-β signaling has been shown by increased nuclear pSmad2 staining of aortic tissue [12, 13, 29]. However, the exact mechanism by which Fibulin-4 deficiency leads to increased TGF-β signaling remains to be determined.

Therefore, we isolated SMCs from the aortic arch of Fibulin-4 deficient mice to further investigate the upregulation of TGF-β signaling in these mice at the molecular level. Due to transcriptional interference, hypomorphic Fibulin-4[R/R] mice (R stands for reduced) have a 4-fold reduced expression of Fibulin-4 resulting in vascular abnormalities, including TAAs, and Fibulin-4[+/R] mice a 2-fold lower expression leading to milder extracellular matrix defects [12]. Our data establishes that TGF-β signaling is enhanced in isolated SMCs derived from the aortas of Fibulin-4 deficient mice. Interestingly, we find that this increased TGF-β signal transduction activity is not only associated with increased bioavailability of TGF-β1, but also with enhanced TGF-β2 levels. In the presence of TGF-β neutralizing antibodies, the proliferation defect seen in Fibulin-4[R/R] SMCs could be reversed, indicating that increased TGF-β signaling is responsible for the growth delay in Fibulin-4 deficient SMCs. Increased secretion of TGF-β2 could also be detected in blood of the Fibulin-4[R/R] mice. Treatment of Fibulin-4[R/R] mice with losartan suppressed the increased TGF-β2 levels in blood plasma. This study shows that increased TGF-β signaling in SMCs of Fibulin-4 deficient mice is caused by an increased bioavailability of different isoforms of the TGF-β ligands.

METHODS

Animals
Mice containing the Fibulin-4[R] allele were generated as previously described [12]. All mice used were bred in a C57Bl/6J background and were kept in individually ventilated cages to keep animals consistently micro-flora and disease free. To avoid stress-related vascular injury, mice were earmarked and genotyped 4 weeks after birth. Animals were housed at the Animal Resource Center (Erasmus University Medical Center), which operates in compliance with the "Animal Welfare Act" of the Dutch government, using the "Guide for the Care and Use of Laboratory Animals" as its standard. As required by Dutch law, formal permission to generate and use genetically modified animals was obtained from the responsible local and national authorities. All animal studies were approved by an independent Animal Ethical Committee (Dutch equivalent of the IACUC).

Treatment
Fibulin-4^{+/+} and Fibulin-4[R/R] mice received losartan (0.6 gram/liter, Sigma) or placebo in their drinking water as previously described [21, 59]. Adult Fibulin-4[R/R] mice and their wild type littermates were treated during 10 weeks, starting at the age of 5 weeks. Blood samples from placebo or losartan treated Fibulin-4^{+/+} and Fibulin-4[R/R] mice were obtained by cardiac puncture and collected in heparin vials (Sarstedt).

Isolation of SMCs and cell culture
Vascular SMCs were isolated from the luminal side of the aortic arch from Fibulin-4^{+/+}, Fibulin-4[+/R] and Fibulin-4[R/R] male mice. The tissue was washed with phosphate-buffered saline (PBS), cut into 5-mm pieces and incubated in 0.1% gelatin coated cell culture dishes. After 7–10 days, smooth muscle-like cell outgrowth was observed. SMCs were maintained in complete DMEM (Lonza, Leusden, the Netherlands), 100 U/ml penicillin and 100 µg/ml streptomycin, supplemented with 10% fetal calf serum (HyClone, Thermo Scientific) and used at passage 5–11.

Immunofluorescent staining

Subconfluent SMCs, human umbilical vein endothelial cells (HUVECs) and mouse embryonic fibroblasts (MEFs) were grown on coverslips and fixed in 1% paraformaldehyde. Cells were permeabilized with 0.1% Triton/PBS and blocked with PBS+ (1.5% bovine serum albumin/0.15% glycine (Sigma) in PBS). Next, coverslips were incubated overnight at 4 °C with the primary antibodies; mouse anti-smooth muscle actin (SMA) 1:1500 (Progen, Heidelberg, Germany), rabbit polyclonal anti-smooth muscle specific protein-22 (SM22) alpha antibody 1:400 (ab14106, Abcam, Cambridge, UK), mouse monoclonal anti-smooth muscle myosin heavy chain II (MHC II) 1G12 1:500 (ab683, Abcam), Rabbit anti-CD31 1:800 (Santa Cruz Biotechnologies, Santa Cruz, USA) and Rabbit anti-fibroblast specific protein (FSP)1/S100A4 1:1600 (Millipore). The next day cells were incubated with secondary antibodies anti-Mouse alexafluor 488 1:1000 (Molecular Probes) for SMA and MHC II and anti-Rabbit alexafluor 594 1:1000 (Molecular Probes, Eugene, Oregon) for SM22, CD31 and FSP1, and mounted with DAPI. Slides were analyzed with the LEICA DMRBE Aristoplan Microscope equipped with the Hamamatsu ORCA-ER Camera. Pictures were taken at 25 x magnification.

Proliferation assay

Fibulin-4$^{+/+}$, Fibulin-4$^{+/R}$ and Fibulin-4$^{R/R}$ SMCs were seeded in triplicate in 6 cm dishes (5000 cells/well) and allowed to attach overnight. Next cells were treated with an IgG control or with TGF-β neutralizing antibodies (nAb), kindly provided by Dr. E. de Heer, Leiden University Medical Center, Dept. of pathology, and counted every day. Medium was replaced every other day. The MTS proliferation assay was performed according to the manufacturer's instructions (Promega, Madison, USA). In short SMCs were seeded in 96-well plates (1500 cells/well) and allowed to attach overnight. At day-1, -2 and -3 medium was changed to 100 μl complete DMEM + 20 μl MTS substrate and the metabolic activity of the cells was analyzed by absorbance change at 490 nm after 2 hours.

TGF-β response assay

TGF-β response in SMCs was determined using (CAGA)$_{12}$−MLP−Luciferase promoter reporter construct [38]. This construct contains 12 palindromic repeats of the Smad3/4 binding element derived from the *PAI-1* promoter and was shown to be highly specific and sensitive to TGF-β. The assay was performed as described previously [60]. In short SMCs were seeded in 1% gelatin coated 24-well plates and allowed to attach overnight. Subconfluent cells were transfected using Lipofectamin 2000 (Invitrogen) according to the manufacturer's protocol. A β-galactosidase plasmid was co-transfected to correct for transfection efficiency. After 6 hours, medium was changed to DMEM containing 10% FCS and the cells were incubated for 24 hours. Next cells were serum-starved overnight and stimulated with 5 ng/ml TGF-β3 in the presence or absence of 10 uM SB431542 (Tocris/R&D systems, Abington, UK) for 6 hours. After stimulation the cells were washed, lysed and luciferase activity was determined according to the manufacturer's protocol (Promega). β-Galactosidase activity in the lysates was determined using β-gal substrate (0.2 M H$_2$PO$_4$, 2 mM MgCl$_2$, 4 mM ortho-nitrophenyl-phosphate, 0.25% β-mercaptoethanol) and measuring absorbance change at 405 nm. The luciferase count was corrected for β-galactosidase activity. The relative increase in luciferase activity was calculated versus controls. All experiments were performed at least three times in triplicate. To determine the transfection efficiency of Fibulin-4$^{+/+}$, Fibulin-4$^{+/R}$ and Fibulin-4$^{R/R}$ SMCs they were transfected with a green fluorescent protein (GFP) plasmid as described above, trypsinized and fixed with 1% PFA. Subsequently, SMCs were analyzed with flow cytometry for the percentage of GFP

5

transfected SMCs compared to the total amount of SMCs.

Western blot analysis

Western blot analysis was performed as described before [61]. In short, equal amounts of protein (DC protein assay, Bio-Rad Laboratories, Hercules, CA) were separated on 10% SDS−polyacrylamide gel electrophoresis under reducing conditions. Proteins were transferred to nitrocellulose membranes (Whattman, Dassel, Germany) and blocked with 5% milk powder in tris-buffered saline containing 0.05% Tween-20 (Merck, Darmstadt, Germany). After washing, blots were overnight incubated with rabbit anti-pSmad2 (Cell signaling Technologies, USA) and rabbit anti-pSmad3 (kindly provided by Dr. E. Leof, Mayo Clinic, Rochester, MN, USA) followed by horseradish peroxidase-conjugated secondary antibodies (all GE Healthcare, Waukesha, WI, USA). Detection was performed by chemoluminescence according to the manufacturer's protocol (Pierce, Rockford, IL, USA). Afterwards, blots were stripped and reprobed with mouse anti-β-actin antibodies as a loading control.

RNA isolation and real-time PCR

Expression of Fibulin-4 and TGF-β2 were analyzed in SMCs. RNA was isolated using RNeasy Mini Kit according to the manufacturer's instructions (Qiagen, Hilden, Germany). RNA concentration and purity was determined spectrometrically. Complementary DNA synthesis was performed using random primers. cDNA samples were subjected to 40 cycles real-time PCR analysis using maxima SYBR Green qPCR Master Mix 2x (Fermentas, Vilnius Lithuania) and primers shown in supplemental table 1. Reactions were performed in triplicates for each sample. Product specificity was determined by melting curve analysis and gel electrophoresis. The average Ct values of the triple reactions were calculated for each gene and all values were normalized for cDNA content by HPRT expression. The levels of fold-change for each gene were calculated relative to the gene expression levels in baseline wild type SMCs. RNA isolated from HUVECs and fibroblasts were used as controls for the SMCs markers.

TGF-β ELISAs

SMC conditioned medium was prepared by seeding the cells and growing them to subconfluence. Medium was changed to serum-free DMEM, containing antibiotics as described above, and incubated for 4 days. Lysates were prepared from aortic arches of 14-15 week old Fibulin-4$^{+/+}$, Fibulin-4$^{+/R}$ and Fibulin-4$^{R/R}$ mice and protein amounts were determined (Pierce BCA protein assay kit, Thermo Scientific). Blood samples from Fibulin-4$^{+/+}$, Fibulin-4$^{+/R}$ and Fibulin-4$^{R/R}$ mice were obtained by cardiac puncture and collected in heparin vials (Sarstedt). Total TGF-β1, TGF-β2, and TGF-β3 levels in CM samples, aortic arch lysates and plasma samples were determined by commercially available duo-sets (R&D Systems) as described before [62, 63].

Statistical analysis

Data are presented as mean ± SEM. The nonparametric Mann-Whitney U-test and unpaired student's t-test were performed to analyze the specific sample pairs for significant differences. A p-value of <0.05 was considered to indicate a significant difference between groups. All analyses were performed using IBM SPSS Statistics version 20.0 (SPSS Inc., Chicago, IL, USA).

RESULTS

Characterization of SMCs derived from Fibulin-4 deficient aortas

To examine TGF-β signaling in Fibulin-4 deficient SMCs we isolated these cells from the aortic arches of Fibulin-4$^{+/+}$, Fibulin-4$^{+/R}$ and Fibulin-4$^{R/R}$ mice. To confirm that the cells we isolated were SMCs, the cells were analyzed for presence of SMC specific markers, including α-smooth muscle actin (SMA), smooth muscle specific protein-22 (SM22), smooth muscle myosin heavy chain II (MHC II) and fibroblast specific protein 1 (FSP1), which stains SMCs with a rhomboid phenotype [35]. Rhomboid SMCs are characterized by a polygonal, flat and elongated shape and are grown by explantation from sliced tissue, together with a proportion of spindle-shaped SMCs [36]. HUVECs stained positive for CD31 and negative for all other markers, while MEFs were positive for FSP1, and SMA and SM22, as described before [37]. Immunofluorescent staining of the isolated SMCs showed positive staining for SMA, SM22, MHC II, FSP-1 and negative staining for CD31 (Figure 1A) confirming the SMC phenotype. QPCR expression analysis also showed absent CD31 expression and von Willebrand Factor, an additional endothelial cell marker (data not shown). SMA was highly expressed and seemed somewhat increased in Fibulin-4$^{+/R}$ and Fibulin-4$^{R/R}$ SMCs (Figure 1B). Next, the levels of Fibulin-4 were analyzed by QPCR. These data revealed that expression levels of Fibulin-4 mRNA in Fibulin-4$^{+/R}$ and Fibulin-4$^{R/R}$ SMCs was downregulated (Figure 1C). These data show that we isolated a population of SMCs with a gradual reduced Fibulin-4 expression level for further studies.

Reduced proliferation of Fibulin-4$^{R/R}$ SMCs due to increased TGF-β signaling

First we analyzed proliferation rates of the SMCs with reduced Fibulin-4 expression. Figure 2A shows similar growth rates of all three genotypes until day 5, after which proliferation was decreased in Fibulin-4$^{R/R}$ SMCs. As TGF-β can inhibit cell proliferation, we determined whether the reduced growth of Fibulin-4$^{R/R}$ SMCs is a consequence of increased TGF-β activity. Therefore SMCs were treated with TGF-β neutralizing antibodies (nAb), which neutralize all three TGF-β isoforms (TGF-β1, TGF-β2 and TGF-β3). Interestingly, treatment with TGF-β nAb reversed the growth inhibition observed in Fibulin-4$^{R/R}$ SMCs compared to Fibulin-4$^{+/+}$ SMCs (Figure 2B-E). On day 7 the number of Fibulin-4$^{R/R}$ SMCs was significantly higher after treatment with TGF-β nAb compared to non-treated Fibulin-4$^{R/R}$ SMCs. Moreover, proliferation was similar to Fibulin-4$^{+/+}$ SMCs. These data indicate that TGF-β might inhibit the proliferation of Fibulin-4 deficient SMCs.

Fibulin-4 expression dose dependently regulates TGF-β signaling in aortic SMCs

Since we observed that TGF-β nAb stimulates Fibulin-4$^{R/R}$ SMC cell number, we analyzed whether this might be due to increased TGF-β signaling in these cells using a Smad3/Smad4 dependent promoter transcriptional reporter construct (CAGA-luciferase) [38]. Although there was a difference in proliferation between different genotypes at later time points, this was not observed during the short duration of the transcriptional response assay (Figure 3A). To determine whether transfection efficiency was similar between the different genotypes a Green Fluorescent Protein (GFP) expressing construct was transfected and GFP expression determined. Flow cytometric analysis showed no differences between the percentages of GFP expressing Fibulin-4$^{+/+}$, Fibulin-4$^{+/R}$ and Fibulin-4$^{R/R}$ SMCs (Figure 3B). Next, we used the Smad3/Smad4 transcriptional reporter construct CAGA-luciferase to assess TGF-β signaling activity in Fibulin-4$^{+/+}$, Fibulin-4$^{+/R}$ and Fibulin-4$^{R/R}$ SMCs. TGF-β treatment of Fibulin-4$^{+/+}$, Fibulin-4$^{+/R}$ and Fibulin-4$^{R/R}$ SMCs showed an increased induction of luciferase activity, which was increased in a Fibulin-4 dose-dependent manner in
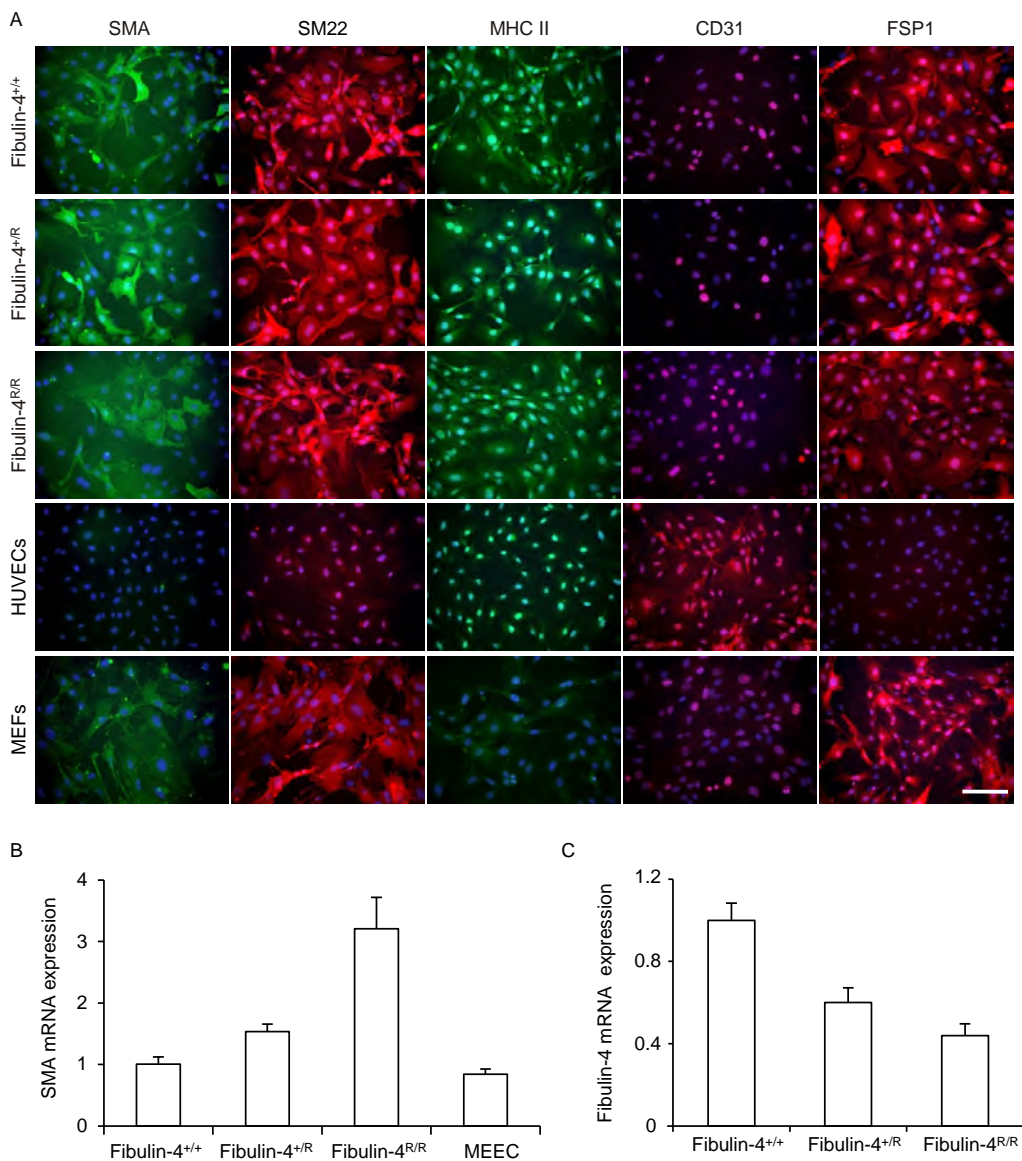
5

Figure 1: Characterization of isolated smooth muscle cells (SMCs) from the aortic arch. (A) Immunofluorescent staining of aortic SMCs isolated from Fibulin-4$^{+/+}$, Fibulin-4$^{+/R}$ and Fibulin-4$^{R/R}$ mice showed that these cells were positively stained for smooth muscle actin (SMA), smooth muscle protein 22 (SM22), myosin heavy chain II (MHC II) and fibroblast specific protein 1 (FSP1). The SMCs were negative for the endothelial marker CD31, while HUVECs were positive. HUVECs were negative for all other stainings. MEFs stained positive for SMA, SM22 and FSP1 and were negative for MHC II and CD31. Magnification 20x, scale bar 100 µm. (B) Fibulin-4 mRNA expression in SMCs. Fibulin-4$^{+/R}$ and Fibulin-4$^{R/R}$ SMCs show gradual decreased Fibulin-4 mRNA expression levels compared to Fibulin-4$^{+/+}$ SMCs. (C) Fibulin-4$^{+/R}$ and Fibulin-4$^{R/R}$ SMCs show gradual increased SMA mRNA expression levels compared to Fibulin-4$^{+/+}$ SMCs. MEEC = mouse embryonic endothelial cells.
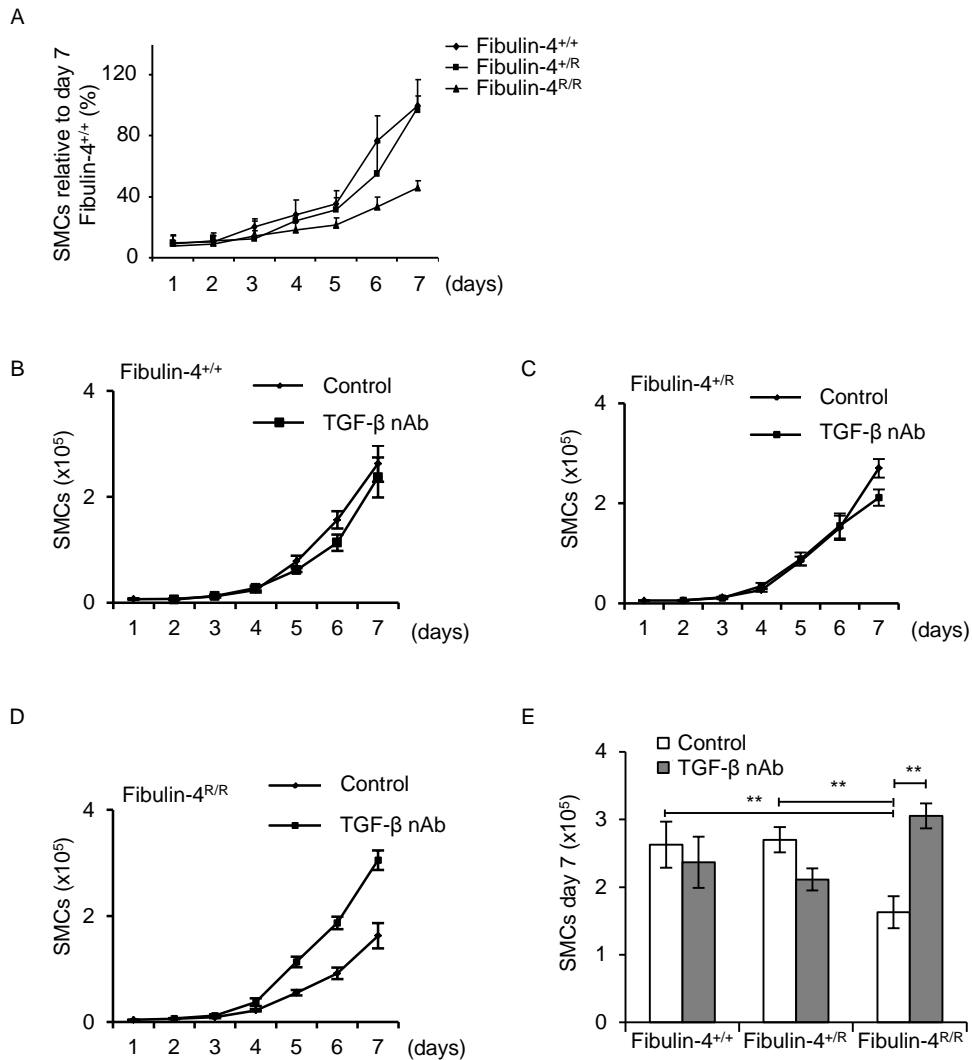
Figure 2: Altered proliferation of Fibulin-4[R/R] SMCs rescued by TGF-β pathway inhibition. (A) Growth analyses of Fibulin-4^{+/+}, Fibulin-4[+/R] and Fibulin-4[R/R] SMCs revealed a reduced growth starting from day 5 for Fibulin-4[R/R] SMCs as compared to Fibulin-4^{+/+} SMCs (3 dishes per experiment were counted and the average of 3 independent experiments is shown). Treatment of (B) Fibulin-4^{+/+}, (C) Fibulin-4[+/R] and (D and E) Fibulin-4[R/R] SMCs with TGF-β neutralizing antibodies significantly increased proliferation of Fibulin-4[R/R] SMCs from day 5. (E) At day 7 the amount of treated Fibulin-4[R/R] SMCs was significantly increased and comparable to the amount of Fibulin-4^{+/+} SMCs ($p<0.05$, ** $p<0.01$). Data represent 3 independent experiments performed in triplicate.

Fibulin-4$^{+/R}$ and Fibulin-4$^{R/R}$ SMCs compared to Fibulin-4$^{+/+}$ SMCs (Figure 3C). Addition of the TβRI kinase inhibitor SB431542 abolished TGF-β induced transcriptional responses. Analysis of downstream pSmad2 and pSmad3 by western blotting revealed a gradual increase in phosphorylation of Smad2 and Smad3 after stimulation with TGF-β in Fibulin-4$^{+/R}$ and Fibulin-4$^{R/R}$ SMCs compared to Fibulin-4$^{+/+}$ SMCs (Figure 3D), confirming the CAGA-luciferase reporter data.

To explore basal TGF-β signaling in Fibulin-4 deficient cells, SMCs were transfected with the CAGA-luciferase reporter and after serum starvation basal TGF-β signaling was analyzed. Interestingly, luciferase activity was already increased in control Fibulin-4$^{R/R}$ SMCs compared to Fibulin-4$^{+/+}$ SMCs (Figure 3E). This activation could be inhibited by addition of SB431542, suggesting a TGF-β mediated effect. These data were confirmed by western blotting, showing gradually increased phosphorylation of Smad2 and Smad3 in Fibulin-4$^{+/R}$ and Fibulin-4$^{R/R}$ SMCs (Figure 3F). Taken together, these data indicate increased TGF-β signaling as a basal property of Fibulin-4 deficient SMCs.

Increased TGF-β1 and TGF-β2 levels by Fibulin-4 deficient SMCs

Since we observed increased basal TGF-β signaling in Fibulin-4 deficient SMCs, we analyzed whether this was due to increased TGF-β levels. Subconfluent Fibulin-4$^{+/+}$, Fibulin-4$^{+/R}$ and Fibulin-4$^{R/R}$ SMCs were serum-starved and conditioned medium was collected for 4 days to determine TGF-β1, 2 and 3 levels. TGF-β3 levels were very low and did not differ between the different genotypes (data not shown). Although TGF-β1 mRNA levels in SMCs did not differ between the genotypes (Figure 4A), TGF-β1 levels in conditioned medium derived from Fibulin-4$^{R/R}$ SMCs were higher compared to Fibulin-4$^{+/+}$ SMCs (Figure 4B), while conditioned medium from Fibulin-4$^{+/R}$ SMCs showed an intermediate level. To analyze whether the increased TGF-β1 levels in conditioned medium was also observed *in vivo*, we prepared lysates from aortic arches of Fibulin-4$^{+/+}$, Fibulin-4$^{+/R}$ and Fibulin-4$^{R/R}$ mice and measured TGF-β1 levels. These data revealed a similar gradual increase in TGF-β1 levels in aortic arch lysates of Fibulin-4$^{+/R}$ and Fibulin-4$^{R/R}$ mice (Figure 4C).

Next, we analyzed TGF-β2 expression by the SMCs. Fibulin-4$^{+/R}$ and Fibulin-4$^{R/R}$ SMCs showed strongly increased TGF-β2 mRNA expression levels (Figure 4D). ELISA analysis on conditioned medium from Fibulin-4$^{+/+}$, Fibulin-4$^{+/R}$ and Fibulin-4$^{R/R}$ SMCs revealed markedly increased TGF-β2 levels in medium from Fibulin-4$^{+/R}$ and Fibulin-4$^{R/R}$ SMCs from respectively day 1 and day 2 compared to Fibulin-4$^{+/+}$ SMCs, in which TGF-β2 was undetectable (Figure 4E). In addition, strongly increased TGF-β2 levels were detectable in Fibulin-4$^{R/R}$ aortic arch lysates, when compared to aortic arch lysates from Fibulin-4$^{+/+}$ and Fibulin-4$^{+/R}$ mice (Figure 4F). These data show that in addition to increased soluble TGF-β1, especially TGF-β2 secretion by Fibulin-4 deficient SMCs is strongly enhanced.

Higher circulating TGF-β2 levels in Fibulin-4$^{R/R}$ mice

AAs we observed increased TGF-β1 and TGF-β2 levels in SMCs and aortic tissue derived from Fibulin-4 deficient mice, we determined TGF-β levels in plasma samples from these Fibulin-4 deficient mice. TGF-β1 levels were high and not enhanced in plasma from Fibulin-4$^{+/R}$ and Fibulin-4$^{R/R}$ mice, compared to plasma of Fibulin-4$^{+/+}$ mice (Figure 5A). In contrast, plasma TGF-β2 levels were very low in wildtype mice and could only be detected in 2 out of 15 Fibulin-4$^{+/+}$ mice and 2 out of 19 Fibulin-4$^{+/R}$ mice (Figure 5B). Strikingly, TGF-β2 could be detected in plasma from 9 out of 17 Fibulin-4$^{R/R}$ mice with higher concentrations compared to Fibulin-4$^{+/+}$ and Fibulin-4$^{+/R}$ mice. Since patients suffering from Marfan syndrome, which is associated with increased TGF-β signaling, benefit from treatment with losartan, adult Fibulin-4$^{R/R}$ mice were treated with losartan (between day35–day100,
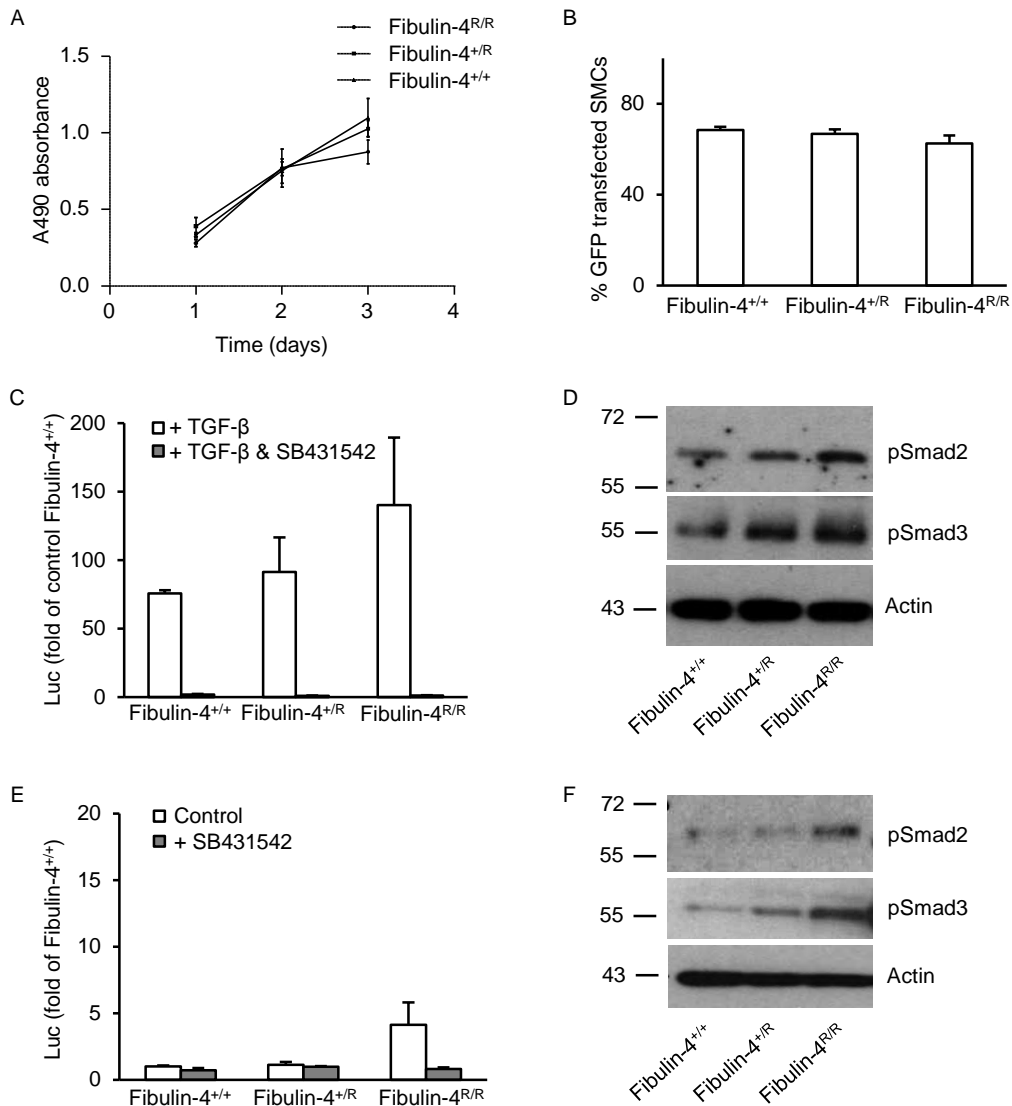
Figure 3: Increased TGF-β signaling in Fibulin-4 deficient SMCs. (A) Fibulin-4$^{+/+}$, Fibulin-4$^{+/R}$ and Fibulin-4$^{R/R}$ SMCs show similar proliferation rates in the time course of the experiment (mitochondrial targeting sequence (MTS) proliferation assay) (B) Transfection with green fluorescent protein (GFP) encoding plasmids display no difference in percentage of transfected SMCs between Fibulin-4$^{+/+}$, Fibulin-4$^{+/R}$ and Fibulin-4$^{R/R}$ SMCs. (C) The TGF-β response assay reveals a gradual increase in TGF-β activity in Fibulin-4$^{+/R}$ and Fibulin-4$^{R/R}$ SMCs compared to Fibulin-4$^{+/+}$ SMCs, after stimulation with TGF-β. Data represent fold change relative to unstimulated Fibulin-4$^{+/+}$ SMCs. Addition of the ALK-5 kinase inhibitor (SB431542) abolishes the TGF-β response in Fibulin-4$^{+/+}$, Fibulin-4$^{+/R}$ and Fibulin-4$^{R/R}$ SMCs. (D) Immunoblot analyses for TGF-β signaling downstream mediators pSmad2 and pSmad3 on TGF-β stimulated SMCs show a gradual increase in TGF-β signaling in Fibulin-4 deficient SMCs compared to Fibulin-4$^{+/+}$ SMCs. (E) Measurement of basal TGF-β activity by the CAGA-luciferase reporter show increased TGF-β activity in Fibulin-4$^{R/R}$ SMCs compared to Fibulin-4$^{+/+}$ SMCs, which can be inhibited by the TβRI kinase inhibitor SB431542. (F) These data are confirmed by immunoblot analyses for pSmad2 and pSmad3.
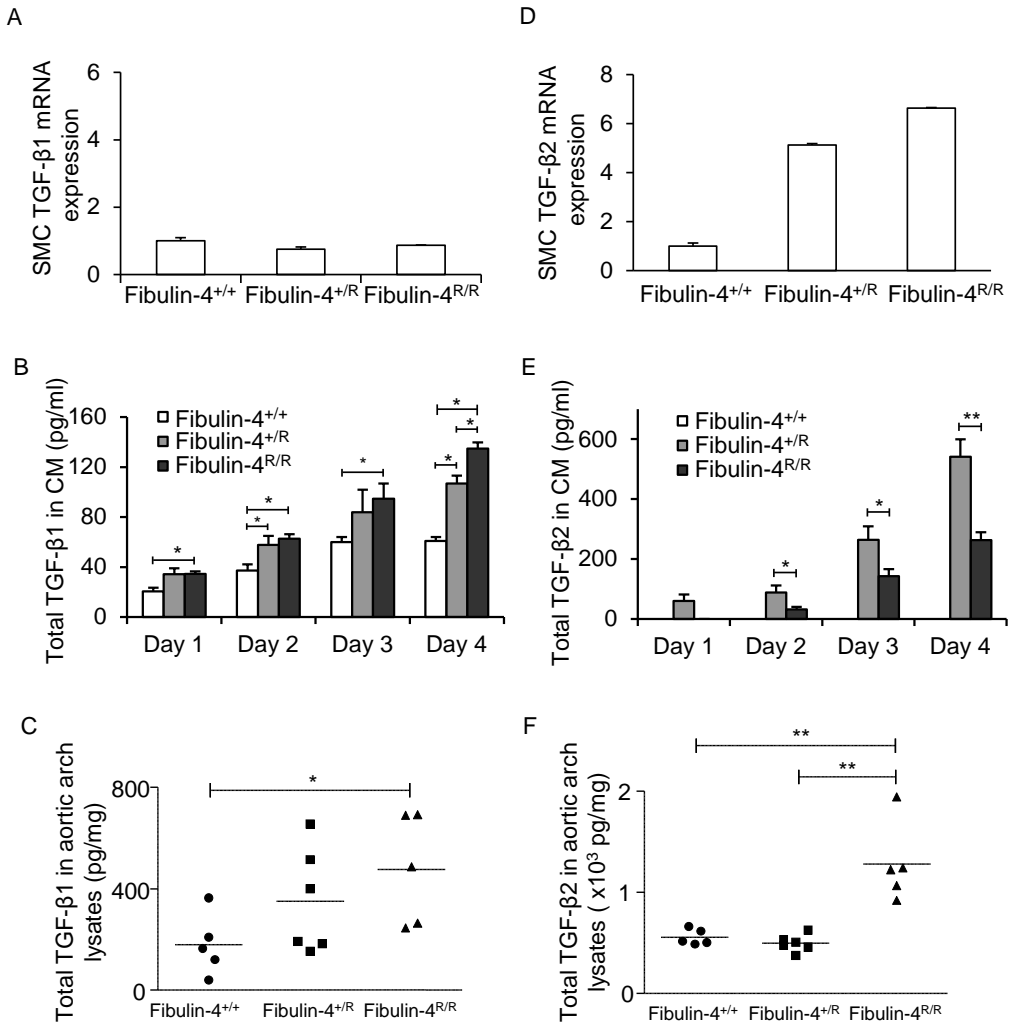
Figure 4: Strong increase of TGF-β2 secretion by Fibulin-4 deficient SMCs. (A) Fibulin-4+/R and Fibulin-4R/R SMCs show equal TGF-β1 mRNA expression levels compared to Fibulin-4+/+ SMCs. (B) Increased TGF-β1 secretion measured in conditioned medium (CM) from Fibulin-4R/R SMCs compared to Fibulin-4+/+ CM on day 1-4 after serum starvation. Fibulin-4+/R SMCs showed significant increased TGF-β1 secretion on day 2 and 4 after serum starvation compared to Fibulin-4+/+ SMCs. Furthermore, on day 4 Fibulin-4R/R SMCs show a significant increased TGF-β1 secretion compared to Fibulin-4+/R SMCs (n=4 per day for each genotype). (C) Gradual increased TGF-β1 is also observed in aortic arch lysates of Fibulin-4+/R (n=6) and Fibulin-4R/R mice (n=5) compared to Fibulin-4+/+ aortas (n=5). This increase is significant in Fibulin-4R/R aortic arch lysates compared to Fibulin-4+/+ aortic arch lysates. (D) Fibulin-4+/R and Fibulin-4R/R SMCs show gradual increased TGF-β2 mRNA expression levels compared to Fibulin-4+/+ SMCs. (E) Measurement of TGF-β2 revealed markedly increased levels in CM of Fibulin-4+/R and Fibulin-4R/R SMCs, while TGF-β2 was undetectable in CM of Fibulin-4+/+ SMCs (n=2, experiments repeated twice). (F) Measurements in aortic arch lysates display significantly increased TGF-β2 in Fibulin-4R/R aortas compared to Fibulin-4+/R and Fibulin-4+/+ aortas (*p<0.05, **p<0.01).

manuscript in preparation). Interestingly, while increased TGF-β2 levels were observed in plasma from 3 out of 7 placebo treated Fibulin-4[R/R] mice, TGF-β2 could be detected in only one out of 10 losartan treated Fibulin-4[R/R] mice, which had a worse disease state compared to other losartan treated Fibulin-4[R/R] mice and died during handling (Figure 5C). These results indicate that especially TGF-β2 secretion from Fibulin-4[R/R] SMCs is increased, which is reflected in TGF-β2 plasma levels in Fibulin-4[R/R] mice. Finally, our data indicate that this increased TGF-β2 secretion can be reduced upon losartan treatment, offering therapeutic potential for the treatment of these patients.

DISCUSSION

In this study we show that the upregulated TGF-β signaling observed in aortas from Fibulin-4 deficient mice is an intrinsic property of the SMCs derived from these aortas. Our data reveal that TGF-β signaling is gradually enhanced in Fibulin-4 deficient SMCs in a Fibulin-4 dose-dependent manner and influences proliferation of these cells. This increased TGF-β signaling is caused by increased TGF-β1 levels, but especially by increased TGF-β2 expression and secretion from Fibulin-4 deficient SMCs resulting in higher TGF-β2 blood plasma levels in Fibulin-4 deficient mice. This increased TGF-β2 expression might suggest an adaptation response by Fibulin-4 deficient SMCs.

      Previous analyses on aortas from Fibulin-4 deficient mice implicated upregulated TGF-β signaling in the pathogenesis of aneurysm formation by gene expression analysis and increased nuclear pSmad2 staining located in the SMCs of these aortas [12]. Isolation of aortic SMCs from these mice provided the opportunity to assess TGF-β signaling *in vitro*. Fibulin-4[R/R] SMCs have a reduced proliferation rate compared to Fibulin-4[+/R] and wild type SMCs, which is reversed by TGF-β inhibition. Subsequent analyses indeed reveal a gradual increase in TGF-β signaling in Fibulin-4 deficient SMCs. In general, a TAA is characterized by degeneration of the extracellular matrix and vascular SMCs, including SMC dropout, phenotypic SMC loss and proliferative changes of the SMCs [39-41]. Furthermore, increased TGF-β signaling inhibits proliferation of SMCs [42]. Indeed, our data on SMCs isolated from aneurismal Fibulin-4[R/R] mice resemble SMC pathology and increased TGF-β signaling, which most likely contributes to the pathogenesis of aortic aneurysm formation in these mice.

      ELISA analyses point to increased secretion of TGF-β1 from Fibulin-4 deficient SMCs and strongly increased TGF-β2 secretion, which is detected in plasma of Fibulin-4[R/R] mice. The three TGF-β isoforms are involved in both overlapping and divergent roles as illustrated by the discrete phenotypes of the respective knockout mouse models, which all show perinatal lethality. While TGF-β1 null mice develop an autoimmune-like inflammatory disease [43] and TGF-β3 knockout mice develop abnormal lung development and cleft palate [44], TGF-β2 knockout mice have multiple developmental defects, including cardiovascular, pulmonary, skeletal, ocular, inner ear and urogenital manifestations. The most commonly involved developmental processes are epithelial-mesenchymal interactions, cell growth, extracellular matrix production and tissue remodeling [45, 46]. However, TGF-β2 heterozygous mutations in patients apparently result in a different phenotype as compared to TGF-β2 knock-out mice [47-49]. TGF-β2 haploinsufficiency predisposes for adult-onset vascular disease, including aortic tortuosity and dilation, cerebrovascular disease and mitral valve disease, which interestingly overlaps with the phenotype of Fibulin-4 deficient patients. The phenotype of the TGF-β2 deficient patients also shows overlap with other TGF-β signalopathies including Marfan syndrome, Loeys-Dietz syndrome, the aneurysm-
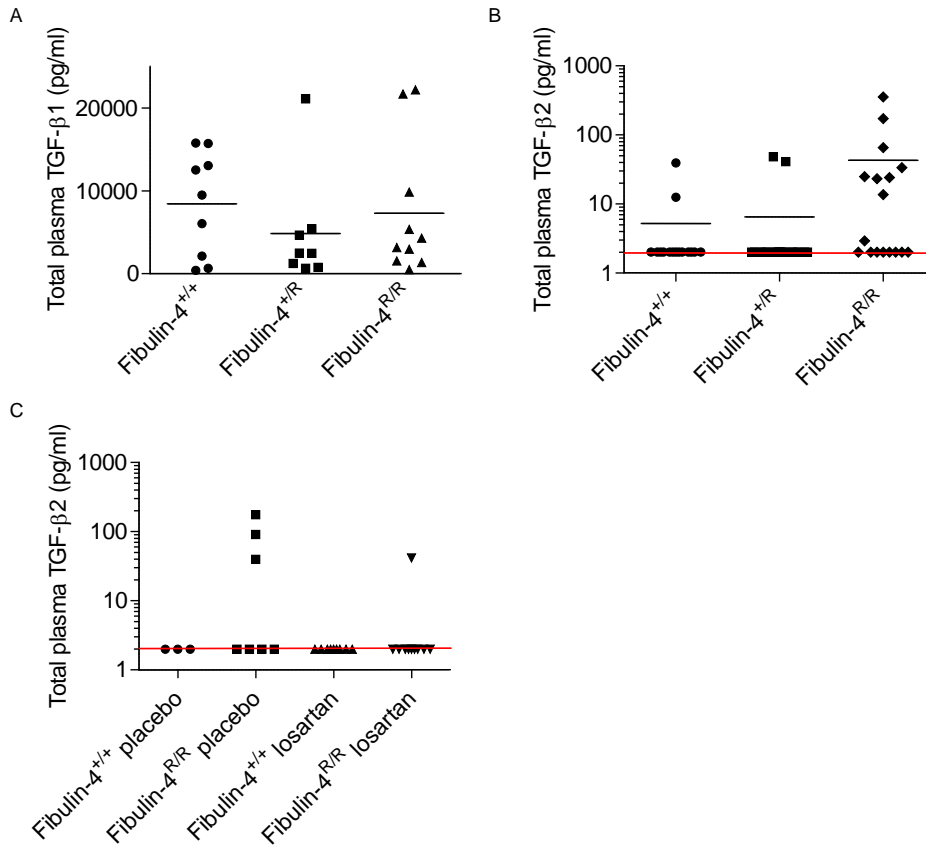
5

Figure 5: Increased secretion of TGF-β2 is detectable in plasma from Fibulin-4^R/R mice. (A) TGF-β1 measurements in plasma samples showed no difference between Fibulin-4^+/+ (n=9), Fibulin-4^+/R (n=8) and Fibulin-4^R/R mice (n=10). (B) TGF-β2 was detectable in plasma of more Fibulin-4^R/R mice (nine out of 17) compared to Fibulin-4^+/+ (two out of 15) and Fibulin-4^+/R (2 out of 19) mice with significantly higher levels compared to Fibulin-4^+/+ and Fibulin-4^+/R mice. (C) Losartan treatment of Fibulin-4^R/R mice seemed to reduce the TGF-β2 levels (one out of 10) as compared to placebo treated Fibulin-4^R/R mice (three out of seven). The losartan treated Fibulin-4^R/R mouse with a detectable TGF-β2 concentration had a worse disease outcome compared to other losartan treated Fibulin-4^R/R mice.

osteoarthritis syndrome and similarly present with a paradoxical, probably compensatory, local increase in TGF-β1 and TGF-β2. This leads to the conclusion that both TGF-β2 and Fibulin-4 mutations result in increased TGF-β1 and TGF-β2 levels, which are both associated with aortic aneurysm formation.

Additionally, TGF-β2 differs in its receptor binding properties from TGF-β1 and TGF-β3. While TGF-β1 and TGF-β3 have a high affinity for binding to TβRII, TGF-β2 primarily binds to the transforming growth factor type III receptor (TβRIII), also called betaglycan, after which it presents the ligand to the TβRI-TβRII signaling complex [50]. Moreover, Bee *et al.* showed a specific regulatory role for the TGF-β receptor IIb (TβRIIb), an alternatively spliced variant of TβRII, in TGF-β2 signal transduction. TβRIIb mutations

result in TGF-β2 dependent increased Smad2 phosphorylation, which is involved in aortic aneurysm progression [51]. Normal human SMCs express all three receptors, TβRI, TβRII and TβRIII, while in cells derived from atherosclerotic lesions TβRII expression is decreased [52]. This might indicate that alterations in the TGF-β receptors probably contribute to the regulation of the TGF-β pathway in the pathogenesis of aortic disease, including aortic aneurysm progression. As our data points to markedly increased TGF-β2 secretion by Fibulin-4 deficient SMCs, analyses on TGF-β receptors on these SMCs might further clarify the process of TGF-β regulation and determine its role in the pathogenesis of Fibulin-4 associated aortic aneurysms.

Increased TGF-β or TGF-β signaling is associated with multiple diseases. Enhanced TGF-β signaling is known to mediate a pathologic increase in ECM secretion and deposition and is causative for fibrosis in multiple disorders throughout the body [53, 54]. Overexpression of TGF-β2 is likely to induce trabecular meshwork ECM deposition [55] and increased ECM deposition is also observed in aortic aneurysm formation. In addition, studies on milk-derived TGF-β shows an immune suppressive role for TGF-β2 in adverse immunological outcomes in infants [56]. TGF-β2 is also frequently overexpressed in malignant cancers, where it regulates immunosuppression and metastasis [57]. This TGF-β2 overexpression can be targeted with antisense oligonucleotides, which is currently under investigation in clinical trials [58]. As inhibition with TGF-β pan nAb is likely to induce target side effects, aortic aneurysms associated with increased TGF-β2 might benefit from an intervention with TGF-β2 as a specific therapeutic target, which could be much more easily tolerated by patients. This needs to be determined in further studies.

In conclusion, these data add to a potential role for SMC derived TGF-β2 in the pathogenesis of aortic aneurysm formation. *In vitro* analyses on isolated SMC provide the opportunity to determine the molecular link between Fibulin-4, TGF-β2 and TGF-β pathway regulation, and to further unravel its contributing biological role in aortic aneurysm formation.

5

ACKNOWLEDGEMENTS

SUPPLEMENTARY

Supplemental Table 1 - Primers used for quantitative real time PCR. Forward and reverse primers are displayed for each gene from 5' to 3'.

| Genes	Forward primers	Reverse primers
Fibulin-4	5'-GGGTTATTTGTGTCTGCCTCG-3'	5'-TGGTAGGAGCCAGGAAGGTT-3'
SMA	5'-GTCCCAGACATCAGGGAGTAA-3'	5'-TCGGATACTTCAGCGTCAGGA-3
TGF-β1	5'-CAACAATTCCTGGCGTTACC-3'	5'-TGCTGTCACAAGAGCAGTGA-3'
TGF-β2	5'-CCGCCCACTTTCTACAGACCC-3'	5'-GCGCTGGGTGGGAGATGTTAA-3'

5

REFERENCES

1. Lindsay ME, Dietz HC. Lessons on the pathogenesis of aneurysm from heritable conditions. Nature. 2011 May 19;473(7347):308-16.
2. Ramanath VS, Oh JK, Sundt TM, 3rd, Eagle KA. Acute aortic syndromes and thoracic aortic aneurysm. Mayo Clin Proc. 2009 May;84(5):465-81.
3. Olsson C, Thelin S, Stahle E, Ekbom A, Granath F. Thoracic aortic aneurysm and dissection: increasing prevalence and improved outcomes reported in a nationwide population-based study of more than 14,000 cases from 1987 to 2002. Circulation. 2006 Dec 12;114(24):2611-8.
4. Dietz HC, Cutting GR, Pyeritz RE, Maslen CL, Sakai LY, Corson GM, Puffenberger EG, Hamosh A, Nanthakumar EJ, Curristin SM, et al. Marfan syndrome caused by a recurrent de novo missense mutation in the fibrillin gene. Nature. 1991 Jul 25;352(6333):337-9.
5. Guo DC, Pannu H, Tran-Fadulu V, Papke CL, Yu RK, Avidan N, Bourgeois S, Estrera AL, Safi HJ, Sparks E, Amor D, Ades L, McConnell V, Willoughby CE, Abuelo D, Willing M, Lewis RA, Kim DH, Scherer S, Tung PP, Ahn C, Buja LM, Raman CS, Shete SS, Milewicz DM. Mutations in smooth muscle alpha-actin (ACTA2) lead to thoracic aortic aneurysms and dissections. Nat Genet. 2007 Dec;39(12):1488-93.
6. Loeys BL, Chen J, Neptune ER, Judge DP, Podowski M, Holm T, Meyers J, Leitch CC, Katsanis N, Sharifi N, Xu FL, Myers LA, Spevak PJ, Cameron DE, De Backer J, Hellemans J, Chen Y, Davis EC, Webb CL, Kress W, Coucke P, Rifkin DB, De Paepe AM, Dietz HC. A syndrome of altered cardiovascular, craniofacial, neurocognitive and skeletal development caused by mutations in TGFBR1 or TGFBR2. Nat Genet. 2005 Mar;37(3):275-81.
7. Pannu H, Tran-Fadulu V, Papke CL, Scherer S, Liu Y, Presley C, Guo D, Estrera AL, Safi HJ, Brasier AR, Vick GW, Marian AJ, Raman CS, Buja LM, Milewicz DM. MYH11 mutations result in a distinct vascular pathology driven by insulin-like growth factor 1 and angiotensin II. Hum Mol Genet. 2007 Oct 15;16(20):2453-62.
8. Wang L, Guo DC, Cao J, Gong L, Kamm KE, Regalado E, Li L, Shete S, He WQ, Zhu MS, Offermanns S, Gilchrist D, Elefteriades J, Stull JT, Milewicz DM. Mutations in myosin light chain kinase cause familial aortic dissections. Am J Hum Genet. 2010 Nov 12;87(5):701-7.
9. Zhu L, Vranckx R, Khau Van Kien P, Lalande A, Boisset N, Mathieu F, Wegman M, Glancy L, Gasc JM, Brunotte F, Bruneval P, Wolf JE, Michel JB, Jeunemaitre X. Mutations in myosin heavy chain 11 cause a syndrome associating thoracic aortic aneurysm/aortic dissection and patent ductus arteriosus. Nat Genet. 2006 Mar;38(3):343-9.
10. van de Laar IM, Oldenburg RA, Pals G, Roos-Hesselink JW, de Graaf BM, Verhagen JM, Hoedemaekers YM, Willemsen R, Severijnen LA, Venselaar H, Vriend G, Pattynama PM, Collee M, Majoor-Krakauer D, Poldermans D, Frohn-Mulder IM, Micha D, Timmermans J, Hilhorst-Hofstee Y, Bierma-Zeinstra SM, Willems PJ, Kros JM, Oei EH, Oostra BA, Wessels MW, Bertoli-Avella AM. Mutations in SMAD3 cause a syndromic form of aortic aneurysms and dissections with early-onset osteoarthritis. Nat Genet. 2011 Feb;43(2):121-6.
11. Neptune ER, Frischmeyer PA, Arking DE, Myers L, Bunton TE, Gayraud B, Ramirez F, Sakai LY, Dietz HC. Dysregulation of TGF-beta activation contributes to pathogenesis in Marfan syndrome. Nat Genet. 2003 Mar;33(3):407-11.
12. Hanada K, Vermeij M, Garinis GA, de Waard MC, Kunen MG, Myers L, Maas A, Duncker DJ, Meijers C, Dietz HC, Kanaar R, Essers J. Perturbations of vascular homeostasis and aortic valve abnormalities in fibulin-4 deficient mice. Circ Res. 2007 Mar 16;100(5):738-46.
13. Renard M, Holm T, Veith R, Callewaert BL, Ades LC, Baspinar O, Pickart A, Dasouki M, Hoyer J, Rauch A, Trapane P, Earing MG, Coucke PJ, Sakai LY, Dietz HC, De Paepe AM, Loeys BL. Altered TGFbeta signaling and cardiovascular manifestations in patients with autosomal recessive cutis laxa type I caused by fibulin-4 deficiency. Eur J Hum Genet. 2010 Aug;18(8):895-901.
14. Renard M, Callewaert B, Baetens M, Campens L, MacDermot K, Fryns JP, Bonduelle M, Dietz HC, Gaspar IM, Cavaco D, Stattin EL, Schrander-Stumpel C, Coucke P, Loeys B, De Paepe A, De Backer J. Novel MYH11 and ACTA2 mutations reveal a role for enhanced TGFbeta signaling in FTAAD. Int J Cardiol. 2013 May 10;165(2):314-21.
15. ten Dijke P, Arthur HM. Extracellular control of TGFbeta signalling in vascular development and disease. Nat Rev Mol Cell Biol. 2007 Nov;8(11):857-69.
16. ten Dijke P, Goumans MJ, Pardali E. Endoglin in angiogenesis and vascular diseases. Angiogenesis. 2008;11(1):79-89.

5

17. ten Dijke P, Hill CS. New insights into TGF-beta-Smad signalling. Trends Biochem Sci. 2004 May;29(5):265-73.

18. Lavoie P, Robitaille G, Agharazii M, Ledbetter S, Lebel M, Lariviere R. Neutralization of transforming growth factor-beta attenuates hypertension and prevents renal injury in uremic rats. J Hypertens. 2005 Oct;23(10):1895-903.

19. Franken R, den Hartog AW, de Waard V, Engele L, Radonic T, Lutter R, Timmermans J, Scholte AJ, van den Berg MP, Zwinderman AH, Groenink M, Mulder BJ. Circulating transforming growth factor-beta as a prognostic biomarker in Marfan syndrome. Int J Cardiol. 2013 Apr 10.

20. Matt P, Schoenhoff F, Habashi J, Holm T, Van Erp C, Loch D, Carlson OD, Griswold BF, Fu Q, De Backer J, Loeys B, Huso DL, McDonnell NB, Van Eyk JE, Dietz HC, Gen TACC. Circulating transforming growth factor-beta in Marfan syndrome. Circulation. 2009 Aug 11;120(6):526-32.

21. Habashi JP, Judge DP, Holm TM, Cohn RD, Loeys BL, Cooper TK, Myers L, Klein EC, Liu G, Calvi C, Podowski M, Neptune ER, Halushka MK, Bedja D, Gabrielson K, Rifkin DB, Carta L, Ramirez F, Huso DL, Dietz HC. Losartan, an AT1 antagonist, prevents aortic aneurysm in a mouse model of Marfan syndrome. Science. 2006 Apr 7;312(5770):117-21.

22. Brooke BS, Habashi JP, Judge DP, Patel N, Loeys B, Dietz HC, 3rd. Angiotensin II blockade and aortic-root dilation in Marfan's syndrome. N Engl J Med. 2008 Jun 26;358(26):2787-95.

23. Hoyer J, Kraus C, Hammersen G, Geppert JP, Rauch A. Lethal cutis laxa with contractural arachnodactyly, overgrowth and soft tissue bleeding due to a novel homozygous fibulin-4 gene mutation. Clin Genet. 2009 Sep;76(3):276-81.

24. Hucthagowder V, Sausgruber N, Kim KH, Angle B, Marmorstein LY, Urban Z. Fibulin-4: a novel gene for an autosomal recessive cutis laxa syndrome. Am J Hum Genet. 2006 Jun;78(6):1075-80.

25. Dasouki M, Markova D, Garola R, Sasaki T, Charbonneau NL, Sakai LY, Chu ML. Compound heterozygous mutations in fibulin-4 causing neonatal lethal pulmonary artery occlusion, aortic aneurysm, arachnodactyly, and mild cutis laxa. Am J Med Genet A. 2007 Nov 15;143A(22):2635-41.

26. Erickson LK, Opitz JM, Zhou H. Lethal osteogenesis imperfecta-like condition with cutis laxa and arterial tortuosity in MZ twins due to a homozygous fibulin-4 mutation. Pediatr Dev Pathol. 2012 Mar-Apr;15(2):137-41.

27. Sawyer SL, Dicke F, Kirton A, Rajapske T, Rebeyka IM, McInnes B, Parboosingh JS, Bernier FP. Longer term survival of a child with autosomal recessive cutis laxa due to a mutation in FBLN4. Am J Med Genet A. 2013 May;161A(5):1148-53.

28. Kappanayil M, Nampoothiri S, Kannan R, Renard M, Coucke P, Malfait F, Menon S, Ravindran HK, Kurup R, Faiyaz-Ul-Haque M, Kumar K, De Paepe A. Characterization of a distinct lethal arteriopathy syndrome in twenty-two infants associated with an identical, novel mutation in FBLN4 gene, confirms fibulin-4 as a critical determinant of human vascular elastogenesis. Orphanet J Rare Dis. 2012;7:61.

29. Huang J, Davis EC, Chapman SL, Budatha M, Marmorstein LY, Word RA, Yanagisawa H. Fibulin-4 deficiency results in ascending aortic aneurysms: a potential link between abnormal smooth muscle cell phenotype and aneurysm progression. Circ Res. 2010 Feb 19;106(3):583-92.

30. Argraves WS, Greene LM, Cooley MA, Gallagher WM. Fibulins: physiological and disease perspectives. EMBO Rep. 2003 Dec;4(12):1127-31.

31. Chen Q, Zhang T, Roshetsky JF, Ouyang Z, Essers J, Fan C, Wang Q, Hinek A, Plow EF, Dicorleto PE. Fibulin-4 regulates expression of the tropoelastin gene and consequent elastic-fibre formation by human fibroblasts. Biochem J. 2009 Oct 1;423(1):79-89.

32. Horiguchi M, Inoue T, Ohbayashi T, Hirai M, Noda K, Marmorstein LY, Yabe D, Takagi K, Akama TO, Kita T, Kimura T, Nakamura T. Fibulin-4 conducts proper elastogenesis via interaction with cross-linking enzyme lysyl oxidase. Proc Natl Acad Sci U S A. 2009 Nov 10;106(45):19029-34.

33. Atsawasuwan P, Mochida Y, Katafuchi M, Kaku M, Fong KS, Csiszar K, Yamauchi M. Lysyl oxidase binds transforming growth factor-beta and regulates its signaling via amine oxidase activity. J Biol Chem. 2008 Dec 5;283(49):34229-40.

34. Doyle JJ, Gerber EE, Dietz HC. Matrix-dependent perturbation of TGFbeta signaling and disease. FEBS Lett. 2012 Jul 4;586(14):2003-15.

35. Brisset AC, Hao H, Camenzind E, Bacchetta M, Geinoz A, Sanchez JC, Chaponnier C,

5

Gabbiani G, Bochaton-Piallat ML. Intimal smooth muscle cells of porcine and human coronary artery express S100A4, a marker of the rhomboid phenotype in vitro. Circ Res. 2007 Apr 13;100(7):1055-62.

36. Hao H, Ropraz P, Verin V, Camenzind E, Geinoz A, Pepper MS, Gabbiani G, Bochaton-Piallat ML. Heterogeneity of smooth muscle cell populations cultured from pig coronary artery. Arterioscler Thromb Vasc Biol. 2002 Jul 1;22(7):1093-9.

37. Wang J, Chen H, Seth A, McCulloch CA. Mechanical force regulation of myofibroblast differentiation in cardiac fibroblasts. Am J Physiol Heart Circ Physiol. 2003 Nov;285(5):H1871-81.

38. Dennler S, Itoh S, Vivien D, ten Dijke P, Huet S, Gauthier JM. Direct binding of Smad3 and Smad4 to critical TGF beta-inducible elements in the promoter of human plasminogen activator inhibitor-type 1 gene. EMBO J. 1998 Jun 1;17(11):3091-100.

39. Isselbacher EM. Thoracic and abdominal aortic aneurysms. Circulation. 2005 Feb 15;111(6):816-28.

40. Guo D, Hasham S, Kuang SQ, Vaughan CJ, Boerwinkle E, Chen H, Abuelo D, Dietz HC, Basson CT, Shete SS, Milewicz DM. Familial thoracic aortic aneurysms and dissections: genetic heterogeneity with a major locus mapping to 5q13-14. Circulation. 2001 May 22;103(20):2461-8.

41. Bunton TE, Biery NJ, Myers L, Gayraud B, Ramirez F, Dietz HC. Phenotypic alteration of vascular smooth muscle cells precedes elastolysis in a mouse model of Marfan syndrome. Circ Res. 2001 Jan 19;88(1):37-43.

42. Merwin JR, Newman W, Beall LD, Tucker A, Madri J. Vascular cells respond differentially to transforming growth factors beta 1 and beta 2 in vitro. Am J Pathol. 1991 Jan;138(1):37-51.

43. Shull MM, Ormsby I, Kier AB, Pawlowski S, Diebold RJ, Yin M, Allen R, Sidman C, Proetzel G, Calvin D, et al. Targeted disruption of the mouse transforming growth factor-beta 1 gene results in multifocal inflammatory disease. Nature. 1992 Oct 22;359(6397):693-9.

44. Kaartinen V, Voncken JW, Shuler C, Warburton D, Bu D, Heisterkamp N, Groffen J. Abnormal lung development and cleft palate in mice lacking TGF-beta 3 indicates defects of epithelial-mesenchymal interaction. Nat Genet. 1995 Dec;11(4):415-21.

45. Sanford LP, Ormsby I, Gittenberger-de Groot AC, Sariola H, Friedman R, Boivin GP, Cardell EL, Doetschman T. TGFbeta2 knockout mice have multiple developmental defects that are non-overlapping with other TGFbeta knockout phenotypes. Development. 1997 Jul;124(13):2659-70.

46. Bartram U, Molin DG, Wisse LJ, Mohamad A, Sanford LP, Doetschman T, Speer CP, Poelmann RE, Gittenberger-de Groot AC. Double-outlet right ventricle and overriding tricuspid valve reflect disturbances of looping, myocardialization, endocardial cushion differentiation, and apoptosis in TGF-beta(2)-knockout mice. Circulation. 2001 Jun 5;103(22):2745-52.

47. Boileau C, Guo DC, Hanna N, Regalado ES, Detaint D, Gong L, Varret M, Prakash SK, Li AH, d'Indy H, Braverman AC, Grandchamp B, Kwartler CS, Gouya L, Santos-Cortez RL, Abifadel M, Leal SM, Muti C, Shendure J, Gross MS, Rieder MJ, Vahanian A, Nickerson DA, Michel JB, National Heart L, Blood Institute Go Exome Sequencing P, Jondeau G, Milewicz DM. TGFB2 mutations cause familial thoracic aortic aneurysms and dissections associated with mild systemic features of Marfan syndrome. Nat Genet. 2012 Aug;44(8):916-21.

48. Lindsay ME, Schepers D, Bolar NA, Doyle JJ, Gallo E, Fert-Bober J, Kempers MJ, Fishman EK, Chen Y, Myers L, Bjeda D, Oswald G, Elias AF, Levy HP, Anderlid BM, Yang MH, Bongers EM, Timmermans J, Braverman AC, Canham N, Mortier GR, Brunner HG, Byers PH, Van Eyk J, Van Laer L, Dietz HC, Loeys BL. Loss-of-function mutations in TGFB2 cause a syndromic presentation of thoracic aortic aneurysm. Nat Genet. 2012 Aug;44(8):922-7.

49. Renard M, Callewaert B, Malfait F, Campens L, Sharif S, del Campo M, Valenzuela I, McWilliam C, Coucke P, De Paepe A, De Backer J. Thoracic aortic-aneurysm and dissection in association with significant mitral valve disease caused by mutations in TGFB2. Int J Cardiol. 2013 May 25;165(3):584-7.

50. Lopez-Casillas F, Wrana JL, Massague J. Betaglycan presents ligand to the TGF beta signaling receptor. Cell. 1993 Jul 2;73(7):1435-44.

51. Bee KJ, Wilkes DC, Devereux RB, Basson CT, Hatcher CJ. TGFbetaRIIb mutations trigger aortic aneurysm pathogenesis by altering transforming growth factor beta2 signal transduction. Circ Cardiovasc Genet. 2012 Dec;5(6):621-9.

52. McCaffrey TA, Consigli S, Du B, Falcone DJ, Sanborn TA, Spokojny AM, Bush HL, Jr. Decreased type II/type I TGF-beta receptor ratio in cells derived from human atherosclerotic

5

lesions. Conversion from an antiproliferative to profibrotic response to TGF-beta1. J Clin Invest. 1995 Dec;96(6):2667-75.

53.   Ghosh AK, Quaggin SE, Vaughan DE. Molecular basis of organ fibrosis: potential therapeutic approaches. Exp Biol Med (Maywood). 2013 May;238(5):461-81.

54.   Samarakoon R, Overstreet JM, Higgins PJ. TGF-beta signaling in tissue fibrosis: redox controls, target genes and therapeutic opportunities. Cell Signal. 2013 Jan;25(1):264-8.

55.   Fuchshofer R, Tamm ER. The role of TGF-beta in the pathogenesis of primary open-angle glaucoma. Cell Tissue Res. 2012 Jan;347(1):279-90.

56.   Oddy WH, McMahon RJ. Milk-derived or recombinant transforming growth factor-beta has effects on immunological outcomes: a review of evidence from animal experimental studies. Clin Exp Allergy. 2011 Jun;41(6):783-93.

57.   Jaschinski F, Rothhammer T, Jachimczak P, Seitz C, Schneider A, Schlingensiepen KH. The antisense oligonucleotide trabedersen (AP 12009) for the targeted inhibition of TGF-beta2. Curr Pharm Biotechnol. 2011 Dec;12(12):2203-13.

58.   Hawinkels LJ, Ten Dijke P. Exploring anti-TGF-beta therapies in cancer and fibrosis. Growth Factors. 2011 Aug;29(4):140-52.

59.   Moltzer E, te Riet L, Swagemakers SM, van Heijningen PM, Vermeij M, van Veghel R, Bouhuizen AM, van Esch JH, Lankhorst S, Ramnath NW, de Waard MC, Duncker DJ, van der Spek PJ, Rouwet EV, Danser AH, Essers J. Impaired vascular contractility and aortic wall degeneration in fibulin-4 deficient mice: effect of angiotensin II type 1 (AT1) receptor blockade. PLoS One. 2011;6(8):e23411.

60.   Hawinkels LJ, Paauwe M, Verspaget HW, Wiercinska E, van der Zon JM, van der Ploeg K, Koelink PJ, Lindeman JH, Mesker W, Ten Dijke P, Sier CF. Interaction with colon cancer cells hyperactivates TGF-beta signaling in cancer-associated fibroblasts. Oncogene. 2012 Dec 3.

61.   Kaijzel EL, van Heijningen PM, Wielopolski PA, Vermeij M, Koning GA, van Cappellen WA, Que I, Chan A, Dijkstra J, Ramnath NW, Hawinkels LJ, Bernsen MR, Lowik CW, Essers J. Multimodality imaging reveals a gradual increase in matrix metalloproteinase activity at aneurysmal lesions in live fibulin-4 mice. Circ Cardiovasc Imaging. 2010 Sep;3(5):567-77.

62.   Hawinkels LJ, Verspaget HW, van Duijn W, van der Zon JM, Zuidwijk K, Kubben FJ, Verheijen JH, Hommes DW, Lamers CB, Sier CF. Tissue level, activation and cellular localisation of TGF-beta1 and association with survival in gastric cancer patients. Br J Cancer. 2007 Aug 6;97(3):398-404.

63.   Hawinkels LJ, Verspaget HW, van der Reijden JJ, van der Zon JM, Verheijen JH, Hommes DW, Lamers CB, Sier CF. Active TGF-beta1 correlates with myofibroblasts and malignancy in the colorectal adenoma-carcinoma sequence. Cancer Sci. 2009 Apr;100(4):663-70.
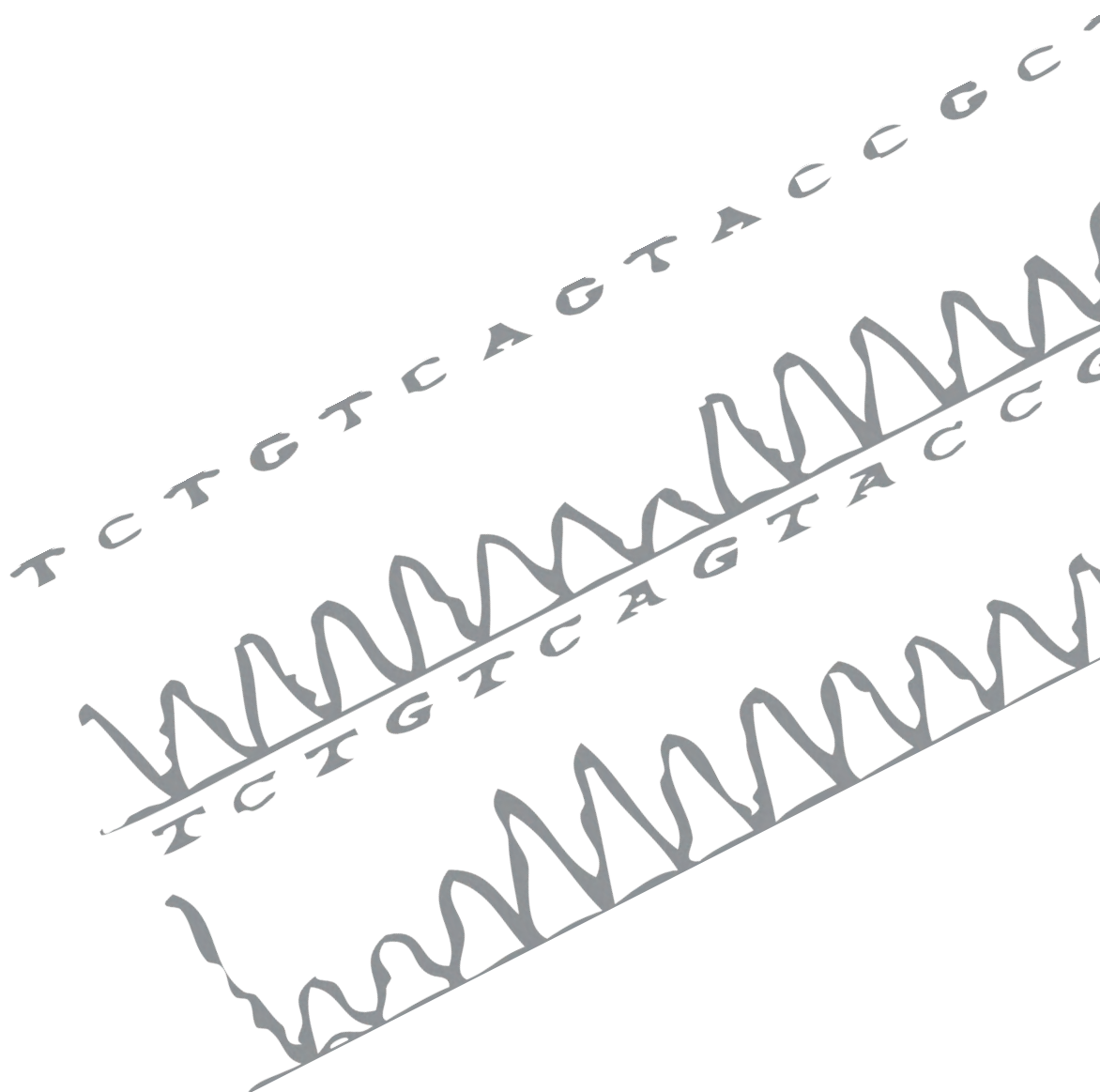
5

Chapter 6

Fibulin-4 mutation analysis of patients with thoracic and abdominal aortic disease
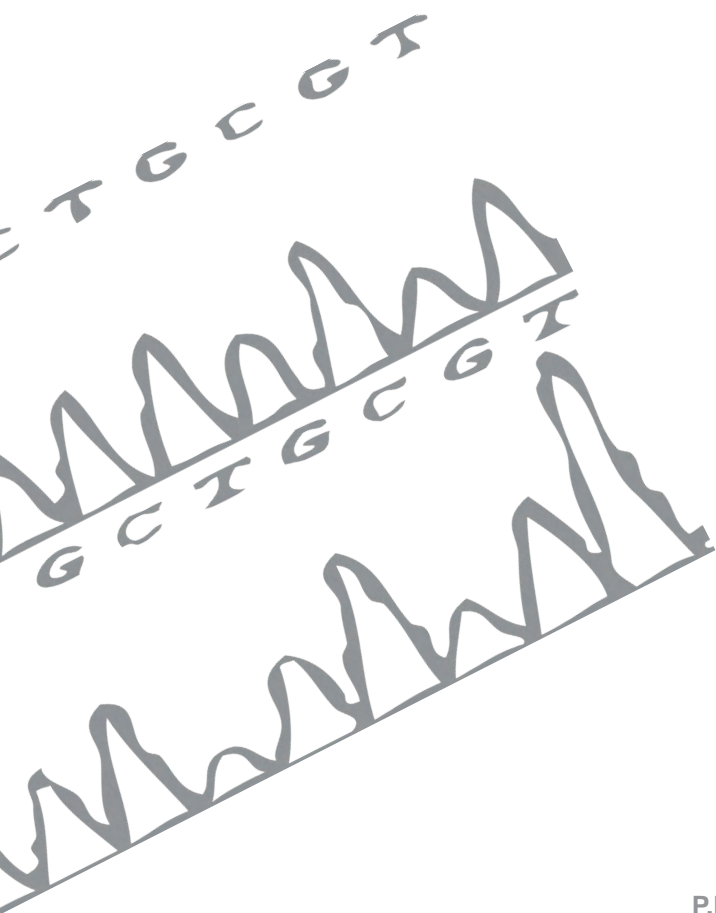
N.W.M. Ramnath[1,2],
P. Elfferich[3],
K.M. van de Luijtgaarden[1],
P.M. van Heijningen[2], H.T. Bruggenwirth[3],
D. Dooijes[6], J.M.A. Verhagen[3], M.W. Wessels[3],
G. Pals[7], D. Majoor-Krakauer[3], J. W. Roos-Hesselink[4],
E.V. Rouwet[1], R. Kanaar[2,5], J. Essers[1,2,5]

[1]Department of Vascular Surgery, [2]Department of Cell Biology & Genetics, Cancer Genomics Centre, [3]Department of Clinical Genetics, [4]Department of Cardiology, Thorax Centre, [5]Department of Radiation Oncology, Erasmus MC, Rotterdam, The Netherlands

[6]Department of Medical Genetics, UMC Utrecht

[7]Department of Clinical Genetics, VU University Medical Centre Amsterdam, Amsterdam, The Netherlands.

ABSTRACT

Thoracic aortic aneurysms occur in a number of connective tissue disorders, such as Marfan syndrome. Patients with homozygous or compound heterozygous mutations in the extracellular matrix protein Fibulin-4 show a Marfan-like phenotype, including ascending aortic aneurysm and tortuosity and stenosis of the thoracic aortic. In some patients abdominal aortic tortuosity and dilation occur. Mutant mice (Fibulin-4$^{R/R}$), with a 4-fold reduced expression level of Fibulin-4, show severe developmental thoracic aortic aneurysms and stenosis. In contrast, Fibulin-4$^{+/R}$ mice, with a 2-fold reduced expression level of Fibulin-4, have extracellular matrix defects in the aortic wall without aortic aneurysms. These Fibulin-4$^{+/R}$ mice develop thoracic and abdominal aortic dilation after atherosclerosis induction. Based on these aortic abnormalities resulting from decreased Fibulin-4 expression, this study investigated whether heterozygous or mild pathogenic Fibulin-4 mutations could genetically predispose to thoracic and abdominal aortic aneurysms in adult patients. This was tested in 4 cohorts of patients with thoracic aortic dilation and/or aortic valve stenosis and coarctation, Ehlers-Danlos syndrome vascular type, and with familial and sporadic thoracic aortic aneurysm, and in 1 cohort consisting of patients with abdominal aortic dilation. All detected variants were analyzed in silico and scored on pathogenicity. Exon sequencing of Fibulin-4 revealed no overtly pathogenic mutations. However, we cannot rule out that subtle mutations affecting the expression level of Fibulin-4 are present in these patients.

6

INTRODUCTION

According to the location aneurysms in the aorta are classified as thoracic aortic aneurysm (TAA) and abdominal aortic aneurysm (AAA). Patients with TAA can be categorized in 3 groups: (1) inherited TAA syndromes such as Marfan Syndrome, Ehlers- Danlos Syndrome, Loeys-Dietz Syndrome and the arterial , (2) familial non-syndromic TAA disease (20% of TAA cases) with a variable age of onset and associated cardiovascular features such as bicuspid aortic valve, and (3) sporadic TAA cases with no family history of TAA detected at older age [1, 2]. TAAs can be caused by a genetic alteration, and mutations within different genes have been shown to be responsible. The gene encoding the extracellular matrix protein Fibrillin-1 (FBN1 gene) is associated with the classical form of Marfan syndrome, and is the most frequently involved gene in familial forms of TAA [3]. Other implicated genes encode contractile proteins of the smooth muscle cell (ACTA2, MYH11 and MYLK) and factors involved in the TGF-β pathway (TGFBR1, TGFBR2, TGFB2, SMAD3) [4-6].

In addition to the FBN1 gene, mutations in other genes encoding extracellular matrix proteins have been identified in patients with thoracic aortic aneurysms, including mutations in the Fibulin-4 gene. Fibulin-4 plays an important role in elastic fiber assembly and function and is a regulatory factor in elastogenesis [7, 8]. The Fibulin-4 deficient patients described so far all had homozygous or compound heterozygous mutations, and presented with a severe stage of the disease in the first months or years of their life [9-15]. A certain proportion of these patients described also presented with abdominal tortuosity and/or dilation on further examination [12, 15].

We have previously demonstrated that mice with a systemic 4-fold (Fibulin-4$^{R/R}$) or 2-fold (Fibulin-4$^{+/R}$) reduced expression of Fibulin-4 share a number of key features with the Fibulin-4 patients and the Marfan syndrome mouse model, including aortic wall degeneration, aneurysm formation, and increased TGF-β expression [16, 17]. In addition, Fibulin-4 deficient mice have impaired vascular contractility, increased arterial stiffness [18], left ventricular hypertrophy and aortic stenosis and regurgitation [16]. The combination of aortic stenosis and ascending aorta dilation is well known in patients with a bicuspid aortic valve and occurs irrespective of altered hemodynamics [19, 20]. However, no clear genetic underlying cause could be identified in the majority of these patients. Since aortic stenosis was observed in Fibulin-4 deficient mice, also Fibulin-4 deficient patients might be expected to have it. However, to date this has not been described.

In addition, Fibulin-4$^{+/R}$ mice present with a milder form of the aortic disease. They do not develop aortic aneurysms spontaneously, but have aortic wall degeneration and slightly increased TGF-β signaling and increased matrix metalloprotease (MMP) activity compared to wild type littermates. A slight increase in MMP activity is also observed in the abdominal aorta of Fibulin-4$^{+/R}$ mice. After atherosclerosis induction in these Fibulin-4$^{+/R}$ mice the MMP activity in the abdominal aorta increases further, and in addition, they develop abdominal aortic dilation (Chapter 2). In patients AAA is a complex disease and occurs due to a combination of both genetic and environmental risk factors. AAAs are almost always associated with atherosclerosis and the risk factors for occurrence of AAAs are similar to those for atherosclerotic disease [21, 22]. The development of abdominal aortic dilation in atherosclerotic Fibulin-4$^{+/R}$ mice indicates that gene defects resulting in minor alterations in the extracellular matrix of the aortic wall in combination with atherosclerosis and other environmental risk factors might trigger AAA formation.

The aim of the present study was to investigate whether Fibulin-4 mutations could genetically predispose to thoracic and abdominal aortic disease in patients. To this end, we developed a PCR protocol for human Fibulin-4 exon sequence analysis and subsequently

6

sequenced DNA of 4 cohorts with thoracic aortic pathology and/or aortic stenosis, and DNA of 1 cohort consisting of AAA patients. With in silico methods the pathogenicity of the detected variants was assessed.

METHODS

Sequencing protocol for the human Fibulin-4 gene

Primers (Table 1) were designed with the Fibulin-4 gene sequence from the Ensemble database (RefSeq IDs: NM_016938 and Accession Number: AF109121) [23]. The exons and approximately 80-100 bp flanking regions were selectively amplified. An M13-DNA sequence was included in each primer for simple and efficient direct sequencing. The M13-DNA sequence 5'-TGTAAAACGACGGCCAGT-3' was included at the 5'-end of all the forward primers, while the sequence 5'-CAGGAAACAGCTATGACC-3' was included at the 5'-end of the reverse primers. Exon 11 was split into 2 fragments (exon 11.1 and exon 11.2) of 462 bp and 593 bp. Amplification reactions were performed in a total volume of 25 μl, containing 10x PCR buffer (Invitrogen), 1.5 mM $MgCl_2$ (Invitrogen), 1.325 μl DMSO (Dimethyl Sulfoxide 99.9%, Sigma-Aldrich), 200 μM of each dNTP (Invitrogen), $4x10^{-4}$ μM forward primer, $4x10^{-4}$ μM reverse primer, 0.1 units Platinum Taq DNA polymerase (Invitrogen) and 100 ng genomic DNA. The PCR conditions were: 2' 94°C, 35 cycles of 1' 94°C, 1' 60°C, and 90'' 72°C with a final extension for 10' 72°C and 5' 20°C. Sequence analysis was done with Seqscape (Applied Biosystems). Noncoding exon 1 was left out of the analysis.

Patient samples

In this study 5 patient cohorts were investigated. From the CONgenital CORvitia (CONCOR), the Dutch registry and DNA-bank for adults with congenital heart disease [24], 400 samples could be obtained from patients with aorta and/or aortic valve abnormalities. Of those, 94 had a similar phenotype as Marfan syndrome patients, but had no Fibrillin-1 mutation, 70 patients had ascending aortic dilation, 173 aortic coarctation (COA), 133 congenital aortic stenosis, 9 aortic stenosis and ascending aorta dilation and 15 patients had combined COA and ascending aorta dilation. 399 DNA samples of the CONCOR patients could be sequenced successfully. One sample had a bad quality and was therefore excluded. The second cohort was obtained from the department of Clinical Genetics, VU University Medical Centre Amsterdam, and consisted of 83 patients with thoracic aortic aneurysms negative for FBN1, TGFBR1, TGFBR2 and SMAD3 mutations. The 47 patients in the third cohort were only clinically diagnosed for the Ehlers-Danlos syndrome vascular type. Exon 10 and 11 from 35 patients of this cohort could not be sequenced successfully due to limited DNA samples. The fourth cohort was obtained from the department of Clinical Genetics, Erasmus MC Rotterdam, and consisted of 31 patients with familial and sporadic TAAs, all screened negative for FBN1, TGFBR1, TGFBR2, SMAD3, TGFB2, ACTA2 and MYL9 mutations, and most of them for MYH11 and MYLK mutations. The fifth cohort included 76 abdominal aortic aneurysm patients. The DNA samples of 190 healthy male and female subjects were obtained from the department of Clinical Genetics of the Erasmus MC.

In silico analysis

The ensemble database was checked for the presence of the observed variants in the different patient cohorts. The variants found in the ensemble database were selected with their reference sequence (rs) numbers, which are linked to the dbSNP database. From this

database the frequencies of the variants in certain populations could be obtained, which were compared to the frequencies of the variants in the patient cohorts, determined by dividing the number of detected variants by the total number of DNA samples per patient cohort.

All detected variants were then tested on the probability of being pathogenic. In order to do so the variants were analyzed with software, Alamut (Biointeractive Software), that integrates genetic information from different sources. Based on the outcome of 5 splice site prediction programs (SpliceSiteFinder-like, MaxEntScan, NNSPLICE, GeneSplicer, Human Splicing Finder), 4 prediction programs on the effect of amino acid changes (Align GVGD, SIFT, Mutation Taster, Polyphen), frequencies in different populations and other available information according to databases such as RefSeq, dbSNP, Ensembl, Uniprot, the UCSC Genome Browser Database and PubMed, the observed variants were classified into 3 classes of pathogenicity according to the department of Clinical Genetics of the Erasmus Medical Centre (Erasmus MC): 1) Not Pathogenic or of No Clinical Significance, 2) Uncertain or Unclassified Variants (UVs) and 3) Definitely Pathogenic. To assess the probability of pathogenicity we used a Minor Allele Frequency (MAF) cut-off of <10% for increased pathogenicity. In addition, splice site predictions with a >10% change in >2 out of 5 programs and predictions on the effect of amino acid changes were used to determine the degree of pathogenicity.

RESULTS

Human Fibulin-4 exon sequencing protocol
In order to screen Fibulin-4 in patient cohorts with cardiovascular diseases, we first set up a PCR amplification and sequencing protocol for all coding exons and flanking introns of the Fibulin-4 gene using a human control Centre d'Etude Polymorphisme Humain (CEPH) cell line. The coding exons with flanking introns and Untranslated Regions (UTRs) were amplified using specific primer pairs, which were screened for the absence of single nucleotide polymorphisms (Figure 1A and Table 1). To successfully amplify and sequence exon 11, which is 633 bp long including the 3' UTR, we split the amplification of this exon over two fragments; exon 11.1 and exon 11.2. A M13-DNA sequence, specific for forward and reverse primers, was included at the 5'-end of every primer to simplify direct sequencing (Table 1). PCR products were analyzed by gel electrophoresis through 2% agarose gels and visualized by ethidium bromide staining (Figure 1B). Subsequently, these amplimers were directly sequenced using the Sanger sequencing method on the ABI3730 XL automated sequencer and compared to the Fibulin-4 wild type sequence available on the Ensembl database (RefSeq IDs: NM_016938 and Accession Number: AF109121). Although different primer pairs, polymerases (Expand Long Template, Roche, and Ex Taq, TaKara) and additives (10x PCR enhancer, Invitrogen, and spermidine, Invitrogen) were used for amplification of exon 1, not enough PCR products could be obtained (Figure 1B) and the sequence was not readable. Therefore, noncoding exon 1 was left out of the analysis. In contrast, amplification of all coding exons and the 3' UTR resulted in products of the expected size and readable sequences.

Fibulin-4 exon sequence analysis in patients with thoracic aortic disease
With the developed exon sequencing protocol for Fibulin-4, four patient cohorts with thoracic aortic disease were screened in this study. As until now a limited amount of Fibulin-4 deficient patients has been described and not much is known of the phenotypic spectrum of
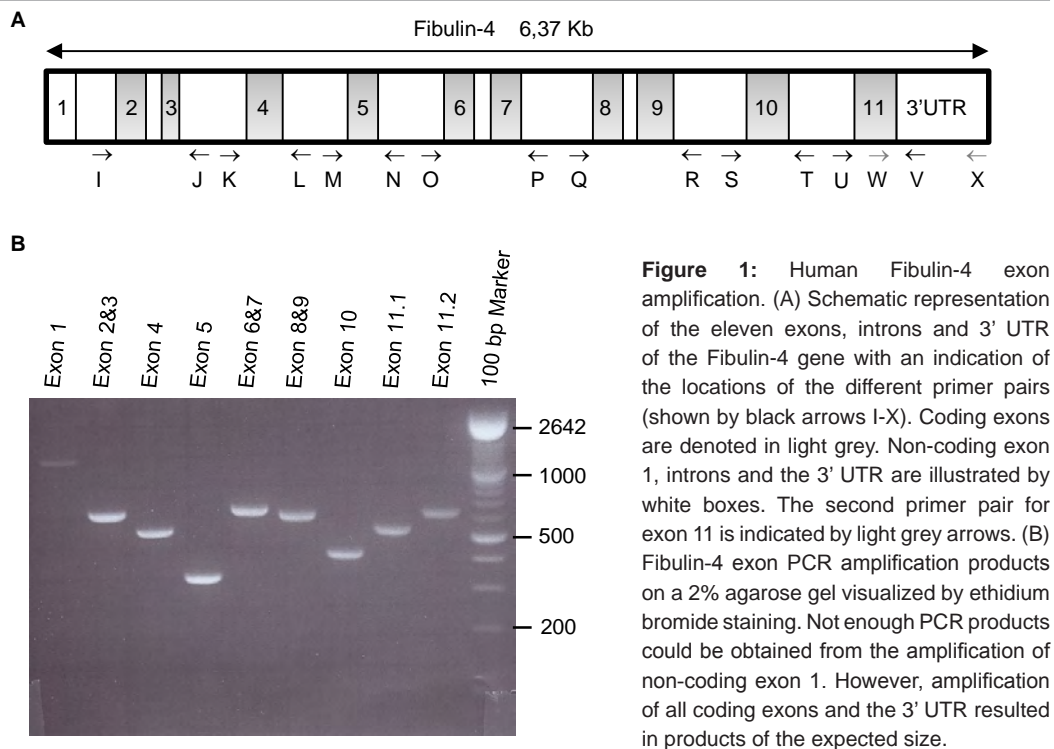
6

A

B

Figure 1: Human Fibulin-4 exon amplification. (A) Schematic representation of the eleven exons, introns and 3' UTR of the Fibulin-4 gene with an indication of the locations of the different primer pairs (shown by black arrows I-X). Coding exons are denoted in light grey. Non-coding exon 1, introns and the 3' UTR are illustrated by white boxes. The second primer pair for exon 11 is indicated by light grey arrows. (B) Fibulin-4 exon PCR amplification products on a 2% agarose gel visualized by ethidium bromide staining. Not enough PCR products could be obtained from the amplification of non-coding exon 1. However, amplification of all coding exons and the 3' UTR resulted in products of the expected size.

Table 1 – Primer sequences used for amplification of the different exons of the human Fibulin-4 gene. M13-tail sequences of the forward and reverse primers are listed. F = Forward, R = Reverse.

Exon	M13-tail – Primer	
2&3	TGTAAAACGACGGCCAGT-CCCAAGCACGGTCCTGAG	F
	CAGGAAACAGCTATGACC- ACGGCAGTTCTTGGAGGTG	R
4	TGTAAAACGACGGCCAGT-TTGTTGAGCAGAGTGGGAAG	F
	CAGGAAACAGCTATGACC-CGGCAGGTCCTAAACAACAT	R
5	TGTAAAACGACGGCCAGT-GTGCTGTTGAGAGAACCGAAT	F
	CAGGAAACAGCTATGACC-GAATGGGGGTCAGGTGCTA	R
6&7	TGTAAAACGACGGCCAGT-GCTCCTCGGACACAGGATTA	F
	CAGGAAACAGCTATGACC-GGGTGCACAGTGACAGGAG	R
8&9	TGTAAAACGACGGCCAGT-TTGTCTCATCCCCCTCTGTC	F
	CAGGAAACAGCTATGACC-TGATTCCCATCATCCCTCA	R
10	TGTAAAACGACGGCCAGT-CCCTGAGGGATGATGGGAATC	F
	CAGGAAACAGCTATGACC-ATAGCAGCCTGGCCGAGT	R
11.1	TGTAAAACGACGGCCAGT-TCAAAGAGCTGCATGAGAGG	F
	CAGGAAACAGCTATGACC-CCCCATTTAGGTGAACTTGG	R
11.2	TGTAAAACGACGGCCAGT-CCTCCCTGCAGCTACCCTA	F
	CAGGAAACAGCTATGACC-GCATTGCAGCTTGGAATCTA	R

especially a haploinsufficiency for Fibulin-4, we screened for mutations in heterogeneous aortic aneurysm patient cohorts. The first cohort consisted of 399 patients from the Concor database with aortic dilation, COA and/or aortic valve stenosis, and were selected based on the phenotypes observed in Fibulin-4 deficient mice and patients. The second cohort contained 83 TAA cases without a FBN1, TGFBR1, TGFBR2 or SMAD3 mutations. The third cohort included 47 patients diagnosed with the Ehlers-Danlos syndrome vascular type, and the fourth cohort contained 31 patients presenting with familial and sporadic thoracic aortic aneurysms negative for FBN1, TGFBR1, TGFBR2, SMAD3, TGFB2, ACTA2 and MYL9 mutations, and most of them for MYH11 and MYLK mutations. Comparison of the sequenced fragments of the Fibulin-4 gene to the reference sequence (Ensemble database) resulted in the detection of in total 16 variants in introns, exons and non-coding regions (Table 2).

To determine whether the detected variants in the thoracic aortic disease patients could be specifically associated with aortic and heart pathology, the frequencies of the variants were compared to their frequencies in control populations. Variants described earlier with a rs (reference sequence) number could be compared with previously determined frequencies (Table 3). The frequencies of novel variants in exons and near splice sites were compared to their frequency in a control group that was sequenced for this purpose specifically (Table 3). However, for variants c.111+29G>C, c.160+19C>T, c.490+30C>T, c.728-3C>T, c.*187G>A and c.*115G>A no frequency information was available in control populations. No major differences were detected between the frequencies of the other variants in the reported populations, control group and the 4 cohorts.

To determine their clinical significance, these variants were analyzed *in silico* with Alamut, which integrates genetic information from different sources using 5 splice site prediction programs, 4 prediction programs on the effect of amino acid changes, frequencies in different populations and other available information, like amino acid conservation, according to databases such as RefSeq, dbSNP, Ensembl, Uniprot, the UCSC Genome Browser Database and PubMed. Based on predicted effects of splice site alterations and amino-acid substitutions, and on whether variants are common in control populations, the 16 observed variants in Fibulin-4 were classified into 3 classes of pathogenicity. Three criteria to evaluate expected pathogenicity were included: 1) a minor allele frequency of <10% or when frequency information was unavailable, 2) splice site predictions with alterations of >10% in more than 2 out of 5 programs, and 3) predicted pathogenic effects of amino acid changes. Variants scored definitely neutral were placed in Class 1; variants likely to be neutral, but without clear evidence, variants for which there is too little information to make any recommendations, and variants likely to be pathogenic but without irrefutable evidence for pathogenicity were assigned to Class 2; and variants proven to be definitely pathogenic were placed in Class 3.

According to this classification 10 variants were assigned to Class 1 'Not pathogenic or of No Clinical Significance' based on a combination of no predicted splice site changes, no functional consequences of amino-acid substitutions and a MAF of >10% in control populations (Table 4). Variant c.139C>T [p.Pro47Ser] had no significant predicted splice site changes, a predicted tolerated non-synonymous amino acid change and a frequency of <10%. As this variant has a low frequency and a probable tolerated amino acid change, we could not classify it as definitely neutral (Class 1), as there was no irrefutable evidence against pathogenicity. This variant was therefore classified in Class 2. According to similar prediction outcomes and a frequency <10% for variant c.277G>A [p.Gly93Ser], this variant was also classified in Class 2. Variant c.1188C>T [p.= (p.Ser396Ser)] had no predicted altered splice sites, a synonymous amino-acid change and a frequency <10% and was

6

Table 2 – Fibulin-4 variants in patients with thoracic and abdominal aortic disease. Found variants in the intron, exon and 3'UTR regions are displayed per exon for the different patient groups. n= number of found variants.

Exon	Concor - Coarctation n=188	Concor - Aortic Valvar Stenosis n=142	Concor - Ascending Aorta Dilation n=94	Thoracic aortic aneurysm n=83	Thoracic aortic aneurysm - Ehlers Danlos Vascular Type n=47	Familial Thoracic Aortic Aneurysm n=31	Abdominal Aortic Aneurysm n=89
2			c.111+29G>C (1)				
3	c.160+19C>T (1) c.139C>T [p.Pro47Ser] (1)	c.160+19C>T (1)					
4	c.276C>T [p.= (p.His92His)] † c.277G>A [p.Gly93Ser] (3)	c.276C>T [p.= (p.His92His)] †	c.276C>T [p.= (p.His92His)] †	c.276C>T [p.= (p.His92His)] †	c.276C>T [p.= (p.His92His)]† c.277G>A [p.Gly93Ser] (1)	c.276C>T [p.= (p.His92His)] †	c.276C>T [p.= (p.His92His)] † c.277G>A [p.Gly93Ser] (2) c.367+90delG (1)
5	c.368-11G>A (2) c.368-4G>A (4) c.490+23G>C †	c.368-11G>A (1) c.368-4G>A (2) c.490+23G>C†	c.368-4G>A (2) c.490+23G>C† c.490+30C>T (1)	c.368-11G>A (1) c.368-4G>A (1) c.490+23G>C†	c.490+23G>C†	c.490+23G>C†	c.368-4G>A (1) c.490+23G>C†
6							c.491-28_491-22del7 (1)
8	c.728-3C>T (1) c.775A>G [p.Ile259Val] †	c.775A>G [p.Ile259Val]†	c.728-3C>T (1) c.775A>G [p.Ile259Val] †	c.775A>G [p.Ile259Val]†	c.775A>G [p.Ile259Val]†	c.775A>G [p.Ile259Val]†	c.775A>G [p.Ile259Val] †
10						c.975-25 G>T (1)	c.1047C>T [p.= (p.Thr349Thr)] (1)
11.1	c.1188C>T [p.= (p.Ser396Ser)] (2)	c.1188C>T [p.= (p.Ser396Ser)] (1)	c.1188C>T [p.= (p.Ser396Ser)] (1)				
11.2	c.*165delG (15) c.*187G>A (1)	c.*165delG (4)	c.*165delG (6)	c.*165delG (8)	c.*165delG (1‡)	c.*115 G>A (1) c.*165delG (3)	c.*165delG (1)

‡ 34 samples could not be analyzed, † these variants have a high frequency

Table 3 - Frequencies of the variants in different populations from dbSNP, control samples and the different cohorts. Frequencies in different populations could be obtained from the dbSNP database for known variants and were compared to the frequencies in the different patients cohorts. For novel variants near splice sites and within exons the frequencies were analyzed in a control group. n=number, ESP= Exome Sequencing project, CSAgilent= ClinSeq Agilent project, ref= reference, del= deletion.

Variants		ESP (%) n≥2604	CSAgilent (%) n≥1049	Control samples (%) n=200	Concor patients (%) n=399	Thoracic aortic aneurysm - no Marfan Syndrome (%) n=83	Thoracic aortic aneurysm - ED Vascular type (%) n=47	Familial Thoracic Aortic Aneurysm (%) n=31	Abdominal Aortic Aneurysm (%) n=76
c.111+29G>C	G/G	n/a	n/a	n/a	99.75	-	-	-	-
	G/C	n/a	n/a	n/a	0.25	-	-	-	-
	C/C	n/a	n/a	n/a	-	-	-	-	-
c.160+19C>T	C/C	n/a	n/a	n/a	99.50	-	-	-	-
	C/T	n/a	n/a	n/a	0.50	-	-	-	-
	T/T	n/a	n/a	n/a	-	-	-	-	-
c.139C>T	C/C	99.80	n/a	n/a	99.75	-	-	-	-
rs144320036	C/T	0.20	n/a	n/a	0.25	-	-	-	-
	T/T	-	n/a	n/a	-	-	-	-	-
c.276G>A	G/G	42	23.50	22.90	24.25	15.70	29.82	29	35.53
rs633800	A/G	42	48.80	54.30	50.30	60.20	48.90	35.50	48.86
	A/A	16	27.70	22.90	25	24.10	21.28	35.50	15.79
c.277G>A	G/G	99.50	99.40	98.9	99.25	-	97.87	-	97.37
rs 2234462	A/G	0.50	0.60	1.1	0.75	-	2.13	-	2.63
	A/A	-	-	-	-	-	-	-	-
c.367+90delG	G/G	n/a	n/a	-	-	-	-	-	98.68
	del/G	n/a	n/a	-	-	-	-	-	1.32
	del/del	n/a	n/a	-	-	-	-	-	-
c.368-11G>A	G/G	n/a	97.60	98.40	99.20	98.80	-	-	-
rs181514768	A/G	n/a	2.40	1.60	0.80	1.20	-	-	-
	A/A	n/a	-	-	-	-	-	-	-
c.368-4G>A	G/G	n/a	99.70	98.9	98	98.80	-	-	98.68
rs111550973	A/G	n/a	0.30	1.1	2	1.20	-	-	1.32
	A/A	n/a	-	-	-	-	-	-	-
c.490+23 G>C	G/G	n/a	46.70	8.50	12.50	12	10.20	12.90	15.79
rs630394	G/C	n/a	43.40	44.70	44	48.20	38.30	35.50	47.36
	C/C	n/a	9.90	45.70	43.50	39.80	51.50	51.60	36.84
c.490+30C>T	C/C	n/a	n/a	n/a	99.75	-	-	-	-
	C/T	n/a	n/a	n/a	0.25	-	-	-	-
	T/T	n/a	n/a	n/a	-	-	-	-	-
c.491-28_491-22del7	ref/ref	n/a	n/a	n/a	-	-	-	-	98.68
	del/ref	n/a	n/a	n/a	-	-	-	-	1.32
rs149021732	del/del	n/a	n/a	n/a	-	-	-	-	-
c.728-3C>T	C/C	n/a	n/a	n/a	99.75	-	-	-	-
	C/T	n/a	n/a	n/a	0.25	-	-	-	-
	T/T	n/a	n/a	n/a	-	-	-	-	-
c.775A>G	T/T	4.40	-	-	-	-	-	-	59.21
rs601314	T/C	18	0.30	2.70	1.50	66.27	n/a	3.20	-
	C/C	77.50	99.70	96.30	98.50	31.33	80.90	96.80	40.79
c.975-25G>T	G/G	99.93	n/a	n/a	-	-	-	96.80	-
rs2234470	G/T	0.07	n/a	n/a	-	-	-	3.20	-
	T/T	-	n/a	n/a	-	-	-	-	-
c.1047C>T	C/C	n/a	n/a	n/a	-	-	-	-	98.68
rs2234470	C/T	n/a	n/a	n/a	-	-	-	-	1.32
	T/T	n/a	n/a	n/a	-	-	-	-	-
c.1188C>T	C/C	99.80	99.80	99.50	99.25	-	-	-	-
rs2234473	C/T	0.20	0.20	0.50	0.75	-	-	-	-
	T/T	-	-	-	-	-	-	-	-
c.*165delG	G/G	n/a	n/a	92	94	90.40	23.50*	90.30	98.68
rs201135561	del/G	n/a	n/a	8	6	8.40	2.0	6.50	1.32
	del/del	n/a	n/a	-	-	1.20	n/a	3.20	-
c.*187G>A	G/G	n/a	n/a	n/a	99.75	-	-	-	-
	A/G	n/a	n/a	n/a	0.25	-	-	-	-
	A/A	n/a	n/a	n/a	-	-	-	-	-
c.*115G>A	G/G	n/a	n/a	n/a	-	-	-	96.80	-
rs187686630	A/G	n/a	n/a	n/a	-	-	-	3.20	-
	A/A	n/a	n/a	n/a	-	-	-	-	-

*74.5% could not be analyzed

therefore also assigned to Class 2. Variants c.*165delG, c.*187G>A and c.*115G>A were positioned in the 3' UTR, which is usually involved in gene regulation. Because no information was available whether these positions are involved in gene regulation, these variants were also classified as 'Unclassified Variants' in Class 2. For variant c.*115G>A 3 out of 5 splice site prediction programs predicted >10% alterations in splice sites. As this variant is positioned 115 bp after the stopcodon, these splice site changes are probably irrelevant and do not influence a change in classification. In short, we found no indications for direct pathogenic mutations in the Fibulin-4 gene of the patients in the 4 cohorts. No variants were found with a higher or exclusive frequency in the thoracic aortic aneurysm patients. Analysis on pathogenicity indicated a subgroup of variants with unknown pathogenicity, assigned as Unclassified Variants, which may be involved in gene regulation and should be further analyzed in the future.

Fibulin-4 exon sequence analysis in patients with abdominal aortic disease
Apart from thoracic aortic disease Fibulin-4 deficiency in heterozygous Fibulin-4$^{+/R}$ mice, which already have minor aortic wall degeneration, also results in abdominal aortic abnormalities upon atherosclerosis induction (Chapter 2). This mouse model mimics the clinical situation of combined atherosclerosis and abdominal aortic dilation, and prompted us to screen for Fibulin-4 mutations in a cohort consisting of 89 abdominal aortic aneurysm patients. Comparison of the sequenced fragments of the Fibulin-4 gene from these patients to the reference sequence (Ensemble database) resulted in the detection of 9 variants in introns, exons and non-coding regions (Table 2). Six out of the 9 variants also occurred in the thoracic aortic disease patients. The c.276C>T [p.= (p.His92His)], c.368-4G>A, c.490+23G>C and c.775A>G [p.Ile259Val] variants, were classified in Class 1 and c.277G>A [p.Gly93Ser] and c.*165delG were classified as UV (Class 2). Frequencies of the other 4 detected variants could not be compared to their frequencies in control populations, and therefore specific association with abdominal aortic aneurysm patients could not be determined (Table 3).

However, the pathogenic effect of these 4 variants were analyzed *in silico* following the same methods and were classified. For variant c.160+17G>T only one program predicted >10% difference for a new splice site, and this was therefore not counted as a significant predicted splice site change. However, also no frequency data was available. Therefore this variant could not be classified as definitely neutral and was assigned to Class 2 (Likely Not Pathogenic/Little Clinical Significance) (Table 4). Variants c.367+90delG and c.491-28_491-22del7 were classified as 'No Clinical Significance' (Class 1) due to no predicted splice site changes, a MAF >10% and their intronic position. Variant c.1047C>T [p.= (p.Thr349Thr)] was classified in Class 2, as it was not predicted to create altered splice sites, resulted in a synonymous amino acid change, but had no frequency data available and could therefore not be classified as definitely neutral. In conclusion, in the patients with abdominal aortic aneurysms we found no indications for direct pathogenic mutations in the Fibulin-4 gene. However, pathogenicity of 3 out 7 variants could not be ruled out and 1 variant in the 3' UTR was classified as an Unclassified Variant.

6

Table 4 – Expected pathogenicity of the Fibulin-4 variants. Frequencies, predictions on splice sites and amino acid substitutions and the pathogenicity classification are indicated per variant. The observed variants were classified into 3 classes of pathogenicity: 1) Not Pathogenic or of No Clinical Significance, 2) Uncertain or Unclassified Variants (UVs) and 3) Definitely Pathogenic. rs=reference sequence, n=number, MAF= Minor Allele frequency.

Variants	rs number	MAF in reported populations (%)	Splice site prediction (5 programs)	Protein change	In silico prediction pathogenic effect	Amino Acid conservation**	Expected pathogenicity Class (1-3)
c.111+29G>C	-	-	<10% difference	-	-	-	1
c.160+19C>T	-	-	<10% difference	-	-	-	1
c.139C>T	rs144320036	0.14	<10% difference	p.Pro47Ser	Missense, tolerated	Moderately	2
c.276C>T	rs633800	31.17	<10% difference	p.= (p.His92His)	-	-	1
c.277G>A	rs2234462	0.42	2> +10% difference, new splice site	p.Gly93Ser	Missense, tolerated	Moderately	2
c.367+90delG	-	-	1> 10% difference, no new splice site	-	-	-	1
c.368-11G>A	rs181514768	0.6	1> +10% difference, 1 > -10% difference, no new splice site	-	-	-	1
c.368-4G>A	rs111550973	0.2	1> +10% difference, no new splice site	-	-	-	1
c.490+23G>C	rs630394	48.2	<10% difference	-	-	-	1
c.490+30C>T	-	-	<10% difference	-	-	-	1
c.491-28_491-22del7	rs149021732	1.8	<10% difference	-	-	-	1
c.728-3C>T	-	-	1> +10% difference, no new splice site	-	-	-	1
c.775A>G	rs601314	8.5 [allele A]	1> 10% difference, new splice site	p.Ile259Val	Missense, tolerated	Weakly	1
c.975-25G>T	rs2234470	0.05	<10% difference	-	-	-	1
c.1047C>T	-	-	<10% difference	p.= (p.Thr349Thr)	-	-	2
c.1188C>T	rs 2234473	0.2	2> +10% difference, no new splice site	p.= (p.Ser396Ser)	-	-	2
c.*165delG	rs201135561	0.2	1> 10% difference, no new splice site	-	-	-	2
c.*187G>A	-	-	1> 10% difference, new splice site	-	-	-	2
c.*115G>A	rs187686630	0.1	3> +10% difference, new 5' splice sites; 1> +10% difference, new 3' splice site; 2> -10% difference, 3' splice sites	-	-	-	2

** Based on 10 species

6

DISCUSSION

In the current study, we developed an exon amplification and sequencing protocol, which successfully screened all coding exons and the 3' UTR of the human Fibulin-4 gene. Subsequent screening of the Fibulin-4 gene in 4 cohorts of patients with syndromic, familial and sporadic TAAs and in 1 cohort consisting of AAA patients revealed no evidence of a definite pathogenic mutation. However, distinct variants were detected that were classified as 'Unclassified Variant', as they could not be categorized as definitely neutral. In addition, variants were detected in the 3' UTR and were classified as UVs, as they may be involved in gene regulation.

It is possible that Fibulin-4 mutations do not underlie the majority of familial and sporadic aortic aneurysms and the combined existence of ascending aortic aneurysms and aortic valve stenosis, however we cannot rule out the occurrence of milder mutations affecting the expression level of the protein. This remains to be determined by genomic sequencing of the Fibulin-4 locus or by Fibulin-4 RNA expression analysis. Furthermore, variants were classified as 'Likely Not Pathogenic' in Class 2 as they could not be assigned as definitely neutral, due to a population frequency cut-off of <10% or the absence of available frequency data. This classification category may be altered if more information and evidence becomes available in the future, converting it from Class 2 to either Class 1 or Class 3.

It is also possible that our set of patients was too heterogeneous to find a pathogenic Fibulin-4 mutation. From previous publications and the chapters in this thesis we may conclude that reduced expression of Fibulin-4 in mice mainly results in cardiovascular abnormalities, including thoracic aorta aneurysms, tortuosity, aortic stenosis and cardiac dysfunction, but also coincide with Fibulin-4 dose-dependent lung emphysema [16-18, 25]. In addition, we observed that a mild Fibulin-4 reduction in combination with atherosclerosis results in thoracic and abdominal aortic disease in heterozygous adult mice (Chapter 2). The Fibulin-4 patients described so far share the clinical features of Fibulin-4$^{R/R}$ mice, and in addition present with cutis laxa (described as Autosomal Recessive Cutis Laxa Type 1B) and severe tortuosity of the cerebral arteries, including the internal carotid arteries. No cardiovascular abnormalities have been described so far in the heterozygous parents of these patients, while hip dysplasia, hernias, and premature rupture and bleedings during pregnancies are described [9-15]. Furthermore, the cohort described in Renard et al, where 3 patients carrying Fibulin-4 mutations were found, consisted of 22 patients with combined arterial tortuosity, stenosis and aneurysms [12]. However, in this study only a small subset of the population had the combined diagnosis of aortic dilation and stenosis.

Although no haploinsufficient heterozygous effect of Fibulin-4 has been reported in patients so far and most of the described Fibulin-4 patients, carrying recessive mutations in the Fibulin-4 gene, do not survive through the first two years of life, two patients were observed that asymptomatically reached the age of 7 years (Table 5) [12, 15]. One patient was observed in a group of 22 patients, described by Kappanayil et al. Of these 22 patients, 21 patients shared an identical homozygous missense c.608A>C (p. Asp203Ala) mutation and reached a median age of 4 months or were described until 20 months of age. The patient that asymptomatically reached the age of 7 years showed compound heterozygosity for this mutation, and carried next to the c.608A>C (p.Asp203Ala) mutation, a missense c.679C>T (p.Arg227Cys) mutation in the same calcium binding epidermal growth factor (cbEGF) domain. The other patient that asymptomatically reached the age of 7 years, described by Renard et al, had a homozygous missense c.1189G>A (p.Ala397Thr) mutation in the Fibulin-type module, while all other mutations described until now are in

Table 5 – Reported pathogenic Fibulin-4 mutations in patients. The mutations in the Fibulin-4 gene of the so far described patients are displayed with their pathogenic effect on the expression of the Fibulin-4 protein and the survival of the patients. BMD= bone mineral density

Patients	Identified mutation	Pathogenic effect	Extracellular Fibulin-4	Age	Clinical features
Patient 1 (Dasouki et al)	c.835C>T (p.Arg279Cys); c.1070_1073dupCCGC (p.Asp359Argfs*2) Compound heterozygous	Missense; Premature stop codon	Near absence, reduced secretion	27 days	Aneurysm, tortuosity, mild cutis laxa, arachnodactyly
Patient 2 (Huchthagowder et al)	c.169G>A (p.Glu57Lys) Homozygous	missense	Severely reduced secretion	2 years	Aneurysm, tortuosity, joint laxity, diaphragmatic hernia, emphysema, fractures at birth
Patient 3 (Hoyer et al)	c.800G>A (p.Cys267Tyr) Homozygous	missense	Complete absence	Died at birth	Cutis laxa, hyperextensibility, emphysema, hypertelorism, retrognathia
Patient 4 (Renard et al)	c.376G>A (p.Glu126Lys) Homozygous	missense	Slightly reduced secretion	20 years	Aneurysm, tortuosity, velvety skin, arched palate, retrognathia
Patient 5 (Renard et al)	c.1189G>A (p.Ala397Thr) Homozygous	missense	Not determined	7 years	Aneurysm, tortuosity, joint laxity, hypertelorism, flat facies
Patient 6 (Renard et al)	c.377A>T (p.Glu126Val); c.577delC (p.Gln193Serfs*12) Compound heterozygous	Missense; Premature stop codon	Not determined	18 months	Aneurysm, tortuosity, long fingers, hypertelorism, stroke
Patient 7 and 8 (Erickson et al)	c.85delG (p.Asp29Ilefs*31) Homozygous	Premature stop codon	Predicted to be completely absent	Died at birth (31 weeks)	Tortuosity, cutis laxa, and limb, rib and skull fractures
Patient 9 (Sawyer et al)	c.376G>A (p.Glu126Lys) Homozygous	missense	In silico predicted to be damaging	8 years	Aneurysm, tortuosity, cutis laxa, baroreceptor reflex failure, reduced BMD
Patient 10‡ (Sawyer et al)	c.376G>A (p.Glu126Lys)** Homozygous	missense	In silico predicted to be damaging	29 months	Aneurysm, tortuosity, pendulous cheeks, inguinal hernia, pectus excavatum, hypotonia
Patient 11‡ (Sawyer et al)	c.376G>A (p.Glu126Lys)** Homozygous	missense	In silico predicted to be damaging	Died at birth (24 weeks)	Aneurysm, tortuosity, skin laxity, hypermobility, bilateral club feet, dislocated hip
Patient 12‡ (Sawyer et al)	c.376G>A (p.Glu126Lys)** Homozygous	missense	In silico predicted to be damaging	4 months	Aneurysm, tortuosity, cutis laxa, hypermobile joints, pyloric stenosis
Patient 13-34 (Kappanayil et al)	c.608A>C (p. Asp203Ala) Homozygous	Missense	In silico predicted to be damaging	4-20 months	Aneurysm, tortuosity, cutis laxa, and other features described in Kappanayil et al.
Patient 35 (Kappanayil et al)	c.608A>C (p. Asp203Ala); c.679C>T (p.Arg227Cys)	missense; missense	In silico predicted to be damaging	7 years	Hypertelorism, joint laxity

‡ Patients were siblings of each other.

** Presumed genotype, as these patients are related to patient 9 and their parents both carry the c.376G>A (p.Glu126Lys) mutation.

6

cbEGF-like domains. In addition, amongst 5 patients with the same homozygous missense c.376G>A (p.Glu126Lys) mutation, two patients were reported with a prolonged survival (8 and 20 years) [12, 14]. In the 20 year old patient this was probably due to only partially affected secretion of the mutant Fibulin-4 protein leading to a better survival than in complete absence of the protein. In addition, the surgery both patients received possibly led to a better survival. These data on survival of the patients indicate that the severity of the disease might indeed be related to the effect of the Fibulin-4 mutation on protein expression, which mirrors the gene dosage effect observed in Fibulin-4 deficient mice [16]. Therefore, besides the described recessive mutations, a haploinsufficiency for Fibulin-4 should also be considered during mutation analyses.

In conclusion, for future cohort inclusions it might be advisable to select adult or older patients with aortic aneurysms in combination with aortic tortuosity and stenosis, with known pulmonary dysfunction like lung emphysema or chronic obstructive pulmonary disease, and/or in combination with known risk factors such as atherosclerosis and smoking, to possibly detect haploinsufficient heterozygous or mild Fibulin-4 mutations. For the detection of homozygous Fibulin-4 pathogenic mutations a cohort consisting of young TAA patients with Marfan features, potentially pulmonary abnormalities and cutis laxa might be selected. In short, a pathogenic Fibulin-4 mutation might be found in a more defined homogeneous and larger population.

6

REFERENCES

1. Booher AM, Eagle KA. Diagnosis and management issues in thoracic aortic aneurysm. Am Heart J. 2011 Jul;162(1):38-46 e1.
2. Albornoz G, Coady MA, Roberts M, Davies RR, Tranquilli M, Rizzo JA, Elefteriades JA. Familial thoracic aortic aneurysms and dissections--incidence, modes of inheritance, and phenotypic patterns. Ann Thorac Surg. 2006 Oct;82(4):1400-5.
3. Dietz HC, Cutting GR, Pyeritz RE, Maslen CL, Sakai LY, Corson GM, Puffenberger EG, Hamosh A, Nanthakumar EJ, Curristin SM, et al. Marfan syndrome caused by a recurrent de novo missense mutation in the fibrillin gene. Nature. 1991 Jul 25;352(6333):337-9.
4. Jondeau G, Boileau C. Genetics of thoracic aortic aneurysms. Curr Atheroscler Rep. 2012 Jun;14(3):219-26.
5. Wang L, Guo DC, Cao J, Gong L, Kamm KE, Regalado E, Li L, Shete S, He WQ, Zhu MS, Offermanns S, Gilchrist D, Elefteriades J, Stull JT, Milewicz DM. Mutations in myosin light chain kinase cause familial aortic dissections. Am J Hum Genet. 2010 Nov 12;87(5):701-7.
6. van de Laar IM, Oldenburg RA, Pals G, Roos-Hesselink JW, de Graaf BM, Verhagen JM, Hoedemaekers YM, Willemsen R, Severijnen LA, Venselaar H, Vriend G, Pattynama PM, Collee M, Majoor-Krakauer D, Poldermans D, Frohn-Mulder IM, Micha D, Timmermans J, Hilhorst-Hofstee Y, Bierma-Zeinstra SM, Willems PJ, Kros JM, Oei EH, Oostra BA, Wessels MW, Bertoli-Avella AM. Mutations in SMAD3 cause a syndromic form of aortic aneurysms and dissections with early-onset osteoarthritis. Nat Genet. 2011 Feb;43(2):121-6.
7. Argraves WS, Greene LM, Cooley MA, Gallagher WM. Fibulins: physiological and disease perspectives. EMBO Rep. 2003 Dec;4(12):1127-31.
8. Chen Q, Zhang T, Roshetsky JF, Ouyang Z, Essers J, Fan C, Wang Q, Hinek A, Plow EF, Dicorleto PE. Fibulin-4 regulates expression of the tropoelastin gene and consequent elastic-fibre formation by human fibroblasts. Biochem J. 2009 Oct 1;423(1):79-89.
9. Hoyer J, Kraus C, Hammersen G, Geppert JP, Rauch A. Lethal cutis laxa with contractural arachnodactyly, overgrowth and soft tissue bleeding due to a novel homozygous fibulin-4 gene mutation. Clin Genet. 2009 Sep;76(3):276-81.
10. Hucthagowder V, Sausgruber N, Kim KH, Angle B, Marmorstein LY, Urban Z. Fibulin-4: a novel gene for an autosomal recessive cutis laxa syndrome. Am J Hum Genet. 2006 Jun;78(6):1075-80.
11. Dasouki M, Markova D, Garola R, Sasaki T, Charbonneau NL, Sakai LY, Chu ML. Compound heterozygous mutations in fibulin-4 causing neonatal lethal pulmonary artery occlusion, aortic aneurysm, arachnodactyly, and mild cutis laxa. Am J Med Genet A. 2007 Nov 15;143A(22):2635-41.
12. Renard M, Holm T, Veith R, Callewaert BL, Ades LC, Baspinar O, Pickart A, Dasouki M, Hoyer J, Rauch A, Trapane P, Earing MG, Coucke PJ, Sakai LY, Dietz HC, De Paepe AM, Loeys BL. Altered TGFbeta signaling and cardiovascular manifestations in patients with autosomal recessive cutis laxa type I caused by fibulin-4 deficiency. Eur J Hum Genet. 2010 Aug;18(8):895-901.
13. Erickson LK, Opitz JM, Zhou H. Lethal osteogenesis imperfecta-like condition with cutis laxa and arterial tortuosity in MZ twins due to a homozygous fibulin-4 mutation. Pediatr Dev Pathol. 2012 Mar-Apr;15(2):137-41.
14. Sawyer SL, Dicke F, Kirton A, Rajapkse T, Rebeyka IM, McInnes B, Parboosingh JS, Bernier FP. Longer term survival of a child with autosomal recessive cutis laxa due to a mutation in FBLN4. Am J Med Genet A. 2013 May;161A(5):1148-53.
15. Kappanayil M, Nampoothiri S, Kannan R, Renard M, Coucke P, Malfait F, Menon S, Ravindran HK, Kurup R, Faiyaz-Ul-Haque M, Kumar K, De Paepe A. Characterization of a distinct lethal arteriopathy syndrome in twenty-two infants associated with an identical, novel mutation in FBLN4 gene, confirms fibulin-4 as a critical determinant of human vascular elastogenesis. Orphanet J Rare Dis. 2012;7:61.
16. Hanada K, Vermeij M, Garinis GA, de Waard MC, Kunen MG, Myers L, Maas A, Duncker DJ, Meijers C, Dietz HC, Kanaar R, Essers J. Perturbations of vascular homeostasis and aortic valve abnormalities in fibulin-4 deficient mice. Circ Res. 2007 Mar 16;100(5):738-46.
17. Kaijzel EL, van Heijningen PM, Wielopolski PA, Vermeij M, Koning GA, van Cappellen WA, Que I, Chan A, Dijkstra J, Ramnath NW, Hawinkels LJ, Bernsen MR, Lowik CW, Essers J. Multimodality imaging reveals a gradual increase in matrix metalloproteinase activity at aneurysmal lesions in live fibulin-4 mice. Circ Cardiovasc Imaging. 2010 Sep;3(5):567-77.

6

18. Moltzer E, te Riet L, Swagemakers SM, van Heijningen PM, Vermeij M, van Veghel R, Bouhuizen AM, van Esch JH, Lankhorst S, Ramnath NW, de Waard MC, Duncker DJ, van der Spek PJ, Rouwet EV, Danser AH, Essers J. Impaired vascular contractility and aortic wall degeneration in fibulin-4 deficient mice: effect of angiotensin II type 1 (AT1) receptor blockade. PLoS One. 2011;6(8):e23411.

19. Hahn RT, Roman MJ, Mogtader AH, Devereux RB. Association of aortic dilation with regurgitant, stenotic and functionally normal bicuspid aortic valves. J Am Coll Cardiol. 1992 Feb;19(2):283-8.

20. Nistri S, Sorbo MD, Marin M, Palisi M, Scognamiglio R, Thiene G. Aortic root dilatation in young men with normally functioning bicuspid aortic valves. Heart. 1999 Jul;82(1):19-22.

21. Michel JB, Martin-Ventura JL, Egido J, Sakalihasan N, Treska V, Lindholt J, Allaire E, Thorsteinsdottir U, Cockerill G, Swedenborg J, consortium FE. Novel aspects of the pathogenesis of aneurysms of the abdominal aorta in humans. Cardiovasc Res. 2011 Apr 1;90(1):18-27.

22. Hinterseher I, Tromp G, Kuivaniemi H. Genes and abdominal aortic aneurysm. Ann Vasc Surg. 2011 Apr;25(3):388-412.

23. Wang J, Chen H, Seth A, McCulloch CA. Mechanical force regulation of myofibroblast differentiation in cardiac fibroblasts. Am J Physiol Heart Circ Physiol. 2003 Nov;285(5):H1871-81.

24. van der Velde ET, Vriend JW, Mannens MM, Uiterwaal CS, Brand R, Mulder BJ. CONCOR, an initiative towards a national registry and DNA-bank of patients with congenital heart disease in the Netherlands: rationale, design, and first results. Eur J Epidemiol. 2005;20(6):549-57.

25. McLaughlin PJ, Chen Q, Horiguchi M, Starcher BC, Stanton JB, Broekelmann TJ, Marmorstein AD, McKay B, Mecham R, Nakamura T, Marmorstein LY. Targeted disruption of fibulin-4 abolishes elastogenesis and causes perinatal lethality in mice. Mol Cell Biol. 2006 Mar;26(5):1700-9.

6

6

Chapter 7
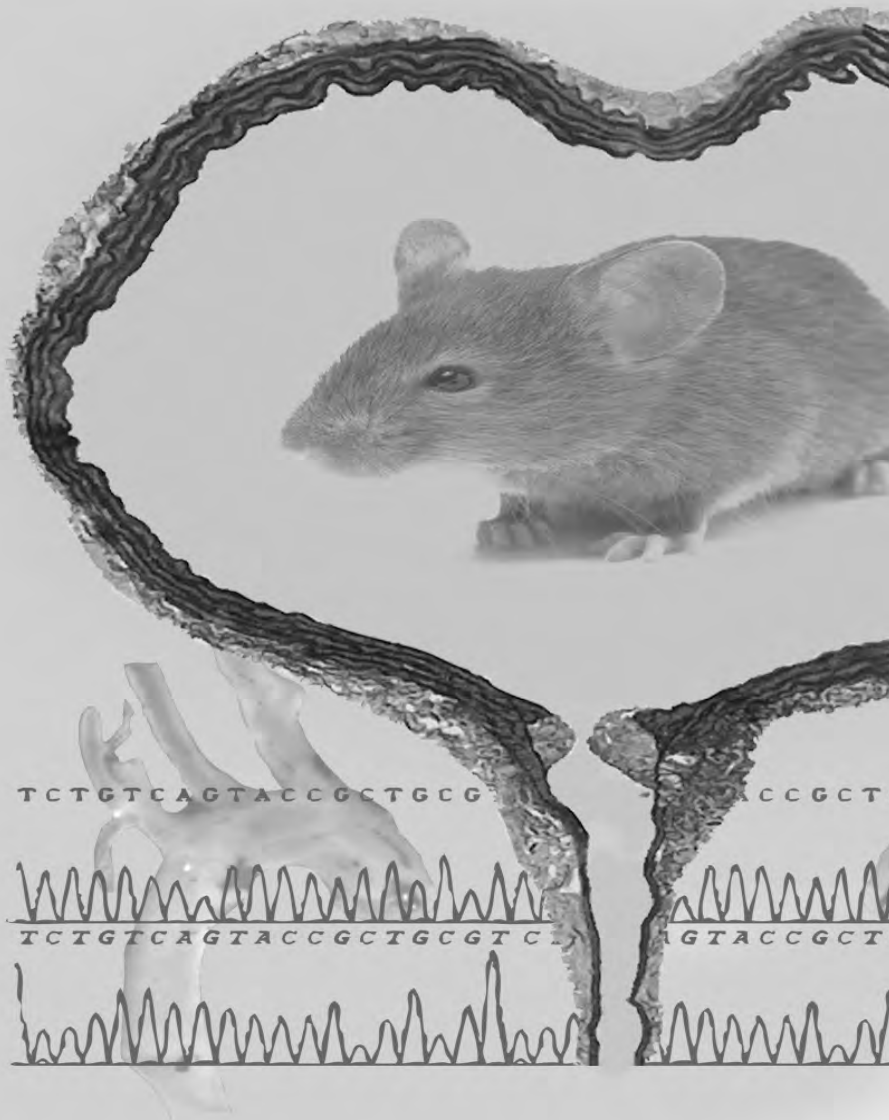
SUMMARY

Aortic disease, such as an aortic aneurysm, is one of the leading causes of mortality and morbidity in industrialized countries. Aortic aneurysms usually progress asymptomatically and are usually detected in a severe stage of the disease. The pathophysiology of aortic aneurysms is largely unknown. Mutations in a number of genes involved in the extracellular matrix structure, the TGF-β signaling pathway and in genes important for the contractile function of vascular smooth muscle cells (SMCs) have been identified so far to be associated with mainly ascending aortic aneurysms, which improved the understanding of the complex pathophysiology to some extent. However, the main mechanisms underlying the remaining forms of thoracic aortic aneurysms (TAAs) and the complex multifactorial processes leading to abdominal aortic aneurysms (AAAs) still need to be determined. Insight in the molecular mechanism underlying aortic aneurysm formation can expose predisposing factors, which can contribute to new and early detection mechanisms. Homozygous or compound heterozygous mutations in the Fibulin-4 gene, which encodes for the glycoprotein Fibulin-4, important for extracellular matrix structure and elastic fiber synthesis, results in early severe TAA formation in both patients and mice. In this thesis a Fibulin-4 deficient mouse model was used to determine the dose-dependent phenotypic and molecular effects of the Fibulin-4 protein. Additionally, cohorts of patients were analyzed on aortic aneurysm associated phenotypic and molecular alterations.

Activity of matrix metalloproteinases (MMPs) contributes significantly to the pathogenesis of aortic aneurysms. Induction of MMP activity may arise from increased TGF-β signaling, which plays a prominent role in aortic aneurysm syndromes. Moreover, aortic transcriptome and protein expression analyses showed increased TGF-β signaling in aortas of Fibulin-4 deficient mice. Homozygous Fibulin-4$^{R/R}$ mice have a 4-fold reduced expression of Fibulin-4 and develop severe TAAs with extracellular matrix degeneration from birth on, while heterozygous Fibulin-4$^{+/R}$ mice, which have a 2-fold reduction of the Fibulin-4 protein, display a milder form of extracellular matrix degeneration without aortic aneurysm formation. To determine whether increased MMP activity associated with TAAs can be monitored in vivo with molecular imaging methods, the use of protease-activatable near-infrared fluorescence (NIRF) probes was tested in the Fibulin-4 deficient mouse model (Chapter 2). The NIRF probes could be detected using a non-invasive 3D quantitative technique, fluorescence molecular tomography (FMT), which in combination with micro-CT, could determine the degree and localization of MMP activity in the Fibulin-4^{R} mice. Using this combined FMT-CT imaging method a dose-dependent increase in MMP activity was identified in Fibulin-4$^{+/R}$ and Fibulin-4$^{R/R}$ mice, which confirmed the results obtained by gelatin zymography. In this way, a combined molecular imaging method was developed which allows in vivo non-invasive coregistration of MMP activity during aneurysm formation, as it detects increased MMP activity in heterozygous Fibulin-4$^{+/R}$ mice that do not yet develop aortic aneurysms.

In patients, both thoracic and abdominal aortic aneurysms often occur concomitantly with chronic obstructive pulmonary disease (COPD). In Chapter 3 we investigated this relationship and show that COPD occurred at statistically significant higher frequencies in patients with aortic aneurysms as compared to patients with atherosclerotic arterial disease. This relation was independent of smoking, inflammation and other known risk factors. As both aortic aneurysms and COPD are characterized by extracellular matrix degeneration, the Fibulin-4 deficient mouse model was used to investigate whether an extracellular

7

matrix defect could provide a pathogenetic link for both diseases. Indeed, gradual alveolar airspace enlargement was observed in lungs of Fibulin-4$^{+/R}$ and Fibulin-4$^{R/R}$ mice. The lung abnormalities were already present in newborn lungs of Fibulin-4$^{R/R}$ mice, while Fibulin-4$^{+/R}$ mice had normal elastin structures and alveolar airspaces at birth and developed airspace enlargement with aging. The alveolar airspace enlargement was associated with gradually enhanced activation of TGF-β signaling in the lungs of Fibulin-4$^{+/R}$ and Fibulin-4$^{R/R}$ mice, which is also found in lungs from Marfan mice. In addition, combined gene expression analyses of lungs of Fibulin-4^R mice and COPD patients revealed a downregulation of SERPINA1, the serine protease inhibitor α-1 antitrypsin, which inhibits elastase. Pathway analyses revealed a link between SERPINA1, Fibulin-4 and MMP9, which was itself not deregulated. However, molecular imaging using the protease activatable probes indeed showed increased MMP and neutrophil elastase activity. Furthermore, gene expression analyses pointed to increased inflammation pathways in lungs of Fibulin-4$^{R/R}$ mice, which was confirmed by histology and flowcytometric measurements. This was not observed in lungs of Fibulin-4$^{+/R}$ mice under baseline conditions, while after LPS inhalation an enhanced respiratory inflammatory response was observed. Thus, mild Fibulin-4 deficiency induces disruption of the extracellular matrix, which subsequently predisposes to an enhanced inflammatory response with further breakdown of alveolar walls. The experimental data from this chapter suggest that a generalized genetic susceptibility to extracellular matrix degradation and secondary inflammation might be a common pathophysiologic mechanism responsible for the tissue destruction in both COPD and aneurysm formation. Genetic screening for mutations related to extracellular matrix degeneration may be a new strategy to identify people with an increased risk for developing both aneurysms and COPD with age.

In addition, mild extracellular matrix degeneration in heterozygous Fibulin-4$^{+/R}$ mice predisposes for late-onset thoracic and abdominal aortic disease after induction of atherosclerosis (Chapter 4). In humans, aneurysms are usually associated with atherosclerosis and most commonly develop in the abdominal aorta with increasing age. However, the molecular mechanism for the relation between aneurysm formation and atherosclerosis is largely unknown. To determine whether a mild extracellular matrix defect might account for the association between aortic dilation and atherosclerosis, a new mouse model was developed. The subtle defect in the extracellular matrix of the Fibulin-4$^{+/R}$ mouse was combined with a representative model for atherosclerosis as observed in humans, the ApoE knockout mouse. Due to absence of the ApoE protein these mice obtain increased LDL levels, which stimulate atherosclerotic plaque formation. At the age of nine weeks the double mutant mice were fed a high fat diet (HFD), control fat diet (CFD) or regular chow diet for 10, 20 or 30 weeks, to study plaque formation and its effect on the aortic wall. Using the protease activatable probes, increased MMP activity was observed in the abdominal aorta of ApoE$^{-/-}$Fibulin-4$^{+/R}$ mice after 10 and 20 weeks of HFD as compared to ApoE$^{-/-}$Fibulin-4$^{+/+}$ mice. Aortic diameter measurements revealed thoracic and abdominal aortic wall dilations already after 20 weeks of CFD, which has a slightly higher fat percentage compared to chow diet and probably induced mild atherosclerosis. However, HFD resulted in increased thoracic aortic dilations in both ApoE$^{-/-}$Fibulin-4$^{+/R}$ as well as ApoE$^{-/-}$Fibulin-4$^{+/+}$ mice. Compared to ApoE$^{-/-}$Fibulin-4$^{+/+}$ mice, HFD led to increased aortic arch stiffness in ApoE$^{-/-}$Fibulin-4$^{+/R}$ mice. Interestingly, HFD led to abdominal aortic dilations after 20 weeks of HFD in ApoE$^{-/-}$Fibulin-4$^{+/R}$ mice. Altogether, a mild Fibulin-4 deficiency led to relatively small (<20%) thoracic dilations after exposure to low fat levels in CFD and abdominal dilations after exposure to high fat levels in HFD indicating a subtle interplay between the

7

processes of aortic wall degeneration and plaque formation. A much more dramatic effect of Fibulin-4 deficiency was observed in plaque size and composition as the extracellular matrix defect in ApoE$^{-/-}$Fibulin-4$^{+/R}$ aortas resulted in an increased plaque area in both the descending and abdominal aorta after 10 weeks of HFD. Additionally, an altered plaque morphology was observed in the aortic arch of ApoE$^{-/-}$Fibulin-4$^{+/R}$ mice after 10 weeks of HFD, characterized by disconnected and overlying plaques with reduced elastin content. Interestingly, between 20 and 30 weeks of HFD some of the ApoE$^{-/-}$Fibulin-4$^{+/R}$ mice developed symptoms of paralysis and 30% did not survive. This indicates that a subtle defect in the extracellular matrix of the aortic wall in association with atherosclerosis predisposes for both the development of thoracic and abdominal aortic dilation, and for an altered plaque morphology.

Fibulin-4 deficient patients and mice show increased TGF-β signaling in the aortic wall, which is observed by increased nuclear pSmad2 staining. To determine the relation between Fibulin-4 deficiency and increased TGF-β signaling, aortic SMCs were isolated from Fibulin-4$^{+/+}$, Fibulin-4$^{+/R}$ and Fibulin-4$^{R/R}$ mice (Chapter 5). Interestingly, Fibulin-4$^{R/R}$ SMCs showed a reduced proliferation rate compared to Fibulin-4$^{+/R}$ and wild type SMCs, which could be reversed by TGF-β inhibition through addition of neutralizing antibodies. Subsequent analyses of TGF-β activity using the CAGA-luciferase reporter assay and expression analyses of TGF-β pathway related proteins, indeed revealed a gradual ligand induced and basal increase of TGF-β signaling in Fibulin-4$^{+/R}$ and Fibulin-4$^{R/R}$ SMCs. An increased amount of TGF-β1 and strongly increased TGF-β2 could be detected in medium from Fibulin-4 deficient SMCs, which likely induced the observed increased TGF-β signaling. Interestingly, elevated levels of TGF-β2 were also measured in blood plasma of some Fibulin-4$^{R/R}$ mice, and were reduced after losartan treatment of these mice. The observed increase in TGF-β2 secretion gives new insights in the molecular interaction between Fibulin-4 and TGF-β pathway regulation, and their roles in the pathogenesis of aortic aneurysms. Additionally, it might prove relevant to use TGF-β2 as a therapeutic target or as a diagnostic, therapeutic and/or prognostic biomarker.

Finally, a Fibulin-4 exon-sequencing protocol was developed to screen for pathogenic Fibulin-4 mutations in patients with syndromic, familial and sporadic forms of TAA and patients with AAA (Chapter 6). As observed in homozygous Fibulin-4$^{R/R}$ mice, patients with homozygous or compound heterozygous Fibulin-4 mutations present with severe cardiovascular abnormalities in the first months or years of their life. Besides ascending aortic aneurysms, abdominal aortic tortuosity and dilations were observed in some of the Fibulin-4 patients. To determine whether heterozygous or mild pathogenic Fibulin-4 mutations could also genetically predispose to thoracic and abdominal aortic disease in patients, four cohorts consisting of patients with TAAs, coarctations and/or aortic stenosis and one cohort consisting of AAA patients were screened. In total 16 variants were found in the different cohorts with TAA patients, and 10 variants in the AAA patients, of which six were already found in the TAA patients. In silico analyses of these variants revealed no direct pathogenic mutations. However, a number of variants were detected that could not be classified as definitely neutral and were assigned as unclassified variants, which might be classified on available information in the future. Additionally, subtle mutations affecting the expression level of Fibulin-4 cannot be ruled out in these patients.

The thesis presented here underscores the importance of the Fibulin-4 mutant mice as a tool in cardiovascular research as it shows that the dosage of a single gene can determine the

7

severity of both aneurysm formation as well as lung emphysema and implies that disturbed TGF-β signaling underlies these multiple phenotypes. These data highlight the importance that a deficiency of elastic fibers is a marker of a more critical event in the pathogenesis of aneurysms, as we found that excessive TGF-β signaling underlies both aneurysm formation and lung emphysema in this model. Besides the genetic link between aneurysm formation and progression and COPD, we also found a considerable association between aneurysms and COPD in human patients, underscoring the relevance of these mouse models for both genetic heritable early-onset as well as genetically predisposed late-onset diseases. If validated, this model opens the possibility to test therapeutic strategies aimed to target TGF-β signaling and the renin angiotensin system, such as losartan, for the treatment of TAA, COPD and other disorders caused by the extracellular matrix degeneration, and to determine their relevance for the treatment of abdominal aortic dilations. The molecular and phenotypic observations of both the mouse model as well as human data additionally provide the possibility to develop methods for early detection of aortic aneurysms.

7

SAMENVATTING

Ziektes van de aorta, zoals aorta aneurysmata, gaan gepaard met een hoge mortaliteit en morbiditeit in de geïndustrialiseerde landen. Aorta aneurysmata hebben meestal een asymptomatisch verloop en worden daarom vaak in een laat en ernstig stadium ontdekt. De pathofysiologie van aorta aneurysmata is voor een groot gedeelte onbekend. Tot zover is bekend dat mutaties in genen betrokken bij de extracellulaire matrix samenstelling, de TGF-β signaleringsroute en genen belangrijk voor de contractiele functie van vasculaire gladde spiercellen geassocieerd zijn met voornamelijk aneurysmata van de aorta ascendens. Hierdoor is de complexe pathofysiologie voor een gedeelte opgehelderd. Echter, de voornaamste onderliggende mechanismen van de overige vormen van thoracale aorta aneurysmata (TAA) en de complexe multifactoriële processen die resulteren in een abdominale aorta aneurysma (AAA) zijn nog onbekend. Inzicht in het moleculaire mechanisme dat leidt tot aneurysmavorming kan predisponerende factoren aan het licht brengen en bijdragen aan nieuwe en vroege detectiemethodes. Homozygote of samengestelde heterozygote mutaties in het Fibuline-4 gen, dat codeert voor het glycoproteïne Fibuline-4 en belangrijk is voor de extracellulaire matrix samenstelling en de aanmaak van elastische vezels, leiden tot vroege ernstige aneurysmavorming van de aorta ascendens in zowel patiënten als muizen. In dit proefschrift is er gebruik gemaakt van een Fibuline-4 deficiënt muismodel om de dosisafhankelijke fenotypische en moleculaire effecten van het Fibuline-4 eiwit te onderzoeken. Daarnaast zijn er patiëntengroepen geanalyseerd voor aneurysma geassocieerde fenotypische en moleculaire afwijkingen.

Matrix metalloproteïnase (MMP) activiteit draagt voor een belangrijk gedeelte bij aan de pathogenese van aorta aneurysmata. De MMP activiteit kan geïnduceerd worden door een verhoogde TGF-β signalering, waarvan bekend is dat het een aanzienlijke rol speelt in thoracale aorta aneurysmata. Bovendien is een verhoogde TGF-β signalering ook gebleken uit aorta transcriptoom en eiwitexpressie analyses van Fibuline-4 deficiënte muizen. Homozygote Fibuline-4$^{R/R}$ muizen hebben een 4-maal verlaagde expressie van Fibuline-4 en ontwikkelen ernstige aneurysmata van de aorta ascendens met extracellulaire matrix degeneratie vanaf de geboorte, terwijl heterozygote Fibuline-4$^{+/R}$ muizen, met een 2-maal verlaagde expressie van het Fibuline-4 eiwit, een mildere vorm van extracellulaire matrix degeneratie laten zien zonder aorta aneurysma formatie. Om te bepalen of de aan TAA gerelateerde MMP activiteit *in vivo* te monitoren is met moleculaire beeldvormingstechnieken, is het gebruik van protease-activeerbare fluorescerende 'near-infrared fluorescence' (NIRF) probes getest in het Fibuline-4 deficiënte muismodel (**Hoofdstuk 2**). De NIRF probes konden worden gedetecteerd door middel van een non-invasieve 3D kwantitatieve techniek, fluorescent moleculaire tomografie (FMT), waarmee in combinatie met micro-CT de graad en lokalisatie van MMP activiteit kon worden bepaald in de Fibuline-4^{R} muizen. Met deze gecombineerde FMT-CT beeldvormingstechniek was er een dosisafhankelijke verhoogde MMP activiteit te zien in de Fibuline-4$^{+/R}$ en Fibuline-4$^{R/R}$ muizen, wat overeenkwam met de resultaten van gelatine zymografie. Op deze manier is er dus een gecombineerde moleculaire beeldvormingstechniek ontwikkeld, die *in vivo* non-invasieve coregistratie van MMP activiteit tijdens aneurysmavorming mogelijk maakt, aangezien ze al een verhoogde MMP activiteit detecteert in heterozygote Fibuline-4$^{+/R}$ muizen die nog geen aneurysma hebben ontwikkeld.

In patiënten komen aorta aneurysmata, zowel thoracale als abdominale aneurysmata, vaak gelijktijdig voor met obstructieve longziekten 'chronic obstructive pulmonary diseases'

7

(COPD). In **Hoofdstuk 3** hebben we deze relatie onderzocht en laten we zien dat COPD statistisch significant vaker voorkomt bij patiënten met aorta aneurysmata dan bij patiënten met arteriële atherosclerose. Deze relatie was onafhankelijk van roken, inflammatie en andere risicofactoren. Aangezien aorta aneurysmata en COPD beide gekarakteriseerd worden door extracellulaire matrix degeneratie, is het Fibuline-4 deficiënte muismodel gebruikt om te bepalen of extracellulaire matrix afwijkingen een pathogenetische link vormt voor beide ziekten. Histologische analyses lieten inderdaad een graduele vergroting van de alveolaire ruimten zien in longen van de Fibuline-4$^{+/R}$ en Fibuline-4$^{R/R}$ muizen. De afwijkingen waren reeds te zien in longen van pasgeboren Fibuline-4$^{R/R}$ muizen, terwijl pasgeboren Fibuline-4$^{+/R}$ muizen normale elastine structuren en alveolaire ruimten hadden, maar wel met toenemende leeftijd vergroting van de alveolaire ruimten ontwikkelden. De vergroting van de alveolaire ruimten was geassocieerd met gradueel toegenomen TGF-β signalering in Fibuline-4$^{+/R}$ en Fibuline-4$^{R/R}$ muizen, en is ook beschreven in longen van Marfan muizen. Daarnaast is uit een combinatie van gen expressie analyses van longen van Fibuline-4^{R} muizen en van COPD patiënten gebleken dat de expressie van SERPINA1 verlaagd is. SERPINA1 is de serine protease remmer α-1 antitrypsine, waarvan bekend is dat het elastases remt. Daaropvolgende analyses van signaleringsroutes hebben op een link gewezen tussen SERPINA1, Fibuline-4 en MMP9, waarvan de laatstgenoemde zelf geen verandering in expressie toonde. Echter, moleculaire beeldvorming met de protease-activeerbare probes liet een verhoogde MMP en neutrofiele elastase activiteit zien. Daarnaast hebben gen expressie analyses van longen van Fibuline-4$^{R/R}$ muizen gewezen op toegenomen inflammatie signaleringsroutes, die ook aangetoond werden door middel van histologie en flowcytometrie metingen. Deze toegenomen inflammatie werd niet gevonden in Fibuline-4$^{+/R}$ muizen onder basale condities, terwijl lipopolysaccharide inhalatie wel leidde tot een toegenomen respiratoire inflammatie in deze muizen. Dus, milde Fibuline-4 deficiëntie zorgt voor een afwijkende extracellulaire matrix, dat vervolgens predisponeert voor een toegenomen inflammatoire reactie met verdere afbraak van de alveolaire wanden. De experimentele data van dit hoofdstuk suggereren dat een genetische susceptibiliteit voor extracellulaire matrix degradatie, en secundair inflammatie, mogelijk een gemeenschappelijk pathofysiologisch mechanisme vormen welke verantwoordelijk zijn voor de weefselafbraak in zowel COPD als aneurysmata. Genetische screening op mutaties gerelateerd aan extracellulaire matrix degeneratie kan een nieuwe strategie zijn voor de identificatie van mensen met een verhoogd risico op het ontwikkelen van zowel aneurysmata als COPD met de leeftijd.

Daarnaast predisponeert een milde extracellulaire matrix degeneratie in heterozygote Fibuline-4$^{+/R}$ muizen voor thoracale en abdominale aorta afwijkingen na inductie van atherosclerose (**Hoofdstuk 4**). In mensen gaan aneurysmata vaak gepaard met atherosclerose en deze ontwikkelen zich vaker in de abdominale aorta en met toenemende leeftijd. Echter, het moleculaire mechanisme onderliggend aan de relatie tussen aneurysmavorming en atherosclerose is voor een groot gedeelte onbekend. Om te bepalen of een mild extracellulair matrix defect verantwoordelijk is voor de relatie tussen aorta dilatatie en atherosclerose, is er een nieuw muismodel ontwikkeld. Het subtiele defect in de extracellulaire matrix van de Fibuline-4$^{+/R}$ muizen werd gecombineerd met een representatief model voor atherosclerose zoals dat ook in mensen voorkomt, de ApoE$^{-/-}$ muizen. Door het uitschakelen van het ApoE gen in muizen, die van zichzelf geen atherosclerose ontwikkelen, krijgen de muizen verhoogde LDL waarden die atherosclerotische plaquevorming stimuleren. Op de leeftijd van negen weken werden de dubbel mutante muizen op een hoog vet dieet ('high fat diet', HFD), controle vet dieet ('control fat diet', CFD) of een normaal

7

chow dieet gezet voor 10, 20 of 30 weken, om atherosclerotische plaquevorming en de effecten op de aortawand, zoals aortadilatatie, te bestuderen. Met behulp van de protease-activeerbare probes was er verhoogde MMP activiteit te zien in de abdominale aorta's van ApoE$^{-/-}$Fibuline-4$^{+/R}$ muizen na 10 en 20 weken HFD in vergelijking met ApoE$^{-/-}$Fibuline-4$^{+/+}$ muizen. Aorta diameter metingen toonden al thoracale aortaboog en abdominale aorta dilataties na 20 weken CFD, dat een licht verhoogd vetpercentage heeft vergeleken met een standaard 'chow' dieet en mogelijk milde atherosclerose induceert. HFD resulteerde in toegenomen thoracale aortaboog diameters in zowel ApoE$^{-/-}$Fibuline-4$^{+/R}$ als ApoE$^{-/-}$Fibuline-4$^{+/+}$ muizen. In ApoE$^{-/-}$Fibuline-4$^{+/R}$ muizen was er na HFD vergeleken met ApoE$^{-/-}$Fibuline-4$^{+/+}$ muizen wel een toename te zien in de stijfheid van de aortaboog. Daarnaast resulteerde HFD na 20 weken in dilataties van de abdominale aorta van ApoE$^{-/-}$Fibuline-4$^{+/R}$ muizen. Samenvattend leidde een milde Fibuline-4 deficiëntie tot relatief kleine (<20%) thoracale aortaboog dilataties na blootstelling aan lage vet gehalten in CFD en abdominale dilataties na blootstelling aan hoge vet gehalten in HFD, wat wijst op een subtiele interactie tussen het proces van aortawand degeneratie en plaquevorming. Een dramatischer effect van Fibuline-4 deficiëntie was te zien in plaque grootte en compositie, aangezien het extracellulaire matrix defect in ApoE$^{-/-}$Fibuline-4$^{+/R}$ aorta's zorgde voor een toegenomen plaque oppervlakte in de aorta descendens en abdominale aorta na 10 weken HFD. Daarnaast werd er een afwijkende plaque morfologie in de aortaboog van ApoE$^{-/-}$Fibuline-4$^{+/R}$ muizen gevonden, gekarakteriseerd door losliggende en overliggende plaques met verminderde elastine. Sommige ApoE$^{-/-}$Fibuline-4$^{+/R}$ muizen ontwikkelden tussen de 20 en 30 weken HFD verlammingsverschijnselen en 30% overleefde het niet. Dit geeft aan dat een subtiel defect in de extracellulaire matrix van de aortawand, in associatie met atherosclerose, predisponeert voor zowel thoracale en abdominale aorta dilatatie, als voor een afwijkende plaque morfologie.

Verder hebben Fibuline-4 deficiënte patiënten en muizen een verhoogde TGF-β signalering in de aortawand, wat aangetoond is door een toegenomen nucleaire pSmad2 kleuring. Om de relatie tussen Fibuline-4 deficiëntie en een verhoogde TGF-β signalering te bepalen, zijn er gladde spiercellen geïsoleerd uit aortabogen van Fibuline-4$^{+/+}$, Fibuline-4$^{+/R}$ en Fibuline-4$^{R/R}$ muizen (**Hoofdstuk 5**). Het was opmerkelijk dat Fibuline-4$^{R/R}$ gladde spiercellen een afgenomen proliferatie lieten zien vergeleken met Fibuline-4$^{+/R}$ en wild type gladde spiercellen. De afgenomen proliferatie kon hersteld worden door TGF-β inhibitie met neutraliserende antilichamen. Daaropvolgend zijn er analyses gedaan van de TGF-β activiteit met de CAGA-luciferase reporter analyse en met expressie analyses van TGF-β signaleringsroute gerelateerde eiwitten. Deze wezen inderdaad op een gradueel verhoogde TGF-β signalering, zowel ligand geïnduceerd als basaal, in Fibuline-4$^{+/R}$ en Fibuline-4$^{R/R}$ gladde spiercellen. Medium van Fibuline-4 deficiënte gladde spiercellen toonden vervolgens verhoogde TGF-β1 en sterk verhoogde TGF-β2 waarden, wat waarschijnlijk resulteerde in de toegenomen TGF-β signalering. Verhoogde TGF-β2 waarden werden ook gevonden in plasma van een aantal Fibuline-4$^{R/R}$ muizen, welke verlaagd was na losartan behandeling van deze muizen. De verhoogde secretie van TGF-β2 geeft nieuwe inzichten in de moleculaire interactie tussen Fibuline-4 en de TGF-β signaleringsroute, en hun rol in de pathogenese van aorta aneurysmata. Daarnaast kan het interessant zijn om TGF-β2 als een therapeutisch doelwit of als een diagnostische, therapeutische en/of prognostische biomarker te gebruiken.

In het laatste hoofdstuk staat beschreven dat er een Fibuline-4 exon-sequencing protocol ontwikkeld is om patiënten met syndromische, familiaire en sporadische vormen van

TAA en patiënten met AAA te screenen op pathogene Fibuline-4 mutaties (**Hoofdstuk 6**). Vergelijkbaar met homozygote Fibuline-4$^{R/R}$ muizen, presenteren patiënten met homozygote of samengesteld heterozygote Fibuline-4 mutaties gedurende de eerste paar maanden of jaren ernstige cardiovasculaire afwijkingen. Naast aneurysmata van de aorta ascendens, worden er ook gekronkelde abdominale aorta's en dilataties gezien in sommige Fibuline-4 patiënten. Om te bepalen of heterozygote of mild pathogene Fibuline-4 mutaties ook genetisch kunnen predisponeren voor thoracale en abdominale aorta aandoeningen in patiënten, zijn er vier patiënten cohorten met TAA, coarctatie en/of aorta stenose, en één cohort met AAA patiënten gescreend. In totaal zijn er 16 varianten gevonden in de verschillende cohorten met TAA patiënten en 10 varianten in de AAA patiënten, waarvan er zes ook gevonden waren in de TAA patiënten. *In silico* analyses van deze varianten hebben geen aanwijzingen gegeven voor direct pathogene mutaties. Echter, zijn er wel een aantal varianten gedetecteerd die niet als neutrale varianten geclassificeerd konden worden. Deze varianten werden als niet-geclassificeerde varianten benoemd, die mogelijk in de toekomst met meer beschikbare informatie geclassificeerd kunnen worden. Daarnaast, kunnen subtiele mutaties die een effect hebben op de expressie van Fibuline-4 niet uitgesloten worden in deze patiënten.

Dit proefschrift onderstreept de relevantie van de Fibuline-4 mutante muizen als model in cardiovasculair onderzoek, aangezien de dosis van een enkel gen de ernst van zowel aneurysma formatie als long emfyseem bepaalt, waarbij een verstoorde TGF-β signalering ten grondslag ligt aan deze fenotypes. Deze data benadrukt dat een deficiëntie van elastische vezels een marker is voor een nog kritischer verloop van de pathogenese van aneurysmata, aangezien we gevonden hebben dat verhoogde TGF-β signalering ten grondslag ligt aan zowel aneurysma formatie als long emfyseem in dit model. Naast de genetische link tussen aneurysma formatie en progressie en COPD, hebben we ook een significante associatie gevonden tussen aneurysmata en COPD in patiënten, welke de relevantie van dit muismodel benadrukt voor zowel genetisch erfelijk vroeg ontwikkelende ziekten, als genetisch predisponerende op latere leeftijd ontwikkelende ziekten. Indien gevalideerd, geeft dit model de mogelijkheid om therapeutische strategieën te testen die aangrijpen op de TGF-β signalering en het renine angiotensine systeem, zoals losartan, voor de behandeling van TAA, COPD en andere aandoeningen die veroorzaakt worden door de extracellulaire matrix degeneratie, en om te bepalen wat hun relevantie is voor de behandeling van abdominale aorta dilataties. De moleculaire en fenotypische bevindingen van zowel het muismodel als de humane data geven tevens de mogelijkheid om methoden voor vroege detectie van aorta aneurysmata te ontwikkelen.

7

LIST OF ABBREVIATIONS

2D	two-dimensional
3D	three-dimensional
α-SMA	alpha-smooth muscle actin
AA	aortic aneurysm
AAA	abdominal aortic aneurysm
ACTA2	actin, alpha 2
ALK	activin receptor like kinase
AOD	arterial occlusive disease
AOS	aneurysm-osteoarthritis
ApoE	apolipoprotein E
ARB	angiotensin II type 1 receptor blocker
AT1	angiotensin II type 1
ATS	arterial tortuosity syndrome
BAL	broncho-alveolar lavage
BAPN	β-aminopropionitrile monofumarate
BMI	body mass index
BMP	bone morphogenetic protein
BSA	bovine serum albumin
cbEGF	calcium-binding epidermal growth factor
CC-10	Clara-cell-specific protein
CEPH	centre d' Etrude polymorphisme humain
CFD	control fat diet
COL3A1	procollagen type III
COPD	chronic obstructive pulmonary disease
DOCA	deoxycorticosterone acetate
ECM	extracellular matrix
EDS	Ehlers Danlos syndrome
ELN	elastin
ERK	extracellular signal-regulated kinase
FBLN4	Fibulin-4
Fbn1	Fibrillin-1
FEV1	forced expiratory volume in one second
FMT	fluorescence molecular tomography
FOV	field-of-view
FSP1	fibroblast specific protein 1
FVC	forced vital capacity
Gd	gadolinium
GFP	green fluorescent protein
GM-CSF	granulocyte-macrophage colony-stimulating factor
HE	Haematoxylin-Eosin
HFD	high fat diet
HRP	horse radish peroxidase
hs-CRP	high-sensitivity C-reactive protein
HUVEC	human umbilical vein endothelial cell
IL	interleukin
ILK	integrin-linked kinase
IPA	Ingenuity pathway analysis

7

LAP	latency associated protein
LDL	low density lipoprotein
LDLR	low density lipoprotein receptor
LDS	Loeys-Dietz syndrome
LLC	large latent complex
Lox	lysyl oxidase
LPS	lipopolysaccharide
LRP	low density lipoprotein receptor-related protein
LTBP	latent TGF-β binding protein
LV	left ventricle
MEF	mouse embryonic fibroblast
MFS	Marfan syndrome
MHC II	smooth muscle myosin heavy chain II
MMP	matrix metalloprotease
MMP9	matrix metalloproteinase-9
MRA	magnetic resonance angiography
MRI	magnetic resonance imaging
MYH11	myosin heacy chain 11
MYLK	myosin light chain kinase
nAb	neutralizing antibodies
NE	neutrophil elastase
NIRF	near-infrared fluorescence
PAI	plasminogen activator inhibitor
PBS	phosphate-buffered saline
PDA	patent ductus arteriosus
PEF	peak expiratory flow
PFA	paraformaldehyde
PIF	peak inspiratory flow
PRKG1	protein kinase, cGMP-dependent, type I
RAS	renin-angiotensin system
ROS	reactive oxygen species
SAM	significance analysis of microarrays
SDS	sodium dodecyl sulfate
SERPINA1	serine protease inhibitor α-1 antitrypsin
SLC	small latent complex
SM22	smooth muscle specific protein-22
Smad	mothers against decapentaplegic
SMC	smooth muscle cell
Smurf1	SMAD specific E3 ubiquitin ligase 1
TβR	transforming growth factor beta receptor
TAA	thoracic aortic aneurysm
TAC	transverse aortic constriction
TGF-β	transforming growth factor- beta
TIMP	tissue inhibitor of metalloproteinases
TNF	tumor necrosis factor
TTF-1	thyroid transcription factor 1
UTR	untranslated region

7

CURRICULUM VITAE

Personal Information:

Name:	Natasja Wanita Monisha Ramnath
Nationality:	Dutch
Date of birth:	24th December 1986
Place of birth:	The Hague, The Netherlands

Education and research:

2009 – 2013	PhD research, department of Genetics and department of Vascular Surgery, Erasmus MC, Rotterdam, The Netherlands Promotors: Prof.dr. R. Kanaar and Prof.dr. H.J.M. Verhagen Co-promotor: Dr. J. Essers
2006 – 2009	Master of Science in Molecular Medicine, Erasmus MC, Rotterdam, The Netherlands
2008 – 2009	Msc thesis, department of Genetics, Erasmus MC, Rotterdam, The Netherlands
2008	Research internship, department of Genetics, Erasmus MC, Rotterdam, The Netherlands
2004 – 2008	Medicine doctorate, Erasmus MC, Rotterdam, The Netherlands
2005-2008	Doctorate
2004-2005	Propaedeutic
2001 – 2004	VWO, V.H.K.-Scholengemeenschap, Nickerie, Suriname

7

LIST OF PUBLICATIONS

Impaired vascular contractility and aortic wall degeneration in fibulin-4 deficient mice: effect of angiotensin II type 1 (AT1) receptor blockade.
*Moltzer E, te Riet L, Swagemakers SM, van Heijningen PM, Vermeij M, van Veghel R, Bouhuizen AM, van Esch JH, Lankhorst S, **Ramnath NW**, de Waard MC, Duncker DJ, van der Spek PJ, Rouwet EV, Danser AH, Essers J.*
PLoS One. 2011;6(8):e23411. doi: 10.1371/journal.pone.0023411. Epub 2011 Aug 9.

Multimodality imaging reveals a gradual increase in matrix metalloproteinase activity at aneurysmal lesions in live fibulin-4 mice.
*Kaijzel EL, van Heijningen PM, Wielopolski PA, Vermeij M, Koning GA, van Cappellen WA, Que I, Chan A, Dijkstra J, **Ramnath NW**, Hawinkels LJ, Bernsen MR, Löwik CW, Essers J.*
Circ Cardiovasc Imaging. 2010 Sep;3(5):567-77. doi: 10.1161/CIRCIMAGING. 109.933093. Epub 2010 Jun 30.

Extracellular matrix defects in aneurysmal Fibulin-4 deficient mice predispose to lung emphysema
***N.W.M. Ramnath**, K.M. van de Luijtgaarden, I. van der Pluijm, M. van Nimwegen, P.M. van Heijningen, S.M.A. Swagemakers, B.S. van Thiel, R.Y. Ridwan, N.van Vliet, M. Vermeij, L.J.A.C. Hawinkels, A. de Munck, O. Dzyubachyk, E. Meijering, P. van der Spek, R. Rottier, H. Yanagisawa, R.W. Hendriks, R. Kanaar, E.V. Rouwet, A. KleinJan, J. Essers*
(manuscript in preparation)

Fibulin-4 deficiency induces thoracic and abdominal aortic wall dilation and altered plaque morphology in apolipoprotein E-deficient mice
N.W.M. Ramnath, B.S. Van Thiel*, K. Van der Heiden*, L. Speelman, R.Y. Ridwan, P.M. van Heijningen, M. Vermeij, E.V. Rouwet, R. Kanaar, I. Van der Pluijm, J. Essers*
* Equal contributors
(manuscript in preparation)

Fibulin-4 deficiency results in enhanced TGF-β signaling in aortic smooth muscle cells and increased TGF-β2 secretion
N.W.M. Ramnath, L.J.A.C. Hawinkels*, P.M. van Heijningen, L. te Riet, M. Paauwe, R. Kanaar, P. ten Dijke, J. Essers*
* Equal contributors
(manuscript in preparation)

Fibulin-4 mutation analysis of patients with thoracic and abdominal aortic disease
***N.W.M. Ramnath**, P. Elfferich, K.M. van de Luijtgaarden, P.M. van Heijningen, H.T. Bruggenwirth, D. Dooijes, J.M.A. Verhagen, M.W. Wessels, G. Pals, D. Majoor-Krakauer, J. W. Roos-Hesselink, E.V. Rouwet, R. Kanaar, J. Essers*
(manuscript in preparation)

7

PHD PORTFOLIO

Name: Natasja W.M. Ramnath
Department: Genetics/Vascular Surgery
Research schools: MGC and COEUR
PhD period: 2009-2013
Promotors: Prof.dr. R. Kanaar and Prof.dr. H.J.M. Verhagen
Co-promotor: Dr. J. Essers

General academic skills:
    2009   Technology Facilities
    2009   Veilig werken in het laboratorium
    2009   Laboratory animal science
    2011   Biomedical English Writing and Communication

Research skills and in-depth courses
    2008   Course on 'SNPs and human diseases'
    2008   Cursusdag Klinische Genetica Diagnostiek
                               'Grasduinen in Genome Browsers'
    2009   Analysis of microarray gene expression data
    2009   Basic data analysis on gene expression arrays
                               (BAGE)
    2009   Cardiovascular Medicine
    2010   Basic introduction course on SPSS
    2012   Atherosclerosis and Aneurysmal Disease-
                               from bed to bench and back

Presentations
    2010   Genetica Retraite, Genetic Epidemiology,
                               Maastricht UMC
                               Oral presentation
    2010   Coeur PhD day, Erasmus MC, Rotterdam
                               Oral presentation
    2011   Stafdag Chirurgie, Erasmus MC, Rotterdam
                               Oral presentation
    2012   Masterclass Aortic Aneurysms, AMC, Amsterdam
                               Oral presentation
    2012   NRS Task Force Animal Models symposium, UMC
                               Utrecht
                               Oral presentation

International conferences
    2011   American Heart Association Scientific Sessions 2011,
                               Orlando, USA
                               Poster presentation
    2012   Arteriosclerosis, Thrombosis and Vascular Biology,
                               Scientific Sessions, Chicago, USA
                               Oral presentation

7

| 2012 | The 8th international symposium on Biomechanics in Vascular Biology and Cardiovascular Disease, Rotterdam, The Netherlands
Poster presentation |

Attended

| 2011 | The 6th international symposium on Biomechanics in Vascular Biology and Cardiovascular Disease, Rotterdam, The Netherlands |
| 2011 | Thoracale aortapathologie- nieuwe inzichten actuele behandeling, Rotterdam, The Netherlands |

Seminars and workshops

2010	Workshop animal imaging by AMIE
2010	17th MGC Graduate student workshop
2010	Photoshop and Illustrator CS4 workshop
2010	Partek training course
2011	18th MGC Graduate student workshop *Organising committee*

Teaching activities

| 2010-2011 | Supervision of bachelor student |
| 2011/2013 | Partially supervision of two bachelor students |

7

DANKWOORD

Het is af, na vier jaar promotieonderzoek en een paar maanden hard doorschrijven. Ik moet het nog even beseffen, maar er ligt nu toch echt een boekje klaar! Echter, dit zou nooit gelukt zijn zonder de hulp en het geloof van velen. Ik wil daarom ook een ieder die heeft bijgedragen aan mijn ontwikkelingen en een ieder die heeft geholpen bij de totstandkoming van dit proefschrift, vooral bij de sprint om het af te krijgen voor de coschappen, hartelijk bedanken.

Om te beginnen wil ik mijn promotoren bedanken. Prof.dr. R. Kanaar, Roland, bedankt dat ik mijn masteronderzoek op uw afdeling mocht voortzetten in promotieonderzoek. U heeft het er bij mij, en ik denk nog bij vele anderen, goed in gekregen dat DNA niet linkshandig, maar rechtshandig afgebeeld dient te worden. Ik heb veel van uw kritische en rationele blik op onderzoek meegekregen tijdens onze wekelijkse werkbesprekingen en van uw regelmatige feedback. Dat controles belangrijk zijn om je resultaten te interpreteren, is mij nu ook goed bijgebleven. Het blijft mij ook nog steeds verwonderen hoe u ondanks uw drukke agenda, binnen een dag of (uiterlijk) twee de stukken voor het proefschrift nagekeken had. Ik ben u daar heel dankbaar voor!

Prof.dr. Hence Verhagen, ook u wil ik als mijn promotor bedanken voor de mogelijkheid om promotieonderzoek te doen, maar dan vanuit de Heelkunde. Vanwege de klinische raakvlakken van dit onderzoek was het van groot belang om op deze manier nauw in contact te staan met de kliniek. Ik heb veel gehad aan ons gesprek voor de aanvang van mijn promotieonderzoek en ik kan nu zeker zeggen dat ik op basis daarvan een goede keuze heb kunnen maken. Bedankt voor uw stimulans en daarnaast wil ik u ook heel erg bedanken voor het nakijken van mijn proefschrift en uw feedback daarop.

Mijn copromotor, dr. J. Essers, Jeroen, toen ik een project moest kiezen voor mijn onderzoeksstage ben ik via dr. Rini de Crom, waar ik één van mijn labrotatie stages heb gedaan, bij jou en het Fibuline-4 onderzoek terecht gekomen. Het is mij blijkbaar goed bevallen, want de onderzoeksstage heb ik mogen doorzetten in een masteronderzoek en uiteindelijk zag ik het toch ook wel zitten om op het project door te gaan met promotieonderzoek. Ik wil je dan ook hartelijk danken dat je mij deze mogelijkheden hebt geboden en mij daarin hebt willen begeleiden. Met een moleculaire achtergrond van de master en een klinische achtergrond vanuit geneeskunde was dit een perfect project met uiteenlopende onderzoekslijnen. Het was vooral in het begin zoeken naar hoe, wat en waar, omdat we een soort exotisch onderwerp binnen de afdeling hadden. In de loop der tijd zijn er samenwerkingen ontstaan, waarbij we naast het moleculair genetische ook gebruik konden maken van andere expertises. Bedankt voor je begeleiding, al je tips, je kritische blik, je vele pogingen om mij assertiever te krijgen (en ik denk dat het ook wel een beetje is gelukt) en het laten zien hoe de wereld van onderzoek eruit ziet.

Prof.dr. Dirk Duncker, bedankt dat u zitting heeft willen nemen in mijn leescommissie. Uw interesse en enthousiasme voor onderzoek heb ik meegekregen op congressen, seminars en symposia, maar ook toen ik mijn proefschrift ter beoordeling langs kwam brengen. Het was een erg positief gesprek met nuttige adviezen en zeker een opbeuring na maandenlang schrijven. Bedankt voor al uw stimulerende tips! Prof.dr. Jolien Roos-Hesselink, ook u wil ik bedanken voor het deelnemen aan mijn leescommissie. Het onderzoek ben ik zowat gestart met het analyseren van de Concor patiënten; bedankt voor deze mogelijkheid en

7

het nakijken van het uiteindelijk hoofdstuk en mijn proefschrift. Prof.dr. Julie de Backer, ook bedankt voor uw deelname aan de leescommissie en uw inbreng voor mijn proefschrift. Prof.dr. Rudi Hendriks, prof.dr. Peter ten Dijke en dr. Danielle Majoor, bedankt voor jullie samenwerkingsmogelijkheden in de afgelopen vier jaar en voor het zitting willen nemen in de grote commissie.

Om vervolgens met mijn collega's te beginnen, wil ik als eerste de Fibuline-4 groep ontzettend bedanken voor een leuke en leerzame tijd. Ingrid, heel erg bedankt voor al jouw hulp en begeleiding. Mede dankzij jouw inzet hebben we een mooie paper kunnen maken over het longemfyseem verhaal en ik hoop dat we het snel een keer kunnen publiceren! Ik heb veel geleerd van jouw enthousiaste, snelle en kritische blik op resultaten en daarmee ben je een groot voorbeeld geweest. Ook bedankt voor alle gezellige, maar ook stimulerende momenten en dat ik me af en toe bij je mocht uitlaten. Succes met je verdere carrière en veel plezier met je gezin (ik zal het hopelijk nog enige tijd volgen via facebook ;)). Ellen, heel erg bedankt voor al je begeleiding, je kritische blik en klinische input voor het tot stand komen van dit proefschrift. Ik heb veel geleerd van jouw manier van schrijven. Ook jij bent voor mij een groot voorbeeld, aangezien je als clinicus nauw betrokken bent bij moleculair genetisch onderzoek. Ook bedankt voor het idee van het topmodel ;). Paula, je was net een maand voor mij begonnen en eigenlijk heb jij mij leren omgaan met een pipet. Daarna heb ik nog veel labwerk, waaronder omgaan met muizen en de muizendatabase, en het zo goed en volledig mogelijk opzetten van experimenten van jou mogen leren. Bedankt voor al je hulp en de gezelligheid op het lab en veel succes met je verdere carrière! Yanto, heel erg bedankt voor al je hulp met de muizen en de snelle analyses. Het bleef lang niet alleen bij imagen, maar hele proeven die wij samen (soms tot laat) deden. Veel geluk met je gezin en zorg ervoor dat je dat bekende Hindoestaanse nummer echt een keer weet ;). Nicole, ook jou wil ik bedanken voor je hulp en geduld bij het muizenwerk en op het lab. Ik vind het knap hoe jij je proefjes altijd netjes gepland en uitgevoerd hebt. Ik wens je nog veel succes met je eigen muizen en hoop dat er wat moois uitkomt. Bibi, bedankt voor je hulp bij het ApoE hoofdstuk en het oppakken van de experimenten. Hopelijk kunnen we het gauw afmaken en opsturen. Ik wens je veel succes met je overige projecten die je hopelijk over ongeveer 2 jaar ook mag verdedigen. Luuk, bedankt voor jouw hulp bij het TGF-β verhaal en bij de kleuringen en ook veel succes met het afronden van jouw promotie. Elza, ook bedankt voor jouw hulp, tips en een gezellige tijd op het lab en succes met je carrière. Suzan en Precious, jullie ook heel erg bedankt voor jullie hulp in de laatste fase van mijn promotie en veel succes met jullie opleidingen. Moara, ook met jou was het leuk en ik wens je ook veel succes verder. Daarnaast wil ik jullie allemaal nogmaals ontzettend bedanken voor jullie hulp, steun en begrip in de zes maanden dat ik amper kon lopen. Ingrid, Bibi en Paula, ook nog bedankt voor jullie hulp met het nakijken ;).

Then I want to thank all the colleagues from the sixth floor for a nice and enjoyable time. Cecile, heel erg bedankt voor al je hulp met de organisatie op het lab, en ook voor alle vragen waarmee je mij hebt geholpen. Bij jou kon ik altijd wel terecht voor een goed gesprek en dan maakt het niet uit waarover. Bedankt daarvoor en voor al je tips. Ook bedankt dat je graag wilt helpen bij het organiseren van mijn receptie! Nathalie, bedankt voor de gezelligheid op het lab, en ik wens je veel succes met je promotie. Berina, ook met jou heb ik af en toe goede gesprekken kunnen voeren die mij weer de motivatie gaven om door te zetten, en van Maurice heb ik ook een aantal goede tips gehad. Ontzettend bedankt en veel succes met jullie carrière! Colleagues from room Ee655a, thanks for a very nice time! You can now put the temperature as low as you guys desire ;). Marcel and Kishan, with

7

7

ik bedanken voor jullie hulp op het lab. Marja en Judith, bedankt voor de mogelijkheid dat we TAA patiënten konden screenen op Fibuline-4, en Danielle bedankt dat het ook bij AAA patiënten kon en voor jouw feedback op het desbetreffende hoofdstuk. Koen, bedankt voor het delen van de data van de AAA patiënten en natuurlijk ook voor het longemfyseem hoofdstuk. Veel succes met je opleiding en het afronden van jouw boekje! Dr. Pals and Aida, thanks for sharing the samples. Hennie, ook bedankt dat jij in de laatste periode ons hebt willen begeleiden bij het interpreteren en rapporteren van de gevonden varianten.

Robbert, bedankt dat we de eerste analyses van de longen met jou samen konden doen. Bedankt voor alle hulp, enthousiasme en vrolijkheid! Marjon en Anna, ook bedankt voor jullie hulp bij het opzetten van de kleuringen. Oleh and Erik, thanks for your expertise on the quantification of the alveoli and for the very nice colorful segmented pictures of the lungs. Oleh, it was a bit of finding the best way to quantify them, but we managed. Hope to publish it soon and good luck with your career! Sigrid en Peter, bedankt dat wij voor de microarray analyses bij jullie terecht konden. Sigrid, binnen een paar klikken had jij analyses klaar; ook bedankt voor al jouw snelle hulp!

Ook wil ik de collega's van de afdeling longziekten bedanken: Alex, toevallig hebben wij bij de proefdierkunde cursus in groepsverband samengewerkt en uiteindelijk ook voor het immunologisch analyseren van de longen van de Fibuline-4 muizen. Heel erg bedankt voor jouw hulp en begeleiding bij het opzetten en uitvoeren van de proeven en de uiteindelijke verwerking in het artikel. Menno, ook ontzettend bedankt voor al jouw hulp en handigheid bij het uitvoeren en interpreteren van de proeven. Ook de overige collega's wil ik bedanken voor een gezellige tijd bij jullie op het lab!

Luuk, onze samenwerking begon met die ene western voor het longemfyseem artikel en is een beetje uit de hand gelopen naar het SMC/TGF-β manuscript. Heel erg bedankt voor al jouw hulp, enthousiasme en begeleiding bij dit project (en voor de soms wat late avonden). Helaas is het niet meer gelukt voor mijn coschappen, maar ik hoop dat we het snel kunnen opsturen. Ook bedankt voor een gezellige tijd bij jullie op het lab en ik ben blij dat ik de 3FM serious request een keer heb mogen meemaken :) ! Veel succes met je verdere carrière. Peter, ook bedankt voor uw nuttige feedback tijdens onze meetings. Marie-Jose, Madelon en alle andere collega's daar: bedankt voor al jullie hulp en een leuke tijd op het lab.

Kim en Lambert, ik wil jullie ook heel erg bedanken voor de samenwerking met het ApoE hoofdstuk. De meeste en langste late avonden waren toch bij jullie op het lab, maar in ruil daarvoor hebben we wel hele mooie schoon-geprepareerde aorta's gekregen en mooie data kunnen genereren. Lambert, je handigheid in het vevo'en heeft enorm geholpen bij de lange dagen. Bedankt voor je hulp en input bij het project! Kim, ook ontzettend bedankt voor al jouw ideeën bij de athero-analyses, en voor alle hulp en tips bij de kleuringen. Kimmetje, Leah en alle andere collega's van de 23ste ook bedankt voor jullie hulp en een gezellige tijd!

En dan wil ik graag nog mijn familie en vrienden bedanken. Chiks, hartelijk dank voor alle mooie momenten die we samen in de afgelopen, ja toch wel 9 jaar hebben mogen meemaken. Ook bedankt voor jullie support en stimulans via onze chik app, de app die soms toch ook wel de nodige afleiding gaf. Kish, ik heb je hierboven al genoemd, maar je hoort ook eigenlijk hier weer bij. Samen met Widia hadden we ervoor gekozen de Molmed master te doen en samen zijn we er door heen gekomen. Bedankt voor alle hulp

7

ooit en de grappige momenten en ervaringen die we gedeeld hebben! Jij houdt echt van verassingen ;). Widia, zoals je al in je boekje schreef hebben we dit traject inderdaad samen doorgemaakt. Bedankt dat je ook mijn paranimf wilt zijn ;). Ook ontzettend bedankt voor al je hulp en steun en dat ik af en toe mijn frustraties bij je kwijt kon. Daarnaast wil ik je nog heel erg bedanken voor het op weg helpen met Indesign en voor een opzet waarin ik verder kon; die heb ik goed kunnen gebruiken! Veel succes straks met je coschappen, maar kom eerst goed bij ;). Naar India gaan we zeker ooit nog wel een keer! Roqziee, ook bedankt voor alle gezellige momenten en dat je er altijd voor mij bent geweest. Ik wens jou en Ackbar samen veel geluk toe! Sa4, bedankt voor je mooie vriendschap, enthousiasme en alle hulp, ook met het nakijken :). Veel succes met je opleiding in Groningen, en ik kom zeker nog een keer langs! Remy, ook bedankt voor al je tips, de gezelligheid en veel succes met jouw opleiding. Ook veel geluk samen met Johan. Fati en Erman, ook veel geluk samen en ook succes met jullie opleidingen. Erman, met jouw op reis betekent of heel veel lopen en gebouwen opzoeken (waar we soms niet van weten wat voor gebouw het is) of urenlang kajakken. Daarna zijn we uitgeput, maar kunnen we altijd wel terugkijken op een leuke tijd. Fati, je bent altijd erg behulpzaam geweest, bedankt! Bushii, ook jij bedankt voor de grappige momenten, ja die auto's en mannen gaan wel uit de weg voor jou ;). Jouw boekje zag er geweldig uit en het zal vast ook goed komen op de neurologie!

Daarnaast wil ik ook graag iedereen van HSFN en Sangh bedanken voor een leuke tijd, veeel leerzame momenten en niet te vergeten jullie geduld en begrip in het afgelopen half jaar. Ik heb veel kunnen leren en ontwikkelen tijdens mijn tijd bij HSFN en heb een hele hoop vrienden gehad! Dit lijstje werd groter toen ik mij bij Sangh aansloot en ik ben blij dat ik daar onderdeel van mag zijn. Ik vind het knap hoe jullie je vrijwillig inzetten voor de maatschappij, ondanks jullie drukke studies en andere werkzaamheden. Avinash, helaas is het niet meer gelukt met die Nobelprijs, maar ik hoop dat dit resultaat voor nu ook genoeg is ;). Nishii, altijd erg lief, behulpzaam en attent, bedankt dat je er bent! Radjnie, ook bedankt voor al jouw hulp, adviezen en zorgzaamheid. Samen met Ranjeev en de rest van GHRD vind ik dat jullie ontzettend belangrijk werk doen. Veel succes met het behalen van jullie doelen.

Als laatste wil ik mijn familie hier en in Suriname hartelijk danken voor alle steun en hulp en de vele mooie momenten. Ik mag blij zijn met zo een familie. Jullie hebben altijd in mij geloofd en adviezen gegeven en dat heeft mij het nodige vertrouwen gegeven om door te kunnen zetten. Pa en Ma, jullie houding tegenover educatie is niet alleen bij ons, maar zo een beetje bij de hele familie bekend. Pa, u heeft mij leren leren toen ik net vanuit Nederland mijn eerste toets in Suriname moest maken, terwijl ik dat nog nooit eerder had gedaan. Jullie beiden hebben ons altijd met alles gestimuleerd. Heel erg bedankt voor jullie vertrouwen in mij en de vele ontwikkelingen die ik mede dankzij jullie vrijheid heb mogen doormaken. Jullie staan altijd voor een ieder klaar en daar heb ik ook veel van geleerd. Jullie zijn allebei voorbeelden voor mij en ik ben erg trots om jullie dochter te mogen zijn! Bedankt voor alles. Santusja en Rewien, we kunnen het soms heel erg gezellig hebben. Niet altijd, maar daar zijn we broer en zussen voor. Ook heel erg bedankt voor jullie begrip en steun de afgelopen paar maanden dat ik nauwelijks thuis was; ik hoop dat ik het een beetje goed heb kunnen maken door jullie ook als mijn paranimfen te kiezen! Adja, adjie, nanie en nana, ik heb ook heel veel van jullie geleerd en veel wijze lessen meegekregen, bedankt daarvoor. Dan denk ik dat ik daarmee aan het einde ben gekomen van mijn dankwoord; het is een lang verhaal geworden, maar naar mijn idee ook wel nodig. Ik wil bij deze nogmaals een ieder hartelijk bedanken!

7

Natasja